2013-04-15

Molecular Mechanism of Calcium Release Activation and Termination

Tian, Xixi

UNIVERSITY OF CALGARY

Molecular Mechanism of Calcium Release Activation and Termination

by

Xixi Tian

A THESIS

SUBMITTED TO THE FACULTY OF GRADUATE STUDIES

IN PARTIAL FULFILMENT OF THE REQUIREMENTS FOR THE

DEGREE OF DOCTOR OF PHILOSOPHY

DEPARTMENT OF CARDIOVASCULAR/RESPIRATORY SCIENCES

CALGARY, ALBERTA

APRIL, 2013

ABSTRACT

It is now well established that sarcoplasmic reticulum (SR) Ca^{2+} release in cardiac muscle is triggered via a mechanism termed Ca^{2+}-induced Ca^{2+} release (CICR). It is unknown, however, how the SR Ca^{2+} release is terminated. The overall objective of the current study is to understand the mechanisms of activation and termination of SR Ca^{2+} release mediated by the cardiac ryanodine receptor (RyR2) and their roles in the pathogenesis of cardiac disease.

A simple HEK293 cell expression system was established to assess the impact of RyR2 mutations on both Ca^{2+} release activation and termination. We found that mutations in the pore-forming region of RyR2 affected either the activation or the termination of Ca^{2+} release or both, indicating that the pore-forming region is a major determinant of Ca^{2+} release termination. Two additional regions, the N-terminal region and the calmodulin binding domain (CaMBD) of RyR2, were also found to be important for the termination of Ca^{2+} release. These results demonstrate that RyR2 itself controls the termination of Ca^{2+} release.

RyR2 and its numerous modulators together form a macromolecular complex. Whether these modulators regulate the activation or termination of Ca^{2+} release is largely unknown. Our results show that both the 12.6 kDa FK506 binding protein (FKBP12.6) and calmodulin (CaM) facilitate the termination of Ca^{2+} release, but have little effect on Ca^{2+} release activation. On the other hand, cytosolic Ca^{2+} affects both the activation and termination of Ca^{2+} release, whereas CaM-dependent protein kinase II (CaMKII) only alters the activation of Ca^{2+} release. These data indicate that Ca^{2+} release termination is a common target of RyR2 regulation.

RyR2 modulators are believed to exert their impact on channel function by inducing conformational changes in the channel, but these ligand-induced conformational changes and their functional correlation have yet to be demonstrated. Using a novel fluorescence resonance energy transfer (FRET)-based conformational probe, we assessed conformational changes in the "clamp" region near the corners of the square-shaped three-dimensional structure of RyR2 upon activation by a number of ligands. Our data demonstrate that conformational changes in the clamp region of RyR2 are ligand dependent, and suggest that RyR2 possesses multiple ligand-dependent gating mechanisms associated with distinct conformational changes.

Enhanced luminal Ca^{2+} activation has been recognized as a common defect of RyR2 mutations linked to catecholaminergic polymorphic ventricular tachycardia (CPVT). However, why some CPVT mutations are also associated with cardiomyopathies is unknown. Single cell luminal Ca^{2+} imaging revealed that RyR2 mutations that are associated with dilated cardiomyopathy (DCM) or arrhythmogenic right ventricular dysplasia type 2 (ARVD2) markedly reduced the threshold for Ca^{2+} release termination and increased the fractional Ca^{2+} release. In contrast, a RyR2 mutation associated with hypertrophic cardiomyopathy (HCM) increased the threshold for Ca^{2+} release termination and reduced the fractional Ca^{2+} release. These results provide the first evidence that abnormal fractional Ca^{2+} release attributable to aberrant termination of Ca^{2+} release is a common defect in RyR2-associated cardiomyopathies.

Overall, these findings provide novel and important insights into the molecular basis and regulation of Ca^{2+} release activation and termination, and their roles in the genesis of cardiac arrhythmias and cardiomyopathies.

ACKNOWLEDGEMENTS

First and foremost, I would like to express my sincere thanks of gratitude to my supervisor Dr. S. R. Wayne Chen, who guided me to the wonderland of science. Without his careful training, continuous support, strong encouragement and constant patience in the past six years, it would have been impossible for me to accomplish even a tiny portion of this project. I am also deeply grateful to have Dr. Robert J. French and Dr. Gary J. Kargacin as the members of my supervisory committee. They regularly gave me excellent advices to ensure the right direction of my project. I am indebted to Dr. Paul Schnetkamp and Dr. Mitsuhiko Ikura for kindly being the internal and external examiner of my doctoral thesis defense. My thanks are also extended to Drs. Zheng Liu, Terence Wagenknecht, Michael Fill, Donald Welsh, Henk ter Keurs, Jonathan Lytton and Andrew Braun for their help in many ways. I also greatly appreciate the financial support provided by Alberta Innovates-Health Solutions.

Besides, my thanks go to all the previous and current colleagues whom I have worked with in our laboratory: Lin Zhang, for teaching me the single channel recordings; Ruiwu Wang, for the significant help in all of the projects; Yijun Tang, for the excellent collaborative work; Bailong Xiao, Jianmin Xiao, Wenqian Chen, Xiaowei Zhong, Yingjie Liu, Yunlong Bai, Tao Mi, Qiang Zhou, Cuihong Xie, Jingqun Zhang, Zhen Tan, Florian Hiess, Peter Jones, Andrea Koop, Jeff Bolstad and Vladimir Vinluan for the precious companioning and support during the long period of my doctoral study.

Finally, an honorable mention goes to my family. Thanks to my parents for their warm consideration and great confidence in me through all these years. They made me what I am today. Thanks to my husband for his pure love and invaluable support.

To my beloved parents and husband

TABLE OF CONTENTS

ABSTRACT ii

ACKNOWLEDGEMENTS iv

DEDICATION v

TABLE OF CONTENTS vi

LIST OF FIGURES xii

LIST OF ABBREVIATIONS xv

CHAPTER I: INTRODUCTION 1

1.1 Cardiac excitation-contraction coupling and Ca^{2+} homeostasis 2

1.1.1 Ca^{2+} influx via L-type Ca^{2+} channel 4

1.1.2 SR Ca^{2+} release 5

1.1.2.1 SR Ca^{2+} release channel 5

1.1.2.2 Activation of SR Ca^{2+} release-CICR 6

1.1.2.2.1 The paradox of CICR 6

1.1.2.2.2 The “local control” theory 7

1.1.2.3 Termination of SR Ca^{2+} release 8

1.1.3 Ca^{2+}-dependent muscle contraction 11

1.1.4 Ca^{2+} re-uptake 12

1.1.4.1 NCX 13

1.1.4.2 SERCA and its modulators 14

1.2 Ryanodine receptors 17

1.2.1 Expression and localization of RyRs 17

1.2.2 Structure of RyRs 18

1.2.2.1 C-terminal transmembrane domain 19

1.2.2.2 N-terminal cytoplasmic domain 20

1.2.2.2.1 Clamp region 23

1.2.2.2.2 Cytoplasmic central rim 24

1.2.2.3 Ligand-dependent conformational changes during channel gating 24

1.2.3 Regulation of RyRs....25
1.2.3.1 Cytosolic Ca^{2+}....28
1.2.3.2 Luminal Ca^{2+}....29
1.2.3.3 ATP....33
1.2.3.4 Phosphorylation....34
1.2.3.4.1 PKA....34
1.2.3.4.2 CaMKII....35
1.2.3.5 CaM....37
1.2.3.6 FKBP12.6....40
1.2.3.7 Pharmological ligands....43
1.2.3.7.1 Ryanodine....43
1.2.3.7.2 Caffeine and other methylxanthines....44
1.2.3.7.3 4-CmC....46
1.3 Cardiac ryanodine receptor and cardiomyopathies....47
1.3.1 RyR2 mutations and cardiac disease....47
1.3.2 General aspects of cardiomyopathies....49
1.3.3 Sarcomeric proteins and cardiomyopathies....50
1.3.4 SR Ca^{2+} handling and cardiomyopathies....51
1.3.5 Fundamental mechanism of cardiomyopathies....53
1.4 Research objective and specific aims....57
1.4.1 Defining the molecular determinants of Ca^{2+} release activation and termination in RyR2....57
1.4.2 Determining the roles of RyR2 modulators in Ca^{2+} release activation and termination....58
1.4.3 Studying the correlation between ligand-regulated channel function and ligand-dependent conformational changes....59
1.4.4 Assessing the impact of cardiomyopathy-linked RyR2 mutations on Ca^{2+} release....59

CHAPTER II: EXPERIMENTAL PROCEDURES....60
2.1 Site-directed mutagenesis....61
2.1.1 Construction of RyR2 deletions and point mutations....61

2.1.2 Construction of GFP-tagged RyR2 and CFP/YFP-dual labeled RyR2 63
2.1.3 Construction of CaM (1-4), CA-CaMKIIδ_C 64
2.2 HEK293 cell culture and DNA transfection 65
2.3 Caffeine-induced Ca^{2+} release measurements 66
2.4 Generation of stable, inducible HEK293 cell lines expressing RyR2 WT and mutants 66
2.5 Western blotting 67
2.6 Single-cell Ca^{2+} imaging (cytosolic Ca^{2+}) of HEK293 cells 68
2.7 Single-cell Ca^{2+} imaging (luminal Ca^{2+}) of HEK293 cells 69
2.8 Measurements of FRET signals from the $RyR2_{S2367\text{-}CFP/Y2801\text{-}YFP}$ FRET pair 71
2.9 [^{3}H]ryanodine binding 72
2.10 Culture, transfection and single cell Ca^{2+} imaging of mouse HL-1 cardiac cells 74
2.11 Statistical analysis 75

CHAPTER III: ROLE OF THE PORE-FORMING REGION OF RYR2 IN CALCIUM RELEASE ACTIVATION AND TERMINATION 76
3.1 Introduction 77
3.2 Results 78
3.2.1 Generation of RyR2 mutations in the pore-forming region 78
3.2.2 Experimental model for studying luminal Ca^{2+} release activation and termination 79
3.2.3 Mutation of the luminal Ca^{2+} sensing residue E4872 elevates both the activation and termination thresholds 88
3.2.4 Mutations in the pore-forming region reduce both the activation and termination thresholds 91
3.2.5 Mutations in the pore-forming region alter either the activation or the termination threshold 95
3.2.6 D4868A increases the activation threshold but decreases the termination threshold 96
3.3 Summary 103

CHAPTER IV: ROLE OF RYR2 MODULATORS IN CALCIUM RELEASE ACTIVATION AND TERMINATION 105
4.1 Introduction 106
4.2 Results 108
4.2.1 Effect of CaM and CaMBD on Ca^{2+} release activation and termination 108
4.2.1.1 Ca^{2+}-CaM inhibits Ca^{2+} release by increasing the threshold for Ca^{2+} release termination 108
4.2.1.2 Effect of CaM on the termination of Ca^{2+} release is mediated by RyR2 112
4.2.1.3 The CaMBD of RyR2 itself is important for Ca^{2+} release activation and termination irrespective of its CaM binding 113
4.2.2 FKBP12.6 accelerates Ca^{2+} release termination 114
4.2.3 Cytosolic Ca^{2+} reduces the thresholds for both Ca^{2+} release activation and termination 121
4.2.4 CaMKIIδc stimulates the activation of Ca^{2+} release 122
4.3 Summary 129

CHAPTER V: MECHANISM OF LIGNAD-DEPENDENT CONFORMATIONAL CHANGES IN THE CLAMP REGION OF RYR2 131
5.1 Introduction 132
5.2 Results 134
5.2.1 Construction of a FRET probe in the clamp region of RyR2 134
5.2.2 S2367-CFP/Y2801-YFP FRET probe is a dynamic, functional conformation sensor 140
5.2.3 Ligand-dependent conformational changes in the clamp region of RyR2 148
5.2.3.1 Pharmalogical compound aminophylline, theophylline and 4-CmC affect the channel conformation differently 148
5.2.3.2 Distinct effects of cytosolic ATP and Ca^{2+} on the conformational dynamics of RyR2 148
5.2.3.3 Ryanodine keeps the channel open, but dose not lock RyR in a fixed conformation 153
5.3 Summary 163

CHAPTER VI: MOLECULAR BASIS OF CARDIOMYOPATHY-ASSOCIATED RYR2 MUTATIONS 165
6.1 Introduction 166
6.2 Results 168
6.2.1 The N-terminal region of RyR2 is an important determinant of Ca^{2+} release termination 168
6.2.2 Deletion of Exon-3 in RyR2 reduces the threshold for Ca^{2+} release termination 169
6.2.3 Exon-3 deletion enhances the propensity for SOICR and the magnitude of Ca^{2+} transients 174
6.2.4 RyR2 N-terminal mutations associated with ARVD2 reduce the threshold for Ca^{2+} release termination 183
6.2.5 HCM-linked RyR2 mutation A1107M increases the threshold for Ca^{2+} release termination 186
6.3 Summary 191

CHAPTER VII: DISCUSSION AND FUTURE STUDIES 193
7.1 Molecular determinants of Ca^{2+} release activation and termination in RyR2 194
7.1.1 Ca^{2+} release terminates at a fixed threshold of ER luminal Ca^{2+} in HEK293 cells 194
7.1.2 Pore-forming region 195
7.1.2.1 Luminal Ca^{2+} sensing residue E4872 is important for Ca^{2+} release termination 195
7.1.2.2 Mechanism of luminal Ca^{2+} dependent activation and termination of Ca^{2+} release 196
7.1.3 Other regions in RyR2 critical for Ca^{2+} release activation and termination 198
7.1.3.1 N-terminal region of RyR2 199
7.1.3.2 CaMBD of RyR2 199
7.2 RyR2 modulators in Ca^{2+} release activation and termination 200
7.2.1 CaM and CaMBD 200
7.2.1.1 Ca^{2+}-CaM facilitates Ca^{2+} release termination 200
7.2.1.2 The CaMBD of RyR2 is important for channel function 203

7.2.2 FKBP12.6 accelerates Ca^{2+} release termination 206
7.2.3 Cytosolic Ca^{2+} sensitizes Ca^{2+} release activation and delays Ca^{2+} release termination 207
7.2.4 CaMKII lowers the SOICR activation threshold 208
7.3 Ligand dependent conformational changes in the clamp region of RyR2 210
7.3.1 Multiple ligand-dependent RyR2 open states 210
7.3.2 Functional and structural impact of ryanodine on RyR 213
7.4 Impaired Ca^{2+} release in the genesis of cardiomyopathies 213
7.4.1 Sarcomeric proteins and cardiomyopathies 214
7.4.2 RyR2 and cardiomyopathies 214
7.4.3 Mechanisms underlying cardiomyopathies 216
7.4.4 Impaired Ca^{2+} release termination is a common target of cardiac disease 217
7.5 Perspectives and future studies 218
7.5.1 Investigating the role of other RyR2 modulators in Ca^{2+} release activation and termination 218
7.5.2 Generation of domain-specific FRET probes for studying conformational changes in RyR 218
7.5.3 Generation of knock-in mouse models for cardiomyopathies and development of a novel luminal Ca^{2+} sensing probe targeting mouse SR 219
7.5.4 Ca^{2+} release termination as a therapeutic drug target 221
7.6 Summary 222

LIST OF FIGURES

Fig. 1 Ca^{2+} transport in ventricular myocytes 3
Fig. 2 A 9.6 Å resolution cryo-EM density map of RyR1 in the closed state 21
Fig. 3 3D map of RyR assembly 26
Fig. 4 Ca^{2+}-dependent transcriptional pathways that reprogram cardiac gene expressions leading to hypertrophy 55
Fig. 5 Proposed pore structure of RyR2 and corresponding amino acid sequence 80
Fig. 6 Experimental model for studying luminal Ca^{2+} dynamics in HEK293 cells expressing RyR2 83
Fig. 7 Effect of xestospongin C on Ca^{2+} release activation and termination in HEK293 cells 85
Fig. 8 D1ER signal is not saturated in HEK293 cells at physiological Ca^{2+} concentrations 87
Fig. 9 Effect of mutation E4872A on Ca^{2+} release activation and termination 89
Fig.10 Effect of G4871E/E4872A double mutation on Ca^{2+} release activation and termination 92
Fig. 11 Effect of A4869G, Q4876A, F4870A, V4880A and K4881A on Ca^{2+} release activation and termination 93
Fig. 12 Effect of I4862A and G4864A on Ca^{2+} release activation and termination 97
Fig. 13 Effect of G4871R, E4882A and D4896A on Ca^{2+} release activation and termination 99
Fig. 14 Effect of D4868A on Ca^{2+} release activation and termination 101
Fig. 15 Construction of a CaM mutant that lacks 4 Ca^{2+} binding sites 109
Fig. 16 Co-expression of CaM or CaM (1-4) alters the threshold for Ca^{2+} release termination 110
Fig. 17 Effect of CaM and CaM (1-4) on SOICR activation and termination thresholds in cells expressing RyR2 Del-3583-3603 115
Fig. 18 Effect of W3587A/L3591A/F3603A, W3587A and L3591A on Ca^{2+} release activation and termination 117
Fig. 19 Effect of F3603A on Ca^{2+} release activation and termination 119

Fig. 20 Co-expression of FKBP12.6 increases the threshold for Ca^{2+} release termination 123
Fig. 21 Effect of cytosolic Ca^{2+} on the SOICR activation and termination thresholds .. 125
Fig. 22 Effect of CaMKIIδc on the SOICR activation and termination thresholds 127
Fig. 23 Construction and characterization of a novel FRET pair S2367-CFP/Y2801-YFP in RyR2 136
Fig. 24 FRET efficiencies in HEK293 cells transfected with $RyR2_{S2367\text{-}CFP/Y2801\text{-}YFP}$ or co-transfected with $RyR2_{S2367\text{-}CFP}$ and $RyR2_{Y2801\text{-}YFP}$ 138
Fig. 25 Caffeine induces correlated structural and functional changes in RyR2 142
Fig. 26 Fluorescence intensity of CFP or YFP in HEK293 cells expressing $RyR2_{S2367\text{-}CFP/Y2801\text{-}YFP}$ with or without D1ER 145
Fig. 27 Effect of caffeine on the FRET efficiency in HEK293 cells expressing $RyR2_{S2367\text{-}CFP/Y2801\text{-}YFP}$ or $RyR2(1\text{-}4770)_{S2367\text{-}CFP/Y2801\text{-}YFP}$ 146
Fig. 28 Caffeine has no effect on fluorescence intensity of HEK293 cells co-transfected with $RyR2_{S2367\text{-}CFP}$ and $RyR2_{Y2801\text{-}YFP}$ 147
Fig. 29 Effect of aminophylline and theophylline on the structure and function of RyR2 149
Fig. 30 Effect of 4-CmC on the structure and function of RyR2 151
Fig. 31 Effect of cytosolic ATP on the structure and function of RyR2 154
Fig. 32 Effects of cytosolic Ca^{2+} on the structure and function of RyR2 156
Fig. 33 Effect of ATP, Ca^{2+} or 4-CmC on the FRET efficiency in permeabilized HEK293 cells expressing $RyR2_{S2367\text{-}CFP/Y2801\text{-}YFP}$ 158
Fig. 34. Impact of ryanodine on the structure and function of RyR2 160
Fig. 35 [^{3}H]ryanodine binding to $RyR2_{S2367\text{-}CFP/Y2801\text{-}YFP}$ 162
Fig. 36 Construction and functional expression of an N-terminally truncated RyR2 in HEK293 cells 170
Fig. 37 Effect of deleting the first 305 N-terminal residues of RyR2 on Ca^{2+} release activation and termination 172
Fig. 38 Construction and functional expression of the RyR2 Exon-3 deletion mutant .. 175
Fig. 39 Disease-causing RyR2 mutation, Exon-3 deletion, reduces the threshold for Ca^{2+} release termination 177

Fig. 40 Exon-3 deletion enhances the occurrence, amplitude and frequency of SOICR in HEK293 cells 179
Fig. 41 Deletion of the first 305 N-terminal residues of RyR2 enhances the propensity for SOICR and the amplitude of Ca^{2+} release 181
Fig. 42 Effect of RyR2 Exon-3 deletion on SOICR in mouse HL-1 cardiac cells 184
Fig. 43 ARVD2-associted RyR2 N-terminal mutations decrease the termination threshold and increase the fractional Ca^{2+} release 187
Fig. 44 HCM-associated RyR2 mutation A1107M increases the termination threshold and decreases the fractional Ca^{2+} release 189

LIST OF ABBREVIATIONS

ADP	Adenosine diphosphate
AM	Acetoxymethyl ester
AMP	Adenosine monophosphate
AMP-PCP	Adenylyl methylenediphosphate
ARVD2	Arrhythmogenic right ventricular dysplasia type 2
ATP	Adenosine triphosphate
cAMP	Cyclic adenosine monophosphate
CaM	Calmodulin
CaMBD	Calmodulin binding domain
CaMKII	Ca^{2+}/calmodulin-dependent protein kinase II
CaMLD	Calmodulin-like domain
CASQ	Calsequestrin
CCD	Central core disease
CFP	Cyan fluorescent protein
CHAPS	3-[(3-cholamidopropyl)dimethylammonio]-1-propanesulfonate
CICR	Ca^{2+}- induced Ca^{2+} release
CLIC2	Chloride intracellular channel protein 2
CPA	Cyclopiazonic acid
CPVT	Catecholaminergic polymorphic ventricular tachycardia
CRS	Calmodulin recognition sequence
DAD	Delayed afterdepolarization
DCM	Dilated cardiomyopathy
DHPR	Dihydropyridine receptor
DMEM	Dulbecco's modified eagle medium
DTT	Dithiothreitol
EC	Excitation-contraction
EM	Electron microscopy
FKBP	FK506 binding protein
FRET	Fluorescence resonance energy transfer

GATA4	Zinc finger-containing transcription factor-4
GFP	Green fluorescent protein
HCM	Hypertrophic cardiomyopathy
HDAC	Histone deacetylases
HEPES	4-(2-hydroxyethyl)-1-piperazineethanesulfonic acid
ICM	Intracellular-like medium
IF	Inner forward
IR	Inner reverse
$IP_3(R)$	Inositol trisphosphate (receptor)
KcsA	K^+ crystallographically-sited activation channel
KRH	Krebs-Ringer-Hepes
MEF2	Myocyte enhancer factor-2
MH	Malignant hyperthermia
MLP	Muscle-specific LIM protein
MthK	Ca^{2+}-dependent K^+ channel from *Methanobacterium thermoautrophicum*
NCX	Na^+/Ca^{2+} exchanger
NFAT	Nuclear factor of activated T-cells
OF	Outer forward
OR	Outer reverse
PBS	Phosphate buffered saline
PCB 95	2,2',3,5',6-pentachlorobiphenyl
PIP2	Phosphatidylinositol 4,5-bisphosphate
PKA	cAMP-dependent protein kinase, Protein kinase A
PKC	Protein kinase C
PKG	cGMP-dependent protein kinase, Protein kinase G
PLB	Phospholamban
PLC	Phospholipase C
PMCA	Plasma membrane Ca^{2+}-ATPase
PMSF	Phenylmethylsulfonyl fluoride
P_o	Open probability

PP1	Protein phosphatase 1
PP2A	Protein phosphatase 2A
RyR	Ryanodine receptor
SLN	Sarcolipin
SERCA	Sarco(endo)plasmic reticulum Ca^{2+}-ATPase
SOICR	Store-overload-induced Ca^{2+} release
SR	Sarcoplasmic reticulum
Tm	Tropomyosin
Tn	Troponin
T-tubule	Transverse tubule
VDCR	Voltage-dependent Ca^{2+} release
WT	Wild type
YFP	Yellow fluorescent protein
3D	Three-dimensional
4-CmC	4-chloro-m-cresol

CHAPTER I: INTRODUCTION

1.1 Cardiac excitation-contraction coupling and Ca^{2+} homeostasis

The heart's main function is to pump blood throughout the body. Rhythmic contraction in the heart is initiated by an electrical excitation signal. As a ubiquitous multifaceted messenger, Ca^{2+} is essential and pivotal in the coupling between excitation and contraction. Aberrant Ca^{2+} cycling has been implicated in a range of pathological conditions, including cardiac arrhythmias, cardiomyopathies, and heart failure [1].

Ca^{2+} signaling in cardiac muscles is a bi-directional process that involves the crosstalk among extracellular Ca^{2+}, cytosolic Ca^{2+} and the Ca^{2+} stored in organelles such as the sarcoplasmic reticulum (SR) and mitochondria. Typically, during an action potential, Ca^{2+} influx through the L-type Ca^{2+} channel activates the cardiac ryanodine receptor (RyR2), resulting in a large reinforcing Ca^{2+} release, a process known as Ca^{2+}-induced Ca^{2+} release (CICR). The combination of Ca^{2+} influx and release from the SR raises the free intracellular Ca^{2+} concentration. This transient increase in intracellular Ca^{2+} concentration has been termed a Ca^{2+} transient. It plays a critical role in cardiac contraction by determining the degree to which Ca^{2+} ions are able to bind to troponin (Tn) C. Ca^{2+} binding to TnC causes a cascade of structural rearrangements within the troponin complex of the myofilament, thereby allowing contraction to occur. During the relaxation phase, cytosolic Ca^{2+} declines as a result of Ca^{2+} reuptake back to the SR via the sarco(endo)plasmic reticulum Ca^{2+}-ATPase (SERCA) or Ca^{2+} extrusion to the extracelluar space via the Na^{+}/Ca^{2+} exchanger (NCX) and the plasma membrane Ca^{2+}-ATPase (PMCA) or Ca^{2+} uptake to the mitochondria via the Ca^{2+} uniporter. Resting intracellular Ca^{2+} is always maintained at a low level (~100 nM) ensuring that myocytes are relaxed, and that improper signaling transduction is prevented [2,3] (Fig. 1). The major

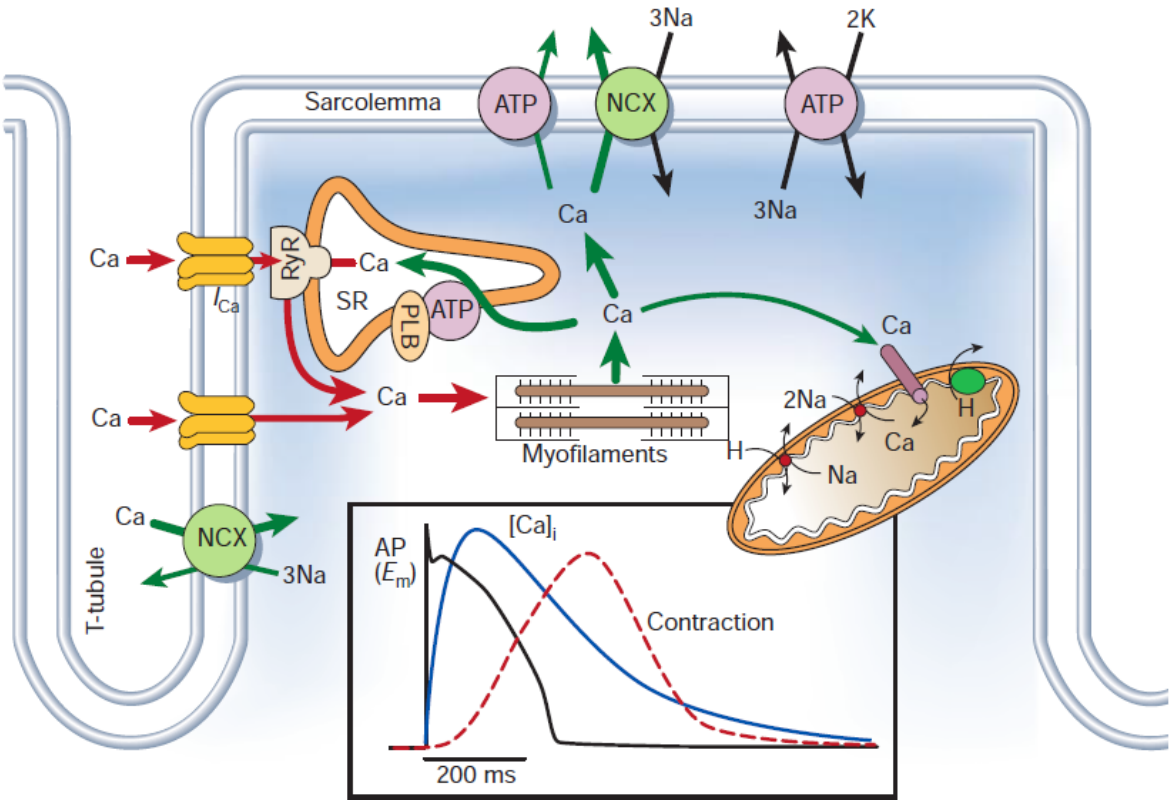

Fig. 1 Ca^{2+} transport in ventricular myocytes

Inset shows the time course of an action potential, Ca^{2+} transient and contraction measured in a rabbit ventricular myocyte at 37 °C. The T-tubule (or transverse tubule), a deep invagination of the sarcolemma, is important for excitation-contraction coupling. NCX, Na^{+}/Ca^{2+} exchange; ATP, ATPase; PLB, phospholamban; SR, sarcoplasmic reticulum. (Taken from "Cardiac excitation–contraction coupling" by Donald M. Bers. *Nature*. 2002 [3])

processes and modulators that maintain Ca^{2+} homeostasis in cardiac excitation-contraction (EC) coupling are reviewed in the following sections.

1.1.1 Ca^{2+} influx via L-type Ca^{2+} channel

Voltage activated Ca^{2+} channels that respond to depolarization account predominantly for the Ca^{2+} influx crossing the plasma membrane. Other types of Ca^{2+} channels, such as stretch-activated Ca^{2+} channels and store-operated Ca^{2+} channels, do mediate Ca^{2+} entry in cardiomyocytes, but are not necessary for the initiation of EC coupling [4].

Five types of Ca^{2+} currents have been classified, of which two (L-type and T-type) are expressed in cardiomyocytes. L-type Ca^{2+} channels are also named dihydropyridine receptors (DHPRs), since they can be effectively blocked by the Ca^{2+} channel antagonist dihydropyridine. The T-type current is rich in pacemaker and conducting cells, whereas the L-type current is ubiquitously expressed in atrial and ventricular tissues [5]. The L-type current is critical to the CICR process because of its large single channel conductance, long opening time and slow voltage-dependent inactivation [6]. During an action potential, L-type Ca^{2+} channels are activated by depolarization, leading to an increase in the Ca^{2+} concentration within a restricted space located between the sarcolemma and the underlying SR. Within this space, known as the "junctional zone" or "dyadic cleft", Ca^{2+} concentration can rise from 100 nM to 10 μM [7]. The elementary Ca^{2+} influx signal produced by a single opening of a DHPR, has been observed in confocal line-scan imaging and termed "Ca^{2+} sparklet" [8]. Inactivation of the L-type Ca^{2+} channel is mediated by both membrane repolarization and Ca^{2+} itself, but the latter is by far predominant. When Ca^{2+} reaches a certain level, Ca^{2+} will bind to CaM, and the Ca^{2+}-bound

calmodulin (Ca^{2+}-CaM) will interact with the carboxy terminus of the L-type Ca^{2+} channel, resulting in channel inactivation [9-11]. This Ca^{2+}-dependent inactivation creates a negative feedback on Ca^{2+} influx and allows for efficient auto-regulation and termination of Ca^{2+} influx.

1.1.2 SR Ca^{2+} release

Muscle cells contain a unique endoplasmic reticulum that has been termed the SR. The SR acts as a specialized Ca^{2+} storage vesicle that enables the control of muscle contraction. The small amount of Ca^{2+} that enters through the L-type channel during the cardiac action potential is not sufficient to activate the contractile machinery and thus a large amount of Ca^{2+} released from the SR is required [2].

1.1.2.1 SR Ca^{2+} release channel

Inositol trisphosphate receptors (IP_3Rs) and ryanodine receptor (RyRs) are two major classes of Ca^{2+} release channels in the SR. They share some common structural and functional features [12]. However, the activation of IP_3Rs requires inositol trisphosphate (IP_3), while the activation of RyR does not. When phospholipase C (PLC) is activated through different mechanisms in various signaling pathways [13], it catalyzes the hydrolysis of membrane-bound phosphatidylinositol 4,5-bisphosphate (PIP2). Hydrolysis of PIP2 generates IP_3. IP_3 then together with cytosolic Ca^{2+} activates the IP_3R, releasing Ca^{2+} from the internal store [14]. IP_3Rs are widely expressed in many tissue types and play a critical role in numerous physiological processes such as apoptosis [15], synaptic transmission [16] and smooth muscle EC coupling [17]. The contribution of IP_3R to EC coupling in cardiac muscle is not well understood.

RyR channels, which are activated by an increase in cytosolic Ca^{2+} in the absence of

IP_3, have been suggested to control the Ca^{2+} release from the SR during EC coupling. Mal-functioning RyR disturbs cardiac Ca^{2+} homeostasis and causes impaired EC coupling. The structure and function of RyRs will be introduced in detail in section 2 of this chapter.

1.1.2.2 Activation of SR Ca^{2+} release-CICR

The primary stimulus for the activation of SR Ca^{2+} release differs between skeletal muscle and cardiac muscle. In skeletal muscle cells, voltage-gated Ca^{2+} channels transform the electrical depolarization signal of the plasma membrane to SR Ca^{2+} release via a direct physical interaction between RyRs and DHPRs. This process is commonly known as voltage-dependent Ca^{2+} release (VDCR). On the other hand, in cardiac muscle, activation of SR Ca^{2+} release is triggered by Ca^{2+} influx through the voltage gated Ca^{2+} channel- a process named CICR [18].

1.1.2.2.1 The paradox of CICR

Although the importance of Ca^{2+} in EC coupling has been known for over a century, it was Fabiato who showed, for the first time, that Ca^{2+} release from the SR can be activated by a moderate increase in cytosolic Ca^{2+} [19]. This process acts to amplify the Ca^{2+} signal in such a way that a small "trigger" Ca^{2+} is able to induce a large SR Ca^{2+} release via RyR2. Theoretically, a small Ca^{2+} influx can trigger Ca^{2+} efflux from the SR and the Ca^{2+} efflux could further activate adjacent unactivated RyR2, leading to uncontrollable positive feedback signaling. However, voltage-clamp studies and single-cell Ca^{2+} measurements unexpectedly showed that Ca^{2+} release from the SR in the normal heart is graded and tightly controlled by the magnitude and duration of the L-type Ca^{2+} current [20]. These findings raise a longstanding and fundamental question in EC coupling:

how can the plasma membrane Ca^{2+} influx amplify the Ca^{2+} release from the SR in a graded manner, despite the theoretical runaway positive feedback mechanism that would occur between adjacent RyRs.

1.1.2.2.2 The "local control" theory

A "local control" theory has been proposed to account for the tight control of SR Ca^{2+} release induced by Ca^{2+} influx [21-26]. In this model, a group of 10-25 DHPRs on the plasma membrane and the co-localized cluster of ~100 individual RyRs within nanometers are considered as a Ca^{2+} release unit (also termed "couplon"). Each release unit is possibly activated only by Ca^{2+} influx through the coupled DHPR and the activation does not spread to neighboring units [27,28]. This would allow for graded control of Ca^{2+} release.

The discovery of "Ca^{2+} sparks" provides firm evidence for the existence of this type of Ca^{2+} release unit. Using a confocal microscope, localized Ca^{2+} release events termed "Ca^{2+} sparks" were first visualized in quiescent cardiomyocytes loaded with the fluorescent Ca^{2+} indicator Fluo-3 acetoxymethyl ester (AM) [29]. Depolarization-triggered Ca^{2+} sparks appear to be identical to spontaneous Ca^{2+} sparks with regard to their amplitude kinetics and spatial properties. This indicates that depolarization-evoked global (cell-wide) Ca^{2+} release and spontaneous Ca^{2+} release share similar properties. Interestingly, these Ca^{2+} sparks occur predominantly along the Z-lines where DHPR-RyR2 couplons are localized. Under physiological condition, these are independent Ca^{2+} release events that do not interfere with each other [29-31]. During a cardiac action potential, around ~20,000 units in one cardiomyocyte are simultaneously activated, leading to a synchronized global Ca^{2+} release [32].

These observations support a "local control" theory in which Ca^{2+} sparks are the elementary events of Ca^{2+} release, and global Ca^{2+} transients arise from the spatio-temporal summation of these independent Ca^{2+} sparks. Hence, the gradation of SR Ca^{2+} release in response to Ca^{2+} influx is thought to occur by recruiting varied numbers of individual Ca^{2+} sparks [28,31,33,34].

1.1.2.3 Termination of SR Ca^{2+} release

The development of the local control theory may satisfactorily resolve the mystery of graded regulation of SR Ca^{2+} release. However it does not explain how CICR is terminated within each release unit. Although the exact number of RyR2s initially activated by the L-type Ca^{2+} current to produce a Ca^{2+} spark is uncertain [35-38], all of the RyR2 channels (~100) in one release unit are thought to be activated because of the inherent positive feedback of CICR. Consequently, Ca^{2+} release in each elementary release unit would continue until the Ca^{2+} store is completely depleted. In contrast to this predicted all-or-none pattern of release, investigators from different groups all found that the SR Ca^{2+} store was only partially depleted during Ca^{2+} sparks or global Ca^{2+} transients [39-42], suggesting the existence of robust mechanisms that turn off SR Ca^{2+} release. Active termination of SR Ca^{2+} release would be essential for maintaining the rhythmic nature of EC coupling and muscle relaxation [20].

A number of theories have been proposed to account for the mechanism of SR Ca^{2+} release termination.

(1) The stochastic attrition [21] and coupled gating [43,44] theory - This theory states that since the opening of any given RyR in a cluster is stochastic, there is always a chance that all of the RyRs may close simultaneously, which would reduce the cytosolic Ca^{2+} to a

level below the activation threshold and break the positive feedback loop. This might work for a limited number of RyRs, but with more realistic numbers of channels, the probability for all of the channels to close at the same time becomes infinitesimal. Coupled gating of RyRs might overcome this limitation. In this case, physically linked RyRs could influence their neighbors through mechanical contact in the presence of FK506 binding protein (FKBPs) [44]. The closing of multiple RyRs within a release unit would then be better synchronized. However, the coupled gating theory remains to be confirmed since other laboratories have not been able to reproduce the results. Even if coupled gating does exist, other additional mechanisms such as RyR2 inactivation would be required to explain the initial decrease in the open probability (P_o) of the channel.

(2) RyR2 adaptation - The activity of RyR2 decreases spontaneously after activation. Decline in Po occurs in both adapted and inactivated channels, but an adapted channel remains responsive to subsequent stimuli. Adaptation of RyR2 was observed following a rapid increase in cytosolic Ca^{2+} by photolysis at the single channel level [45-47]. However, not every group was able to observe the phenomenon of RyR2 adaptation. More importantly, if adaptation of RyR2 is a real channel property, its kinetics (100 ms to seconds) are not fast enough to adequately account for Ca^{2+} release termination (ms to tens of ms) [31].

(3) Cytosolic Ca^{2+}-dependent inactivation - It has been postulated that elevated cytosolic Ca^{2+} levels are able to close RyR2s [48]. Although RyR2s can be inactivated by high levels of cytosolic Ca^{2+} (>1 mM) in artificial lipid bilayers, the physiological cytosolic Ca^{2+} concentrations (100 nM-10 μM) during EC coupling may not be sufficient

to inactivate the channel. Moreover, there are no experimental data showing that SR Ca^{2+} release can be terminated by increasing cytosolic Ca^{2+} in ventricular cardiomyocytes.

(4) Regulatory proteins – Regulatory proteins associated with RyR2 such as CaM and sorcin may play a critical role in the termination of SR Ca^{2+} release by regulating the activity of RyR2. CaM has been found to bind and inhibit RyR in the presence of low levels of cytosolic Ca^{2+} [49]. Mice with impaired CaM regulation of RyR2 were associated with defective SR Ca^{2+} release [50]. This evidence raises the possibility that CaM is the Ca^{2+} sensor that mediates Ca^{2+}-dependent inactivation of the RyR. Sorcin, a 21.6 kDa Ca^{2+}-binding protein has been shown to inhibit both the spontaneous activity of RyRs in quiescent cells (visualized as Ca^{2+} sparks) and the triggered activity of RyRs that gives rise to Ca^{2+} transients, thus sorcin is also a candidate for controlling the termination of CICR [51,52]. Nevertheless, the roles of CaM and sorcin in SR Ca^{2+} release termination remain largely undefined.

(5) Local depletion of SR Ca^{2+} and luminal Ca^{2+}-dependent deactivation - Instead of cytosolic Ca^{2+}, luminal Ca^{2+} has been suggested to play a critical role in Ca^{2+} release termination since a decrease in SR luminal Ca^{2+} level during CICR deactivates the RyR2. A major advance in understanding luminal Ca^{2+}-dependent termination comes from the development of a dye named Fluo-5N that has a low Ca^{2+} binding affinity. Using this dye to directly monitor luminal Ca^{2+} dynamics, the reciprocal events of Ca^{2+} sparks, called "Ca^{2+} blinks", were detected as rapid nanoscopic decreases in luminal Ca^{2+}. Interestingly, Ca^{2+} depletion in a blink only corresponds to about 54% reduction in the free Ca^{2+} in the SR and 28% liberation of the CASQ-bound Ca^{2+}, indicating that SR luminal Ca^{2+} is only partially depleted during Ca^{2+} blinks [53]. Similarly, Zima and his colleagues found that SR

Ca^{2+} release terminated at a fixed level of SR Ca^{2+}, called the termination threshold (~60% of the resting SR Ca^{2+} level). This threshold seems to be an intrinsic property of the cells, as it was independent of the initial SR Ca^{2+} load, the magnitude of Ca^{2+} release flux, or the level of cytosolic Ca^{2+} [42]. Because clear and convincing evidence has shown that a decrease in luminal Ca^{2+} significantly reduces the open probability of the RyR2 channels [40,41,54-56], it is likely that partial luminal Ca^{2+} depletion contributes markedly to the Ca^{2+} release termination. However, mechanistic and molecular studies regarding luminal Ca^{2+} sensing by RyR2 and Ca^{2+} release termination are lacking.

1.1.3 Ca^{2+}-dependent muscle contraction

Ca^{2+} release activation and termination both play a significant role in maintaining Ca^{2+} homeostasis, as they cooperatively shape the amount of Ca^{2+} release from SR. Ca^{2+} release from SR together with extracellular Ca^{2+} influx is essential for the initiation of muscle contraction. Contractile myofilaments consist of myosin-containing thick filaments and thin filaments, which are made up of actin polymers and troponin/tropomyosin (Tn/Tm) regulatory units [57]. In the resting state, the C terminal of TnI binds specifically to actin preventing the myosin head from interacting with actin. Once Ca^{2+} binds to the regulatory sites of TnC, the interaction of TnC with TnI is strengthened and the inhibitory activity of TnI on actin is destabilized thereby allowing for the attachment of TnT to Tm. These re-organizations of the myofilament allow myosin to interact with actin, increasing the ability of myosin ATPase to hydrolyze ATP. Chemical energy stored in the form of ATP is then transformed to kinetic energy to produce force and shortening of the muscle. Upon decreased cytosolic Ca^{2+} concentration

during muscle relaxation, Ca^{2+} is released from TnC, leading to a detachment of the myosin heads from actin filaments. [58].

The Ca^{2+} sensitivity of myofilaments is critical to sarcomere function. The Frank-Starling law of the heart states that enlarged diastolic filling (increased sarcomere length) leads to enhanced contractile force –a phenomenon known as length-dependent activation. In this phenomenon, enhanced contractile force is known to be due to increased overlap between thick and thin filaments as well as elevated myofilament Ca^{2+} sensitivity [59, 60]. The Ca^{2+} sensitivity of myofilaments can be modulated by a number of factors and conditions. Cytosolic Mg^{2+} acidosis (e.g. during ischemia) and β-adrenergic stimulation are found to reduce the Ca^{2+} sensitivity, whereas caffeine and certain inotropic drugs increase the Ca^{2+} sensitivity [3].

Since TnCs are able to bind ~50% of the released Ca^{2+} during a typical SR Ca^{2+} release [2], the myofilament complex plays an important role in Ca^{2+} buffering. Alterations in Ca^{2+} association with, or dissociation from, myofilaments can markedly affect intracellular Ca^{2+} homeostasis in cardiomyocytes. For instance, upon isoproterenol (Iso) stimulation, protein kinase A (PKA)-mediated TnI phosphorylation accelerates the Ca^{2+} off-rate from TnC and thus enhances re-uptake of Ca^{2+} and relaxation of the muscle [61-64]. Several groups also observed impaired Ca^{2+} transients in mice harboring myofilament mutations that either increase or decrease the Ca^{2+} sensitivity [65-69].

1.1.4 Ca^{2+} re-uptake

Clearance of cytosolic Ca^{2+} in cardiac cells mainly involves NCX and SERCA, and to a small degree, the PMCA. Mitochondria and some cytosolic Ca^{2+} binding proteins may also play a role in Ca^{2+} buffering.

1.1.4.1 NCX

NCX is one of the essential regulators of Ca^{2+} homeostasis and contractility in cardiac muscle. It catalyzes electrogenic countertransport of three Na^+ for one Ca^{2+} across the plasma membrane in either the Ca^{2+} efflux (forward mode) or Ca^{2+} influx mode (reverse mode). The direction in which the exchanger will move Ca^{2+} is determined by the Na^+ gradient, the Ca^{2+} gradient, and the membrane potential. High intracellular Ca^{2+} favors Ca^{2+} efflux (inward $I_{Na/Ca}$), whereas positive membrane potential (E_m) and high intracellular Na^+ favor Ca^{2+} influx (outward $I_{Na/Ca}$) [70].

NCX is present in the plasma membrane of most cells with different alternatively spliced variants, of which NCX1.1 is predominantly expressed in the heart [71]. Under normal physiological condition, upon Ca^{2+} elevation in the cytosol, the primary function of NCX in the heart is to extrude Ca^{2+}, thus contributing to muscle relaxation. This process requires the energy of the Na^+ gradient maintained by the Na^+-K^+-ATPases.

The physiological significance of reverse mode of NCX in EC coupling is controversial. It is thought that both DHPR and NCX are involved in Ca^{2+} entry during membrane depolarization. However, the efficiency of triggering SR Ca^{2+} release by Ca^{2+} influx via NCX has been shown to be much lower than that via DHPR. While the role of NCX in mediating Ca^{2+} entry under physiological conditions is debatable, it is generally believed that the reverse mode of NCX is important under pathological conditions [72-75]. Prolonged action potential duration, increased intracellular Na^+ and lowered SR Ca^{2+} release, commonly observed in failing hearts, promote NCX to reverse its mode of operation and favor Ca^{2+} influx [76]. Further, NCX expression is markedly elevated and its role in both Ca^{2+} efflux and influx become more prominent in failing cardiomyocytes, in

which the SR function is often impaired [71].

1.1.4.2 SERCA and its modulators

SERCA is a ~110-kDa membrane protein that pumps cytosolic Ca^{2+} into the SR store. Both SERCA and PMCA belong to the family of P-type ATPases. These Ca^{2+} pumps interconvert between two different conformations (E1 and E2) during the reversible cycle of ATP hydrolysis and Ca^{2+} transport [77]. In the E1 state, the enzyme has a high affinity for cytosolic Ca^{2+}. Upon binding of Ca^{2+}, a series of structural rearrangements occur to promote the phosphorylation of the enzyme using ATP. Hydrolysis of ATP permits the transfer of the enzyme from the E1 to the E2 state. Once in the E2 state, decreased Ca^{2+} affinity leads to the release of the bound Ca^{2+} to the lumen of the SR [78]. More than 10 isoforms of SERCA mainly resulting from alternative splicing have been identified. Among them, SERCA2a is the most abundantly expressed isoform and serves a fundamental role in establishing the intracellular Ca^{2+} gradients in cardiomyocytes [79].

SERCA2a transports Ca^{2+} with a fast turnover rate and a high transport capacity. The Ca^{2+}/ATP stoichiometry for SERCA2a is 2:1. In comparison, the PMCA pumps Ca^{2+} across the sarcolemma with much lower turnover rate and transport capacity and with a 1:1 Ca^{2+}/ATP stoichiometry. SERCA is also more cost-effective than NCX in terms of the amounts of ATP required per Ca^{2+} transported. Although the transport of Ca^{2+} via NCX does not require ATP consumption directly, it does require a Na^+ gradient that is expensive to maintain. NCX removes one cytosolic Ca^{2+} in exchange for three extracellular Na^+ ions. Cytosolic Na^+ is pumped out of the cell by Na^+-K^+-ATPases at a ratio of 3 Na^+ : 2 K^+ : 1 ATP, resulting in a net ratio of one Ca^{2+} transported per ATP

hydrolyzed. If the same amount of Ca^{2+} is to be removed by SERCA2a and NCX, Ca^{2+} uptake by SERCA2a into the SR would only require half of the energy needed for Ca^{2+} extrusion via NCX [80]. Theoretically, this may explain why cardiomyocytes employ SERCA as the major Ca^{2+} removal machine, and SR as the main source of Ca^{2+} for muscle contraction.

Although the proportion of Ca^{2+} cycling via SERCA varies among different species, SERCA remains the predominant mechanism of Ca^{2+} removal. During relaxation, in the rat ventricle, about 92% of the cytosolic Ca^{2+} returns to the SR, while 7% is removed via NCX and 1% via the slow systems (PMCA and mitochondria). In humans and some other mammals, including rabbits and dogs, SERCA contributes up to 70% of the Ca^{2+} removal, while 28% is removed by the NCX and 2% is removed by other mechanisms such as PMCA and mitochondria [3].

The activity of SERCA2a can be modulated by a number of factors, including cytosolic Ca^{2+}, SR Ca^{2+} content, ATP levels and pH. SERCA2a is also regulated by two membrane proteins, namely phospholamban (PLB) and sarcolipin (SLN). PLB is a 52-residue, single transmembrane protein that reversibly binds to and regulates the SERCA2a. In the resting state, PLB works as an inhibitor of SERCA2a and its inhibitory effect can be relieved upon increase in Ca^{2+} concentration. During β-adrenergic stimulation, dissociation of PLB from SERCA2a is enhanced by phosphorylation of PLB via PKA at Ser-16 or via Ca^{2+}/calmodulin-dependent protein kinase II (CaMKII) at Thr-17 [81]. On the other hand, dephosphorylation of PLB by type 1 phosphatase (PP1) results in the inhibition of SERCA2a [82]. Another regulator, the 31-amino acid peptide SLN, which was originally found to interact with SERCA1 in skeletal muscle, is also

abundantly expressed in the heart. Both PLB and SLN inhibit SERCA2a activity by lowering the Ca^{2+} binding affinity of the pump, and their inhibitory effects are removed upon β-adrenergic stimulation. However, unlike PLB, the inhibitory effect of SLN on SERCA2a is not relieved even at high intracellular Ca^{2+} concentrations, suggesting that SLN and PLB may have different functional roles [81].

As the fundamental determinant of SR Ca^{2+} re-uptake in cardiomyocytes, impaired SERCA2a function has been linked to cardiac diseases. SERCA2a gene expression and activity are reduced in human heart failure as well as a variety of animal models of heart failure. Naturally occurring mutations of SERCA2a, on the other hand, are rarely found in patients. Some mutations in the SERCA2a gene are embryonically lethal in mouse models. These findings suggest that alterations as a result of mutations in SERCA2a can cause early death and thus may not be tolerated [83].

Both SERCA2a and its regulatory protein PLB are suggested to be crucial for the cure of contractile failure. In recent years, investigators have tried to improve the systolic and diastolic cardiac function by overexpressing SERCA2a and by reducing the inhibitory effect of PLB. Overexpression of SERCA2a or reduced PLB inhibition of SERCA2a has been shown to improve SR Ca^{2+} handing and cardiac function. However, enhanced SERCA2a function may increase the risk of cardiac arrhythmias due to SR Ca^{2+}overload [84].

In summary, SERCA2a is important for maintaining normal Ca^{2+} homeostasis and cardiac function by re-cycling Ca^{2+} back to the SR and building up the SR Ca^{2+} content required for subsequent Ca^{2+} release and contraction.

1.2 Ryanodine receptors

As discussed above, SR has been recognized as the major intracellular Ca^{2+} store in cardiomyocytes. While SERCA2a controls the uptake of Ca^{2+} ions into the SR, there must be a group of channels responsible for SR Ca^{2+} release. A plant alkaloid, ryanodine, greatly benefits the identification of the SR Ca^{2+} release channel. Early studies showed that ryanodine produces irreversible contractures of skeletal muscle and inhibits twitches of cardiac muscle [85-87]. Later studies revealed direct regulation of Ca^{2+} release from SR membrane vesicles by ryanodine [88,89]. Using this specific ligand, the ryanodine binding protein, RyR, was purified from the junctional terminal cisternae of SR and visualized using electron microscopy [90-94]. After decades of intensive investigation, RyR is now recognized as the major governor of SR Ca^{2+} release in skeletal and cardiac muscles.

1.2.1 Expression and localization of RyRs

Three isoforms of RyRs (RyR1, RyR2 and RyR3) have been identified in mammalian tissues. They are encoded by three different genes, which share ~70% identity in amino acid sequence [95] with three major regions of diversity: D1 (residues 4254−4631 in RyR1 and residues 4210−4562 in RyR2), D2 (residues 1342−1403 in RyR1 and residues 1353−1397 in RyR2), and D3 (residues 1872−1923 in RyR1 and residues 1852−1890 in RyR2). RyR1 is the dominant isoform expressed in skeletal muscle, while RyR2 is the most abundant isoform in cardiac muscle. The expression of RyR3 has been detected at relatively low levels in lymphocytes, thalamus, hippocampus and smooth muscles [96-99]. The levels of expression of different RyR isoforms vary in different developmental stages and under different physiological or pathophysiological conditions [100-102].

RyRs are commonly believed to reside in the SR membrane in striated muscle and in the ER membrane in other cell types. In cardiomyocytes, the SR has two structurally and functionally distinct membrane regions, the longitudinal SR and terminal cisternae. The terminal SR is mainly involved in Ca^{2+} release and contains RyR2. It forms very close contacts (~12 nm) with the deep invagination of the sarcolemma, termed T-tubules. In skeletal muscle, junctional sites between the SR and T-tubules are known as triads. They are formed by a T-tubule and the flanking terminal cisternae of the SR on either side of the T-tubule. In cardiac muscle where T-tubule is only associated with one terminal cisterna, the junctional sites are known as dyads. The close proximity between the terminal SR and the T-tubules allows for a rapid and precise communication between the voltage sensor DHPR and the signal amplifier RyR2. In skeletal muscle, DHPRs form tetrads, which are organized in arrays that face in exact correspondence of arrays of RyR tetramers. Although, in cardiac muscle, the organization of DHPRs and RyRs is less rigid compared to that in skeletal muscle, functional local Ca^{2+}-release units still exist. As previously mentioned, in each junctional cleft, a cluster of about 100 individual RyRs and a closely localized group of ~10-25 L-type Ca^{2+} channels form a local Ca^{2+} release unit, which is capable of generating Ca^{2+} sparks [30].

1.2.2 Structure of RyRs

RyR is a homotetrameric channel composed of four identical subunits. Each subunit has ~5,000 amino acids. Although the structure of the full-length RyR channel has not been solved at a high resolution, models of RyR structures have been proposed based on mutational analyses and homologies with other better characterized ion channels, such as the bacterial potassium channel KcsA from *Streptomyces lividans*. The overall features of

the structures of the three RyR isoforms are similar, which is not surprising given their high sequence homology. Based on the amino acid sequence, RyR has been predicted to possess two major domains, the transmembrane domain located in the C-terminal region and the large cytoplasmic domain located in the N-terminal region.

1.2.2.1 C-terminal transmembrane domain

Sequence analysis reveals that one-fifth of the RyR molecule at the C-terminus is likely to form the channel pore. Several transmembrane topological models derived from the hydropathy profile of RyR have been proposed, in which the number of the transmembrane (TM) segments vary from 4 to 12 [103]. Because four potential transmembrane sequences are clearly more hydrophobic than others, they are designated as M1-M4 to form the pore region in Takeshima's model in early days [104]. Zorzato et al. identified eight additional hydrophobic sequences and proposed a model with 10 transmembrane segments from M1 to M10 and 2 tentative helices M', M'' [105]. Later, Du et al found that the previously proposed M', M'', M1, M2, and M3 sequences were not associated with membrane and proposed a model with 8 transmembrane segments named M4a, M4b, M5, M6, M7a, M7b, M8 and M10 [106]. Recent progress in three-dimensional (3D)-reconstruction of RyR has enabled the visualization of the TM domain of RyR1 at 8–10 Å resolution under conditions favoring the closed state. Samso et al. suggested at least six transmembrane helices per RyR2 monomer based on the similarities between RyR2 and the bacterial KcsA channel [107]. Ludtke et al. identified five helix-like densities and found that the conformation of pore-lining helices of the closed state of RyR1 corresponded well to that of open MthK channel [108,109]. Further studies are required to resolve these discrepancies.

Although debates continue regarding the number of transmembrane segments, two of the putative hydrophobic helices, TM8, the proposed outer helix, and TM10, the proposed inner helix, as well as the loop joining them, are generally accepted to form the channel pore of both RyR1 and RyR2. Using site-directed mutagenesis, the ion-conducting pore has been found to be located in the luminal region of the RyR. It includes the GVRAGGGIGD amino acid sequence conserved among all RyRs [110,111]. The sequence GGIGD in the pore-forming loop has been proposed to form the selectivity filter based on its homology with the selectivity filter of K^+ channels [112,113]. The helix bundle crossing region, which is also conserved in all RyR isoforms from different species, has been identified as the luminal Ca^{2+} ion gate (unpublished data). The predicted transmembrane topology of RyR2 and the putative model of the pore based on the KcsA-template are shown in Figs. 5A,B [114].

1.2.2.2 N-terminal cytoplasmic domain

The gigantic cytoplasmic domain of RyR is the site of interaction with a large number of channel modulators and harbors many mutations that underlie RyR channelopathies. The cytoplasmic domain comprised of 4000 amino acid residues constitute the apparent junctional “foot” structure as observed about half a century ago by electron microscopy [115]. The “foot” structure has been found in native muscle tissues, isolated SR vesicles and purified RyRs [90-92,94]. Further efforts, which improve the resolution of the RyR1 structure to ~30 Å in cryo-electron microscopy (cryo-EM), led to more detailed discoveries of the RyR structure. It is found that the “clamp”-like structures are located at the corners and there are “handles” connecting these corners. A central rim is found on the cytoplasmic face around the four-fold axis. Between the cytoplasmic and

Fig. 2 A 9.6 Å resolution cryo-EM density map of RyR1 in the closed state

The map is displayed at the threshold level corresponding to a molecular mass of ~2.3 MDa and viewed from cytoplasm (*A*) and in a side view (*B*). Clamp, handle, central rim and column are indicated by the arrows. The subdomains numbered from 1 to 12 are distinguished and highlighted by various colors. (Taken from "Subnanometer-resolution electron cryomicroscopy-based domain models for the cytoplasmic region of skeletal muscle RyR channel" by Irina I. Serysheva. *Proceedings of the National Academy of Sciences*. 2008 [109])

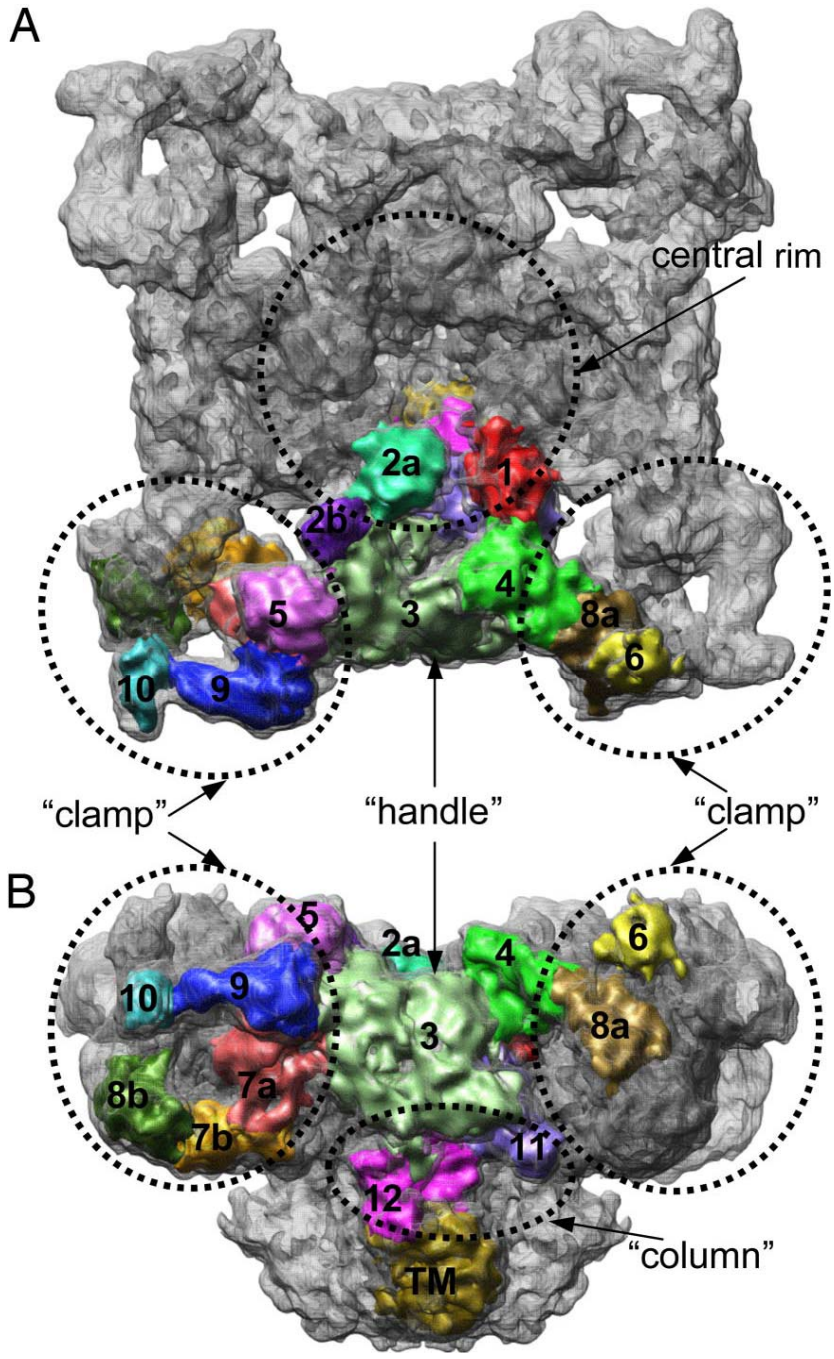
A
central rim
2a
1
2b
4
5
3
8a
6
10
9
"clamp"
"handle"
"clamp"
B
5
2a
4
6
10
9
3
8a
8b
7a
7b
11
12
"column"
TM

transmembrane regions, there is a column [116-118] (Fig. 2). Subnanometer-resolution cryo-EM also enables the dividing of the cytoplasmic domain into 15 subdomains, which are interpreted as entities with compact protein density and with only weak connections to adjacent entities. The clamp is formed by subdomains 5, 7a, 7b, 8b, 9, and 10 from one monomer and by subdomains 6 and 8a from adjacent monomers. The handle is formed by subdomains 3 and 4. The central rim is formed by subdomains 1, 2a, and 2b and the column is formed by subdomains 11 and 12 [109] (Fig. 2).

1.2.2.2.1 Clamp region

The clamp region has been suggested to contain several key structural domains that are crucial for channel gating and regulation. Based on the spacing of the DHPR arrangement and that of the homotetrameric RyR, the clamp region has been implicated in the interaction with neighboring RyRs and in the activation of RyRs by DHPRs during EC coupling in skeletal muscle [119-121]. Additionally, DR2 and DR3 in RyR2 have been mapped to the cytoplasmic clamp subdomains 6 and 9, respectively [122,123]. The central disease-causing mutation hotspot has also been localized to this clamp region [124]. Domains of RyR1 and RyR2 containing phosphorylation sites have recently been crystallized. Docking of these domains into cryo-EM maps suggests a putative location of the phosphorylation domain in the clamp region [125,158]. Consistent with this prediction, GFP inserted into RyR2 after residue Tyr-2801, close to the Ser-2808 phosphorylation site, has been mapped to the clamp region [126]. The clamp region also harbors the binding sites for the natrin toxin, a cysteine-rich secretory protein isolated from snake venom, and the chloride intracellular channel protein 2 (CLIC2), both of which have been shown to modulate the activity of RyR [127,351]. All of these findings suggest that the clamp region

plays an important role in channel function.

1.2.2.2.2 Cytoplasmic central rim

The N-terminal domain is now known to form the cytoplasmic central rim of the 3D structure of the channel. Since the N-terminal region of RyR is a disease hotspot including a large number of disease-associated mutations, several crystallographic studies have focused on this region. Ikura and coworkers reported the first crystal structure of this region, covering residues 1-210 of RyR1 [128]. Tung et al. later published the crystal structure of an N-terminal fragment of RyR1, encompassing the first 559 amino acids. The first 559 amino acids of RyR1 fold into three well-defined domains (A, B, and C). Interestingly, lots of disease-causing RyR1 mutations are located at domain-domain interfaces. In docking analysis, the N-terminal domains (A, B and C) were placed at the center rim in the low-resolution cryo-EM structure of the full-length RyR1[129]. The crystal structure of the first 217 amino acids of mouse RyR2 has been solved at 2.5 Å resolution [130]. Recently, the crystal structure of the corresponding N-terminal region of IP_3R has also been solved. The N-terminal region of IP_3R also encompasses three well-defined domains folded in a manner nearly identical to that seen in RyR1 [12, 157]. These studies provide the essential framework for understanding the mechanisms of disease-causing mutations and the gating of RyRs.

1.2.2.3 Ligand-dependent conformational changes during channel gating

Considerable efforts over the past decades have been focused on understanding conformational changes during RyR gating. The open state of RyR was stabilized by Ca^{2+} and other activators, such as ryanodine, PCB95 and AMP-PCP. Upon binding of these ligands to RyR, significant conformational changes were observed [131-136].

Ikemoto and colleagues labeled RyR with a thiol-reacting fluorescent probe and showed that channel ligands such as Ca^{2+} and ATP changed the fluorescence intensity of the labeled RyR, suggesting ligand-induced conformational changes during RyR channel gating [131,132,135]. Consistent with these biochemical studies, cryo-EM and single particle image analysis also revealed major structural rearrangements in the 3D structure of the RyR [133,134,136]. Particularly, large conformational changes were observed in the transmembrane domain and in the clamp region upon binding of ryanodine and Ca^{2+} or binding of a non-hydrolyzable analog of ATP, AMP-PCP, and Ca^{2+} [133,134]. Using a compound named PCB95, the highest resolution so far for the open-state of RyR was obtained at 10.2 Å. Upon activation of the channel by PCB95, the clamp region and central rim were found to move outwards and away from the center, while the transmembrane region was detected to be kinked [136].

These studies clearly demonstrate that RyR contains various ligand-specific binding sites, and that ligand binding to these sites induces conformational changes in the channel that consequently lead to the opening of the channel gate. Moreover, unlike the conventional notion that upon opening, structural changes happen mainly at the pore region, they suggest that global conformational changes in the clamp region and central rim region also occur. Nevertheless, how the clamp region and central rim region are allosterically coupled to the C-terminal pore-forming region during modulation by diverse ligands is a question beyond our understanding so far.

1.2.3 Regulation of RyRs

Consistent with its functional importance, RyR2 can be regulated by numerous modulators, including physiological agents (e.g. Ca^{2+}, ATP, and Mg^{2+}), small proteins

Fig. 3 3D map of RyR assembly

The large grey structure shows a side view of the RyR homotetramer. In order to show the interactions between SR membrane-bound RyR and its associated modulators, the single particle cryo-EM reconstruction map of rabbit RyR1 in the closed state at resolution of 10 Å was used. Location of each subdomain is labeled with a red number. RyR-interacting proteins are illustrated in blue, green and light brown. D1&3 (white) and TA (brown) indicate the DR and TM assembly domain, respectively. DR2 is located in the groove hidden by domains 5 and 6. (Modified from "Ryanodine receptor assembly: a novel systems biology approach to 3D mapping" by Dong Woo Song. Progress in Biophysics and Molecular Biology. 2011 [138])

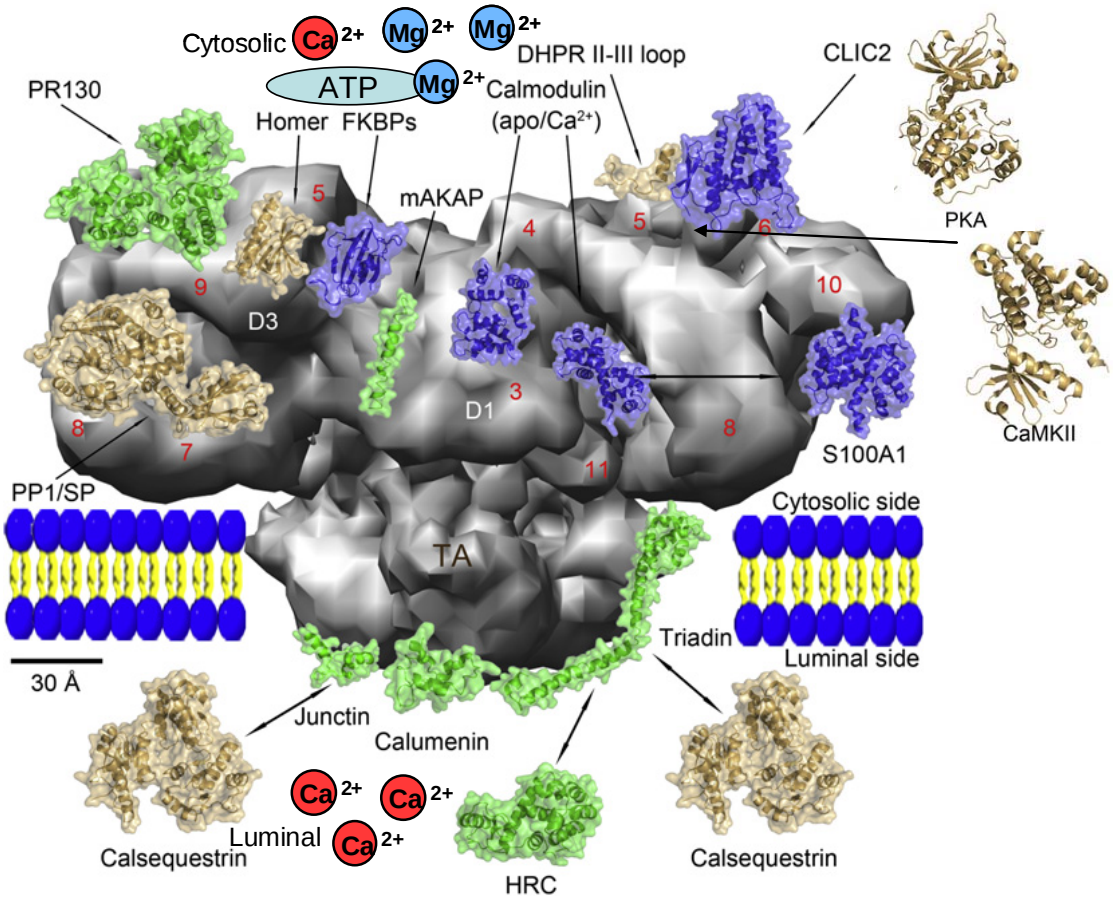
Cytosolic Ca2+
Mg2+
Mg2+
ATP
Mg2+
DHPR II-III loop
CLIC2
PR130
Homer
FKBPs
Calmodulin
(apo/Ca2+)
PKA
mAKAP
5
4
5
6
9
D3
10
3
D1
8
8
7
11
S100A1
CaMKII
PP1/SP
Cytosolic side
TA
Triadin
Luminal side
30 Å
Junctin
Calumenin
Ca2+
Ca2+
Luminal
Ca2+
Calsequestrin
HRC
Calsequestrin

(e.g. CASQ, FKBP and CaM), kinases (e.g. PKA and CaMKII) and pharmacological agents (e.g. ryanodine, caffeine, and 4-chloro-m-cresol (4-CmC)) [137]. In cardiomyocytes, numerous physiological regulators are associated with RyR2, making it a huge macromolecular complex as seen in Fig. 3 [138]. Note that Fig. 3 is intended to show a large number of regulators associated with RyR2. The exact binding locations of these modulators in the 3D structure of RyR have yet to be determined.

1.2.3.1 Cytosolic Ca^{2+}

Since cytosolic Ca^{2+} plays a central role in the activation of RyR2 during CICR, the molecular mechanism of cytosolic Ca^{2+} sensing by RyR has been extensively studied. Regulation of RyRs by cytosolic Ca^{2+} is affected by a number of cellular factors and varies with different RyR isoforms, leading to different characteristics of EC coupling in cardiac and skeletal muscles.

In the absence of cytosolic Mg^{2+}, both RyR1 and RyR2 show a bell-shaped dependence on Ca^{2+} concentrations, which suggests that Ca^{2+} can activate and inhibit RyR activity. RyR is activated by low Ca^{2+} concentrations via Ca^{2+} binding to its high affinity Ca^{2+} binding sites. On the other hand, RyR can be inhibited by high Ca^{2+} concentrations via Ca^{2+} binding to less selective and low-affinity Ca^{2+} binding sites. Cytosolic Mg^{2+} is also able to bind to Ca^{2+} binding sites in RyR, especially the low-affinity inhibitory sites [139,140]. The affinity for Ca^{2+}/Mg^{2+} binding to the inhibitory site is higher in RyR1 than in RyR2. The inhibition of RyR1 by Mg^{2+} is important for maintaining low RyR activity in the resting state, and can only be relieved by voltage for full activation. The inhibition of RyR2 by Mg^{2+} is greatly reduced by elevated cytosolic

Ca^{2+}. During EC coupling, physiological levels of Ca^{2+} alone are able to fully open the RyR2 channel and generate subsequent Ca^{2+} release from the SR.

Mutagenesis studies have provided some evidence regarding the location of the Ca^{2+} activation and Ca^{2+} inactivation sites in RyR. A single point mutation E3885A in RyR3 was found to form a functional channel with a normal conductance and unaltered modulation by other ligands, but a 10,000-fold reduction in Ca^{2+} sensitivity [141]. The corresponding glutamate 4032 of RyR1 was also found to be essential for channel function. Mutation E4032A in RyR1 abolished caffeine response and [^{3}H] ryanodine binding [142]. In line with the importance of this glutamate, Chen's group identified glutamate 3987 located in the predicted transmembrane segment M2 of the mouse RyR2 as the cytosolic Ca^{2+} sensor for channel activation [143]. These studies suggest that the cytosolic Ca^{2+} activation site is located in the C-terminal region. Since Ca^{2+}/Mg^{2+} inhibition differs between RyR isoforms as stated above, the inhibitory Ca^{2+}/Mg^{2+} binding sites may be located in the divergent regions of RyR1 and RyR2. As expected, studies with RyR1/RyR2 chimeras indicate that the C-terminal region (3687–4968) encompassing the divergent region 1 (4254–4631) of RyR1 contains the Ca^{2+} inhibitory binding sites [144-146].

1.2.3.2 Luminal Ca^{2+}

In addition to cytosolic Ca^{2+}, RyR2 is also regulated by luminal Ca^{2+}. The total amount of luminal Ca^{2+} in the SR is determined by Ca^{2+} uptake via SERCA2a, Ca^{2+} efflux via RyR2 and the binding capacity of intra-SR Ca^{2+} binding proteins. The SR Ca^{2+} buffering protein calsequestrin (CASQ2) allows Ca^{2+} to be stored at a total concentration of up to 20 mM, while the free Ca^{2+} concentration in the SR remains at ~1 mM. The

presence of bound Ca^{2+} in the SR lumen allows this organelle to supply sufficient amount of Ca^{2+} for activation of the contractile machinery despite its minuscule luminal space (3.5% of cell volume) [2].

The physiological role of luminal Ca^{2+} regulation has been intensively studied. Using single channel recordings in planar lipid bilayers to assess the effect of luminal Ca^{2+} on RyR2, most groups consistently found that luminal Ca^{2+} is able to regulate the activity of RyR2. Increased luminal Ca^{2+} enhances RyR2 activity, whereas decreased luminal Ca^{2+} reduces RyR2 activity [147-149]. Further, a large body of experimental evidence indicates that an increased SR Ca^{2+} content stimulates Ca^{2+} release, whereas a decreased SR Ca^{2+} content inhibits Ca^{2+} release from the SR in cardiomyocytes [40,54-56].

Impaired luminal Ca^{2+} regulation of RyR2 have been implicated in the pathogenesis of various cardiac diseases. As early as 1972, Fabiato demonstrated that increased SR Ca^{2+} load could generate propagating Ca^{2+} waves and periodical contraction in skinned muscle fibers [150]. This type of store-overload-induced Ca^{2+} release (SOICR) is distinct from physiological CICR. The resulting large SR Ca^{2+} spillover can lead to delayed afterdepolarizations (DADs) and triggered arrhythmias. A number of catecholaminergic polymorphic ventricular tachycardia (CPVT) RyR2 mutations, such as N4104K, R4496C, and N4895D, were found to enhance RyR2 luminal Ca^{2+} activation and reduce the threshold for SOICR, which in turn increases the propensity for triggered arrhythmia. Similar to CPVT RyR2 mutations, loss of function in CASQ2 lowers the Ca^{2+} buffering capacity of the SR and increases the level of free Ca^{2+} in the SR, thereby likewise increasing the propensity for SOICR [151]. These studies suggest that an increased sensitivity to luminal Ca^{2+} may be a common defect in cardiac diseases, including heart

failure and CPVT. Unlike other RyR2 mutations, a unique RyR2 mutation A4860G associated with catecholaminergic idiopathic ventricular fibrillation diminishes the response of RyR2 to activation by luminal Ca^{2+}, indicating that a decreased sensitivity to luminal Ca^{2+} can also cause disease [152]. Additionally, while cytosolic Ca^{2+} initiates CICR, the decline of luminal Ca^{2+} following SR Ca^{2+} release may contribute to the termination of CICR and Ca^{2+} signaling refractoriness through the process of luminal Ca^{2+}-dependent deactivation of RyR2, as discussed in section 1.1.2.3.

Although it becomes increasingly apparent that luminal Ca^{2+} plays a major role in RyR2 regulation, the mechanism by which luminal Ca^{2+}-dependent regulation occurs is unclear. Meissner's group has suggested that luminal Ca^{2+} acts on RyR2 via a "feed-through" regulatory mechanism [153,154]. In other words, luminal Ca^{2+} flowing through an open RyR channel affects the channel activity by binding to the cytosolic Ca^{2+} activation and inhibition sites. This "feed-through" theory would require luminal to cytosolic Ca^{2+} flux for luminal Ca^{2+} to be able to act on the cytosolic side of the channel.

Alternatively, it is possible that luminal Ca^{2+} can directly modulate RyR2 channel by binding to low affinity Ca^{2+} binding sites on the luminal side of the channel. Indeed, an increasing body of evidence has challenged the "feed-through" theory and supported the existence of a true luminal Ca^{2+} sensor in RyR2. In contrast to observations from Meissner's group, studies from other groups showed that increased luminal Ca^{2+} (1 μM-10 mM) enhanced channel activity at both positive and negative membrane holding potentials [148,155,156], suggesting that luminal to cytosolic Ca^{2+} flux through the open RyR2 channel is not a major determinant of luminal Ca^{2+} activation of RyR2. Furthermore, single channel studies demonstrated that luminal Ca^{2+} activation and cytosolic Ca^{2+}

activation of RyR2 could be selectively modulated. By applying luminal trypsin to sheep RyR2 in lipid bilayers, Williams' group found that trypsin digestion led to a selective abolishment of luminal Ca^{2+} activation, but not cytosolic Ca^{2+} activation, of the channel [149]. Chen's group revealed that, unlike previously characterized disease-linked RyR2 mutations, the A4860G mutation diminishes the response of RyR2 to luminal Ca^{2+} activation, whereas it has little effect on the sensitivity of the channel to activation by cytosolic Ca^{2+}. The selective impact of the A4860G mutation on Ca^{2+} activation indicates that the luminal Ca^{2+} activation of RyR2 is distinct from its cytosolic Ca^{2+} activation, and argues against the existence of luminal Ca^{2+} "feed-through" regulation and the idea of luminal Ca^{2+} acting on the cytosolic Ca^{2+} activation site [152].

The location of the luminal Ca^{2+} sensor has been investigated recently. CASQ2, the SR luminal Ca^{2+} binding protein, was proposed to serve as the SR luminal Ca^{2+} sensor [161,162]. However, the RyR2 channel in CASQ2-null cardiomyocytes is still capable of sensing luminal Ca^{2+} in the SR [163]. Purified native and recombinant RyRs that lack CASQ2 can also be modulated by luminal Ca^{2+} [154,164,165]. Furthermore, a putative luminal Ca^{2+} sensor has been identified in the helix bundle crossing of RyR2, which contains a number of negatively charged amino acids. A single mutation of one of these negatively charged residues (E4872A) completely abolishes luminal, but not cytosolic, Ca^{2+} activation of RyR2. Other mutations in the helix bundle crossing also affect the luminal Ca^{2+} activation to various extents (unpublished data). Taken together, it is likely that luminal Ca^{2+} regulates the RyR2 channel through direct interactions with the luminal activation sites of the channel.

1.2.3.3 ATP

Activation of RyR2 by Ca^{2+} alone can not achieve maximum activation of the channel. It is thought that ATP acts as a co-activator of RyR2 that can markedly increase the channel activity during EC coupling. Various other adenine nucleotides (ADP, AMP, cAMP, adenosine, and adenine) also potentiate SR Ca^{2+} release but are less effective than ATP [139,166,167].

The effect of ATP is influenced by a number of factors, such as Mg^{2+}, cytosolic Ca^{2+} and luminal Ca^{2+}. At the cellular level, Mg^{2+} and ATP form a MgATP complex. Considering the high concentration of cytosolic Mg^{2+} (~1 mM) in cardiomyocytes, it is possible that the MgATP complex rather than free ATP regulates Ca^{2+} release under physiological conditions. Activation of RyR by ATP is generally thought to occur under the influence of cytosolic Ca^{2+}. By studying adenine nucleotide stimulated Ca^{2+} efflux from isolated SR vesicles, it has been demonstrated that skeletal RyR1 can be partially activated by ATP alone [139,168], whereas RyR2 can not be activated by ATP in the absence of cytosolic Ca^{2+}. Moreover, adenine nucleotides have been reported to be more effective in stimulating Ca^{2+} release from skeletal than from cardiac SR vesicles [169]. However, later single channel studies suggest that ATP is a more potent activator (EC_{50} = 0.22 mM) of RyR2 than previously suggested from flux studies indicating that it is equipotent in activating skeletal and cardiac RyRs [166]. Interestingly, a recent single channel study shows that ATP-dependent activation of RyR2 is not only influenced by cytosolic Ca^{2+}, but also by luminal Ca^{2+}. Luminal Ca^{2+} at physiological concentrations (~1 mM) significantly increases the binding affinity of ATP to the RyR2 channel. High levels of luminal Ca^{2+} (8~53 mM) in the presence of very low concentrations of cytosolic Ca^{2+}

(100 nM) are capable of amplifying the effect of ATP on RyR2 by increasing the P_o without changing the ATP binding affinity [170].

The exact ATP binding sites in RyR are currently unknown. A number of potential ATP-binding sites, which contain the signature ATP binding motif, GXGXXG, have been predicted in RyR [103]. Further site-specific mutation analysis and functional characterization will be required to identify the residues that form the ATP-binding sites. Meanwhile, structural studies will also be required to locate these sites on the 3D structure of RyR.

1.2.3.4 Phosphorylation

RyR2 is known to be regulated by multiple protein phosphatases and kinases including phosphoprotein phosphatase (PP1), protein phosphatase 2A (PP2A), PKA, protein kinase C (PKC), cGMP-dependent protein kinase (PKG) and CaMKII [171]. Of these, the effects of PKA and CaMKII on RyR2 function have been most widely studied.

1.2.3.4.1 PKA

It is well accepted that PKA plays a central role in β-adrenergic signaling pathway. β-adrenergic receptor stimulation activates adenylyl cyclase mediated by specific G proteins and results in the generation of cAMP, which in return activates PKA. PKA phosphorylates several major Ca^{2+} cycling proteins (L-type Ca^{2+} channel, PLB, and RyR2) in cardiac cells [172], leading to an increase in SR Ca^{2+} content, SR Ca^{2+} release, and cardiac output [3].

It has been shown that RyR2 in failing hearts is hyperphosphorylated by PKA at a single residue, Ser-2808, which has also been previously suggested to be a CaMKII phosphorylation site [173]. Hyperphosphorylation of RyR2 by PKA at Ser-2808 was found

to cause dissociation of FKBP12.6 from RyR2, and, consequently, result in an increased sensitivity of the channel to Ca^{2+} activation [174]. However, several studies have clearly shown no correlation between PKA phosphorylation of RyR2 at Ser-2808 and FKBP12.6 dissociation [175-179]. FKBP12.6 was found to bind to both the Ser-2808 phosphorylated and nonphosphorylated forms of RyR2. Complete phosphorylation at Ser-2808 by exogenous PKA disrupted neither the recombinant nor native FKBP12.6-RyR2 complex. Furthermore, Chen's group identified another PKA phosphorylation site, Ser-2030. Later functional studies suggest that PKA-dependent phosphorylation enhances the response of RyR2 to luminal Ca^{2+} and reduces the threshold for SOICR, and that the effect of PKA is largely mediated by phosphorylation at Ser-2030 but not Ser-2808 [181]. Using a GFP insertion after Thr-2023, cryo-EM studies show that the Ser-2030 site lies in domain 4 within the cytoplasmic assembly of the RyR2 structure [182].

1.2.3.4.2 CaMKII

In addition to PKA, the predominant isoform of CaMKII in cardiomyocytes, CaMKIIδ_C, can also phosphorylate several Ca^{2+} handling proteins in response to Ca^{2+} elevation. With elevated cytosolic Ca^{2+} during systole, Ca^{2+} binds to CaM and the resultant Ca^{2+}-CaM complex then binds to the regulatory domain of CaMKII, leading to the activation of the enzyme. Activated CaMKII targeting to L-type Ca^{2+} channels, PLB, and RyR2 can generate multiple functional consequences. Additionally, CaMKII also regulates a number of proteins that are not directly involved in Ca^{2+} cycling such as Na^+ [183] and K^+ channels [184], making their regulation sensitive to Ca^{2+} handling as well.

An increasing body of evidence indicates that abnormal phosphorylation of RyR2 by CaMKII is involved in the pathogenesis of cardiac diseases, including heart failure and

cardiac arrhythmias [185]. However, even after decades of studies, the functional significance of phosphorylation of RyR2 by CaMKII is complex and controversial. Single channel and [^{3}H]-ryanodine binding studies with isolated RyR2 have suggested that CaMKII phosphorylation either increases [173,186-188] or decreases [189,190] the sensitivity of the RyR2 channel to Ca^{2+}. Recent studies from Bers's laboratory using isolated cardiac myocytes overexpressing CaMKIIδ_C indicate that CaMKII-mediated phosphorylation increases the fractional SR Ca^{2+} release during EC coupling and the frequency and duration of spontaneous Ca^{2+} release, causing increased diastolic SR Ca^{2+} leak [186]. Similarly, Currie et al. showed that in rabbit hearts the CaMKII peptide inhibitor (AIP) depressed Ca^{2+} spark frequency, indicating that CaMKII activates RyR2 in myocytes [188]. However, Cheng's group suggests that CaMKII negatively regulates RyR2 activity and spontaneous SR Ca^{2+} release, thereby forming a negative feedback mechanism that stabilizes local and global CICR in the heart [190]. Further studies are needed to resolve these discrepancies.

Phosphopeptide mapping has revealed that RyR2 could be phosphorylated by CaMKII at multiple sites [172]. Witcher et al. first reported that direct phosphorylation of rabbit RyR2 by CaMKII at Ser-2809 (corresponding to Ser-2808 in mouse RyR2) activated the channel [173]. Their hypothesis that Ser-2809 is a CaMKII site is supported by other studies [191,192]. However, Marks' group suggested that Ser-2809 in rabbit RyR2s is not a CaMKII site, but a unique PKA site. Instead, they identified an adjacent site, Ser-2815, in human RyR2 (corresponding to Ser-2814 in mouse RyR2), as the sole CaMKII site [187].

Ser-2808, Ser-2814 and other potential phosphorylation sites (Thr-2810 and Ser-

2811) in this region form a phosphorylation "hotspot" in RyR2. Recently, the phosphorylation domains of RyR1 and RyR2, including residues Ser-2843 (RyR1) and Ser-2808/Ser-2814 (RyR2), have been crystallized [125,158]. Docking this domain into the cryo-EM maps of RyR1 suggests a putative location of this domain in the clamp region, implying that phosphorylation may affect conformational changes within this region [125,158]. Consistent with these studies, residue Tyr-2801, which is close to the phosphorylation site Ser-2808, has been mapped to the bridge between domains 5 and 6, in each of the corner (clamp) regions of RyR2. Interestingly, the Ser-2808 site and the previously mentioned Ser-2030 site are far away from the FKBP12.6-binding site, indicating that neither of these PKA phosphorylation sites is directly involved in FKBP12.6 binding [126,182].

1.2.3.5 CaM

CaM is a key mediator in a wide range of cellular processes. This small 16.7 kDa cytosolic protein has a dumbbell-like structure with 4 EF-hand Ca^{2+} binding sites that form two symmetrical domains linked by a central alpha helix. Two high affinity (Kd~1 μM) Ca^{2+} binding sites are located at the C-domain, while 2 low affinity binding sites are located at the N-domain (Kd~12 μM) [193]. Ca^{2+} binding to each domain alters interhelical angles in the EF-hand motifs, causing a conformational change. The flexible central helix and exposure of the hydrophobic sites allow CaM to wrap around its target proteins. Using this unique conformational change of CaM upon Ca^{2+} binding, a number of "cameleon" proteins have been generated to measure intracellular Ca^{2+} [194]. A cameleon construct normally consists of a CaM sequence, a CaM recognition sequence (CRS), a pair of fluorescent proteins sequence (e.g. CFP and YFP) linked together by the

CaM sequence and CRS, and a targeting sequence for organelle-specific expression. Upon Ca^{2+} elevation, Ca^{2+}-CaM wraps around the CRS peptide, bringing CFP and YFP closer, thus increasing the fluorescence resonance energy transfer (FRET) efficiency between them [159,195]. CRS peptide derived from CaM-dependent kinase kinase has been used to replace the CRS peptide derived from myosin light chain kinase to enhance the FRET efficiency [160]. CaM mutations are also incorporated to fine tune the Ca^{2+} binding kinetics and affinities for measuring free Ca^{2+} concentrations in the range of 10^{-8} to 10^{-2} M [195]. These cameleons have been successfully applied to study cytosolic, nuclear and ER Ca^{2+} dynamics[160, 194-197].

In cardiomyocytes, CaM influences SR Ca^{2+} release by modulating a variety of ion channels, including DHPRs, IP_3Rs and RyR2s. Specifically, RyR2 is not only regulated by CaM through the CaM-CaMKII pathway, but also through direct interaction with CaM. The purified RyR2 is able to bind to either Ca^{2+}-CaM (Ca^{2+}-bound form of CaM) or apoCaM (Ca^{2+}-unbound form of CaM) [198]. CaM modulates the activity of different RyR isoforms differently. Ca^{2+}-CaM inhibits all three types of RyR, whereas apoCaM stimulates the RyR1 and RyR3, but not RyR2. RyR2 is reported to be either unaffected [49,199,200] or inhibited [201] by apoCaM.

The physiological role of RyR2 inhibition by CaM in EC coupling has not been well defined. Interestingly, CaM binds to and dissociates from RyR2 on a time scale of seconds to minutes [201], which suggests that CaM occupancy of the RyR2 channel remains unchanged during a cardiac action potential. Nevertheless, during the SR Ca^{2+} release process in EC coupling, whether CaM is always effective in inhibiting RyR2 has been questioned. Xu et al. found that CaM most effectively reduced the channel open

probability, open events and mean open time at Ca^{2+} concentrations <10 μM. At Ca^{2+} concentrations >10 μM, CaM was less effective in inhibiting RyR2 at the single channel level. This observation suggests that during the active phase of Ca^{2+} release, SR Ca^{2+} release is not significantly affected by CaM due to the presence of a high concentration of local cytosolic Ca^{2+}. CaM may have a role in the termination of SR Ca^{2+} release by reducing the probability of channel reopening when cytosolic Ca^{2+} is reduced to a low level [49]. In contrast, studies of the effect of CaM in permeabilized frog skeletal muscle fibers suggest that CaM modulates the initiation of Ca^{2+} release via RyR1, but does not play a significant role in the termination of Ca^{2+} release [202].

Mutagenesis studies have shown that the effect of CaM on RyR2 is mainly mediated through the binding of CaM to a domain comprised of highly conserved amino acid residues 3583-3603 in RyR2. The deletion of residues 3583-3603 resulted in a decrease of [^{35}S]CaM binding to background levels and prevented CaM inhibition of RyR2 in single channel studies[200]. Single residues in this region such as W3587 and L3591 were also identified to be crucial for the CaM effect on RyR2. Corresponding region in RyR1 including residues 3614-3643 has also been identified as a calmodulin binding domain (CaMBD) for both Ca^{2+}-CaM and apo-CaM [203,204]. Interestingly, another region including residues 4064-4210 in RyR1 has been found to interact with the CaMBD and regulate the function of the channel [205,206].

In 3D structural studies, CaM was found to bind within a cleft that separates the "handle" and "clamp" regions in the RyR cytoplasmic assembly [107,207-209]. Till now, cryo-EM mapping of CaM binding sites has only been done for apoCaM-RyR2, but not for Ca^{2+}-CaM-RyR2 [209]. Apo-CaM was localized to the gap between subdomain 3 and 7 in

RyR2, which is different from the apo-CaM binding site in RyR1. The 3D structures of RyR1 with and without added CaM suggested that the Ca^{2+}-CaM binding site is located in subdomain 3 and the apo-CaM binding site is located at the outer surface of subdomain 3, just above the binding site for Ca^{2+}-CaM [107,207,208]. The centers of mass of apo-CaM and Ca^{2+}-CaM were separated by 33 Å in the structure of RyR1 [208]. Recent FRET-based mapping has, however, challenged the idea that there are different binding locations on RyR1 for Ca^{2+}-CaM and apo-CaM, and suggested a co-localization of Ca^{2+}-CaM and apo-CaM, since the distance between FKBP and CaM is almost the same in the presence or absence of Ca^{2+} [210].

1.2.3.6 FKBP12.6

FKBPs belong to a family of highly conserved proteins called immunophilins that bind immunosuppressive drugs such as FK506 and rapamycin. FKBPs are named according to their molecular mass (e.g. FKBP12, FKBP12.6, FKBP13 and FKBP25). FKBP12.6 is a 12.6 kDa protein that shares 85% sequence identity with FKBP12, which has only 18 residues different from FKBP 12.6. FKBP12 and FKBP12.6 physically interact with all three isoforms of RyR but show different expression levels and binding affinity in different tissues. FKBP 12 is the predominant form bound to RyR1 in skeletal muscle. In cardiac muscle, although the concentration of FKBP12 is higher compared with that of FKBP12.6, FKBP12.6 plays a major role in regulating RyR2 function due to its high binding affinity [211].

The functional role of FKBP12.6 in RyR2 regulation has been a hot subject of research in recent years, though some controversies remain. In early studies, several groups reported that dissociation of FKBP12.6 from RyR2 by immunosuppressants

(rapamycin or FK506) activated RyR2 and induced subconductance states at the single channel level [212-214]. In cardiomyocytes, FK506 was reported to increase Ca^{2+} spark frequency and Ca^{2+} transients [179,213-215]. Marks and coworkers further proposed that impaired interaction between RyR2 and FKBP12.6 is a major mechanism underlying cardiac dysfunction in heart failure. In their model, hyperphosphorylation of RyR2 by PKA at a single residue Ser-2809 induces dissociation of FKBP12.6, which increases the P_o of the channel and causes long-lasting subconductance states. Increased RyR2 activity is believed to cause diastolic SR Ca^{2+} leak and triggered arrhythmias. K201(JTV519), an experimental cardioprotective and anti-arrhythmic drug, was found to stabilize the interaction between FKBP12.6 and RyR2, and thus prevent the development of arrhythmias [174,187].

However, several other groups have challenged the hyperphosphorylation-hypothesis in heart failure. In single channel studies, removal of FKBP12.6 was found to have no effect on RyR2 activity [175,216] and no subconductance was observed in RyR2 channels isolated from FKBP12.6 knockout mice [217]. Using Western blotting analysis, Xiao et al. found that PKA phosphorylation at Ser-2808 in mouse RyR2 (corresponding to Ser-2809 in rabbit RyR2) did not dissociate FKBP12.6 [178]. Using fluorescently-labeled FKBP12.6/12, Guo et al. directly measured in situ binding of FKBP12.6/12 to RyR2 in rat and mouse ventricular myocytes, and found that PKA phosphorylation did not alter the binding kinetics or affinity of FKBP12.6/12 [179]. Furthermore, no significant changes in the level of RyR2 phosphorylation at Ser-2808 or of binding of FKBP12.6 were detected in humans and canine heart failure models. Instead, Jiang et al. found a significant decrease in the expression level of SERCA2a in failing hearts [176,178]. In

addition, the inhibitory action of K201 on spontaneous Ca^{2+} release was found to be independent of FKBP12.6 [218]. This large array of evidence indicates that removal of FKBP12.6 does not alter the conductance, activation of the RyR2 channel and the susceptibility to ventricular arrhythmias, and that RyR2 hyperphosphorylation by PKA does not disrupt FKBP12.6-RyR2 binding. The exact physiological role of FKBP12.6 in cardiac function remains to be defined.

Both FKBP12 and 12.6 bind to RyRs with a stoichiometry of four FKBPs per RyR homotetramer. A critical residue in RyR1 required for the binding of FKBP12 is Val-2461. Mutations of the Val2461 residue in RyR1 to Gly, Glu, or Ile greatly reduce the affinity of binding of FKBP12 to RyR1, but not the affinity for binding of FKBP12.6 [219]. In line with this finding, Bultynck et al. reported that the conserved residue Val-2322 located in the central domain of RyR3 (corresponding to Val-2461 in RyR1) was also responsible for the interaction of RyR3 with FKBP12 [220]. It is likely that the equivalent residue in RyR2 (Ile-2427) also plays a similar role. Although studies by Marx et al. supported this hypothesis [174], several other groups challenged the importance of Ile-2427 in FKBP12.6 binding to RyR2. Masumiya et al. found that none of the mutations of residue Ile-2427 abolished FKBP12.6 binding. Instead, it was suggested that FKBP 12.6 binds to amino acid residues in the N-terminal region of RyR2, between residues 305–1937 which includes the DR3 region [221]. Zhang et al. further demonstrated that the FKBP12.6 binding site in the 3D structure of RyR is close to the DR3 region, and that a region including residues 1815–1855, upstream of the DR3 region, is essential for FKBP12.6 binding [123]. Further, Zissimopoulos and Lai suggested that the C-terminal region, which encompasses the transmembrane domain of the channel, interacts with

FKBP12.6 [222,223]. These studies indicate that multiple domains from different regions of the channel may contribute to the formation of the FKBP12.6 binding site. The location of FKBP binding site in the 3D structure of RyR lies between subdomains 3, 5, and 9 based on 3D reconstruction and FRET studies [207,224-227]. Interestingly, FKBP12 binding site and CaM binding site are found only 9 nm apart on the opposite sides of subdomain 3 [207].

1.2.3.7 Pharmological ligands

Besides a wide array of physiological channel modulators, RyR is also regulated by various pharmacological ligands, such as ryanodine, caffeine and 4-CmC.

1.2.3.7.1 Ryanodine

Ryanodine is a natural poisonous alkaloid found in the South American plant *Ryania speciosa,* which was originally used as an insecticide. The RyR derives its name from this specific, high-affinity compound, which made possible the initial purification of the RyR from skeletal and cardiac SR [2].

Equilibrium binding experiments suggested that up to four ryanodine molecules are able to bind to a RyR tetramer with varied binding affinities [228,229]. The binding of ryanodine is slow and irreversible. It is commonly believed that ryanodine at nM to hundred μM concentrations "locks" the channel in an open subconductance state by binding to its high affinity site. At higher concentrations (0.3~2 mM), ryanodine inhibits the channel by binding to its low affinity site [228,230,231].

In vitro high-affinity ryanodine binding is influenced by temperature, pH, ion concentrations, and other RyR modulators. A number of ligands known to open the channel and stimulate Ca^{2+} release increase ryanodine binding to the channel. Among

these known ligands, Ca^{2+} is able to increase both the binding affinity and the apparent maximum binding capacity (B_{max}) of ryanodine to RyR. Generally, the binding of ryanodine is strictly Ca^{2+} dependent. Caffeine was also found to facilitate ryanodine binding to skeletal and cardiac RyRs. On the other hand, ligands known to close the channel and inhibit Ca^{2+} release, such as micromolar ruthenium red and millimolar Mg^{2+}, inhibit ryanodine binding to the channel [232]. Thus, it becomes apparent that ryanodine binds preferentially to the open state of the channel and it can be used as a conformational probe to study the gating of RyR.

Biochemical and functional studies have localized the ryanodine binding sites to the C-terminal region of RyR, which forms the channel pore [233,234]. Mutations in the conserved pore-forming motif GVRAGGGIGD abolished or markedly reduced high affinity [^{3}H]ryanodine binding to RyR, suggesting that this region is essential for ryanodine binding[110,111,113,235]. In addition, mutations in the TM10 region of RyR2 also diminished [^{3}H]ryanodine binding. Among these mutations, a single point mutation Q4863A, dramatically altered the kinetics and affinity of ryanodine interaction with RyR2 channels without affecting the response of the channel to other ligands, such as caffeine, ATP and Mg^{2+}, indicating that the TM10 sequence and in particular the Q4863 residue constitute an important determinant of ryanodine interaction [236].

1.2.3.7.2 Caffeine and other methylxanthines

The methylxanthine compound, caffeine, is a nonselective adenosine receptor antagonist that has long been used as a pharmacological agonist of RyR-mediated Ca^{2+} release. Caffeine has also been used in the clinical diagnosis for the skeletal muscle disorder malignant hyperthermia (MH) [237]. Other methylxanthine compounds,

aminophylline and theophylline, have been used clinically for the treatment of pulmonary diseases, but their use was limited largely due to their pro-arrhythmic properties [238-240].

Caffeine and other methylxanthines activate both RyR1 and RyR2, though RyR2 displays higher sensitivity [241,242]. The mechanism of caffeine activation on RyR remains incompletely defined. Caffeine is generally thought to sensitize the RyR2 channel to activation by cytosolic Ca^{2+}, leading to an increase in the P_o of the channel [242,243]. However, the unique feature of caffeine-induced Ca^{2+} release termed "quantal" Ca^{2+} release indicates a mechanism of luminal/store Ca^{2+}-dependent regulation. That is multiple additions of caffeine at submaximal concentrations can each induce a partial and transient Ca^{2+} release from intracellular Ca^{2+} stores in cells expressing RyRs or from SR vesicles. When the luminal Ca^{2+} level is below a threshold level, caffeine is no longer able to induce Ca^{2+} release despite its continued presence [244,245]. Recent studies have confirmed that single RyR2 channels are insensitive to caffeine in the absence of luminal Ca^{2+} [246]. Interestingly, caffeine, aminophylline and theophylline were all demonstrated to potentiate luminal Ca^{2+} activation of RyR2 and increase the propensity for spontaneous Ca^{2+} release, mimicking the effects of disease-linked RyR2 mutations [165]. These findings suggest that luminal Ca^{2+} plays a pivotal role in caffeine dependent RyR2 activation. It is most likely that both cytosolic and luminal Ca^{2+} modulate caffeine-dependent RyR2 activation [247], though luminal Ca^{2+} is probably more effective [165].

The exact binding site for caffeine in RyR has not been identified, largely because mutations throughout the channel sequence cause alterations in caffeine sensitivity. All MH and central core disease (CCD) mutations in the N-terminal and central regions of RyR1 displayed increased caffeine sensitivity [248,249]. CPVT mutations in the N-terminal

[250,251] and C-terminal regions [252] of RyR2 also showed altered sensitivity to caffeine. Caffeine activation of RyR was affected by mutations throughout the amino acid sequence, suggesting that caffeine activation may involve multiple regions of RyR.

1.2.3.7.3 4-CmC

The phenol-based compound, 4-CmC, is a strong activator of both skeletal and cardiac RyR isoforms [253,254] but is less effective in stimulating RyR3 [255]. 4-CmC activates RyR1 with an EC_{50} value of 50 to 200μM, which is about 20 times more potent when compared with caffeine. [253,256]. Sensitivity to activation by 4-CmC is increased for RyR1 mutations associated with the skeletal muscle disorder MH. This finding led to the clinical use of 4-CmC as a tool to distinguish between MH susceptible and normal muscle [257-260]. At the single channel level, the sensitivity to 4-CmC was found to be higher when applied to the luminal side of the channel, suggesting that the binding site of 4-CmC is different from caffeine, which was normally applied to the cytosolic side of the channel [256]. At the cellular level, 4-CmC can produce a contractile response in skinned and intact skeletal muscle [256,261,262]. Since 4-CmC activation of RyR3 is much weaker, RyR1-RyR3 chimeric proteins were generated to identify the 4-CmC activation site in RyR1. The activation site of 4-CmC was localized to residues 4007-4180 in the RyR1 primary sequence [263] and two amino acids (Gln4020 and Lys4021) in this region were identified to be essential for 4-CmC activation [264].

Although not as widely used as caffeine, 4-CmC is also a common pharmacological agonist of RyR2. It is capable of generating caffeine-like responses in saponin-skinned cardiac muscles at the concentrations of 0.1 to 2 mM, but not in intact fibers. Choisy et al. claimed that the failure of 4-CmC to induce contraction in intact cardiac muscle is

probably due to the side effect of 4-CmC on cardiac sarcolemmal membrane-associated proteins, especially the Ca^{2+} extruders, PMCA and NCX. The effects of 4-CmC and caffeine on SR Ca^{2+} release are independent from each other in cardiac muscle fibers, suggesting that the binding site for 4-CmC in RyR2 is different from that for caffeine [254]. To date, the specific 4CmC activation site in RyR2 has not been identified.

1.3 Cardiac ryanodine receptor and cardiomyopathies

1.3.1 RyR2 mutations and cardiac disease

Giving the significant role of RyR2 in cardiac function, it is no surprise that dysregulation of RyR2 can contribute to various cardiac abnormalities. Naturally occurring mutations in RyR2 have been linked to at least two autosomal dominant forms of cardiac arrhythmias, namely CPVT and arrhythmogenic right ventricular dysplasia type 2 (ARVD2) [265-268]. More recently, mutations in RyR2 have also been associated with dilated cardiomyopathy (DCM) [269-271] and hypertrophic cardiomyopathy (HCM) [270,272], in addition to cardiac arrhythmias.

CPVT is an arrhythmogenic cardiac disorder, manifesting as syncopal events and sudden cardiac death, usually in response to intensive exercise or emotional stress. Dominant mutations in RyR2 could lead to the genesis of CPVT. The mechanism of CPVT caused by RyR2 mutations has been uncovered by recent studies [273,274]. Under physiological conditions, initiation of SR Ca^{2+} release is controlled by membrane depolarization via the mechanism of CICR. In the absence of regular membrane depolarizations, spontaneous Ca^{2+} waves or Ca^{2+} oscillations can occur. These spontaneous Ca^{2+} events have been found to be highly dependent on SR Ca^{2+} store and

thus termed SOICR. A number of conditions, including β-adrenergic stimulation, digitalis intoxication, elevated extracellular Ca^{2+}, and fast pacing can lead to SR Ca^{2+} overload and subsequently SOICR in cardiac cells. SOICR may activate NCX to generate a transient inward current. This inward current is capable of depolarizing the surface membrane after the action potential is ended, thus producing delayed afterdepolarizations (DADs), which can lead to triggered arrhythmias. A common defect of CPVT RyR2 mutations is an enhanced sensitivity of the channel to luminal Ca^{2+} activation and a reduced threshold for SOICR. A reduced SOICR threshold would increase the propensity for DADs and thus triggered arrhythmias [151,250,251,275-278].

Interestingly, some of these CPVT mutations cause cardiac arrhythmias without structural modifications of the heart, while other CPVT mutations lead to both cardiac arrhythmias and cardiomyopathies. The mechanism by which RyR2 mutations are able to contribute to the progression of cardiomyopathies is still a mystery.

To date, there are eleven RyR2 mutations that have been linked to three distinct types of cardiomyopathies in addition to cardiac arrhythmias. These include 2 DCM mutations (exon 3 deletion and R3570W) [269-271], 7 ARVD2 mutations (A77V [279], R176Q/T2504M (double mutations) [280,281], R420W [281-283], L433P [280], G1885E/G1886S (compound heterozygous) [284], N2386I [280], and Y2392C[282]) and 2 HCM mutations (T1107M, and G2367R) [270,272]. It is particularly interesting that a large portion of these mutations is located at the N-terminal region of RyR2. Exon 3 deletion is an in-frame deletion of 35 amino acids in the N-terminal region of RyR2. This large genomic deletion in RyR2 elicits extended clinical phenotypes, including progressive atrioventricular node block, sinoatrial node dysfunction, atrial fibrillation and DCM

combined with CPVT. Besides, a number of point mutations including A77V, R176Q/T2504M (double mutations), R420W and L433P in the N-terminal region are found to be associated with ARVD2. Missense mutations of RyR2 in the N-terminal region are also linked to HCM. Although patients with novel missense mutation T1107M only show moderate hypertrophy, the disease prevalence with this mutation is high in the pedigree (100%), while this mutation was completely absent in the other 299 probands or 200 controls [270,272]. These findings provide new insights into the pathogenic mechanism whereby mutations in RyR2 can lead to hypertrophic or dilated cardiomyopathies. Further functional studies need to be performed to resolve the intriguing question of why deletion of exon 3 and other missense mutations lead to DCM, ARVD, or HCM in addition to CPVT.

1.3.2 General aspects of cardiomyopathies

Numerous conditions, either primary or acquired from chronic ischemia, hypertension or diabetes, can lead to the muscle disorder, known as cardiomyopathy [285]. As a major cause of heart failure, cardiomyopathy is always associated with abnormalities in cardiac wall thickness, chamber size, contraction, relaxation, conduction, or rhythm. Primary cardiomyopathies are due to the intrinsic weakness in the muscle of the heart rather than identifiable external causes. Based on pathological phenotypes, the primary cardiomyopathies were traditionally classified as HCM, DCM and restrictive cardiomyopathy. New clinical entities such as ARVD and other unclassified cardiomyopathies have also been defined in recent years [286].

In HCM the wall of the heart is thickened due to enlarged cardiomyocytes and/or increased myocardial interstitial fibrosis. These anatomic abnormalities can obstruct

blood flow and prevent the heart from pumping effectively [287]. DCM is characterized by dilation of the heart, especially the left ventricle, which leads to depressed myocardial contractility and impaired systolic pumping function [288]. Restrictive cardiomyopathy is a less common type of cardiomyopathy, in which the ventricle size is normal (nondilated and nonhypertrophied). However, in this scenario, the diastolic function of the heart is affected due to the increased stiffness of the ventricular tissue, while systolic function is still normal in most cases. ARVD is characterized by a substitution of the right ventricular myocardium with progressive fibrofatty tissue, which results from apoptosis, inflammation of cardiomyocytes or myocardial dystrophy. ARVD may eventually lead to congestive heart failure that mimics DCM [289].

1.3.3 Sarcomeric proteins and cardiomyopathies

Cardiomyopathies with distinct clinical phenotypes, including HCM and DCM are generally associated with mutations in various sarcomeric proteins. To date, hundreds of mutations in more than 20 genes that encode protein constituents of the sarcomere have been identified in HCM [290]. A missense mutation in the β-myosin heavy chain gene is the first identified gene linked to HCM [291]. Mutations in genes encoding the β-myosin heavy chain, myosin-binding protein C, TnI and TnT account for most reported cases. Mutations have also been found in other genes encoding sarcomeres or myofilament related proteins, such as titin, actin and essential myosin light chain. On the other hand, the genetics of DCM has been under intensive investigation lately. Inherited DCM is commonly autosomal dominant, but also presents autosomal recessive, X-linked, or mitochondrial inheritant patterns [285]. Of the 20 reported defective genes responsible for DCM, genes encoding sarcomeric proteins such as β-myosin heavy chain, Tn, and Tm

are the majority [288].

Interestingly, most of the mutations linked to HCM increase myofilament Ca^{2+} sensitivity [58,67], whereas most of the mutations in sarcomeric proteins that are linked to DCM decrease the Ca^{2+} sensitivity of myofilaments [292,293]. Numerous HCM mutations in Tn and several in Tm have been found to result in an increase in the Ca^{2+} sensitivity of force development *in vitro* [294]. Several transgenic mice harboring TnT HCM mutations (such as TnT-I79N [66,295,296], TnT-R92Q [297] and TnT-F110I [298]) or TnI HCM mutation (TnI-R146G [299,300]) have been generated. In all of these cases, the Ca^{2+} sensitivity of force development in these transgenic mice is increased compared with wild type mice in *in vitro* studies. TnT, TnC and Tm mutations in DCM are also related to defective Ca^{2+} sensitivity of the myofilament. In contrast to the mutations in HCM, all of these mutations show decreased Ca^{2+} sensitivity of contractile regulation. Mouse models expressing deletion of K210 [293] and missense mutation R141W [301] in TnT have been created. As expected, cardiac muscle fibers of these mutant mice showed significantly lower Ca^{2+} sensitivity in force generation than those of wild type mice.

1.3.4 SR Ca^{2+} handling and cardiomyopathies

Aside from sarcomeric protein malfunction, alterations in SR Ca^{2+} handling have also been implicated in cardiomyopathies.

SR Ca^{2+} has been recognized as an important signal driving the pathogenesis of HCM. In mice bearing an Arg403Gln missense mutation in the α cardiac myosin heavy chain, SR Ca^{2+} content and the expression levels of CASQ2 and RyR2 are reduced prior to changes in cardiac histology or morphology [65,302]. In another HCM mouse model, SR Ca^{2+} uptake was found to be suppressed due to reduced SERCA2a expression and

hypophosphorylation of PLB [303]. Lowered SR Ca^{2+} levels and altered expression of SR Ca^{2+} handling proteins seem to be two of the earliest detectable manifestations in these HCM models, which indicates that malfunction of SR Ca^{2+} homeostasis is closely associated with HCM.

In DCM, the important role of SR Ca^{2+} handling became evident after the discovery of direct correlation of PLB and DCM. PLB is a small regulatory protein of the SERCA2a pump. Phosphorylation of PLB relieves the inhibition of SERCA2a and consequently accelerates SR Ca^{2+} uptake and cardiac relaxation as introduced in section 1.1.4.2. Interestingly, impaired PLB function has been recognized as a cause for cardiomyopathies. A missense mutation (R9C) in PLB has been linked to inherited human DCM with refractory congestive heart failure. Transgenic mice carrying this mutation recapitulated human cardiomyopathy and heart failure with premature death. Further cellular and biochemical studies revealed that the R9C mutation significantly reduced the phosphorylation of PLB by PKA and thus enhanced SERCA inhibition. Increased SERCA inhibition, which slowed down SR Ca^{2+} re-uptake and prolonged the decay of cytosolic Ca^{2+} transients in myocytes, may eventually result in the development of DCM [304]. On the other hand, cardiac contractility and the DCM phenotype can be rescued by enhanced SR Ca^{2+} re-uptake. Mice with a deficiency in a cytoskeletal protein, the muscle-specific LIM protein (MLP), developed DCM after birth. Ablation of PLB, which up-regulated SERCA activity, rescued a wide spectrum of morphological and ultrastructural defects including chamber dilation in the MLP-deficient mice, indicating that SR Ca^{2+} handling is an important therapeutic target for preventing the progression of DCM [305].

1.3.5 Fundamental mechanism of cardiomyopathies

The fact that sarcomeric protein mutations, PLB mutation and RyR2 mutations all result in clinical phenotypes of cardiomyopathies is particularly interesting. Myofilaments represent a major pool of Ca^{2+} buffering in the cytosol. RyR2 and PLB are the major players in SR Ca^{2+} handling. The cross-talk between the cytosolic Ca^{2+} and SR Ca^{2+} shapes the Ca^{2+} environment in cardiomyocytes, a critical factor in the development of cardiomyopathies. Thus, it is possible that mutations in these three types of Ca^{2+} handling proteins share the same mechanism of genesis of cardiomyopathy.

Since myofilaments play a pivotal role in cytosolic Ca^{2+} buffering, changes in myofilament Ca^{2+} sensitivity will alter the amplitude or decay of cytosolic Ca^{2+} transients [67]. It is believed that increased myofilament Ca^{2+} sensitivity will reduce the amplitude and slow the decay of the cytosolic Ca^{2+} transients, whereas decreased myofilament Ca^{2+} sensitivity will increase the amplitude and hasten the decay of the transients [65-69]. Impaired cytosolic Ca^{2+} transients that arise as a result of altered myofilament Ca^{2+} sensitivity have been proposed to trigger subsequent cardiac remodeling leading to cardiomyopathies [306-309].

Similar to changes caused by mutations in sarcomeric proteins, altering the termination of SR Ca^{2+} release as a result of RyR2 mutations or altering Ca^{2+} re-uptake as a consequence of PLB mutations would also result in changes in cytosolic Ca^{2+} transients. Delayed termination or weakened Ca^{2+} re-uptake would lead to increased Ca^{2+} transients, whereas premature termination or enhanced Ca^{2+} re-uptake would result in decreased Ca^{2+} transients. While the influences of cardiomyopathy-linked sarcomeric protein mutations and PLB mutations on cytosolic Ca^{2+} transients are clear, the impact of RyR2

mutations on SR Ca^{2+} release termination have not yet been determined.

Cytosolic Ca^{2+} transients are capable of affecting the formation of Ca^{2+}-CaM complex. Ca^{2+}-CaM dependent signaling pathways such as the calcineurin/NFAT pathway [306,307], HDAC/MEF2 pathway [308] and apoptotic signaling [309], have been suggested to be critical in the development of cardiomyopathies, including HCM (Fig. 4) and DCM.

Calcineurin is a Ca^{2+}-CaM-dependent phosphatase. In contrast to CaMKII, which responds to high and transient Ca^{2+} oscillations, calcineurin has a relatively higher CaM binding affinity and can be activated by low but sustained Ca^{2+} plateaus. This indicates that Ca^{2+}-CaM can work as a key signaling molecule acting on substrates with different affinities on different time scales. Moderate elevated levels of Ca^{2+}-CaM can activate calcineurin, which dephosphorylates nuclear factor of activated T-cells (NFAT) [306]. Consequently, dephosphorylated NFAT is imported into the nucleus where it works cooperatively with cardiac-restricted zinc finger-containing transcription factor-4 (GATA4) to activate genes responsible for cardiac hypertrophy [310].

The formation of Ca^{2+}-CaM complex also activates CaMKIIδ_B. Activation of CaMKIIδ_B in the nucleus is able to phosphorylate and dissociate histone deacetylases (HDAC) from transcription factors including myocyte enhancer factor-2 (MEF2) [308]. Activation of MEF2 has been suggested to act as a common end point for hypertrophic signaling pathways in the myocardium [311,312]. When the calcineurin/NFAT pathway synergizes with HDAC/MEF2 pathway, profound hypertrophy can be evoked [313].

On the other side, activation of another form of CaMKII, CaMKIIδ_C, by cytosolic Ca^{2+}-CaM can induce a series of downstream events, including phosphorylation of

Fig. 4 Ca^{2+}-dependent transcriptional pathways that reprogram cardiac gene expressions leading to hypertrophy

Increased intracellular Ca^{2+} promotes the formation of Ca^{2+}-CaM, which activates calcineurin or CaMKII. Activation of CaMKII can phosphorylate and disssociate HDAC from transcription factors including MEF2 in the nucleus. Activation of the phosphatase calcineurin can dephosphorylate NFAT, which works cooperatively with the transcription factor GATA4. Activation of these transcriptional pathways eventually leads to the expression of hypertrophic genes. (HDAC, histone deacetylases; NFAT, nuclear factor of activated T-cells; MEF-2, myocyte enhancer factor-2; GATA4, zinc finger-containing transcription factor-4).

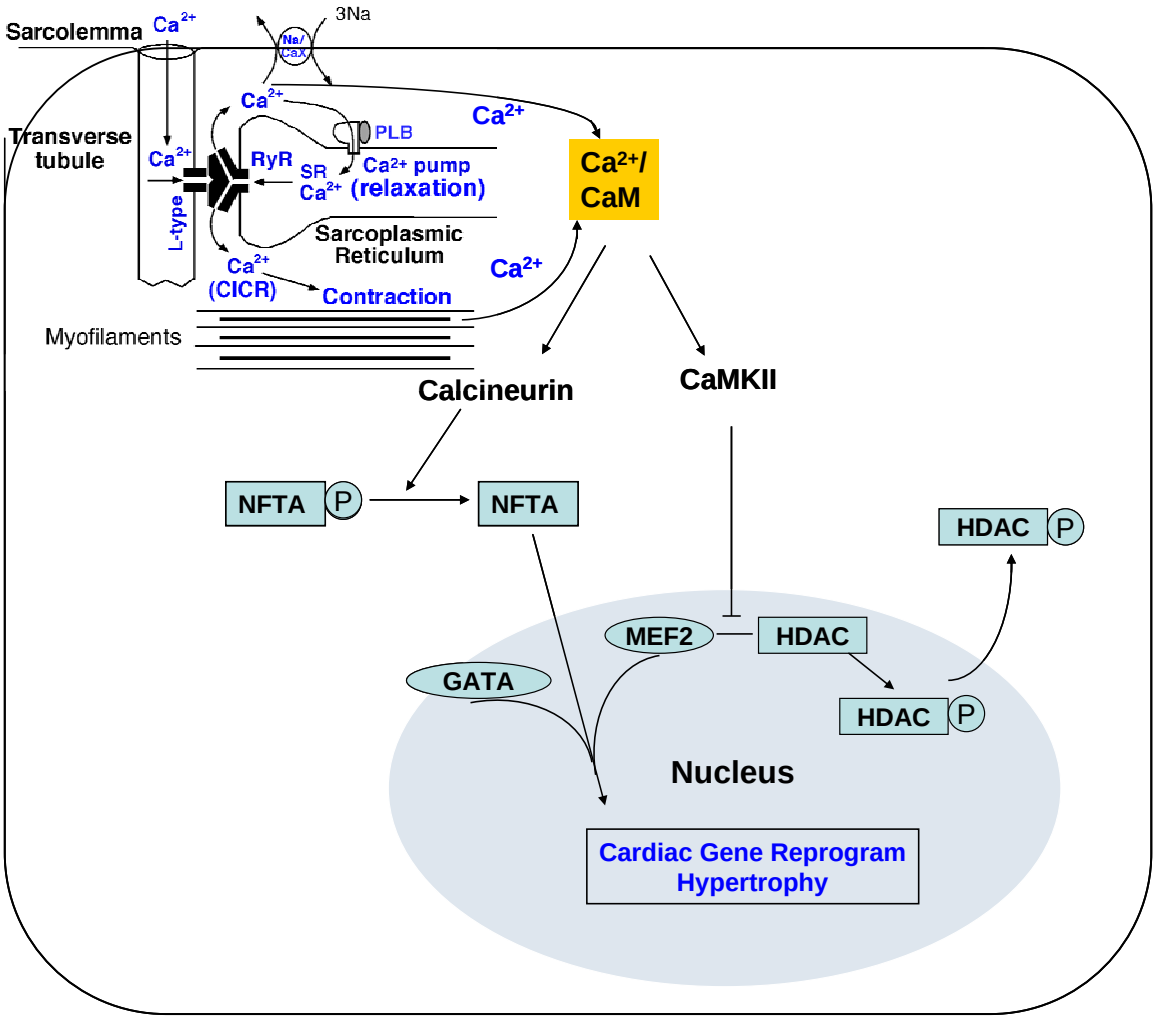
Sarcolemma
Ca2+
3Na
Na/Ca X
Transverse tubule
Ca2+
L-type
Ca2+
RyR
SR
Ca2+
PLB
Ca2+ pump
(relaxation)
Sarcoplasmic Reticulum
Ca2+
(CICR)
Contraction
Myofilaments
Ca2+
Ca2+
Ca2+/ CaM
Calcineurin
CaMKII
NFTA
P
NFTA
HDAC
P
MEF2
HDAC
GATA
HDAC
P
Nucleus
Cardiac Gene Reprogram
Hypertrophy

proteins involved in apoptotic pathways. Initiation of apoptosis will result in the loss of cardiomyocytes, thus possibly contributing to DCM [308]. Toko et al. found that p53, a tumor suppressor protein, was crucial in the induction of cardiomyocyte apoptosis in a DCM mouse model [309]. However, detailed signaling cascades involved in this process are still unknown.

It is worth mentioning that the mechanisms through which altered cytosolic Ca^{2+} transient induces remodelling of the heart and eventually results in distinct phenotypes of HCM and DCM are complex due to the presence of various signaling pathways operated in cardiomyocytes. Nevertheless, the role of cytosolic Ca^{2+} transients in the development of cardiomyopathies warrants further investigations.

1.4 Research objective and specific aims

The **overall objective** of this study is to understand the molecular basis and regulation of Ca^{2+} release activation and termination as well as the role of RyR2 in the pathogenesis of cardiac arrhythmias and cardiomyopathies. The **central hypotheses** are that (i) the activation and termination of Ca^{2+} release are controlled by RyR2 and regulated by RyR2 modulators; and (ii) altered Ca^{2+} release by RyR2 mutations can lead to cardiomyopathies.

1.4.1 Defining the molecular determinants of Ca^{2+} release activation and termination in RyR2

Since CICR is a re-enforcing process, a mechanism accounting for SR Ca^{2+} release termination is needed. RyR2 has been commonly accepted as the governor of Ca^{2+} release activation, however, little is known about its role in Ca^{2+} release termination.

Here we aim to investigate the structure-function relationship of RyR2 in Ca^{2+} release termination by studying mutations in regions potentially involved in Ca^{2+} release termination. Recent studies have suggested that the regulation of RyR2 gating by luminal Ca^{2+} is responsible for Ca^{2+} release termination and a luminal Ca^{2+} sensor formed by residues in the pore-forming region of RyR2 has been identified. In addition, the N-terminal region of the channel undergoes large conformational changes during channel gating and thus may be involved in Ca^{2+} release activation or termination. Therefore, a number of mutations in the pore-forming region and N-terminal region will be constructed and expressed in HEK293 cell lines. Using a FRET based luminal Ca^{2+} sensing probe D1ER, luminal Ca^{2+} dynamics reflecting ER Ca^{2+} release activation and termination will be monitored in cells expressing these mutants.

1.4.2 Determining the roles of RyR2 modulators in Ca^{2+} release activation and termination

RyR2 has been shown to interact with a large array of modulators, ranging from small proteins to physiological ions. An increasing number of studies have demonstrated that these modulators are capable of altering the channel function. However, it is unclear whether these RyR2-interacting proteins affect Ca^{2+} release primarily by modulating the activation or the termination aspect of Ca^{2+} release. To this end, a number of experiments are designed to determine the roles of several RyR2 modulators in Ca^{2+} release activation and termination. The RyR2 regulatory proteins, CaM, FKBP12.6 and CaMKII, will be overexpressed in HEK293 cells and their impact on Ca^{2+} release activation and termination will be characterized. The properties of some regulatory protein-binding deficient RyR2 mutations will also be studied. Moreover, permeabilized cells will be

used for directly assessing the effect of cytosolic Ca^{2+} on Ca^{2+} release activation and termination.

1.4.3 Studying the correlation between ligand-regulated channel function and ligand-dependent conformational changes

Physiological or pharmacological ligands of RyR are able to activate the channel and induce global conformational changes in the 3D structure of the channel. However, it is not known whether these structurally diverse ligands induce the same or different conformational changes. To answer this question, we plan to construct a FRET-based probe by inserting a CFP and a YFP into RyR2 after specific residues that have previously been mapped to the clamp region of RyR2. This clamp region consists of several key structural domains that are crucial for channel regulation and gating. The extents of conformational changes in the clamp region and the extents of Ca^{2+} release upon binding of various ligands will be monitored and compared.

1.4.4 Assessing the impact of cardiomyopathy-linked RyR2 mutations on Ca^{2+} release

Naturally occurring mutations in RyR2 have been linked not only to cardiac arrhythmias and sudden death, but also to cardiomyopathies, such as HCM and DCM. Why some CPVT mutations are also associated with cardiomyopathies is unknown. To study the mechanism underlying cardiomyopathies, the impact of RyR2 mutations associated with cardiomyopathies on Ca^{2+} release activation and termination will be studied using single cell luminal Ca^{2+} imaging. In addition, the properties of CPVT-only mutations will also be characterized to understand the important question of why some RyR2 mutations cause cardiac arrhythmias only, whereas other mutations lead to both cardiac arrhythmias and cardiomyopathies.

CHAPTER II: EXPERIMENTAL PROCEDURES

2.1 Site-directed mutagenesis

2.1.1 Construction of RyR2 deletions and point mutations

The RyR2 deletion mutant Del-305 (deletion of the first 305 N-terminal residues) was constructed as follows. A NheI-AflII adaptor was generated by annealing two primers: 5'-CTA GCA GCG CGG AGC CAT GGC TGA TTA C-3' (forward) and 5'-TTA AGT AAT CAG CCA TGG CTC CGC GCT G-3' (reverse). The full-length mouse RyR2 cDNA was digested with NheI and AflII. The NheI (vector)-AflII (915) fragment was discarded, and the remaining fragment was ligated with the NheI-AflII adaptor to form the N-terminal deletion mutant Del-D305.

The RyR2 deletion mutant Del-Exon-3 and Del-3583-3603 as well as the RyR2 point mutations A77V, R176Q/T2504M, R420W, L433P, A1107M, I4862A, G4864A, D4868A, A4869G, F4870A, G4871R, E4872A, Q4876A, V4880A, K4881A, E4882A, D4896A, W3587A, L3591D, F3603A and W3587A/L3591D/F3603A were constructed using the polymerase chain reaction (PCR) mediated overlap extension method [314].

Briefly, a fragment containing the deletion or mutation was produced by performing PCR twice and then subcloned into the full-length mouse RyR2 WT using specific restriction enzymes. In each case, PCRs were carried out with four designed primers: the outer forward (OF) primer, the inner reverse (IR) primer, the inner forward (IF) primer, and the outer reverse (OR) primer. The inner primers contain the mutated nucleotides and the outer primers include restriction digestion sites.

In the first step, two fragments of the RyR2 cDNA sequence encompassing the point mutation were amplified by PCR using two pairs of the primers (OF and IR; IF and OR). The 50 μl first-step PCR system contained 38 μl H_2O, 400 μM dATP, dCTP, dGTP, and

dTTP (dNTP) (Invitrogen), 0.5 unit of Pfu DNA polymerase (Pfu) (Stratagene), 5 µl 10 x Pfu buffer (Stratagene), 0.5 mM forward primer, 0.5 mM reverse primer, and 1 µl (100-200 ng) of template DNA (RyR2 WT plasmid). The DNA was denatured for 4 min at 94 °C followed by 26-30 cycles of amplification. Each cycle consisted of 45 seconds denaturation at 94 °C, 1 min annealing at 56 °C, and 1-3 min extension at 72 °C. An additional elongation step for 5 min at 72 °C was performed after the final cycle. The annealing temperature and the number of cycles for each pair of primers in PCR were determined empirically. The first PCR products were then subjected to DNA electrophoresis and purified using Qiaex® beads (Qiagen).

In the second step, these two purified fragments were then denatured and annealed in the presence of the two out primers in a subsequent PCR reaction. The 100 µl second PCR system contained 57 µl H_2O, 400 µM dNTP, 1 unit of cloned Pfu, 10 µl 10 x Pfu buffer, 0.5 mM OF primer, 0.5 mM OR primer, 5 µl of each paired first-PCR product. Reaction conditions for the second PCR were the same as the first PCR except that the extension step at 72 °C was longer. The second PCR generated fragments multiplying the RyR cDNA sequence between the two outer primers with the desired mutation. The positions of the two outer primers on the cDNA sequence were chosen so that there was one unique restriction endonuclease site present at each end of the fragment. The products of the second PCR, the amplified full fragments containing the desired mutated nucleotides, were then purified using the QIAquick PCR purification kit (Qiagen).

Using restriction enzyme, each of the constructs was finally made by subcloning the purified second PCR product containing the specific mutation to the full-length WT

RyR2 in pcDNA3 vector for transient transfection or pcDNA5 vector for generation of cell lines.

In several cases, additional steps are required to generate the full-length RyR2 DNA. For example, double mutation R176Q/T2504M was made by subcloning R176Q into the full-length RyR2-T2504M cDNA using NheI and ClaI. A fragment containing the point mutation A1107M was generated by PCR and subcloned into RyR2 WT cDNA using ClaI (2350) and KpnI (3823, 7553). The missing KpnI (3823)-KpnI (7553) fragment was then ligated back to form a full length RyR2-A1107M construct. The fragment containing double mutation W3587A/L3591D was first made and subcloned to a RyR2-Del-(NheI-BsiwI) truncation in pBluescript vector. The fragment containing W3587A/L3591D/F3603A triple mutation was generated by PCR using F3603A inner primers and RyR2-W3587A/L3591D template. The fragment containing the triple mutation was then cloned to the full length RyR2 in pcDNA3 or PcDNA5 using NheI (vector) and BsiwI (8864).

All mutations and the sequence of the PCR-amplified region were confirmed by DNA sequencing analysis.

2.1.2 Construction of GFP-tagged RyR2 and CFP/YFP-dual labeled RyR2

GFP-tagged RyR2 constructs RyR2 $_{\text{D4365-GFP}}$, and RyR2 $_{\text{D4365-GFP/ Del-Exon-3}}$ was generated according to previously described procedures [122,315,316]. Briefly, the DNA encoding GFP flanked by glycine-rich linkers and an AscI site was obtained by PCR using the following primers: 5′-GGG CGC GCC GGT GGA GGT GGA AGT GGA GGT GGA GGT ACT ATG GTG AGC AAG GGC GAG GAG CTG-3′ and 5′-GGC GCG CCC ACC ACC TCC TCC AGA TCC TCC ACC ACC CTT GTA CAG CTC GTC CAT

GCC GAG-3′. The AscI site was introduced into RyR2 WT or Del-Exon-3 after Asp-4365 by overlap-extension PCR. A fragment containing GFP and the glycine-linkers was then subcloned into the full-length RyR2 wt or Del-Exon-3 via the AscI site.

$RyR2_{S2367\text{-}CFP}$ and $RyR2_{Y2801\text{-}YFP}$ cDNAs were constructed by replacing the GFP in previously made GFP-tagged RyR2 [124,126] with CFP or YFP via the AscI site. To generate the cDNA construct of $RyR2_{S2367\text{-}CFP/Y2801\text{-}YFP}$, the full-length RyR2 cDNA containing S2367-CFP in pcDNA3 was released by the NheI-NotI restriction digestion and subcloned to the pBluescript vector. A cDNA fragment containing Y2801-YFP was introduced into $RyR2_{S2367\text{-}CFP}$ via the SphI restriction sites to form the full-length RyR2 containing both S2367-CFP and Y2801-YFP. The full-length $RyR2_{S2367\text{-}CFP/Y2801\text{-}YFP}$ construct was then transferred from pBluescript to pcDNA3 or pcDNA5. To generate the 1–4770 COOH-terminal deletion mutant, the BsiWI (8864)-NotI (vector) fragment in the pcDNA3 plasmid was digested with HpaI and ligated with a linker containing a stop codon, 5′-CTAGCTAG-3′ [221]. The BsiWI (8864)-NotI (vector) fragment containing the inserted stop linker was then used to replace the corresponding fragment in the full-length $RyR2(wt)_{S2367\text{-}CFP/Y2801\text{-}YFP}$ cDNA to yield the $RyR2(1\text{-}4770)_{S2367\text{-}CFP/Y2801\text{-}YFP}$ construct. The sequences and the orientation of the inserted GFP, CFP or YFP cDNA were verified by DNA sequencing analysis.

2.1.3 Construction of CaM (1-4), CA-CaMKIIδ_C

Residues Asp 20, 56, 93, and 129 in bovine CaM gene were mutated to Ala to generate the CaM (1-4) construct using PCR mediated overlap extension method as described previously [317]. The constitutively active CaMKIIδ_C (CA-CaMKIIδ_C), T287D mutation was made using the same method with the wt CaMKIIδ_C as the template, which

was kindly provided by Dr. Andrew Braun from the Faculty of Medicine, University of Calgary. All mutations were confirmed by DNA sequencing analysis.

2.2 HEK293 cell culture and DNA transfection

To express the WT and mutant RyRs, a human embryonic kidney (HEK) 293 cell line was used. The HEK293 cell line has been extensively used as an expression system for the functional and biochemical study of ion channel proteins. It has also been used for the expression of RyRs. It is important to note that there is no detectable expression of RyR in HEK293 cells at either the protein or the functional levels. HEK293 cells were maintained in standard Dulbecco's modified eagle medium (DMEM) with 0.1 mM minimum Eagle's medium nonessential amino acids, 4 mM L-glutamine, 100 units of penicillin/ml, 100 g of streptomycin/ml, and 10% fetal calf serum at 37 °C in a 5% CO_2 atmosphere. The cells were grown to 95% confluency in a 75 cm^2 flask, split with phosphate buffered saline (PBS) (137 mM NaCl, 8 mM Na_2HPO_4, 1.5 mM KH_2PO_4, 2.7 mM KCl), and plated in 100 mm tissue culture dishes at ~10% confluence 18 h before transfection. A Ca^{2+}-phosphate precipitation protocol was employed for transfection. Briefly, 12 μg of DNA was diluted into a final volume of 500 μl of solution containing 248 mM $CaCl_2$. This solution was then added drop-wise to 500 μl of 2X HEPES buffer containing 274 mM NaCl, 1.8 mM Na_2HPO_4, and 50 mM HEPES, pH 7.04. The mixture was thoroughly mixed, incubated for 1 min at room temperature, and then added to the cells.

2.3 Caffeine-induced Ca^{2+} release measurements

Measurements of free cytosolic Ca^{2+} concentrations in the transfected HEK293 cells expressing RyR2 WT or mutants using the fluorescent Ca^{2+} indicator dye Fluo-3 AM were carried out as described follows. The cells grown for 18-20 hr after transfection were washed four times with PBS and incubated in Krebs-Ringer-Hepes (KRH) buffer without $MgCl_2$ and $CaCl_2$ (KRH buffer: 125 mM NaCl, 5 mM KCl, 1.2 mM KH_2PO_4, 6 mM glucose, 1.2 mM $MgCl_2$, 2 mM $CaCl_2$, and 25 mM Hepes, pH 7.4) at room temperature for 40 min and then at 37°C for 40 min. After being detached from culture dishes by pipetting, cells were collected by centrifugation at 1,000 rpm for 2 min in a Beckman TH-4 rotor. Cell pellets were washed twice with KRH buffer and loaded with 10 μM Fluo-3 AM in KRH buffer plus 0.1 mg/ml BSA and 250 μM sulfinpyrazone at room temperature for 60 min., followed by washing with KRH buffer three times and resuspended in 150 μl KRH buffer plus 0.1 mg/ml BSA and 250 μM sulfinpyrazone. The Fluo-3-loaded cells were added to 2 ml (final volume) KRH buffer and challenged with various concentrations of caffeine (0.025-5 mM) or ryanodine (100 μM) in a cuvette. Fluorescence intensity of Fluo-3 AM at 530 nm was measured in an SLM-Aminco series 2 luminescence spectrometer with 480 nm excitation at 25 °C (SLM Instruments, Urbana, IL).

2.4 Generation of stable, inducible HEK293 cell lines expressing RyR2 WT and mutants

Stable, inducible HEK293 cell lines expressing RyR2 WT or mutants were generated using the Flp-In T-REx Core Kit from Invitrogen. Flp-In T-REx-293 cells were

co-transfected with the inducible expression vector pcDNA5/FRT/TO containing the WT or mutant cDNAs and the pOG44 vector encoding the Flp recombinase in 1: 4 ratios (2 μg RyR cDNA and 8 μg pOG44 per dish) using the Ca^{2+} phosphate precipitation method. The transfected cells were washed with PBS 24 h after transfection followed by a change into fresh media for 24 h. The cells were then washed again with PBS, harvested, and plated onto new dishes. After the cells had attached (~4 h), the growth medium was replaced with a selection medium containing 200 μg/ml hygromycin B (Invitrogen). The selection medium was changed every 3-4 days until the desired number of cells was reached. The hygromycin-resistant cells were pooled, aliquoted, and stored at -80 °C. These positive cells are believed to be isogenic, because the integration of RyR2 cDNA is mediated by the Flp recombinase at a single FRT site.

2.5 Western blotting

HEK293 cell lines grown for 24 h after induction were washed with PBS plus 2.5 mM EDTA and harvested in the same solution by centrifugation for 8 min at 2000 rpm. The cells were then washed with PBS without EDTA and centrifuged again at 2000 rpm for 8 min. The PBS-washed cells were solubilized in a lysis buffer containing 25 mM Tris/50 mM Hepes (pH 7.4), 137 mM NaCl, 1% 3-[(3-cholamidopropyl)dimethylammonio]-1-propanesulfonate (CHAPS), 0.5% soybean phosphatidylcholine, 2.5 mM dithiothreitol (DTT) and a protease inhibitor mix (1 mM benzamidine, 2 μg/ml leupeptin, 2 μg/ml pepstatin A, 2 μg/ml aprotinin and 0.5 mM PMSF). This mixture was incubated on ice for 1 hr. Cell lysate was obtained by centrifuging twice at 16,000 x g in a microcentrifuge at 4°C for 30 min to remove

unsolubilized materials. 25 µl of cell lysate of RyR2 WT or mutant was diluted with 25 µl H_2O, mixed with 50 µl of 2 x Laemmli sample buffer including 5 % β-mercaptoethanol and boiled for 5 min. According to the protein concentration measured using the Bradford protein assay (Bio-Rad), a certain volume of boiled sample containing ~15 µg of proteins was loaded into a SDS-polyacrylamide gel electrophoresis (SDS-PAGE). The RyR2 WT and mutant proteins were separated by the 6% SDS-PAGE and transferred to nitrocellulose membranes at 45 V for 18-20 h at 4 °C in the presence of 0.01% SDS. The nitrocellulose membranes containing the transferred proteins were blocked for 30 min with PBS containing 0.5% Tween-20 and 5% skimmed-milk powder. The blocked membrane was incubated with anti-RyR2 antibodies (34c) (1:1000) and then incubated with the secondary anti-mouse IgG (H&L) antibodies conjugated to horseradish peroxidase (1:20000). After washing for 15 min, three times, the bound antibodies were detected using an enhanced chemiluminescence kit from Pierce.

2.6 Single-cell Ca^{2+} imaging (cytosolic Ca^{2+}) of HEK293 cells

Intracellular cytosolic Ca^{2+} changes in stable, inducible HEK293 cells expressing RyR2 WT or mutant channels were monitored using single-cell Ca^{2+} imaging and the fluorescent Ca^{2+} indicator dye Fura-2 AM. Cells grown on glass coverslips for 18-22 h after induced by 1 µg/ml tetracycline (Sigma) were loaded with 5 µM Fura-2 AM in modified KRH (Krebs-Ringer-Hepes) buffer (125 mM NaCl, 5 mM KCl, 1.2mM KH_2PO_4, 6 mM glucose, 1.2 mM $MgCl_2$ and 25 mM Hepes, pH 7.4) plus 0.02% pluronic F-127 (Molecular Probes) and 0.1 mg/ml BSA for 20 min at room temperature (23°C). The coverslips were then mounted in a perfusion chamber (Warner Instruments, Hamden,

CT, U.S.A.) on an inverted microscope (Nikon TE2000-S). The cells were continuously perfused with KRH buffer containing increasing extracellular Ca^{2+} concentrations (0-2.0 mM). Caffeine (10 mM) was applied at the end of each experiment to confirm the expression of active RyR2 channels. The ratio of Fura-2 AM fluorescence was captured every 4 seconds with excitation at 340 or 380 nm and emission at 510 nm through a Fluor 20x objective and a Chroma filter set (Photon Technology International, Lawrenceville, NJ). Only cells that responded to caffeine were analyzed using the Compix Simple PCI 6 software (Compix Inc.)

2.7 Single-cell Ca^{2+} imaging (luminal Ca^{2+}) of HEK293 cells

Luminal Ca^{2+} transients in HEK293 cells expressing RyR2 WT or mutant channels were measured using single-cell Ca^{2+} imaging and the Ca^{2+} sensitive FRET based cameleon protein D1ER [197]. Stable, inducible HEK293 cells expressing WT or mutant channels were transfected with D1ER using the Ca^{2+} phosphate precipitation method 18-20 h after subculture. After transfection for 24 h, the growth medium was then changed to an induction medium containing 1μg/ml tetracycline.

In order to exclude the possibility of D1ER saturation, an experiment was performed to measure the D1ER signal at 0.5, 1, 1.5 and 10 mM free Ca^{2+} concentrations respectively. The HEK293 cells expressing WT was first permeabilized by 50μg/ml saponin in an incomplete intracellular-like medium (incomplete ICM containing 125 mM KCl, 19 mM NaCl, and 10 mM HEPES, pH 7.4 with KOH) for 3-4 min and then saponin was washed off. The cells were then incubated with ICM buffer (incomplete ICM plus 1 mM ATP, 1 mM Mg^{2+}, pH 7.4 with KOH) containing 600 nM A23187 (a Ca^{2+} ionophore,

sigma-aldrich) for 6 min at each concentration of free Ca^{2+} from 0.5 to 10 mM. Finally the cells were treated with 20 mM caffeine to deplete the store and 20 mM EGTA to chelate all of the remained Ca^{2+} ions.

After induced for ~22 h, in a typical experiment, HEK293 cells expressing RyR2 WT and mutants in the pore-forming region, CaMBD and N-terminal region were perfused continuously with KRH buffer containing various concentrations of $CaCl_2$ (0-2 mM), tetracaine (1 mM) and caffeine (20 mM) or variouse concentrations of caffeine (1-20 mM) at room temperature (22 °C). In the study of permeabilized cells, the cells were first permeabilized by 50μg/ml saponin in an incomplete ICM for 3-4 min. The cells were then switched to a complete ICM (incomplete ICM plus 2 mM ATP, 2 mM $MgCl_2$, and 0.05 mM EGTA, and 50 nM free Ca^{2+}, pH 7.4 with KOH) for 5-6 min to remove the saponin in the buffer and recorded for 6 min as the control. The permeabilized cells were then challenged with 200nM free Ca^{2+} and 20 mM caffeine. Images were captured every 2 seconds with excitation at 430 nm and emission at 470 nm or 535 nm using an inverted microscope (Nikon TE2000-S) equipped with an S-Fluor 20x/0.75 objective. The FRET signal was determined from the ratio of the light emission at 535 and 470 nm. Data were analyzed with the Compix Simple PCI 6 software.

For intact cells expressing $RyR2_{S2367\text{-}CFP/Y2801\text{-}YFP}$ or the WT control, the cells were perfused with KRH buffer containing 1mM $CaCl_2$, 1-10 mM caffeine, 10 mM aminophylline or 10mM theophylline at room temperature (22 °C). For permeabilized cells expressing $RyR2_{S2367\text{-}CFP/Y2801\text{-}YFP}$ or the WT control, the cells were first permeabilized by 50μg/ml saponin in an incomplete ICM buffer for 3 to 4 min. The cells were then switched to a complete ICM (incomplete ICM plus 2 mM ATP, 2 mM $MgCl_2$,

and 0.05 mM EGTA, and 200nM free Ca^{2+}, pH 7.4 with KOH) for 5-6 min to remove the saponin in the buffer. The permeabilized cells were then challenged with caffeine (10mM), 4-CmC (1mM), ATP (5mM), Ca^{2+} (1μM), or ryanodine (100μM) plus caffeine (10mM). Images were captured by a QuantEM 512SC camera (Photometrics) every 2 seconds using the NIS-Elements AR software (Nikon Instruments Inc.). The cells were excited at 430nm and the emission was split into 465 nm and 535 nm beams by a dual view device (Photometrics) placed in a Nikon eclipse Ti microscope equipped with the QuantEM 512SC camera (Photometrics). D1ER signals were determined from the ratios of the emissions at 535±30 nm (YFP) and 465±30 nm (CFP). Data were analyzed with the NIS-Elements AR software (Nikon Instruments Inc.).

2.8 Measurements of FRET signals from the $RyR2_{S2367\text{-}CFP/Y2801\text{-}YFP}$ FRET pair

FRET signals from the $RyR2_{S2367\text{-}CFP/Y2801\text{-}YFP}$ pair were measured using two approaches.

In the first approach, we determined the acceptor-donor emission ratio, i.e. the emission ratio of YFP and CFP fluorescence after CFP excitation only in intact or permeabilized HEK293 cells expressing $RyR2_{S2367\text{-}CFP/Y2801\text{-}YFP}$ as described above for measuring ER luminal Ca^{2+} using D1ER. To increase the expression level of $RyR2_{S2367\text{-}CFP/Y2801\text{-}YFP}$ and thus the fluorescence signals, HEK293 cells were induced by 1μg/ml tetracycline for two days.

In the second approach, HEK293 cells grown for 24-48 h after transfection with $RyR2_{S2367\text{-}CFP/Y2801\text{-}YFP}$ were washed 3 times with KRH buffer without $MgCl_2$ or $CaCl_2$ and examined on a Leica TCS SP5 confocal laser scanning microscope with a 63×/NA1.4

oil-immersion objective lens [318]. Cells were kept at 37°C using a water-heated stage incubator. To test the impact of RyR2 ligands on FRET, buffer in the cultured dishes was exchanged by peristaltic pumps. We utilized the acceptor photobleaching method to detect and measure FRET signals in the live cells. Briefly, CFP and YFP were excited with separate laser channels of 458nm and 514nm, respectively. Emission fluorescence intensity data were obtained at 465-495nm (CFP) and 520-550nm (YFP). We used a 700 Hz line frequency scan speed with bidirectional scan mode in combination with an image format of 1024 × 1024 pixels, which can record one image every 754 ms. Repeated scans (30-60) with maximum laser intensity at 514nm were used to photobleach YFP which lasted about 23-45 seconds, and the FRET efficiency was calculated according to the equation:

$$E = \left(\frac{I_{CFPpost} - I_{CFPpre}}{I_{CFPpost}} \right) \times 100\%$$

where I_{CFPpre} and $I_{CFPpost}$ are the respective background-corrected CFP fluorescence intensities before and after photobleaching YFP [319]. The photobleaching, fluorescence intensity measurements, and FRET efficiency calculation were controlled automatically by the software Leica Application Suite Advanced Fluorescence (LAS AF). Measurements of the FRET efficiency were carried out in the laboratories of Dr. Zheng Liu and Dr. Terence Wagenknecht.

2.9 [^{3}H]ryanodine binding

HEK293 cells expressing $RyR2_{S2367\text{-}CFP/Y2801\text{-}YFP}$ for 2 days were collected in a 50 ml tube and permeabilized by 50μg/ml saponin in an incomplete ICM buffer for 3 min. After

saponin was washed off, the cells were split into two 50 ml tubes with an equal amount. The two tubes of cells were incubated in a complete ICM buffer with or without 100μM ryanodine plus 10 mM caffeine for 10 min. The ryanodine-treated or non-treated cells were washed with the complete ICM buffer to remove caffeine and free ryanodine. The washed cells were solubilized with the lysis buffer containing 25 mM Tris, 50 mM HEPES, pH 7.4, 137 mM NaCl, 1% CHAPS, 0.5% soybean phosphatidylcholine, 2.5 mM DTT, and a protease inhibitor mix (1 mM benzamidine, 2 μg/ml leupeptin, 2 μg/ml pepstatin A, 2 μg/ml aprotinin and 0.5 mM PMSF) on ice for 15 min. Cell lysate was obtained after removing the unsolubilized materials by centrifugation in microcentrifuge at 4°C for 2 min. Equilibrium [^{3}H]ryanodine binding to cell lysate was performed as described previously [320] with some modifications. [^{3}H]Ryanodine binding was carried out in a total volume of 600 μl binding solution containing 60 μl of cell lysate, 500 mM KCl, 25 mM Tris, 50 mM HEPES (pH 7.4), 30 μM Ca^{2+}, 10 mM caffeine, 5 nM [^{3}H]ryanodine, and a protease inhibitor mix at 37 °C for 20 min. The binding mix was diluted with 5 ml of ice-cold washing buffer containing 25 mM Tris, pH 8.0, and 250mM KCl and immediately filtered through Whatman GF/B filters presoaked with 1% polyethylenimine. The filters were washed three times, and the radioactivities associated with the filters were determined by liquid scintillation counting. Nonspecific binding was determined by measuring [^{3}H]ryanodine binding in the presence of 50 μM unlabeled ryanodine. All binding assays were done in duplicate.

2.10 Culture, transfection and single cell Ca^{2+} imaging of mouse HL-1 cardiac cells

HL-1 cardiac cells were kindly provided by Dr. William C. Claycomb from the Louisana State University Health Sciences Center. Cells were thawed and grown in a $75cm^2$ tissue culture flask coated with 0.02% (wt/vol) gelatin. The cells were grown in the Claycomb media (JRH Biosciences) supplemented with 10% (volume/volume) fetal bovine serum, penicillin/streptomycin (100U/ml/100ug/ml), 2 mM L-glutamine and 0.1 mM norepinephrine. For transfection, HL-1 cells were washed with PBS and collected in a 13ml-Falcon tube. The cells were then centrifuged at 1200 rpm for 2 min and the supernatant was removed. The cell pellet was then gently mixed with 10 μg of RyR2 WT or Del-Exon-3 cDNA in the Cell Line Nucleofection Solution V (Lonza Bioscience) in a total volume of 100 μl. The mixture of cells and DNA was subjected to Nucleofection by using the Amaxa apparatus with the A033 program. Transfected cells were then plated onto a 6-well plate containing 12-mm glass coverslips coated with gelatin and fibronectin and grown for 24-28 h. Intracellular Ca^{2+} transients in transfected HL-1 cells were measured by using single-cell Ca^{2+} imaging and the fluorescence Ca^{2+} indicator dye Fura-2 AM. Briefly, cells grown on glass coverslips for 24-28 h after transfection were loaded with 5 μM Fura-2 AM in KRH buffer plus 0.02% Pluronic F-127 and 0.1 mg/ml BSA for 20 min at room temperature. The coverslips were then mounted in a perfusion chamber (Warner Instruments, Hamden, CT) on an inverted microscope (Nikon 6 TE2000-S). The cells were continuously perfused with KRH buffer containing different concentrations of $CaCl_2$ (0 to 10 mM) at room temperature (23°C). Time-lapse images (0.5 frame/s) were captured with excitation at 340 nm or 380 nm and emission at 510 nm through a Fluor-20x objective and a Chroma filter set using the Simple PCI System. Data were analyzed

with the Compix Simple PCI 6 software. All chemicals were obtained from Sigma (St. Louis, MO) unless otherwise specified.

2.11 Statistical analysis

All values shown are mean ± SEM unless indicated otherwise. To test for differences between groups, we used Student's *t* test (2-tailed) or one-way ANOVA with *post hoc* test. A *P* value <0.05 was considered to be statistically significant.

CHAPTER III: ROLE OF THE PORE-FORMING REGION OF RYR2 IN CALCIUM RELEASE ACTIVATION AND TERMINATION

3.1 Introduction

Over the past 50 years, enormous progress has been made in the field of EC coupling concerning the mechanism of Ca^{2+} release activation. However, the longstanding question of how SR Ca^{2+} release terminates remains unanswered. Since CICR is an intrinsically self-reinforcing process, it seems reasonable to expect that the positive feedback process of CICR would deplete all of the Ca^{2+} stored in the SR. In contrast to the predicted all-or-none pattern of release, a complete depletion of Ca^{2+} was not observed during CICR in most studies [39-42,53]. Robust mechanisms that turn off SR Ca^{2+} release are essential for stable EC coupling and muscle relaxation [20]. During SR Ca^{2+} release, there is an apparent sudden decrease of luminal Ca^{2+}. The reduced luminal Ca^{2+} has been found to be capable of deactivating the RyR2 channel either in studies at the single channel level or at the cellular level [40,41,54,55,147-149]. Interestingly, Zima et al. showed that Ca^{2+} release from SR terminated at a fixed luminal Ca^{2+} level in cardiomyocytes [42]. These findings indicate that luminal Ca^{2+} may play an important role in Ca^{2+} release termination.

We have recently found that the pore-forming region of RyR2 is essential for luminal Ca^{2+} activation. A single point mutation, E4872A, located at the helix bundle crossing abolished the luminal, but not cytosolic, Ca^{2+} activation of the channel. Luminal Ca^{2+} sensing was markedly reduced in a knock-in mouse model harboring the E4872Q mutation (unpublished data). In addition, the inner helix (TM10) in the pore-forming region was also found to play a critical role in luminal Ca^{2+} sensing and gating [152,321]. Mutations in TM10 displayed varied properties. Some of these mutations abolished or reduced the sensitivity of the RyR2 channel to activation by caffeine, while others

enhanced the basal activity of the channel [321]. These observations raise an important question of whether the same pore-forming region pivotal to luminal Ca^{2+} activation is also crucial for Ca^{2+} release termination.

In the present study, we established a simple system to directly assess the impact of RyR2 mutations on both Ca^{2+} release activation and termination. Stable, inducible HEK293 cell lines expressing RyR2 WT and mutants in the pore-forming region were generated and characterized. We found that HEK293 cells expressing RyR2 displayed robust Ca^{2+} release termination similar to that observed in cardiac cells [42]. This simple HEK293 cell system was used to systematically assess the role of a number of amino acids in the pore-forming region of RyR2 in Ca^{2+} release termination. Our results indicate that mutations in the pore-forming region can affect either the activation or the termination of Ca^{2+} release or both, suggesting that the pathways for Ca^{2+} release activation and termination are distinct but overlap. Moreover, the pore-forming region, including the helix bundle crossing and inner helix of RyR2, responsible for luminal Ca^{2+} activation is also a major determinant of Ca^{2+} release termination.

3.2 Results

3.2.1 Generation of RyR2 mutations in the pore-forming region

According to Williams's model of the RyR2 channel pore (Figs. 5A,B,C) [114], the predicted transmembrane segment TM10 is believed to correspond to the pore inner helix lining the internal pore of the channel (Figs. 5 B,C). The luminal mouth of the pore is formed by the loop between TM8 and TM10 (Figs. 5 B,C). This region is identified to encompass the selectivity filter important for ion selection and conduction. On the other

hand, the cytosolic mouth of the pore is formed by residues in the C-terminal region of the TM10 inner helices, corresponding to the crossover of the pore inner helices (Fig. 5 B). This helix bundle crossing is proposed to constitute the ion gate of the channel [107]. Interestingly, a number of conserved negatively charged residues in the helix bundle crossing have been shown to be involved in the luminal Ca^{2+} regulation of the channel (unpublished data). Among them, E4872 was identified as a critical residue for Ca^{2+} sensing. We have also previously shown that the TM10 transmembrane sequence (inner helix) constitutes an essential determinant of luminal Ca^{2+} activation and gating[152,321]. Mutations in this region could either reduce or enhance the channel activity. Interestingly, single I4862A mutant channels exhibited considerable channel openings and altered gating at very low concentrations of Ca^{2+} [321]. Since luminal Ca^{2+} has been proposed to be important in Ca^{2+} release termination, it is likely that the helix bundle crossing and the inner helix, which are pivotal for luminal Ca^{2+} activation, also play a crucial role in Ca^{2+} release termination. To test this hypothesis, a number of critical residues within the helix bundle crossing (from D4868A to E4885) and the inner helix (from I4844 to I4867) were mutated by using the PCR-mediated overlap extension method. Mutations including D4896A, located near the helix bundle crossing have also been made. The amino acids that have been studied and mentioned in the following Results Section are labeled in red in Fig. 5C.

3.2.2 Experimental model for studying luminal Ca^{2+} release activation and termination

A powerful approach to studying the termination of Ca^{2+} release is to directly monitor the SR luminal Ca^{2+} dynamics. However, the luminal Ca^{2+} probes currently used, such as Fluo-5N, have never been successfully loaded to mouse cardiac cells for some

Fig. 5A Predicted Transmembrane Topology of RyR

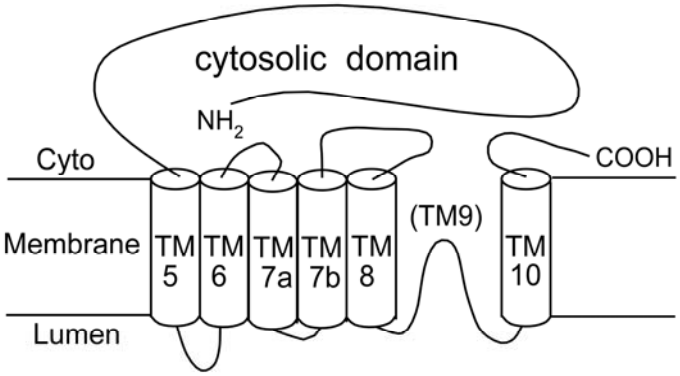

Fig. 5B A putative Model of RyR2 Pore

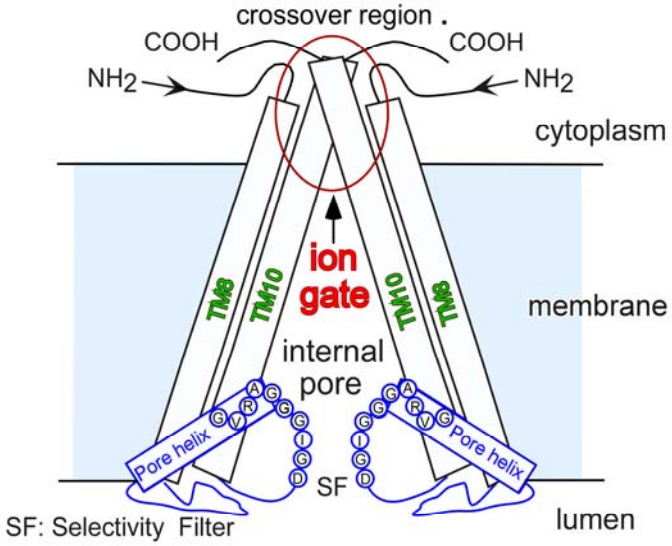

Fig. 5C Amino Acid Sequence of the Pore Region of RyR2

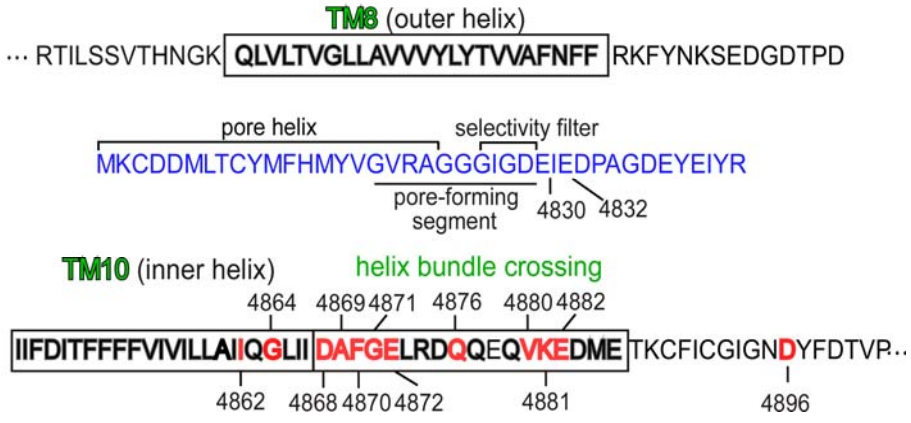

Fig. 5 Proposed pore structure of RyR2 and corresponding amino acid sequence

unknown reasons, although they are effective for monitoring SR Ca^{2+} dynamics in rat and rabbit cardiac cells [42,53,322,323]. In addition, the extremely large size of the RyR2 cDNA (~15 kb) eliminates the use of adenovirus-mediated gene transfer techniques for introducing RyR2 mutations into adult cardiac myocytes. Further, it is impractical to generate knock-in mouse for each of the RyR2 mutations proposed to be investigated. In summary, the lack of proper luminal Ca^{2+} probes and animal models harboring RyR2 mutations makes the study of the molecular basis of Ca^{2+} release termination in cardiomyocytes very difficult at present.

Alternatively, the HEK293 cell system could be used to assess the effect of RyR2 mutations on Ca^{2+} release termination. Stable, inducible HEK293 cell lines expressing each of the RyR2 mutations in the helix bundle crossing and inner helix were generated using the Flp-In™ T-Rex™ system. To be able to monitor the luminal Ca^{2+} dynamics, RyR2 WT or mutant cells were transfected with the FRET based luminal Ca^{2+} sensing protein, D1ER, which is a modified cameleon protein specifically expressed within the ER due to its KDEL ER retention motif [197] (Fig. 6A). The FRET signal of D1ER, which reflects the luminal Ca^{2+} dynamics, was determined by calculating the ratios of the YFP and CFP fluorescence. Typically, as shown in Fig. 6B, elevating extracellular Ca^{2+} from 0 to 2 mM induced SOICR in the form of Ca^{2+} oscillations in HEK293 cells expressing RyR2 WT. These Ca^{2+} oscillations were observed as the downward deflections of the FRET signal (indicated with red circle in Fig. 6B). Spontaneous Ca^{2+} release (or SOICR) occurred when the ER Ca^{2+} increased to a threshold level (the SOICR activation threshold, F_{SOICR}) and terminated when the ER Ca^{2+} declined to another threshold level (the SOICR termination threshold, F_{termi}; Fig. 6B, C). SOICR in HEK293 cells expressing

RyR2 WT occurred at a threshold of ~94% of the store capacity and terminated at a threshold of 57% of the store capacity (Figs. 6B, C). The termination threshold in HEK293 cells is similar to that (60%) observed in cardiomyocytes [42]. Following the addition of 1~2 mM tetracaine, RyR2 activity was inhibited to get the maximum Ca^{2+} store level (F_{max}), and following 20 mM caffeine, the Ca^{2+} store was depleted to obtain the minimum Ca^{2+} store level (F_{min}). This model allows us to monitor the luminal Ca^{2+} dynamics and to determine the SOICR threshold (F_{SOICR}) and the termination threshold (F_{termi}) of WT and each RyR2 mutant.

Note that SOICR is mediated by RyR2, but not by endogenous IP_3Rs that may be present, because xestospongin C, an inhibitor of IP3Rs, had no effect on SOICR in HEK293 cells expressing RyR2 WT (Fig.7). Furthermore, these cells lack some major Ca^{2+} handling proteins present in cardiac cells, such as CASQ, DHPR and PLB. Thus, the properties of spontaneous Ca^{2+} oscillations observed in RyR2-expressing HEK293 cells largely reflect the intrinsic properties of the RyR2. It should also be noted that, similar to that reported previously[197], the D1ER signal in HEK293 cells was not saturated at 0.5-10 mM free Ca^{2+} concentrations (Fig. 8).

Taken together, these results demonstrate that HEK293 cells expressing RyR2 can reproduce cardiac SOICR, and thus offer a readily accessible and manageable cell system for investigating the impact of RyR2 mutations and regulators on SOICR activation and termination.

Fig. 6 Experimental model for studying luminal Ca^{2+} dynamics in HEK293 cells expressing RyR2

Stable, inducible HEK293 cell lines expressing RyR2 WT were transfected with the FRET-based ER luminal Ca^{2+} sensing protein D1ER 48 h before single cell FRET imaging. The expression of RyR2 WT was induced 24 h before imaging. HEK293 cells transfected with D1ER are shown in (A). The cells were perfused with KRH buffer containing increasing levels of extracellular Ca^{2+} (0-2 mM) to induce SOICR, followed by the addition of 1-2 mM tetracaine to inhibit SOICR, and then 20 mM caffeine to deplete the ER Ca^{2+} stores. A representative FRET recording trace from one of the 330 RyR2 WT cells is shown (B). The activation threshold and termination threshold were determined using the equations shown in panel B. F_{SOICR} indicates the FRET level at which SOICR occurs, while F_{termi} depicts the FRET level at which SOICR terminates. The fractional Ca^{2+} release was calculated by subtracting the termination threshold from the activation threshold (C). The maximum FRET signal (F_{max}) is defined as the FRET level after 1 mM tetracaine treatment, whereas the minimum FRET signal (F_{min}) is defined as the FRET level after 20 mM caffeine treatment. The store capacity was calculated by subtracting F_{min} from F_{max}. Data shown are mean ± SEM (n = 24).

A HEK293 Cells Transfected with D1ER

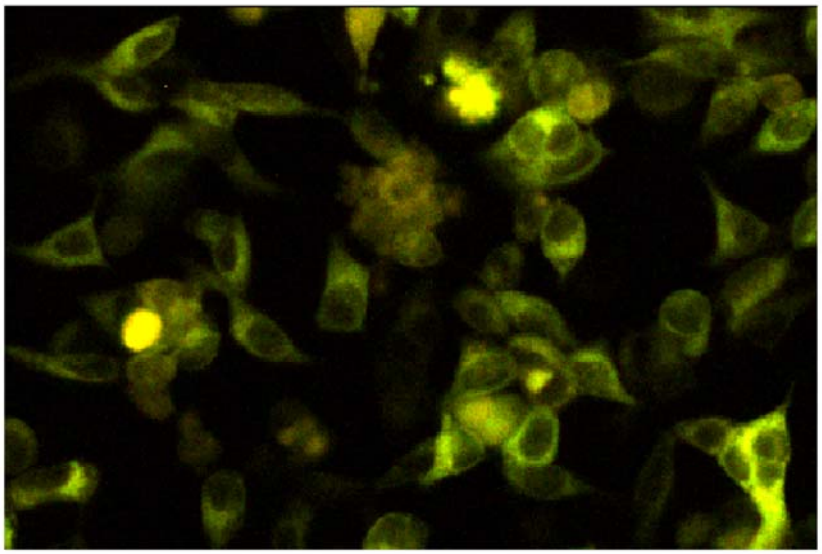

B Trace (RyR2-WT)

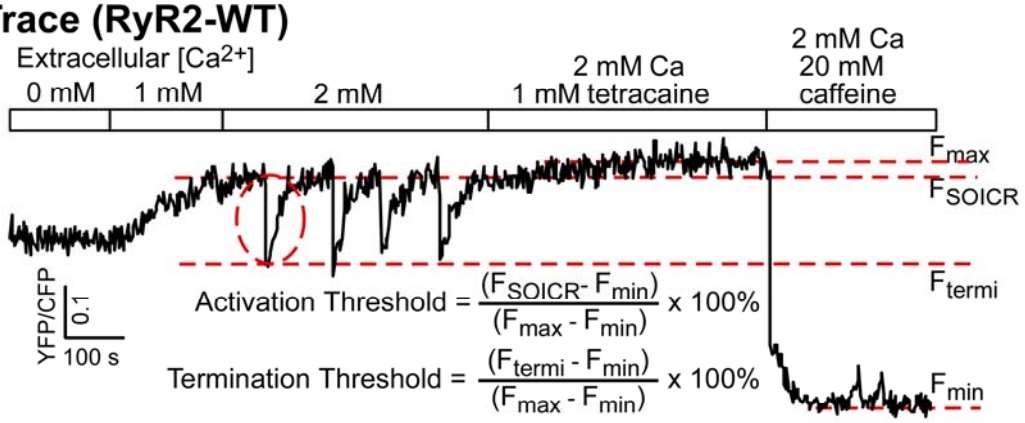

C Thresholds and Fractional Ca^{2+} Release (RyR2-WT)

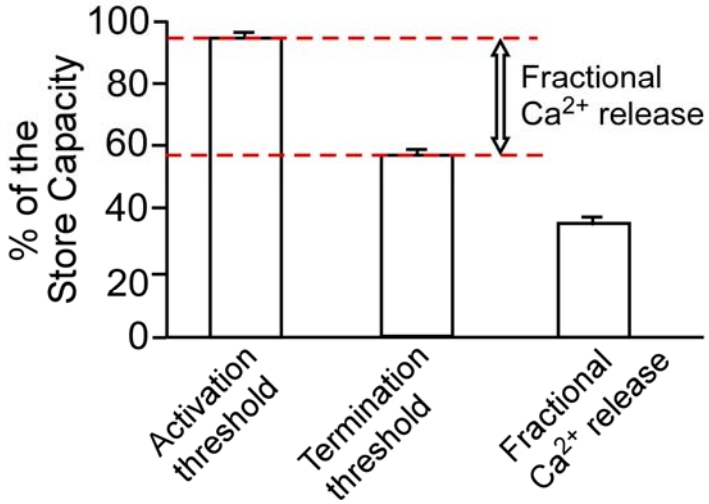

Fig. 7 Effect of xestospongin C on Ca^{2+} release activation and termination in HEK293 cells

Stable, inducible HEK293 cells expressing RyR2-WT were transfected with the D1ER cDNA 48 h before single cell FRET imaging. The expression of RyR2-WT was induced 24 h before imaging. The cells were perfused with KRH buffer containing increasing levels of extracellular Ca^{2+} (0-2 mM) to induce SOICR. This was followed by the addition of 1 μM xestospongin C, 1.0 mM tetracaine, and then 20 mM caffeine. (A) D1ER FRET signals from a representative RyR2-WT expressing cell. The activation threshold (B) and termination threshold (C) of SOICR before (-XesC) and after (+XesC) the addition of xestospongin C to RyR2-WT cells (50 cells) were determined using the equations shown in panel A. F_{SOICR} indicates the FRET level at which SOICR occurs. F_{termi} depicts the FRET level at which SOICR terminates. The maximum FRET signal (F_{max}) is defined as the FRET level after tetracaine treatment. The minimum FRET signal (F_{min}) is defined as the FRET level after caffeine treatment. Data shown are mean ± SEM (n = 4).

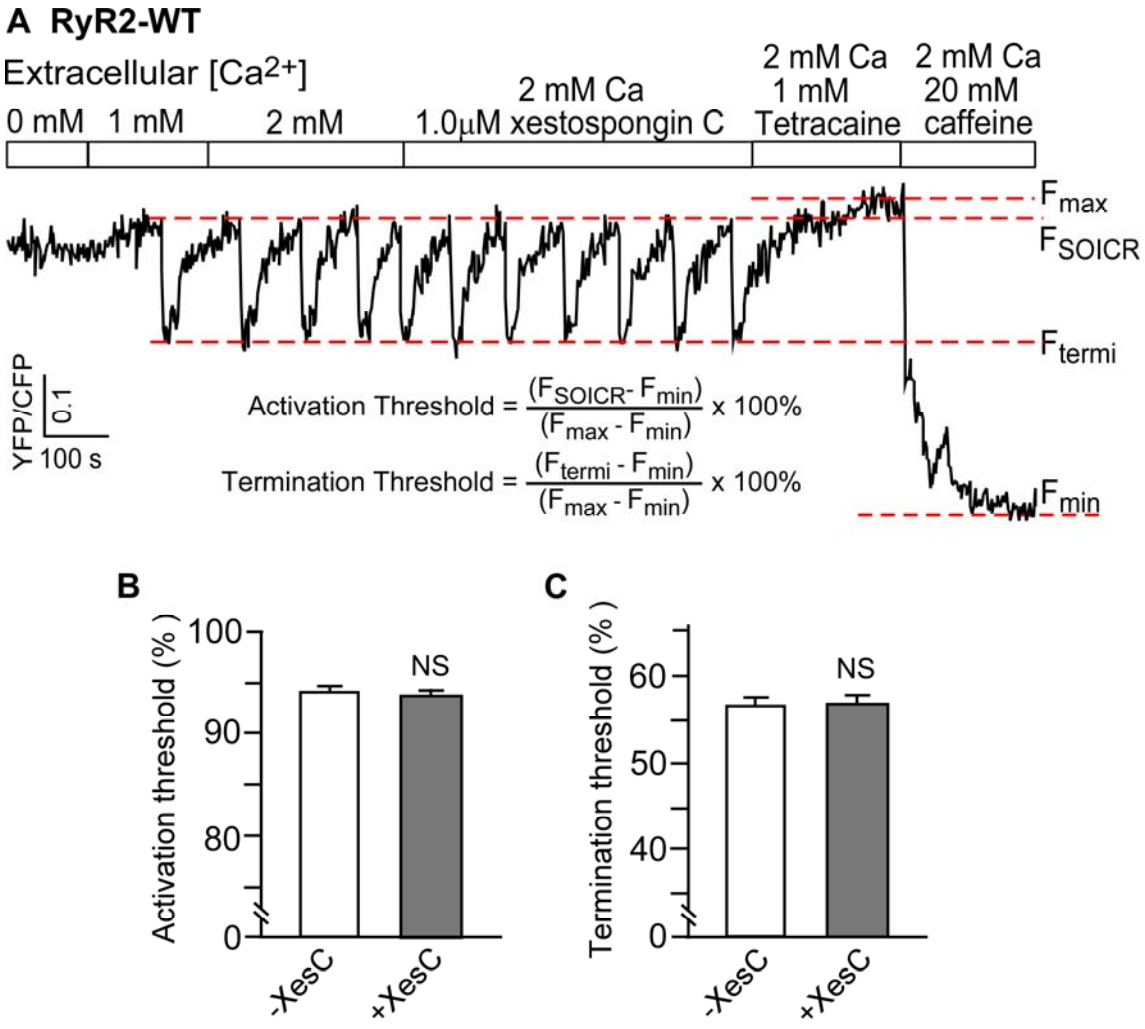
A RyR2-WT
Extracellular [Ca2+]
0 mM
1 mM
2 mM
2 mM Ca
1.0μM xestospongin C
2 mM Ca
1 mM
Tetracaine
2 mM Ca
20 mM
caffeine
Fmax
FSOICR
Ftermi
Fmin
YFP/CFP
0.1
100 s
Activation Threshold = (FSOICR - Fmin) / (Fmax - Fmin) x 100%
Termination Threshold = (Ftermi - Fmin) / (Fmax - Fmin) x 100%
B
Activation threshold (%)
100
90
80
0
NS
-XesC
+XesC
C
Termination threshold (%)
60
50
40
0
NS
-XesC
+XesC

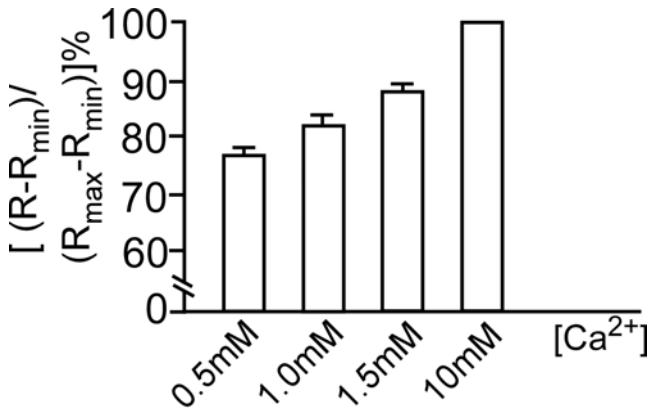

Fig. 8 D1ER signal is not saturated in HEK293 cells at physiological Ca^{2+} concentrations

Stable, inducible HEK293 cells expressing RyR2-WT were transfected with the D1ER cDNA 48 h before single cell FRET imaging. The expression of RyR2-WT was induced 24 h before imaging. The cells (50-68) were permeabilized with incomplete ICM buffer containing 50μg/ml saponin. After the saponin was washed off, the cells was perfused with complete ICM buffer with 1 mM ATP, 1 mM Mg^{2+}, 600 nM A23187 and Ca^{2+} from 0.5 to 10 mM. Finally 20 mM caffeine and 20 mM EGTA was applied to deplete the store and chelate Ca^{2+}. The level of D1ER signal were determined with the equation as $(R-R_{min})/(R_{max}-R_{min})$. The maximum FRET signal (R_{max}) is defined as the FRET level at 10 mM Ca^{2+}. The minimum FRET signal (Rmin) is defined as the FRET level after 20 mM caffeine and 20 mM EGTA treatment. Data shown are mean ± SEM (n = 3-7).

3.2.3 Mutation of the luminal Ca^{2+} sensing residue E4872 elevates both the activation and termination thresholds

Residue E4872 at the helix bundle crossing (the proposed gate) of RyR2 has been identified as a critical residue for luminal Ca^{2+} sensing. A single mutation E4872A in the helix bundle crossing completely abolishes luminal, but not cytosolic Ca^{2+} activation of RyR2. Given the significant role of luminal Ca^{2+} in termination, it is possible that the E4872A mutation with impaired luminal Ca^{2+} activation will also cause impaired termination. Since the E4872A mutant does not show SOICR induced by elevated extracellular Ca^{2+}, various concentrations of caffeine were applied to trigger SOICR, so that the impact of this mutation on SOICR could be studied. As shown in Fig. 9, caffeine caused a concentration-dependent reduction in the SOICR and termination thresholds in both RyR2 WT and the E4872A mutant cells (Fig.9A, B). However, at a given concentration of caffeine (e.g. 5 mM), the thresholds for Ca^{2+} release activation and termination were much higher in the E4872A mutant cells (90% and 46%) than in the RyR2 WT cells (33% and 20%) ($P<0.01$) (Figs. 9C, D), indicating that the E4872A mutation markedly inhibits the activation and enhances termination. There were no significant differences in the store capacity between WT and the mutant (Fig. 9F). Note that since 20mM caffeine may not be able to completely deplete the store, 100 μM SERCA blocker cyclopiazonic acid (CPA) and 20 mM caffeine were applied together to promote the Ca^{2+} store depletion. The results showed that the minimum Ca^{2+} store detected using 20 mM caffeine alone was similar to that detected using caffeine and CPA together (data not shown). Thus, 20 mM caffeine alone can be used for detecting the minimum Ca^{2+} store level in the present study.

Fig. 9 Effect of mutation E4872A on Ca^{2+} release activation and termination

HEK293 cells expressing RyR2 WT (A) and E4872A (B) were transfected with D1ER and perfused with elevating extracellular Ca^{2+} and caffeine concentrations. Representative traces of FRET signal (YFP/CFP ratio) from single cells are shown. Since in cells expressing RyR2 WT, SOICR occurred at a threshold of 94% of the store capacity as shown in Fig. 6C, the store capacity here ($F_{SOICR(0)}$ - F_{min}) is normalized to 94% ($F_{SOICR(0)}$, FRET level at which SOICR occurs in the presence of 0 mM caffeine; F_{min}, FRET level after 20 mM caffeine treatment). In cells expressing E4872A, the store capacity is directly calculated from (F_{max} - F_{min}). Since the cells were fully loaded by Ca^{2+} at 2 mM extracellular Ca^{2+} and no oscillation took place under this condition. Accordingly, the thresholds for activation (C) and Ca^{2+} release termination (D) at 5 mM caffeine for cells expressing WT (40) and E4872A (39) were calculated using the equations shown in panel A and B. $F_{SOICR\ (5)}$ and $F_{termi\ (5)}$ indicate the FRET levels at which Ca^{2+} release occurs and terminates in the presence of 5 mM caffeine respectively. Fractional release was determined by subtracting the termination threshold from the activation threshold as previously described (E). Data shown are mean ± SEM (n = 3) (* $P < 0.01$; vs. WT).

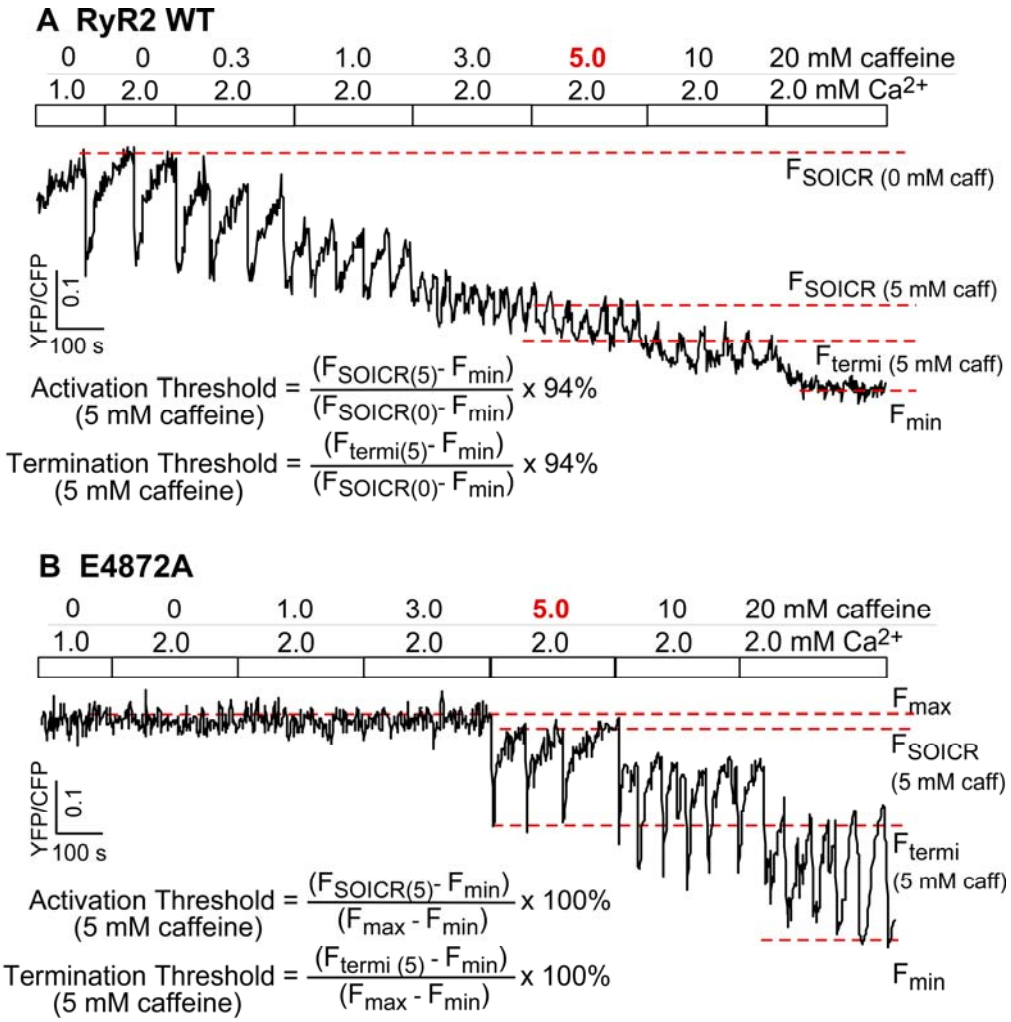
A RyR2 WT
0 0 0.3 1.0 3.0 5.0 10 20 mM caffeine
1.0 2.0 2.0 2.0 2.0 2.0 2.0 2.0 mM Ca2+
FSOICR (0 mM caff)
FSOICR (5 mM caff)
Ftermi (5 mM caff)
Fmin
YFP/CFP
0.1
100 s
Activation Threshold = (FSOICR(5)- Fmin) / (FSOICR(0)- Fmin) x 94%
(5 mM caffeine)
Termination Threshold = (Ftermi(5)- Fmin) / (FSOICR(0)- Fmin) x 94%
(5 mM caffeine)
B E4872A
0 0 1.0 3.0 5.0 10 20 mM caffeine
1.0 2.0 2.0 2.0 2.0 2.0 2.0 mM Ca2+
Fmax
FSOICR (5 mM caff)
Ftermi (5 mM caff)
Fmin
YFP/CFP
0.1
100 s
Activation Threshold = (FSOICR(5)- Fmin) / (Fmax - Fmin) x 100%
(5 mM caffeine)
Termination Threshold = (Ftermi (5) - Fmin) / (Fmax - Fmin) x 100%
(5 mM caffeine)

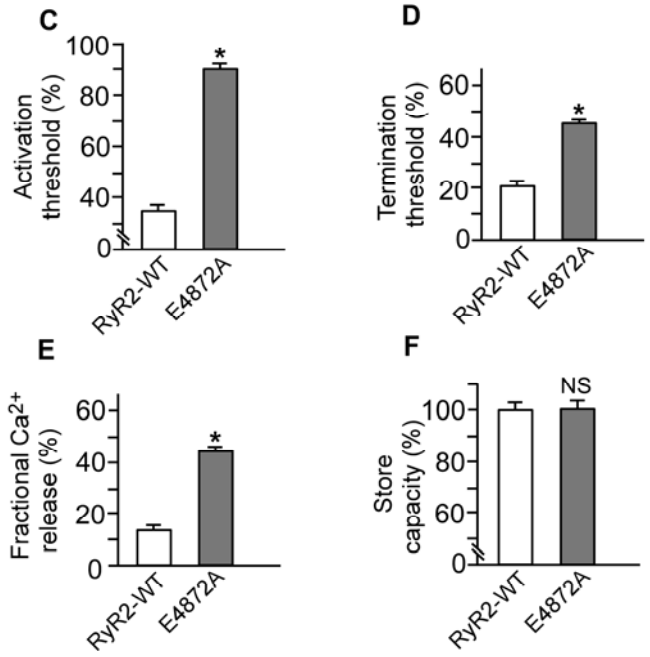
C
Activation threshold (%)
100
80
60
40
0
*
RyR2-WT
E4872A
D
Termination threshold (%)
60
40
20
0
*
RyR2-WT
E4872A
E
Fractional Ca2+ release (%)
60
40
20
0
*
RyR2-WT
E4872A
F
Store capacity (%)
NS
100
80
60
0
RyR2-WT
E4872A

To further study the significant role of the residue E4872 in Ca^{2+} release, double mutation G4871E/E4872A was generated to relocate the "glutamic acid" from site 4872 to the closely positioned site 4871. As shown in Fig.10, the double mutant retained a similar SOICR activation threshold (Fig.10B) and a slightly decreased termination threshold compared with WT (Fig. 10C) (54% vs. 57%, $P<0.05$). As a result, fractional release (activation threshold - termination threshold) was not altered in this double mutant. This result indicates that introducing a negative charge next to residue E4872 (G4871E) is capable of restoring the missing luminal Ca^{2+} activation of the E4872A mutant channel. Taken together, these data suggest that the E4872 residue as a luminal Ca^{2+} binding site plays a crucial role in both luminal Ca^{2+} activation and termination.

3.2.4 Mutations in the pore-forming region reduce both the activation and termination thresholds

It has been shown that a single mutation, E4872A, increased both the activation and termination thresholds for Ca^{2+} release. However, it is unknown whether other mutations in this pore-forming region also play a role in regulating Ca^{2+} release. As shown in Fig. 11, a number of point mutations in the pore-forming region were found to reduce both the activation and termination thresholds. In other words, both the activation and termination of Ca^{2+} release occurred at a lower luminal Ca^{2+} level in the mutant cells as compared with the RyR2 WT cells (Figs. 11A,B,C,D) ($P<0.01$). These mutations can be further divided in to two groups: while A4869G and Q4876A decreased both the activation and termination thresholds to a similar extent and thus did not alter the fractional Ca^{2+} release (Figs. 11A,C,D,E), F4870A, V4880A and K4881A reduced the activation threshold to a greater extent than the termination threshold, consequently, leading to decreased

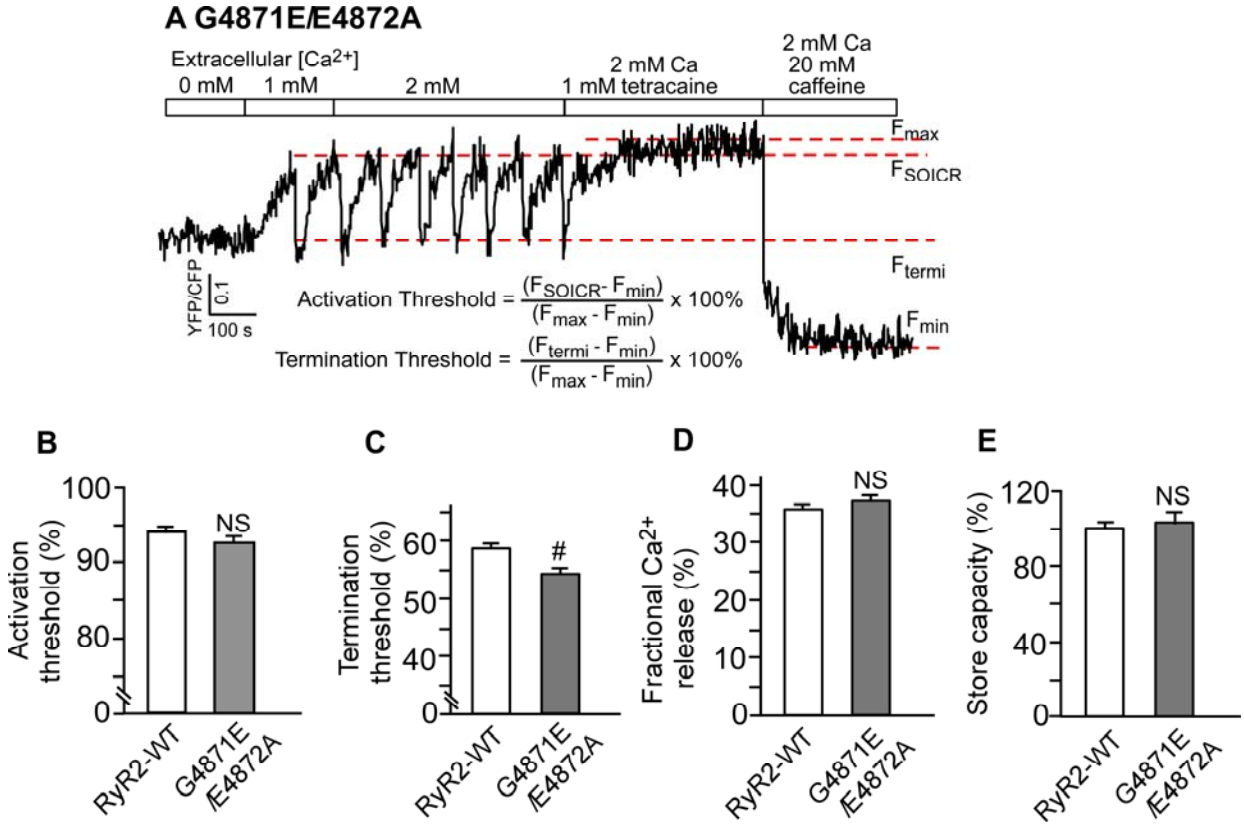

Fig.10 Effect of G4871E/E4872A double mutation on Ca^{2+} release activation and termination

D1ER FRET signals were recorded in HEK293 cells expressing WT and the G4871E/E4872A double mutant. A representative trace of the FRET signal from single cells expressing G4871E/E4872A is shown (A). The activation threshold (B), termination threshold (C), fractional Ca^{2+} release (D), and store capacity (E) in RyR2 WT (330) and mutant (89) cells were determined as described in the legend to Fig. 6. Data shown are mean ± SEM (n = 6-24) (# $P < 0.05$; vs. WT).

Fig. 11 Effect of A4869G, Q4876A, F4870A, V4880A and K4881A on Ca^{2+} release activation and termination

D1ER FRET signals were recorded in HEK293 cells expressing WT, A4869G, Q4876A, F4870A, V4880A and K4881A mutants. Representative traces of FRET signals from single cells expressing A4869G (A) or V4880A (B) are shown. The activation threshold (C), termination threshold (D), fractional Ca^{2+} release (E), and store capacity (F) in RyR2 WT (330) and mutant (56-135) cells were determined as described in the legend to Fig. 6. Data shown are mean ± SEM (n = 4-24) (* $P < 0.01$; vs. WT).

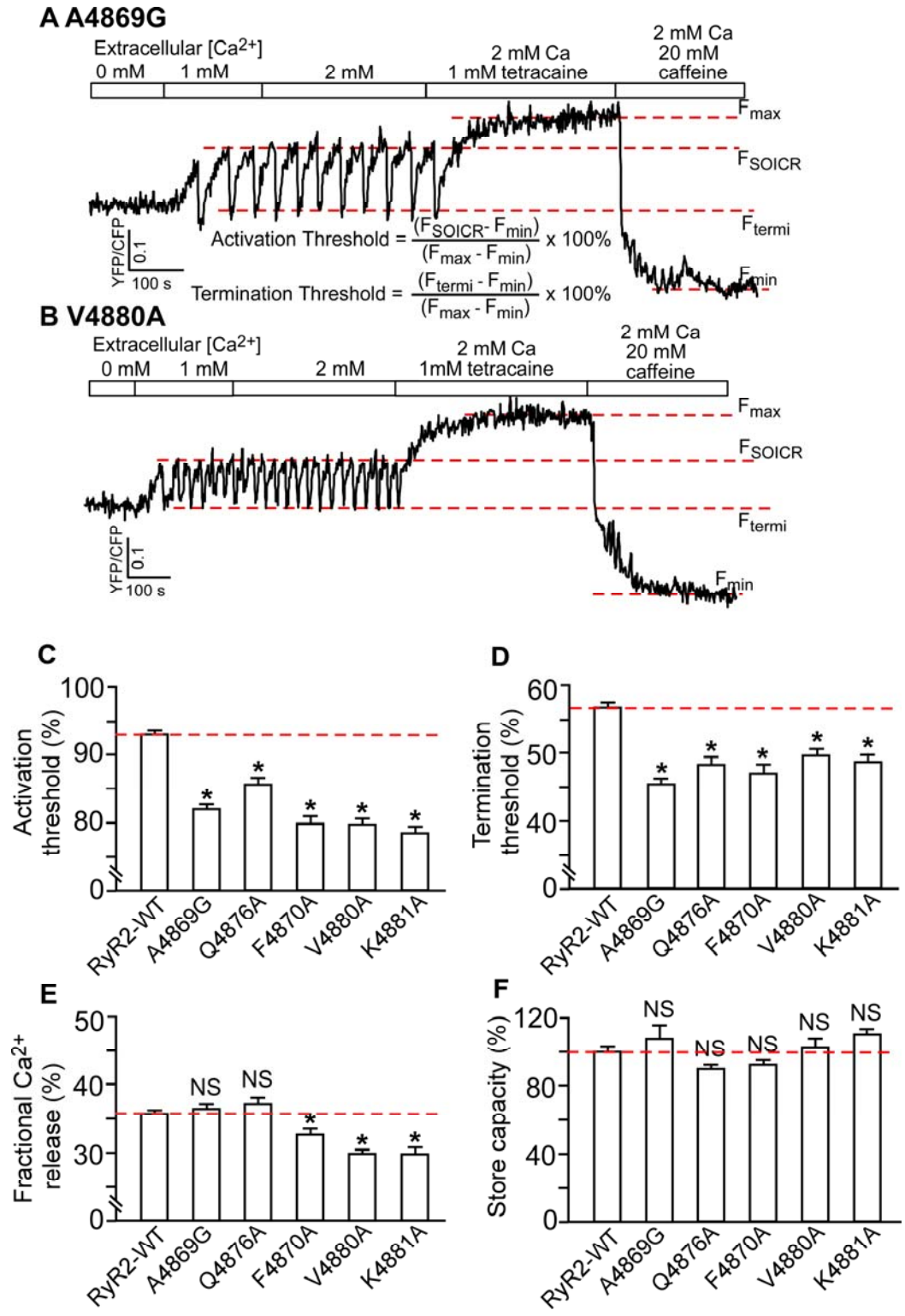
A A4869G
Extracellular [Ca2+]
0 mM
1 mM
2 mM
2 mM Ca
1 mM tetracaine
2 mM Ca
20 mM
caffeine
Fmax
FSOICR
Ftermi
Fmin
YFP/CFP
0.1
100 s
Activation Threshold = (FSOICR- Fmin) / (Fmax - Fmin) x 100%
Termination Threshold = (Ftermi - Fmin) / (Fmax - Fmin) x 100%
B V4880A
Extracellular [Ca2+]
0 mM
1 mM
2 mM
2 mM Ca
1mM tetracaine
2 mM Ca
20 mM
caffeine
Fmax
FSOICR
Ftermi
Fmin
YFP/CFP
0.1
100 s
C
Activation threshold (%)
100
90
80
0
RyR2-WT
A4869G
Q4876A
F4870A
V4880A
K4881A
D
Termination threshold (%)
60
50
40
0
RyR2-WT
A4869G
Q4876A
F4870A
V4880A
K4881A
E
Fractional Ca2+ release (%)
50
40
30
0
NS
NS
RyR2-WT
A4869G
Q4876A
F4870A
V4880A
K4881A
F
Store capacity (%)
120
80
40
0
NS
NS
NS
NS
RyR2-WT
A4869G
Q4876A
F4870A
V4880A
K4881A

fractional Ca^{2+} release (33%, 30%, 30%) compared with WT (36%) (Figs. 11B,C,D,E) ($P<0.01$). Traces of A4869G and V4880A, representing the oscillation pattern for each group, are shown in Figs. 11A, B. There were no significant differences in the store capacity between WT and all of the mutants (Fig. 11F). These results indicate that mutations in the pore-forming region can reduce the thresholds for both Ca^{2+} release activation and termination.

3.2.5 Mutations in the pore-forming region alter either the activation or the termination threshold

Since E4872A and a number of mutations in the pore-forming region showed an increase or a decrease in both the activation and termination thresholds, it is interesting to know that whether the activation and termination of Ca^{2+} release are always modulated together with the same trend. As shown in Fig, 12, in I4862A and G4864A mutant cells, SOICR occurred at a significantly lower luminal Ca^{2+} level (82% and 89%) compared with WT (94%) ($P<0.01$), but the Ca^{2+} release termination was hardly affected (Figs.12 B,C,D,E). The fractional releases of SOICR in I4862A and G4864A cells were also reduced (25% and 32% vs. 36% in WT, $P<0.01$). Note that I4862A and its control WT were only induced for 8 h instead of 24 h, because high expression levels of I4862A caused constant spillover of ER Ca^{2+} preventing synchronized Ca^{2+} oscillations. Interestingly, although fewer numbers of oscillating WT cells were detected when they were induced for 8 h, once they oscillated, the properties of Ca^{2+} release activation and termination were similar to those in cells induced for 24 h (Fig.12C,D,E,F), indicating that the SOICR properties are likely independent of the expression level of RyR2. These

results suggest that mutations in the pore-forming region can alter Ca^{2+} release activation without changes in Ca^{2+} release termination.

Furthermore, it was also found that the G4871R, E4882A and D4896A mutations in the pore-forming region altered the threshold for Ca^{2+} release termination but did not change the threshold for Ca^{2+} release activation ($P<0.01$) (Figs.13 A,B,C,D,E). While G4871R markedly decreased the termination threshold (40% vs. 57% in WT, $P<0.01$), E4882A and D4896A significantly increased the termination threshold (60% and 63% vs. 57% in WT, $P<0.01$). In line with the change in termination threshold, the fractional Ca^{2+} release in G4871R cells (54%) was dramatically enhanced compared with that in WT cells (36%) ($P<0.01$), whereas the fractional releases were reduced in E4882A (33%) and D4896A (30%) cells ($P<0.01$) (Fig. 13F). There were no significant differences in the store capacity between WT and all of the mutants (Fig. 13G). In summary, these results demonstrate that mutations in the pore-forming region could either change the SOICR activation or termination threshold without affecting the other.

3.2.6 D4868A increases the activation threshold but decreases the termination threshold

A negatively charged residue D4868 located in the helix-bundle crossing in the RyR2 channel pore was also found to be crucial in luminal Ca^{2+} sensing. As with E4872A, D4868A mutant cells were insensitive to elevated extracellular Ca^{2+}. Caffeine was required to induce SOICR in D4868A mutant cells. As revealed in Fig. 14, in the presence of 3 mM caffeine, the threshold for SOICR was greatly increased in D4868A mutant cells (80%) in comparison with that in WT cells (45%) ($P<0.01$) (Figs. 14A,B,C). However, D4868A affected the Ca^{2+} release termination completely differently from

Fig. 12 Effect of I4862A and G4864A on Ca^{2+} release activation and termination

Stable, inducible HEK293 cell lines expressing RyR2 WT, I4862A or G4864A were transfected with D1ER 48 h before single cell FRET imaging. The expression of RyR2 WT, G4864A was induced 24 h before imaging. The expression of I4862A and its corresponding control WT was induced for 8 h before imaging. FRET recordings from representative I4862A (A) and G4864A (B) cells are shown. The activation threshold (C), termination threshold (D), fractional Ca^{2+} release (E), and store capacity (F) in RyR2 WT (28-330) and mutant (33-102) cells were determined as described in the legend to Fig. 6. Data shown are mean ± SEM (n = 3-24) (* $P < 0.01$; $^{\#}$ $P < 0.05$; vs. WT).

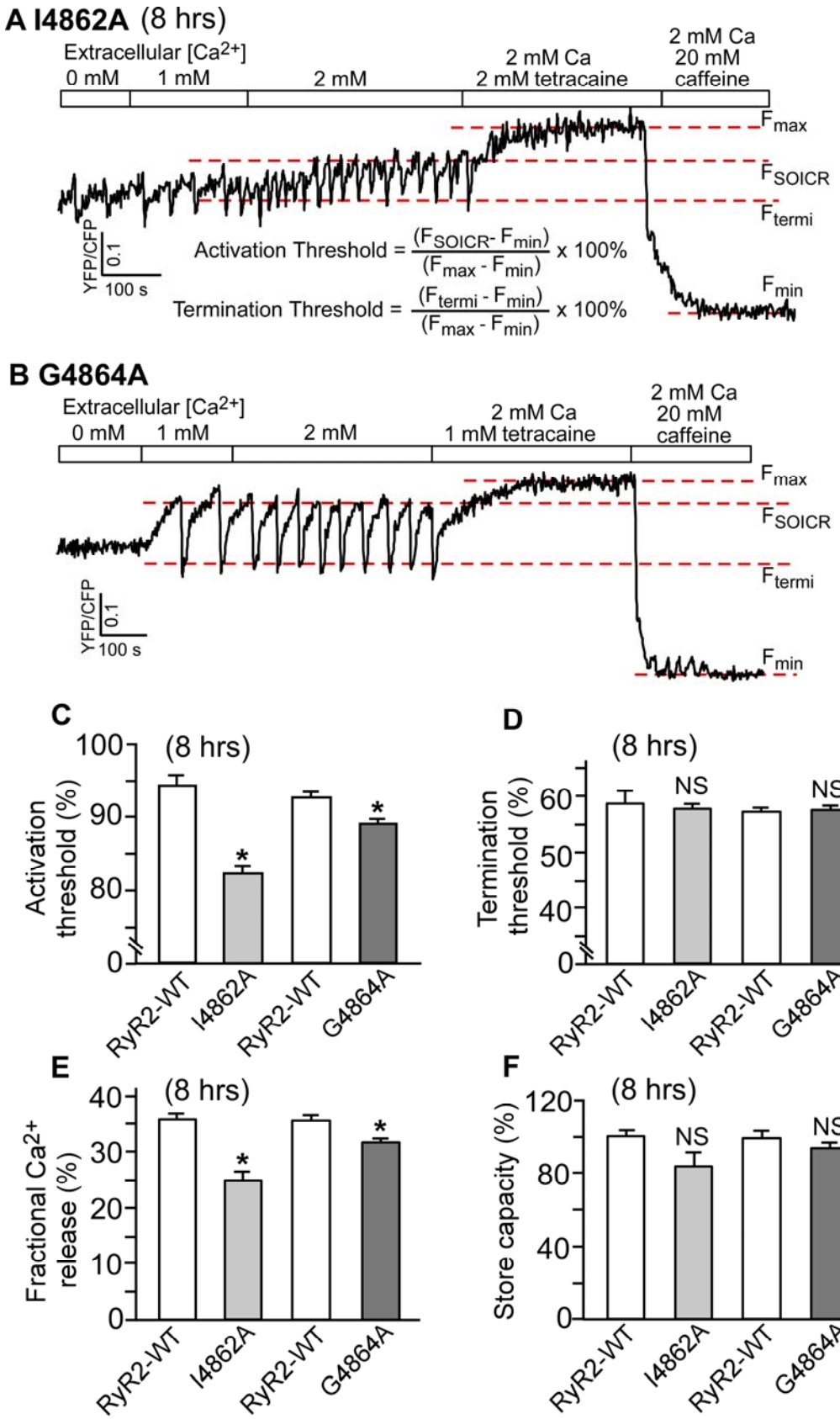
A I4862A (8 hrs)
Extracellular [Ca2+]
0 mM
1 mM
2 mM
2 mM Ca
2 mM tetracaine
2 mM Ca
20 mM
caffeine
Fmax
FSOICR
Ftermi
Fmin
YFP/CFP
0.1
100 s
Activation Threshold = (FSOICR - Fmin) / (Fmax - Fmin) x 100%
Termination Threshold = (Ftermi - Fmin) / (Fmax - Fmin) x 100%
B G4864A
Extracellular [Ca2+]
0 mM
1 mM
2 mM
2 mM Ca
1 mM tetracaine
2 mM Ca
20 mM
caffeine
Fmax
FSOICR
Ftermi
Fmin
YFP/CFP
0.1
100 s
C
(8 hrs)
Activation threshold (%)
100
90
80
0
*
*
RyR2-WT
I4862A
RyR2-WT
G4864A
D
(8 hrs)
Termination threshold (%)
60
50
40
0
NS
NS
RyR2-WT
I4862A
RyR2-WT
G4864A
E
(8 hrs)
Fractional Ca2+ release (%)
40
30
20
10
0
*
*
RyR2-WT
I4862A
RyR2-WT
G4864A
F
(8 hrs)
Store capacity (%)
120
80
40
0
NS
NS
RyR2-WT
I4862A
RyR2-WT
G4864A

Fig. 13 Effect of G4871R, E4882A and D4896A on Ca^{2+} release activation and termination

HEK293 cells expressing G4871R (A), E4882A (B) or D4896A (C) were transfected with D1ER 48 h before imaging and induced 24 h before imaging. During single cell FRET imaging, cells were perfused with elevated extracellular Ca^{2+} concentrations (0-2 mM), followed by 1 mM tetracaine and 20 mM caffeine. The activation threshold (D), termination threshold (E), fractional Ca^{2+} release (F), store capacity (G) in these cells (61-330) were determined as described in the legend to Fig. 6. Data shown are mean ± SEM (n = 5-24) (* $P < 0.01$; vs. WT).

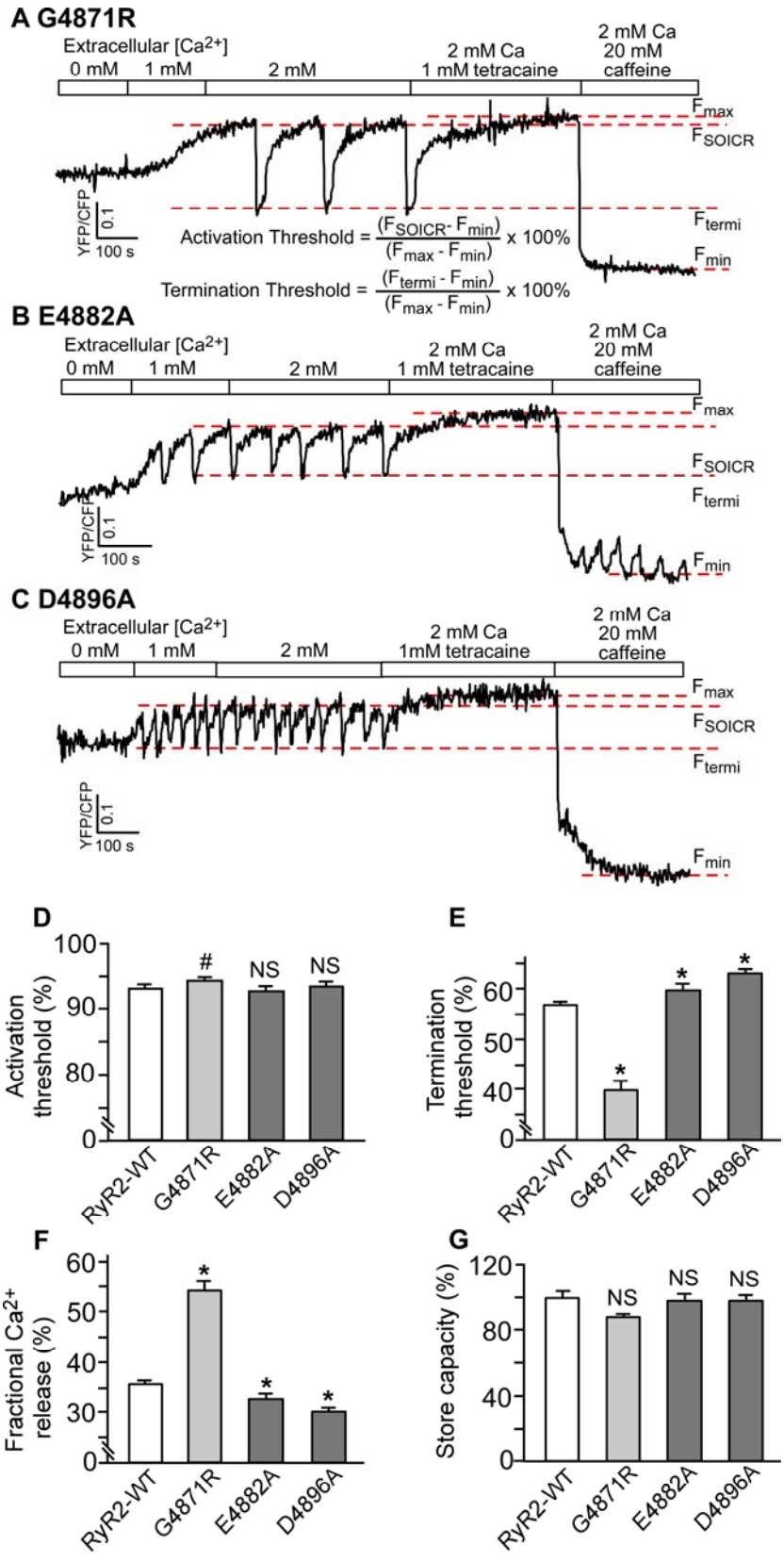
A G4871R
Extracellular [Ca2+]
0 mM
1 mM
2 mM
2 mM Ca
1 mM tetracaine
2 mM Ca
20 mM
caffeine
Fmax
FSOICR
Ftermi
Fmin
YFP/CFP
0.1
100 s
Activation Threshold = (FSOICR - Fmin) / (Fmax - Fmin) x 100%
Termination Threshold = (Ftermi - Fmin) / (Fmax - Fmin) x 100%
B E4882A
C D4896A
1mM tetracaine
D
Activation threshold (%)
E
Termination threshold (%)
F
Fractional Ca2+ release (%)
G
Store capacity (%)
RyR2-WT
G4871R
E4882A
D4896A
#
NS
*

Fig. 14 Effect of D4868A on Ca^{2+} release activation and termination

HEK293 cells expressing RyR2 WT (A) and D4868A (B) were transfected with D1ER and perfused with elevating extracellular Ca^{2+} and caffeine concentrations. Representative traces of FRET signal (YFP/CFP ratio) from single cells are shown. The activation threshold (C) and termination threshold (D) at 3 mM caffeine in RyR2 WT (95) and D4868A (92) mutant cells were calculated using the equation shown in panel A and B. Fractional Ca^{2+} release (E) and store capacity (F) were determined as described in the legend to Fig. 9. $F_{SOICR\ (3)}$ and $F_{termi\ (3)}$ indicated the FRET level at which Ca^{2+} release occurs and terminates in the presence of 3 mM caffeine. Data shown are mean ± SEM (n = 5) (* $P < 0.01$; $^{\#}$ $P < 0.05$; vs. WT).

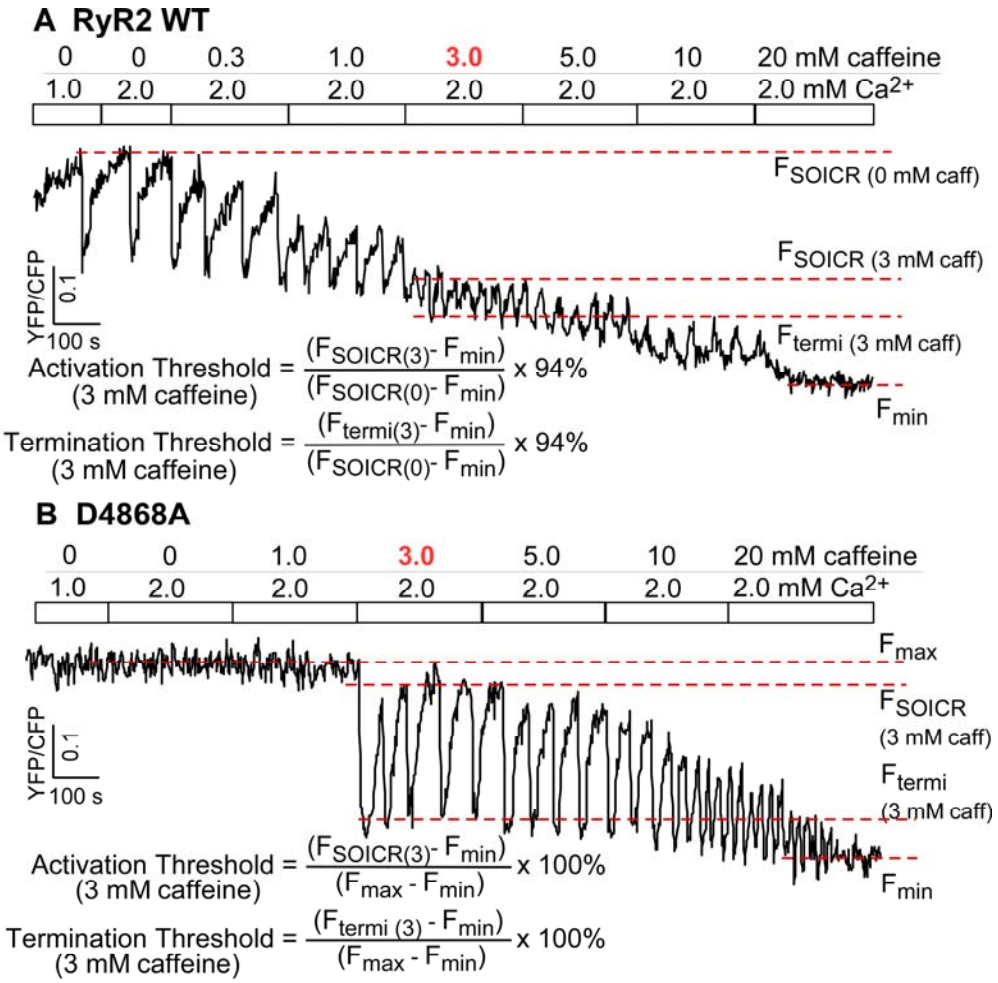
A RyR2 WT
0 0 0.3 1.0 3.0 5.0 10 20 mM caffeine
1.0 2.0 2.0 2.0 2.0 2.0 2.0 2.0 mM Ca2+
FSOICR (0 mM caff)
FSOICR (3 mM caff)
Ftermi (3 mM caff)
Fmin
YFP/CFP
0.1
100 s
Activation Threshold = (FSOICR(3)- Fmin) / (FSOICR(0)- Fmin) x 94%
(3 mM caffeine)
Termination Threshold = (Ftermi(3)- Fmin) / (FSOICR(0)- Fmin) x 94%
(3 mM caffeine)
B D4868A
0 0 1.0 3.0 5.0 10 20 mM caffeine
1.0 2.0 2.0 2.0 2.0 2.0 2.0 mM Ca2+
Fmax
FSOICR (3 mM caff)
Ftermi (3 mM caff)
Fmin
YFP/CFP
0.1
100 s
Activation Threshold = (FSOICR(3)- Fmin) / (Fmax - Fmin) x 100%
(3 mM caffeine)
Termination Threshold = (Ftermi (3) - Fmin) / (Fmax - Fmin) x 100%
(3 mM caffeine)

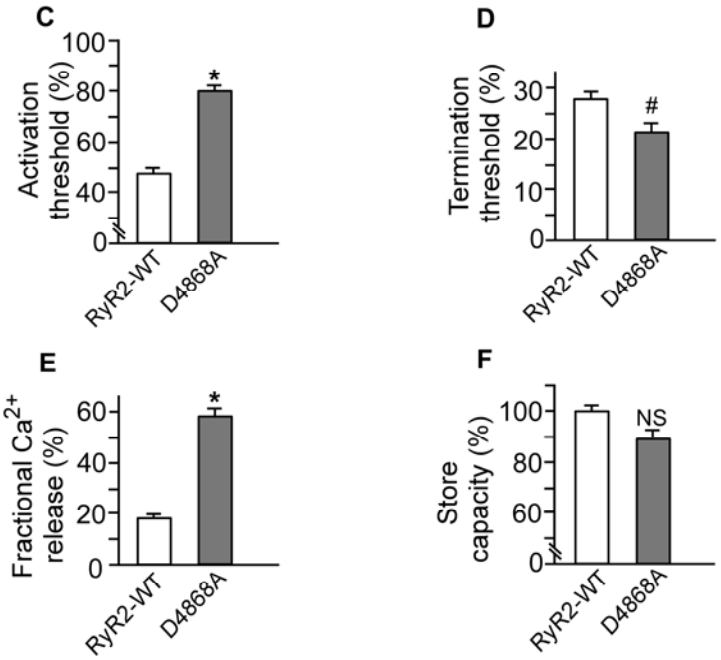
C
Activation threshold (%)
100
80
60
40
0
*
RyR2-WT
D4868A
D
Termination threshold (%)
30
20
10
0
#
RyR2-WT
D4868A
E
Fractional Ca2+ release (%)
60
40
20
0
*
RyR2-WT
D4868A
F
Store capacity (%)
100
80
60
0
NS
RyR2-WT
D4868A

E4872A. It reduced rather than elevated the termination threshold (21% Vs. 28% in WT) ($P<0.05$) (Figs. 14 A,B,D). Consequently, the fractional release triggered by 3mM caffeine was markedly increased in cells expressing D4868A (59% Vs.18% in WT). There were no significant differences in the store capacity between WT and D4868A (Fig. 14F). Interestingly, this result indicates that the activation and termination thresholds for Ca^{2+} release can be regulated in an opposite manner.

3.3 Summary

While the mechanism of Ca^{2+} release activation has been intensively studied in the past decades, the mechanism of Ca^{2+} release termination remains undefined. It has been suggested that luminal Ca^{2+} is responsible for Ca^{2+} release termination. We have previously identified a luminal Ca^{2+} sensor critical in channel activation and gating. In this study, whether this luminal Ca^{2+} sensor is also involved in Ca^{2+} release termination and the molecular basis of luminal Ca^{2+} dependent termination were investigated.

A simple system was established using D1ER to readily study the luminal Ca^{2+} dynamics in HEK293 cells expressing RyR2 WT and mutants. Taking advantage of this system, a systematic study of mutations in the pore-forming region, which are crucial for luminal Ca^{2+} sensing and channel gating, was carried out. It was found that a critical luminal Ca^{2+} sensing residue E4872A increased both SOICR activation and termination thresholds, whereas A4869G, Q4876A, F4870A, V4880A and K4881A decreased both thresholds. Furthermore, G4871R, E4882A and D4896A significantly altered the Ca^{2+} release termination threshold, but they had little impact on Ca^{2+} release activation. In contrast, the I4862A and G4864A mutations mainly enhanced the Ca^{2+} release activation

without altering the Ca^{2+} release termination. Taken together, these results indicate that mutations in the pore-forming region can alter either the activation threshold or the termination threshold or both. Therefore, the pore-forming region of RyR2 is a key determinant of both luminal Ca^{2+}-dependent activation and termination. Further, these results also indicate that the pathways for Ca^{2+} release activation and termination are distinct but overlap.

CHAPTER IV: ROLE OF RYR2 MODULATORS IN CALCIUM RELEASE ACTIVATION AND TERMINATION

4.1 Introduction

It is clear that the pore-forming region of RyR2 represents an important determinant of both Ca^{2+} release activation and termination. Functional and biochemical studies have shown that RyR2 directly interacts with a number of physiological modulators, such as CaM, FKBP12.6, Ca^{2+} and CaMKII [324,325]. It is likely that these RyR2 regulators also play a critical role in modulating the Ca^{2+} release process.

Both apoCaM and Ca^{2+}-CaM have been reported to bind to and dissociate from RyR2 in a time scale of seconds to minutes [198,201]. Although CaM is thought to be an inhibitor of RyR2 based on single channel studies, the physiological role of CaM remains not well understood [49,199,200]. The CaM binding domain (CaMBD) (residues 3583-3603) in RyR2 has been identified. Deletion of this CaMBD completely abolishes CaM binding to RyR2, as revealed by [^{35}S]CaM binding assays, and the CaM inhibitory effect on RyR2 at single channel level [200]. More interestingly, this CaMBD was suggested to directly interact with other domains in RyR2 [206,326], indicating its potential role in regulating the channel via domain-domain interactions.

FKBP12.6 is a ligand tightly bound to RyR2 with a high affinity [179,327,328]. Nevertheless, its role in regulating RyR2 is debatable. Early studies suggested that dissociation of FKBP12.6 from RyR2 by immunosuppressants such as FK506 activates RyR2 channels and induces subconductance states [212-214]. On the contrary, later findings showed that the removal of FKBP12.6 neither influences the activity of RyR2 nor generates subconductance states [175,216,217]. Whether FKBP12.6-RyR2 interaction is regulated by RyR2 phosphorylation is also controversial [176,178,179]. Overall, the functional role of FKBP12.6 still remains to be determined.

Cytosolic Ca^{2+}, as the primary activator of CICR, was found to activate the channel at low concentrations and to inhibit the channel at high concentrations. It is not known whether physiological concentrations of Ca^{2+} that sensitize the channel to activation would affect the inactivation of the channel as well.

The molecular basis and functional consequences of phosphorylation of RyR2 by PKA is becoming clear [180,181], whereas the impact of phosphorylation on RyR2 by CaMKII is still controversial. CaMKII phosphorylation has been reported to increase [173,186-188] or decrease [189,190] the sensitivity of the RyR2 channel to Ca^{2+}.

Impaired interactions of RyR2 with these regulators have also been shown to cause or affect the development of cardiac disease as a result of altered SR Ca^{2+} release. For instance, knock-in mice harboring CaM binding deficient RyR2 mutant [50] and FKBP12.6 null mice [329] both displayed cardiac hypertrophy and abnormal Ca^{2+} release. Transgenic CaMKIIδc overexpression mice exhibited heart failure and impaired Ca^{2+} handling [186]. On the other hand, reduced CaMKII activity normalized cardiac function and rescued disease phenotypes [330-333]. It is unclear, however, whether abnormal regulation of RyR2 by these RyR2-interacting proteins affects Ca^{2+} release primarily by modulating the activation or the termination aspect of Ca^{2+} release. In the present study, it was found that FKBP12.6 and CaM both promote Ca^{2+} release termination without changing the activation of Ca^{2+} release. In addition, the CaMBD of RyR2 itself was found to be involved in the regulation of Ca^{2+} release activation and termination. Cytosolic Ca^{2+} is capable of affecting both the activation and termination thresholds, whereas CaMKII targets the activation aspect of Ca^{2+} release only. These findings indicate that, in addition to activation, Ca^{2+} release termination is a common target for RyR2 modulators, and that

Ca^{2+} release activation and termination can be altered by various regulatory proteins and factors respectively.

4.2 Results

4.2.1 Effect of CaM and CaMBD on Ca^{2+} release activation and termination

4.2.1.1 Ca^{2+}-CaM inhibits Ca^{2+} release by increasing the threshold for Ca^{2+} release termination

To test whether CaM affect ER Ca^{2+} release, HEK293 cells expressing RyR2 were transfected with CaM wt and ER luminal Ca^{2+} dynamics in these cells were monitored by Ca^{2+} imaging. The effect of CaM on SOICR is shown in Fig. 16B. Co-expression of CaM in RyR2-expressing HEK293 cells had no effect on the activation threshold (Fig. 16D), but it significantly increased the termination threshold (65% vs 57% in control, $P < 0.01$) (Fig. 16E). As a result, the fractional Ca^{2+} release during SOICR was significantly reduced in HEK293 cells transfected with CaM (29%) than in control cells (37%) ($P < 0.01$) (Fig.16F).

CaM contains 4 EF-hand Ca^{2+} binding sites. To determine whether Ca^{2+} binding to these sites is required for its action on Ca^{2+} release termination, a Ca^{2+} binding mutant of CaM, CaM (1-4), was employed. In CaM (1-4), all 4 Ca^{2+} binding sites have been mutated. In contrast to co-expression of CaM wt, co-expression of the CaM (1-4) mutant significantly reduced the termination threshold (49%) compared with non-transfected cells (57%) (Fig. 16C,E) ($P<0.01$). As a result, fractional Ca^{2+} release was enhanced in cells transfected with CaM (1-4) (44% vs 37% in control, $P < 0.01$) (Fig. 16F). There were no significant differences in the store capacity between the control and the CaM or

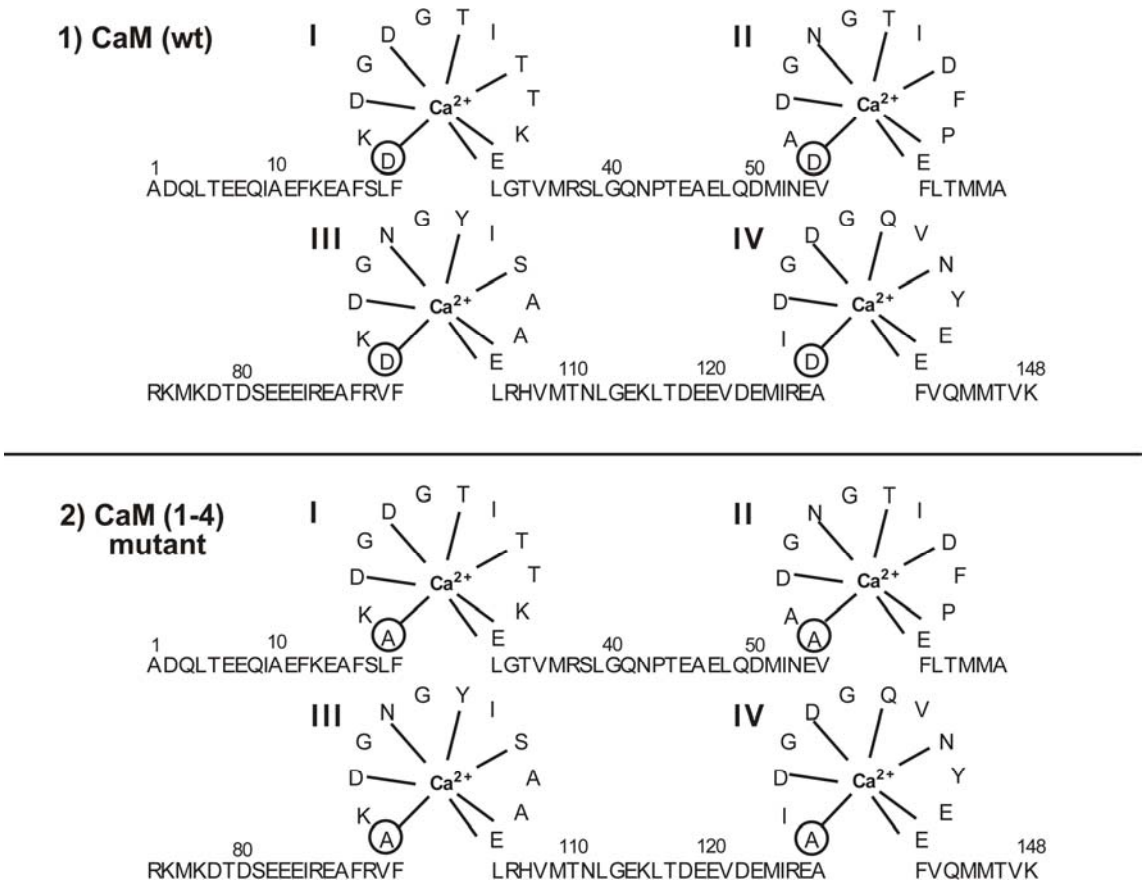

Fig. 15 Construction of a CaM mutant that lacks 4 Ca^{2+} binding sites

CaM(1-4) mutant: aspartates 20, 56, 93, and 129 in Ca^{2+} binding loops I-IV were all mutated to alanine.

Fig. 16 Co-expression of CaM or CaM (1-4) alters the threshold for Ca^{2+} release termination

HEK293 cells expressing RyR2 WT were co-transfected with D1ER and CaM or CaM (1-4). During single cell FRET imaging, cells were perfused with elevated extracellular Ca^{2+} concentrations (0-2 mM), followed by 1 mM tetracaine and 20 mM caffeine (A, B). The activation threshold (C), termination threshold (D), fractional Ca^{2+} release (E), store capacity (F) in these cells and non-transfected control cells (88-150) were determined as described in the legend to Fig. 6. Data shown are mean ± SEM (n = 4-10) (* $P < 0.01$; vs. WT).

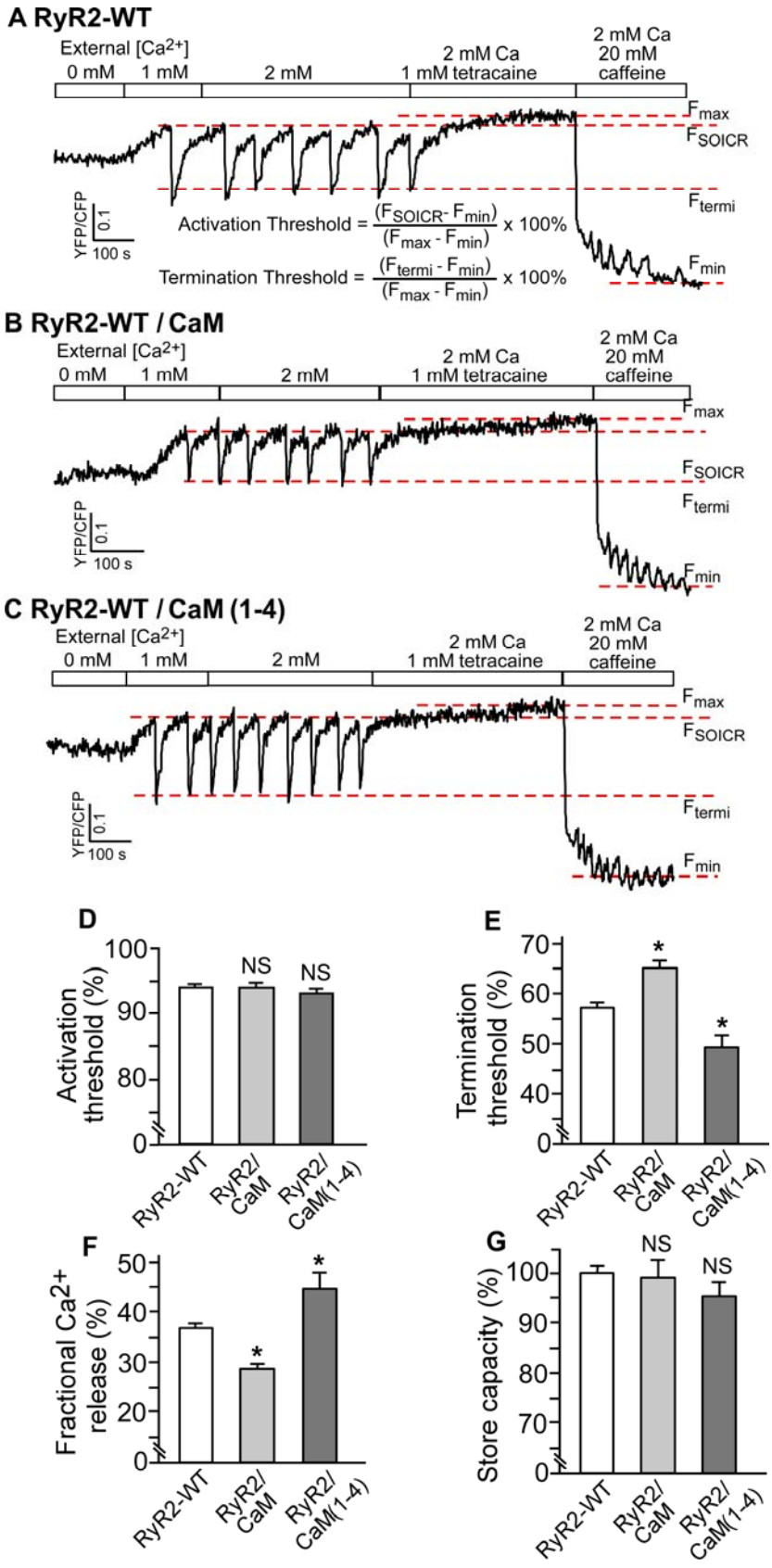
A RyR2-WT
External [Ca2+]
0 mM
1 mM
2 mM
2 mM Ca
1 mM tetracaine
2 mM Ca
20 mM
caffeine
Fmax
FSOICR
Ftermi
Fmin
YFP/CFP
0.1
100 s
Activation Threshold = (FSOICR - Fmin) / (Fmax - Fmin) x 100%
Termination Threshold = (Ftermi - Fmin) / (Fmax - Fmin) x 100%
B RyR2-WT / CaM
C RyR2-WT / CaM (1-4)
D
Activation threshold (%)
NS
NS
E
Termination threshold (%)
F
Fractional Ca2+ release (%)
G
Store capacity (%)
RyR2-WT
RyR2/ CaM
RyR2/ CaM(1-4)

CaM (1-4) co-expressing cells (Fig. 16G). Note that endogenous CaM is expressed in HEK293 cells. Therefore, in Figs. 16C,E, weakened Ca^{2+} release termination is probably due to suppression of the endogenous CaM by overexpression of CaM (1-4). In addition, the inhibitory effect of CaM on Ca^{2+} release termination may have been underestimated if we simply compare the termination thresholds in CaM wt transfected and non-transfected cells (a change of 8% in termination threshold). The effect of CaM on termination is actually more potent based on the comparison of the Ca^{2+} release termination threshold in cells overexpressing CaM wt with that in cells overexpressing the dominant negative CaM (1-4) (a change of 15% in termination threshold).

Taken together, these observations suggest that CaM inhibits Ca^{2+} release by raising the threshold for Ca^{2+} release termination without affecting the activation threshold. Meanwhile, unlike CaM wt, the Ca^{2+}-insensitive mutant of CaM is unable to enhance Ca^{2+} release termination, indicating that Ca^{2+} binding to CaM is required for its action on Ca^{2+} release termination.

4.2.1.2 Effect of CaM on the termination of Ca^{2+} release is mediated by RyR2

Since CaM has a number of targets and is involved in a wide range of cellular processes, it is possible that the altered termination threshold observed above is unrelated to the direct binding of CaM to RyR2, but is due to some complicated remodeling caused by overexpression of CaM wt or CaM (1-4). To determine whether CaM modulates the termination of Ca^{2+} release in HEK293 cells by directly interacting with RyR2, we generated a HEK293 cell line expressing a CaM-binding deficient mutant of RyR2, RyR2-Del-3583-3603, in which the CaMBD (amino acids 3583-3603) in RyR2 has been deleted. Then the impacts of CaM wt and CaM (1-4) on Ca^{2+} release in cells expressing

RyR2-Del-3583-3603 were assessed. As shown in Fig. 17, deletion of the CaM binding site in RyR2 significantly lowered the termination threshold (32% vs 57% in control, $P < 0.01$) (Fig. 17A,E), but had no effect on the activation threshold (Figs. 17A,D). As a result, the fractional Ca^{2+} release is significantly increased (62% Vs. 37% in WT) ($P < 0.01$) (Fig. 17F). Furthermore, co-expression of CaM wt or CaM (1-4) in HEK293 cells expressing RyR2-del(3583-3603) had no effect on either the termination threshold or the activation threshold for Ca^{2+} release (Figs.17 B,C,D,E). Thus, the termination or activation of Ca^{2+} release in HEK293 cells expressing the CaM binding mutant of RyR2 is no longer modulated by CaM wt or CaM (1-4). These observations indicate that the action of CaM on Ca^{2+} release termination is mediated by RyR2, particularly by the CaMBD of RyR2.

4.2.1.3 The CaMBD of RyR2 itself is important for Ca^{2+} release activation and termination irrespective of its CaM binding

It is clear that the CaMBD of RyR2 mediates the action of CaM in Ca^{2+} release termination by providing the binding site for CaM. However, it is unclear whether the CaMBD of RyR2 itself is important for the Ca^{2+} release process unrelated to its CaM binding function. To this end, the impact of a number of CaMBD mutations on Ca^{2+} release was assessed. These mutations, including W3587A/L3591A/F3603A triple mutation and each single mutation, affect CaM binding to different extents [200].

Similar to Del-3583-3603, W3587A/L3591A/F3603A (33%), W3587A (34%) and L3591A (40%), greatly reduced the termination threshold compared with WT (57%), while they hardly changed the activation threshold (Figs. 18A,B,C,D,E,). Consequently, fractional release in Del-3583-3603 (62%), W3587A/L3591A/F3603A (62%), W3587A

(60%) and L3591A (56%) were all increased in comparison with WT (37%) (Figs. 18A,B,C,F, & Figs. 17A,F). Interestingly, Del-3583-3603 and W3587A/L3591A/F3603A, which fully abolished the binding of CaM to RyR2, reduced the termination threshold to the same level as W3587A, which only partially eliminated CaM binding. These observations raise the possibility that W3587A and other mutations may cause allosteric effects on RyR2 in addition to the failure of CaM binding. Alternatively, delayed termination in these deletion/mutations may arise from the combined effect of dissociation of CaM and conformational changes in RyR2.

As F3603A showed no Ca^{2+} oscillation at 2 mM Ca^{2+}, 1 mM caffeine was applied to trigger SOICR. Similar to other mutations, F3603A also delayed the Ca^{2+} release termination (27% vs. 37%) and generated a large amount of fractional release (61%) in contrast to WT (33%) (Figs. 19 A,B,D,E). Note that in addition to the change of termination threshold, F3603A mutation caused an unique effect on RyR2 with increased activation threshold (Figs. 19 A,B,C). This is unlikely due to deficient binding of CaM since the change in activation threshold was not observed in cells expressing the Del-3583-3603, which completely abolishes CaM binding. These observations suggest that the CaMBD may also be involved in Ca^{2+} release activation. Taken together, these data indicate that the CaMBD of RyR2 itself is important for the activation and termination of Ca^{2+} release irrespective of its CaM binding.

4.2.2 FKBP12.6 accelerates Ca^{2+} release termination

The role of FKBP12.6 in RyR2 channel function has been the subject of intensive investigations but it is still highly controversial. Interestingly, cardiac myocytes from FKBP12.6 null mice display a significant increase in Ca^{2+} spark amplitude and duration,

Fig. 17 Effect of CaM and CaM (1-4) on SOICR activation and termination thresholds in cells expressing RyR2 Del-3583-3603

HEK293 cells expressing RyR2 Del-3583-3603 were co-transfected with D1ER and CaM or CaM (1-4). During single cell FRET imaging, cells were perfused with elevated extracellular Ca^{2+} concentrations (0-2 mM), followed by 1 mM tetracaine and 20 mM caffeine (A, B, C). The activation threshold (D), termination threshold (E), fractional Ca^{2+} release (F), store capacity (G) in these cells and non-transfected control cells (51-150) were determined as described in the legend to Fig. 6. Data shown are mean ± SEM (n = 4-10) (* $P < 0.01$; vs. WT).

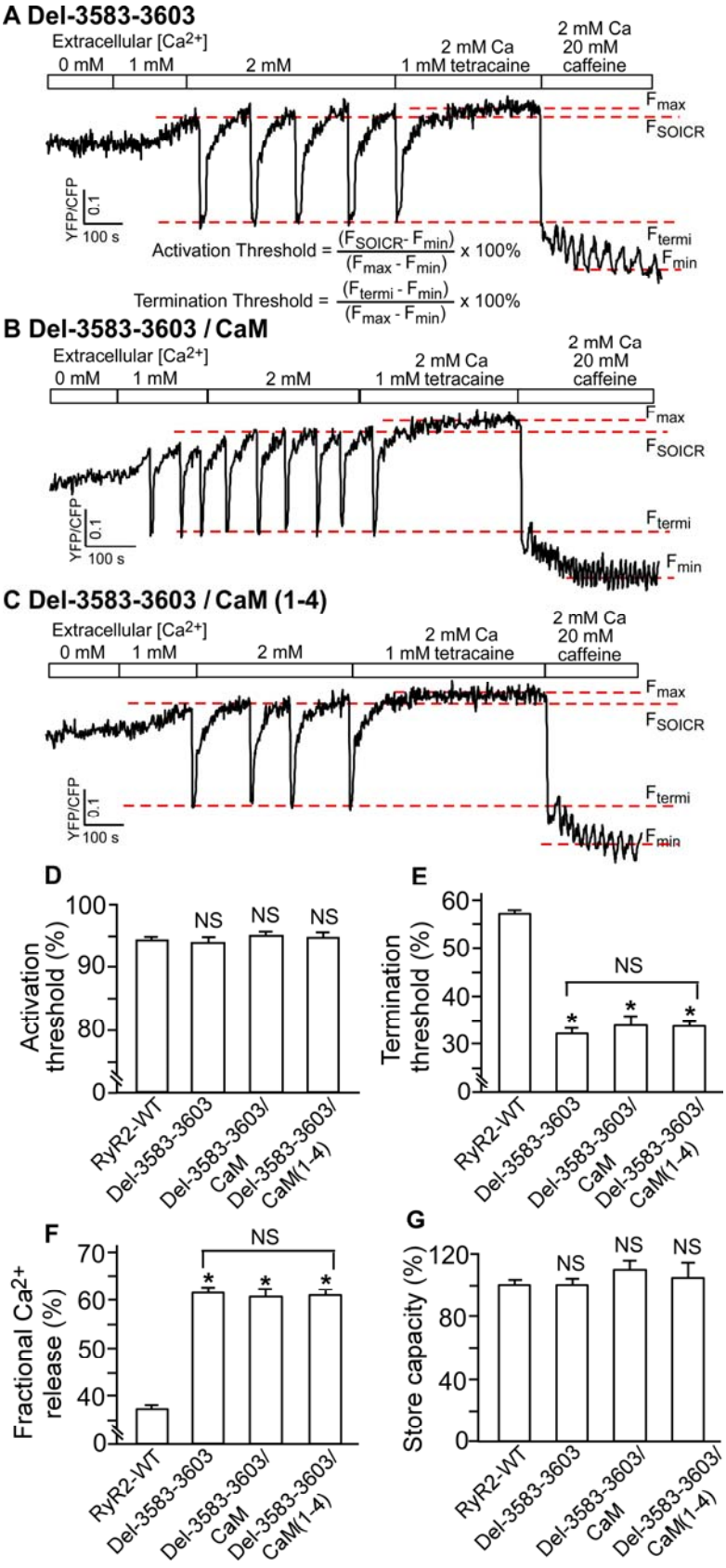
A Del-3583-3603
Extracellular [Ca2+]
0 mM
1 mM
2 mM
2 mM Ca
1 mM tetracaine
2 mM Ca
20 mM
caffeine
Fmax
FSOICR
YFP/CFP
0.1
100 s
Ftermi
Fmin
Activation Threshold = (FSOICR - Fmin) / (Fmax - Fmin) x 100%
Termination Threshold = (Ftermi - Fmin) / (Fmax - Fmin) x 100%
B Del-3583-3603 / CaM
C Del-3583-3603 / CaM (1-4)
D
Activation threshold (%)
NS
E
Termination threshold (%)
F
Fractional Ca2+ release (%)
G
Store capacity (%)
RyR2-WT
Del-3583-3603
Del-3583-3603/ CaM
Del-3583-3603/ CaM(1-4)

Fig. 18 Effect of W3587A/L3591A/F3603A, W3587A and L3591A on Ca^{2+} release activation and termination

D1ER FRET signals were recorded in HEK293 cells expressing WT, W3587A/L3591A/F3603A (A) W3587A (B) or L3591A (C) mutant. Cells were perfused with elevated extracellular Ca^{2+} concentrations (0-2 mM), followed by 1 mM tetracaine and 20 mM caffeine. The activation threshold (D), termination threshold (E), fractional Ca^{2+} release (F), store capacity (G) in these cells (70-177) were determined as described in the legend to Fig. 6. Data shown are mean ± SEM (n = 5-10) (* $P < 0.01$; vs. WT).

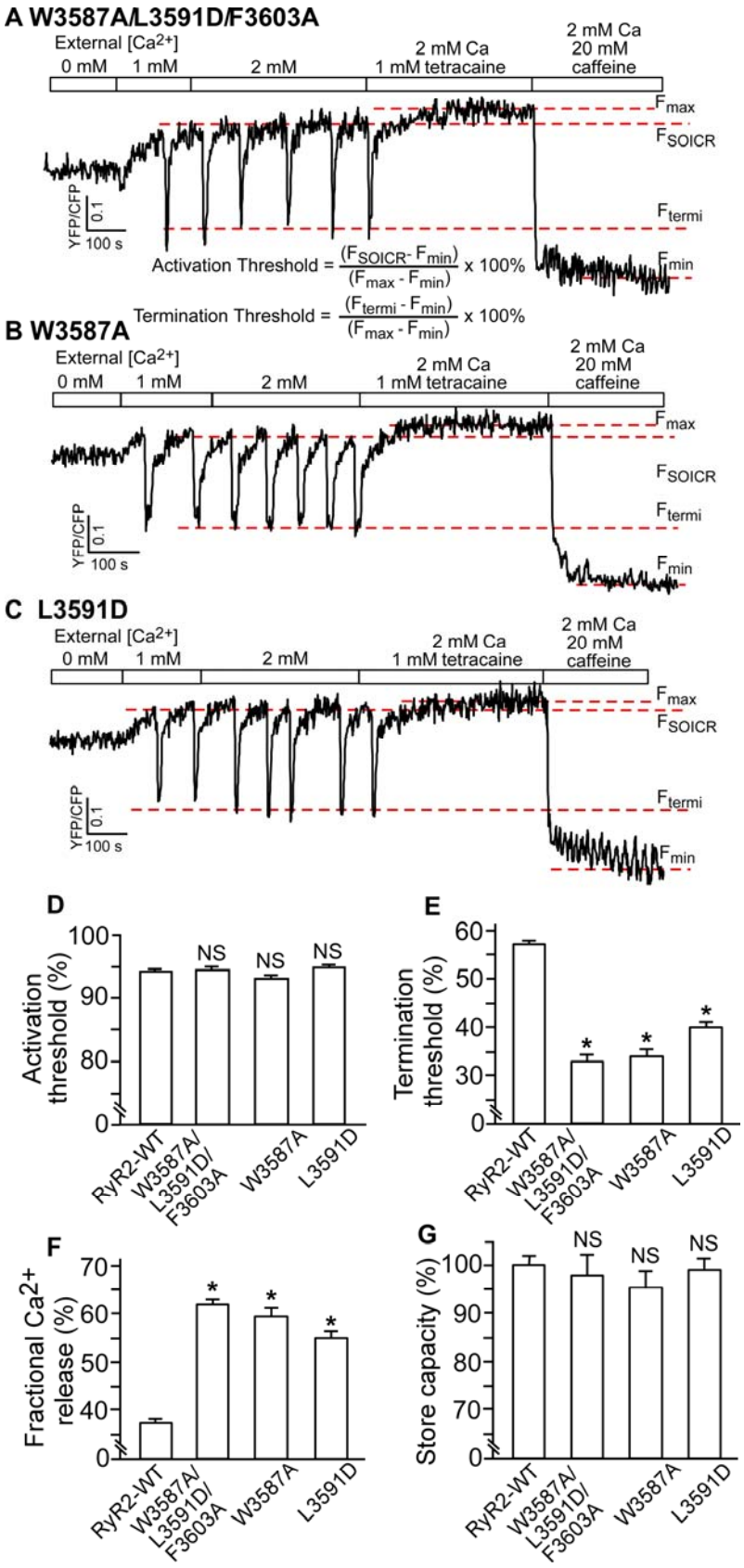
A W3587A/L3591D/F3603A
External [Ca2+]
0 mM
1 mM
2 mM
2 mM Ca
1 mM tetracaine
2 mM Ca
20 mM
caffeine
Fmax
FSOICR
Ftermi
Fmin
YFP/CFP
0.1
100 s
Activation Threshold = (FSOICR - Fmin) / (Fmax - Fmin) x 100%
Termination Threshold = (Ftermi - Fmin) / (Fmax - Fmin) x 100%
B W3587A
C L3591D
D
Activation threshold (%)
NS
E
Termination threshold (%)
*
F
Fractional Ca2+ release (%)
G
Store capacity (%)
RyR2-WT
W3587A/ L3591D/ F3603A
W3587A
L3591D

Fig. 19 Effect of F3603A on Ca^{2+} release activation and termination

D1ER FRET signals were recorded in HEK293 cells expressing WT (A) and F3603A (B) mutant. These cells (103-112) were perfused with elevated extracellular Ca^{2+} concentrations (0-2 mM), followed by 1 mM caffeine and 20 mM caffeine. The SOICR activation threshold (C), termination threshold (D), in these cells were calculated as indicated in panel A and B from F_{max} (maximum FRET level), $F_{SOICR\ (1\ or\ 0)}$ (FRET level at which SOICR occurs in the presence of 1 or 0 mM caffeine), $F_{termi\ (1)}$ (FRET level at which SOICR occurs in the presence of 1 mM caffeine) and F_{min} (minimum FRET level). Data shown are mean ± SEM (n = 4-5) (* $P < 0.01$; vs. WT).

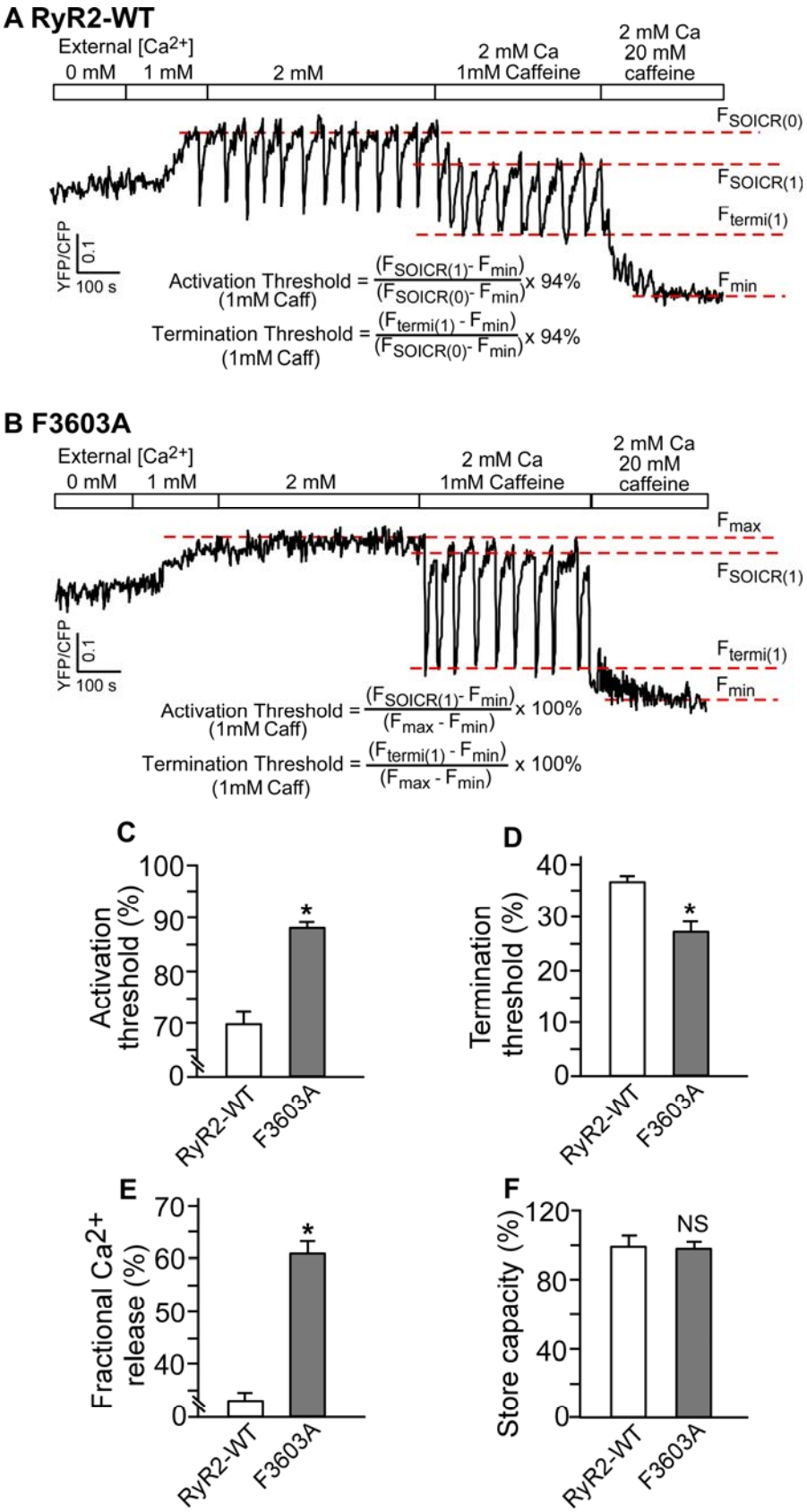
A RyR2-WT
External [Ca2+]
0 mM
1 mM
2 mM
2 mM Ca
1mM Caffeine
2 mM Ca
20 mM
caffeine
FSOICR(0)
FSOICR(1)
Ftermi(1)
Fmin
YFP/CFP
0.1
100 s
Activation Threshold = (FSOICR(1)- Fmin) / (FSOICR(0)- Fmin) x 94%
(1mM Caff)
Termination Threshold = (Ftermi(1) - Fmin) / (FSOICR(0)- Fmin) x 94%
(1mM Caff)
B F3603A
External [Ca2+]
0 mM
1 mM
2 mM
2 mM Ca
1mM Caffeine
2 mM Ca
20 mM
caffeine
Fmax
FSOICR(1)
Ftermi(1)
Fmin
YFP/CFP
0.1
100 s
Activation Threshold = (FSOICR(1)- Fmin) / (Fmax - Fmin) x 100%
(1mM Caff)
Termination Threshold = (Ftermi(1) - Fmin) / (Fmax - Fmin) x 100%
(1mM Caff)
C
Activation threshold (%)
100
90
80
70
0
*
RyR2-WT
F3603A
D
Termination threshold (%)
40
30
20
10
0
*
RyR2-WT
F3603A
E
Fractional Ca2+ release (%)
70
60
50
40
0
*
RyR2-WT
F3603A
F
Store capacity (%)
120
80
40
0
NS
RyR2-WT
F3603A

indicating the role of FKBP12.6 in the regulation of Ca^{2+} release process [329]. However, how the removal of FKBP12.6, which does not affect the activation and conductance of the RyR2 channel, could lead to prolonged openings is puzzling and interesting.

Considering the direct role of Ca^{2+} release termination in determining the size of Ca^{2+} release, it is possible that FKBP 12.6 affects the termination of Ca^{2+} release. To test this hypothesis, HEK293 cells expressing RyR2 WT were transfected with or without FKBP12.6. It was found that co-expression of FKBP12.6 significantly increased the termination threshold (Fig. 20A,C) ($P<0.01$). In other words, FKBP 12.6 makes Ca^{2+} release termination occur at a higher luminal Ca^{2+} level. Interestingly, co-expression of FKBP12.6 did not seem to alter the threshold for SOICR activation (Fig. 20.B), which is consistent with our previous observations that the removal of FKBP12.6 does not affect Ca^{2+} activation, conduction, or the propensity for spontaneous Ca^{2+} release [217]. This result suggests that the functional role of FKBP12.6 is to accelerate Ca^{2+} release termination.

4.2.3 Cytosolic Ca^{2+} reduces the thresholds for both Ca^{2+} release activation and termination

Cytosolic Ca^{2+} plays a central role in the CICR process. Physiological Ca^{2+} at the concentrations of 0.1~10μM activates RyR2. However, whether it sensitizes the channel by promoting the Ca^{2+} release activation or by delaying the Ca^{2+} release termination is unknown. To directly manipulate the concentrations of cytosolic Ca^{2+}, we permeabilized the plasma membranes of the HEK293 cells expressing RyR2 WT with saponin. After washing off saponin, the cells were perfused with ICM buffer containing different concentrations of Ca^{2+}. Elevating the cytosolic Ca^{2+} concentration from 50 nM to 200 nM increased the propensity for SOICR in HEK293 cells expressing RyR2 WT, as revealed

by a reduction in the Ca^{2+} release activation threshold (from 100% to 86%, calculated as described in the legend to Fig. 21), (Fig 21, A, B) ($P<0.01$). On the other hand, the threshold for Ca^{2+} release termination declined from 66% to 55% (calculated as described in the legend to Fig. 21), (Fig 21, A, C) ($P<0.01$). These observations suggest that cytosolic Ca^{2+} at physiological concentrations is able to lower both the activation and termination thresholds.

4.2.4 CaMKIIδc stimulates the activation of Ca^{2+} release

CaMKIIδc is thought to be the major isoform of CaMKII that modulates RyR2. However, the specific effect of CaMKIIδc on RyR2 is highly controversial. To study the effect of CaMKIIδc on RyR2 mediated Ca^{2+} release, constitutively active $CaMKII\delta_C$ (CA-CaMKIIδc) and D1ER were co-expressed in HEK293 cells expressing RyR2 WT. The results showed that SOICR occurred at a lower level of luminal Ca^{2+} in the presence of CA-CaMKIIδc (86%) compared with that in the absence of CA-CaMKIIδc (94%) (Fig. 22A,B,C) ($P<0.01$). Because the activation threshold was reduced and the termination threshold not altered, fractional Ca^{2+} release (activation threshold - termination threshold) was decreased (Fig. 22A,B,D,E). These results indicate that CaMKIIδc may enhance the SOICR propensity by lower the threshold for Ca^{2+} release activation, and that CaMKIIδc does not alter Ca^{2+} release termination. Notably, it is well known that CaMKIIδc is involved in multiple signaling pathways and has multiple targets in cells [334]. The observed change in Ca^{2+} release activation may not reflect the direct phosphorylation of the channel by CaMKIIδc. It may reflect some adapted alternations in the cells caused by global overexpression of CaMKIIδc. Since this condition mimics environments in failing human myocardium and in animal models of cardiac hypertrophy and heart failure, where

Fig. 20 Co-expression of FKBP12.6 increases the threshold for Ca^{2+} release termination

HEK293 cells expressing RyR2 WT were co-transfected with D1ER and FKBP 12.6. During single cell FRET imaging, cells were perfused with elevated extracellular Ca^{2+} concentrations (0-2 mM), followed by 1 mM tetracaine and 20mM caffeine (A). The activation threshold (B), termination threshold (C), fractional Ca^{2+} release (D), store capacity (E) in transfected cells (62) and non-transfected control cells (150) were determined as described in the legend to Fig. 6. Data shown are mean ± SEM (n = 4-10) (* $P < 0.01$; vs. WT).

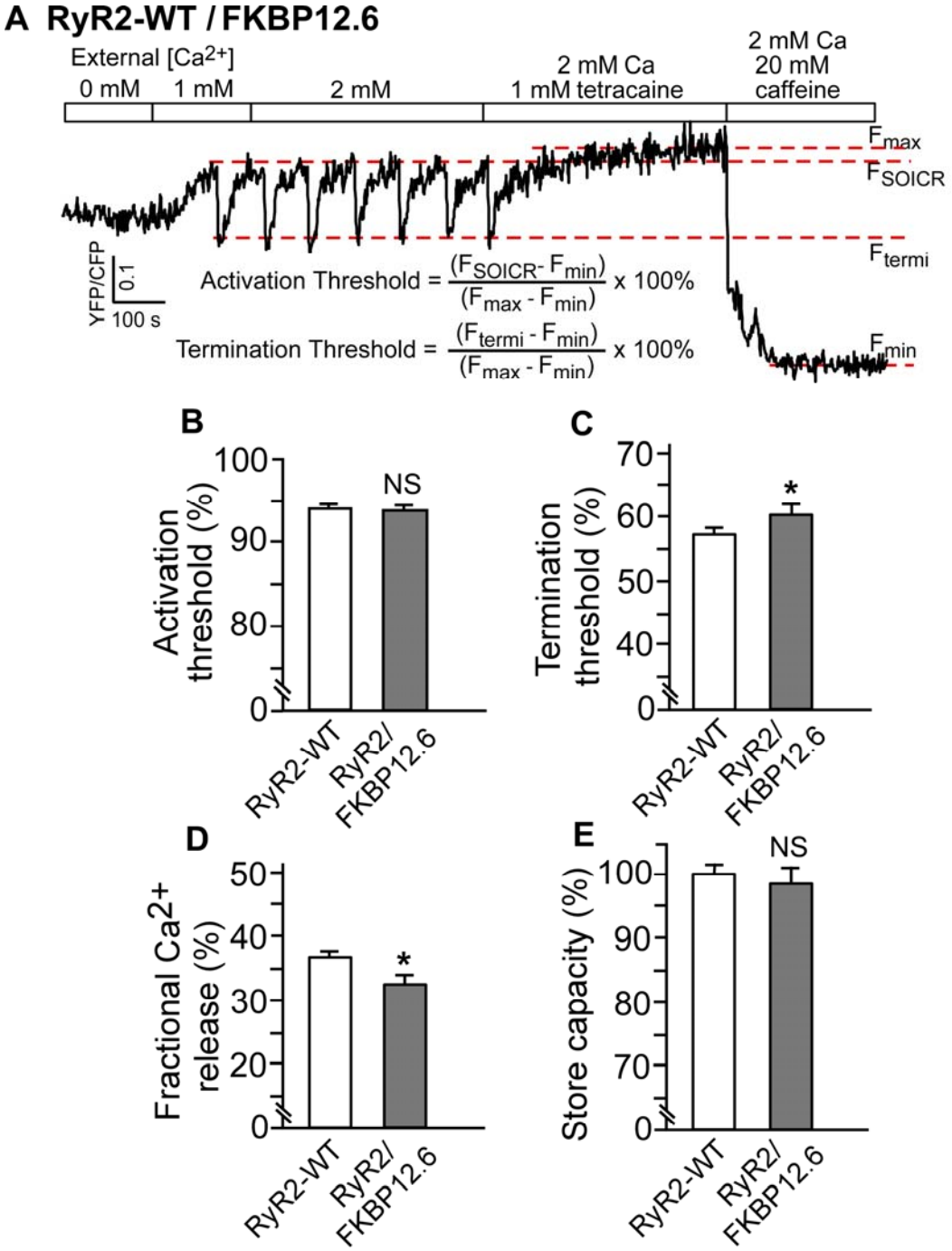
A RyR2-WT / FKBP12.6
External [Ca2+]
0 mM
1 mM
2 mM
2 mM Ca
1 mM tetracaine
2 mM Ca
20 mM
caffeine
Fmax
FSOICR
Ftermi
Fmin
YFP/CFP
0.1
100 s
Activation Threshold = (FSOICR - Fmin) / (Fmax - Fmin) x 100%
Termination Threshold = (Ftermi - Fmin) / (Fmax - Fmin) x 100%
B
Activation threshold (%)
NS
C
Termination threshold (%)
*
D
Fractional Ca2+ release (%)
*
E
Store capacity (%)
NS
RyR2-WT
RyR2/ FKBP12.6

Fig. 21 Effect of cytosolic Ca^{2+} on the SOICR activation and termination thresholds

HEK293 cells expressing RyR2 WT (118) were permeabilized and perfused with ICM buffer containing 50-200 nM Ca^{2+}, followed by 20 mM caffeine (A). The thresholds for activation (B) and termination (C) at each concentration were determined based on the equations indicated in panel A for $F_{SOICR\ (50\ or\ 200)}$ (FRET level at which SOICR occurs in the presence of 50 or 200 nM Ca^{2+}), $F_{termi\ (50\ or\ 200)}$ (FRET level at which Ca^{2+} release terminates in the presence of 50 or 200 nM Ca^{2+}), and F_{min} (minimum FRET). Note that Ca^{2+} release activation and termination thresholds were calculated using the maximum change of FRET signal ($F_{SOICR(50)}$ minus F_{min}) as 100% in this experiment but not the store capacity. Fractional release (D) was defined by subtracting the termination threshold from the activation threshold. Data shown are mean ± SEM (n = 15) (* $P <$ 0.01; 50 nM vs. 200 nM).

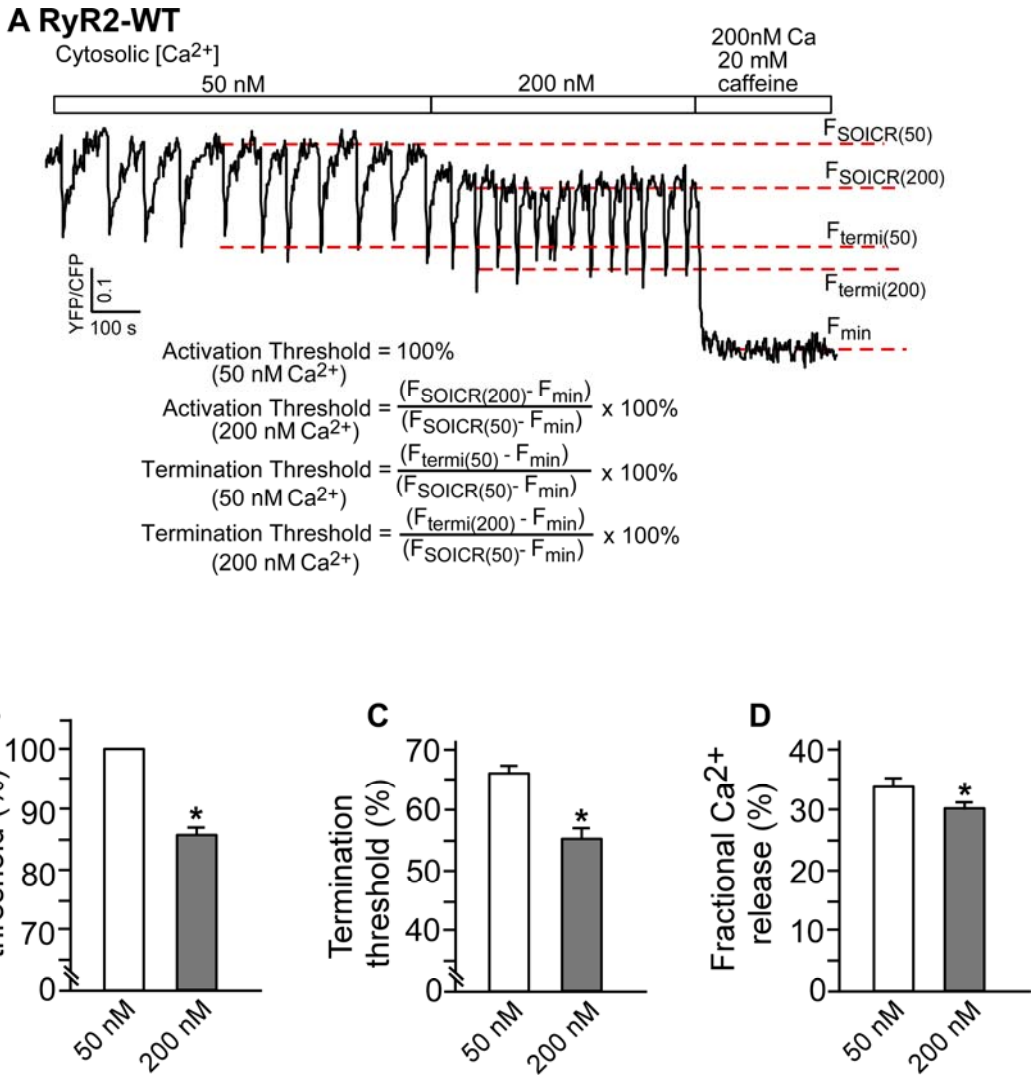
A RyR2-WT
Cytosolic [Ca2+]
50 nM
200 nM
200nM Ca
20 mM
caffeine
FSOICR(50)
FSOICR(200)
Ftermi(50)
Ftermi(200)
Fmin
YFP/CFP
0.1
100 s
Activation Threshold = 100%
(50 nM Ca2+)
Activation Threshold = (FSOICR(200)- Fmin) / (FSOICR(50)- Fmin) x 100%
(200 nM Ca2+)
Termination Threshold = (Ftermi(50) - Fmin) / (FSOICR(50)- Fmin) x 100%
(50 nM Ca2+)
Termination Threshold = (Ftermi(200) - Fmin) / (FSOICR(50)- Fmin) x 100%
(200 nM Ca2+)
B
Activation threshold (%)
100
90
80
70
0
*
50 nM
200 nM
C
Termination threshold (%)
70
60
50
40
0
*
50 nM
200 nM
D
Fractional Ca2+ release (%)
40
30
20
10
0
*
50 nM
200 nM

Fig. 22 Effect of CaMKIIδc on the SOICR activation and termination thresholds

HEK293 cells expressing RyR2 WT were co-transfected with D1ER and constitutively active CaMKIIδ_C (CA-CaMKIIδc). During single cell FRET imaging, cells were perfused with elevated extracellular Ca^{2+} concentrations (0-2 mM), followed by 1 mM tetracaine and 20mM caffeine (A, B). The activation threshold (C), termination threshold (D), fractional Ca^{2+} release (E), store capacity (F) in these cells (42) and non-transfected control cells (150) were determined as described in the legend to Fig. 6. Data shown are mean ± SEM (n = 4-10) (* $P < 0.01$; vs. WT).

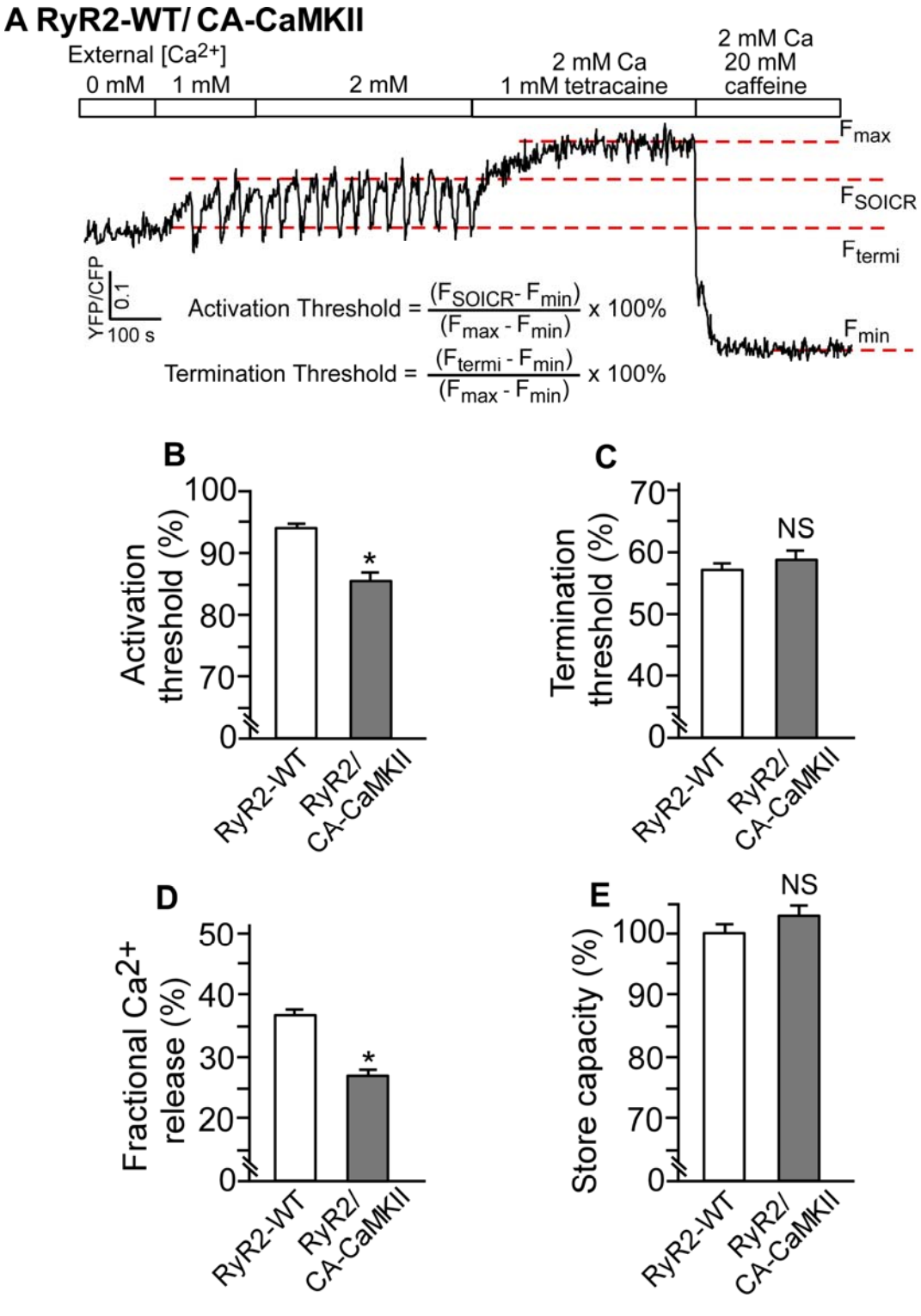
A RyR2-WT/ CA-CaMKII
External [Ca2+]
0 mM
1 mM
2 mM
2 mM Ca
1 mM tetracaine
2 mM Ca
20 mM
caffeine
Fmax
FSOICR
Ftermi
Fmin
YFP/CFP
0.1
100 s
Activation Threshold = (FSOICR - Fmin) / (Fmax - Fmin) x 100%
Termination Threshold = (Ftermi - Fmin) / (Fmax - Fmin) x 100%
B
Activation threshold (%)
RyR2-WT
RyR2/ CA-CaMKII
C
Termination threshold (%)
NS
D
Fractional Ca2+ release (%)
E
Store capacity (%)

CaMKII expression and activity are increased globally, this result may be useful for understanding the actions of CaMKII in pathological conditions.

4.3 Summary

Although numerous modulators have been found to be associated with RyR2, the functional consequences mediated by these modulators are not entirely understood. In this study, it was found that co-expression of CaM wt increased the threshold for Ca^{2+} release termination, whereas co-expression of Ca^{2+} binding deficient CaM mutant, CaM (1-4), greatly reduced the termination threshold. These results suggest that Ca^{2+}-CaM accelerates the termination of Ca^{2+} release. Enhanced Ca^{2+} release termination by CaM was not observed in HEK293 cells expressing CaM binding deficient RyR2-Del-3583-3603, indicating that the effect of CaM on Ca^{2+} release termination is mediated by RyR2. Interestingly, a deletion and a triple mutation that fully abolished the binding of CaM to RyR2 reduced the termination threshold to the same level as a single mutation in the CaMBD that only partially reduced CaM binding. Cells expressing the F3603A mutant showed an increased activation threshold, which was not observed in the deletion or mutations that fully abolished the CaM binding. Thus, it is likely that the CaMBD of RyR2 itself exerts an important influence on Ca^{2+} release activation and termination.

Several other RyR2 regulators have also been investigated. FKBP12.6, whose functional role is highly controversial, was found to attenuate ER Ca^{2+} release by elevating the termination threshold. Cytosolic Ca^{2+} sensitizes the activation and delays the termination of ER Ca^{2+} release, whereas CaMKII appears only to enhance the activation of the channel by lowering the activation threshold. These results suggest that

various RyR2 modulators regulate Ca^{2+} release activation and termination in different ways, and that Ca^{2+} release termination is a common target of physiological RyR2 regulators. Considering the controversies regarding the functional roles of RyR2 modulators, this study is significant because it reveals novel information on the functional consequences of regulation of RyR2 by these modulators at the cellular level, and establishes the link between specific RyR2 modulators and their impact on the activation and/or termination of Ca^{2+} release.

CHAPTER V: MECHANISM OF LIGNAD-DEPENDENT CONFORMATIONAL CHANGES IN THE CLAMP REGION OF RYR2

5.1 Introduction

As shown in the previous chapter, RyR is regulated by various physiological ligands, such as CaM, FKBP, CaMKII and Ca^{2+}, to ensure proper SR/ER Ca^{2+} release [324,325]. In addition, RyR is also modulated by a number of pharmacological ligands including the well known agonists, caffeine and ryanodine [335,336]. As with physiological ligands, altered RyR regulation by abnormal RyR response to pharmacological ligands has also been linked to muscle disorders such as heart failure, cardiac arrhythmias, and MH [274,335,337-340]. These RyR modulators are believed to exert their impact on channel function by inducing conformational changes in the channel, but the ligand-induced conformational changes and their functional correlation have yet to be demonstrated.

A fundamental unresolved question is how this large array of ligands with diverse structures activates the RyR channel through directly interacting with RyRs [324,335,336]. It is thought that RyR contains ligand-specific binding sites, and that ligand binding to these sites induces conformational changes in the channel that consequently lead to the opening of the channel gate and Ca^{2+} release [131-136]. Considerable efforts over the past decades have been focused on the understanding of ligand-induced conformational changes in RyR. Particularly, large conformational changes were observed in the transmembrane domain and in the four corners of the square-shaped cytoplasmic assembly, also known as clamp regions, in the 3D architecture of RyR. Substantial structural rearrangements in the clamp region, the central cytoplasmic region, and the transmembrane domain were also detected when RyR was activated by another channel ligand, PCB 95 [136]. Hence, these studies clearly demonstrate that conformational changes occur in RyR upon ligand binding.

While the transmembrane domain primarily serves as the channel conducting pore, an increasing body of evidence suggests that the cytoplasmic clamp region consisting of several key structural domains are also crucial for channel regulation and gating. The phosphorylation domain [125,126,158], central disease-causing mutation hotspot and one of the divergent regions (DR2) were all localized to this region [122,124]. Based on the spacing of the DHPR arrangement in tetrads and that of the homotetrameric RyR, the clamp region has also been implicated in the activation of RyRs by DHPRs during EC coupling in skeletal muscle [119-121,134]. The clamp region also harbors the binding sites for the natrin toxin, a cysteine-rich secretory protein isolated from snake venom, and the chloride intracellular channel protein 2 (CLIC2), both of which have been shown to modulate the activity of RyR [127,351]. Thus, studying conformational changes in the clamp region is likely to yield important insights into the mechanism of ligand dependent gating of RyR.

Although cryo-EM studies revealed ligand-induced structural rearrangements in the clamp region, little is known about the ligand dependence of these conformational changes and their correlation with function. In the present study, we employed the FRET approach to determining conformational changes in the clamp region of RyR2 upon binding with various ligands in live cells. The ligand-induced conformational changes were then correlated with the extent of Ca^{2+} release induced by the same ligand. To monitor conformational changes in the clamp region, we constructed a FRET probe in the clamp region by inserting a CFP after residue Ser-2367 and a YFP after residue Tyr-2801, both of these insertion sites have been previously mapped to the clamp region by cryo-EM [124,126]. Using this novel FRET probe, we found that caffeine, ATP, and ryanodine induced conformational changes in the clamp region and Ca^{2+} release in HEK293 cells,

whereas Ca^{2+} and 4-chloro-*m*-cresol (4-CmC) induced Ca^{2+} release but caused no detectable conformational changes in the clamp region. Our results indicate that conformational changes in the clamp region are ligand-dependent, and that RyR can be activated by different mechanisms associated with different conformational changes in the channel structure.

5.2 Results

5.2.1 Construction of a FRET probe in the clamp region of RyR2

The clamp region located at the corners of the square-shaped 3D structure of RyR has been shown to display major structural rearrangements when the channel transitions from the closed to the open state [133,134,341]. The clamp region thus represents a potential location for building a FRET-based probe for sensing the conformational changes in RyR. We have previously mapped the 3D locations of a number of GFPs inserted into different sites in the primary sequence of RyR2 [123,124,126,182,315,316]. Two of these GFPs, one inserted after residue Ser-2367 (S2367-GFP) and the other after residue Tyr-2801 (Y2801-GFP), were located close to each other (30Å center to center) in the clamp region [124,126]. Thus, Ser-2367 and Tyr-2801 represent two suitable sites for inserting a pair of fluorescent proteins to build a FRET probe in the clamp region. To this end, we inserted a CFP after residue Ser-2367 (S2367-CFP) and a YFP after residue Tyr-2801 (Y2801-YFP) to generate the dual CFP- and YFP-labeled RyR2, $RyR2_{S2367\text{-}CFP/Y2801\text{-}YFP}$ (Figs. 23A and 23B). Fig. 23C shows that $RyR2_{S2367\text{-}CFP/Y2801\text{-}YFP}$ forms a functional Ca^{2+} release channel in HEK293 cells with a caffeine response similar to that of RyR2(wt). Note that the level of Ca^{2+} release induced by 2.5 mM or 5.0 mM caffeine is lower than that induced by the

prior addition of 1.0 mM caffeine due to ER Ca^{2+} store depletion caused by the preceding cumulative additions of caffeine. To assess whether $RyR2_{S2367\text{-}CFP/Y2801\text{-}YFP}$ is capable of producing FRET, we determined its FRET efficiency by measuring the fluorescence intensity of CFP (donor) before and after bleaching YFP (acceptor) in live cells. As expected based on their close proximity in the 3D structure of RyR2, HEK293 cells expressing $RyR2_{S2367\text{-}CFP/Y2801\text{-}YFP}$ displayed a significant level of FRET with a FRET efficiency of 14.4 ± 1.1% (n=20) (Fig. 24A,C).

RyR is a homotetramer consisting of four identical subunits. It is possible that the FRET signal observed in $RyR2_{S2367\text{-}CFP/Y2801\text{-}YFP}$ results from the interaction between S2367-CFP and Y2801-YFP in the same RyR2 subunit (intra-subunit interaction) or between S2367-CFP in one subunit and Y2801-YFP in the neighboring subunit (inter-subunit interaction). To distinguish an intra-subunit from an inter-subunit interaction between the donor and acceptor in a FRET probe in tetramic RyRs, we have previously developed a co-expression approach [342]. Using the same approach, we constructed RyR2 fusion proteins with a single insertion of S2367-CFP ($RyR2_{S2367\text{-}CFP}$) or a single insertion of Y2801-YFP ($RyR2_{Y2801\text{-}YFP}$), and co-expressed $RyR2_{S2367\text{-}CFP}$ and $RyR2_{Y2801\text{-}YFP}$ in HEK293 cells. Fig. 24 shows that, unlike cells transfected with $RyR2_{S2367\text{-}CFP/Y2801\text{-}YFP}$, HEK293 cells co-transfected with $RyR2_{S2367\text{-}CFP}$ and $RyR2_{Y2801\text{-}YFP}$ displayed no detectable FRET signals (Fig. 24B,C). In other words, there is no detectable interaction between S2367-CFP of one subunit and Y2801-YFP of the neighboring subunit, indicating that the FRET signal in $RyR2_{S2367\text{-}CFP/Y2801\text{-}YFP}$ results from intra-subunit interactions. Thus, collectively, our results indicate that S2367-CFP/Y2801-YFP pair is a functional, intra-subunit FRET probe.

Fig. 23 Construction and characterization of a novel FRET pair S2367-CFP/Y2801-YFP in RyR2

(A) Schematic illustration of the linear sequence of RyR (open box) showing the three major hotspots (pink boxes) where disease-causing mutations frequently occur (CPVT, catecholaminergic polymorphic ventricular tachycardia; ARVD2, arrhythmogenic right ventricular dysplasia type 2; MH, malignant hyperthermia; CCD, central core disease). The locations of S2367-CFP (cyan box), Y2801-YFP (yellow box), the S2808 and S2814 phosphorylation sties, the cytosolic Ca^{2+} sensor, and the pore-forming segment (circles inside the open box) are also indicated. The inserted CFP and YFP are flanked by short glycine-rich linkers. (B) Locations of S2367-CFP (cyan spheres) and Y2801-YFP (yellow spheres) in the 3D architecture of RyR (left, top view; right, side view) based on the previous 3D reconstructions of the $RyR2_{S2367\text{-}GFP}$ and $RyR2_{Y2801\text{-}GFP}$ fusion proteins [124,126]. The distance between CFP and YFP is 30Å. The clamp region (red dashed ellipse) and subdomains (red numbers) are indicated. (C) Caffeine-induced Ca^{2+} release in HEK293 cells transfected with RyR2 (wt) (a) or $RyR2_{S2367\text{-}CFP/Y2801\text{-}YFP}$ (b). Transfected HEK293 cells were loaded with Fluo-3 AM. The fluorescence intensity of the Fluo-3-loaded cells was monitored continuously before and after the sequential additions of increasing concentrations of caffeine (0.025 to 5 mM).

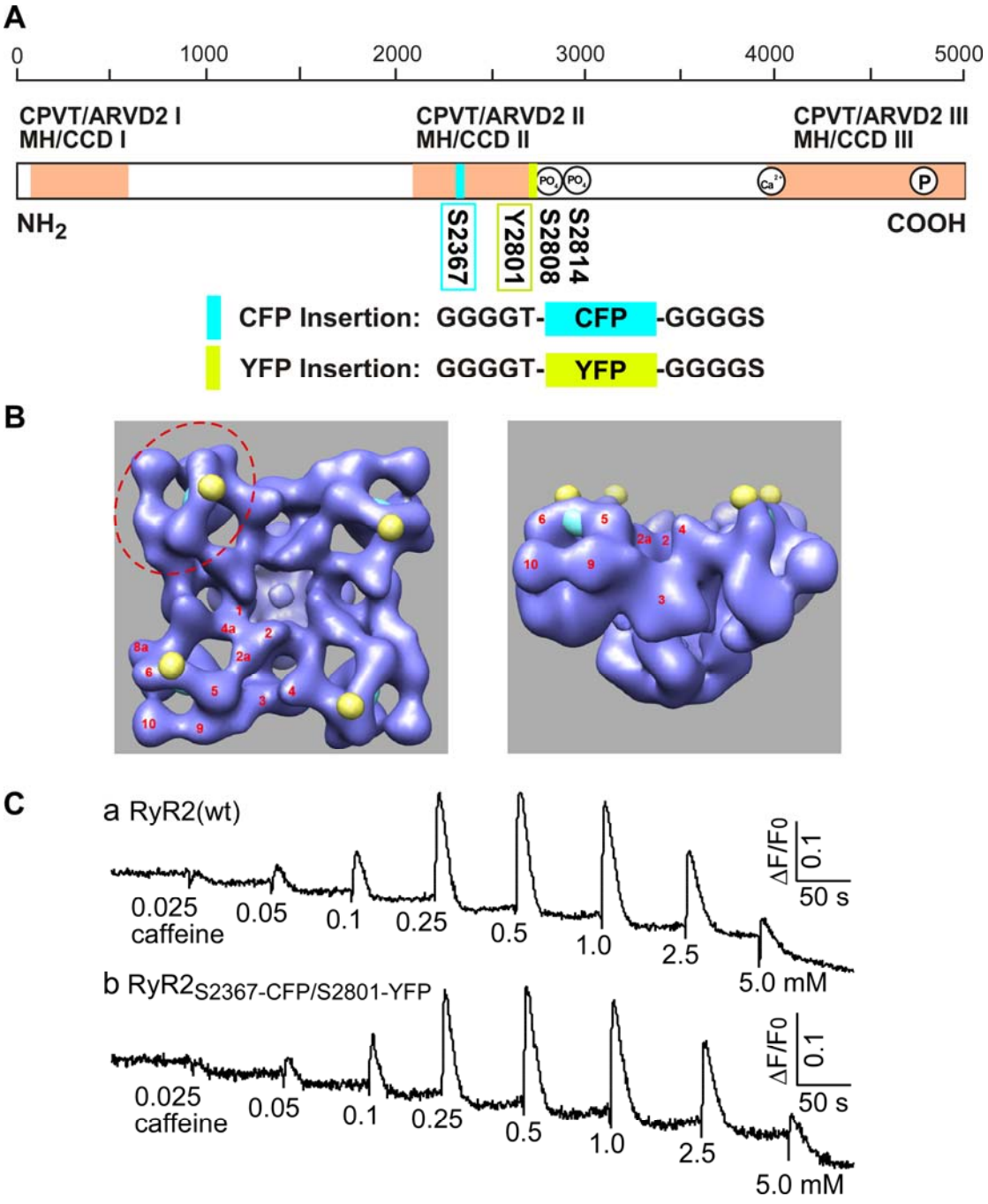
A
0
1000
2000
3000
4000
5000
CPVT/ARVD2 I
MH/CCD I
CPVT/ARVD2 II
MH/CCD II
CPVT/ARVD2 III
MH/CCD III
NH2
COOH
S2367
Y2801
S2808
S2814
CFP Insertion: GGGGT- CFP -GGGGS
YFP Insertion: GGGGT- YFP -GGGGS
B
C
a RyR2(wt)
0.025
caffeine
0.05
0.1
0.25
0.5
1.0
2.5
5.0 mM
ΔF/F0
0.1
50 s
b RyR2S2367-CFP/S2801-YFP

Fig. 24 FRET efficiencies in HEK293 cells transfected with $RyR2_{S2367\text{-}CFP/Y2801\text{-}YFP}$ or co-transfected with $RyR2_{S2367\text{-}CFP}$ and $RyR2_{Y2801\text{-}YFP}$

Confocal images showing cyan fluorescence of the donor CFP and yellow fluorescence of the acceptor YFP before (top panels) and after (bottom panels) photobleaching of a small area (indicated by a green ellipse) in HEK293 cells transfected with $RyR2_{S2367\text{-}CFP/Y2801\text{-}YFP}$ (A) or co-transfected with $RyR2_{S2367\text{-}CFP}$ and $RyR2_{Y2801\text{-}YFP}$ (B). The corresponding FRET efficiencies were shown and calculated according to the equation in panel (C). I_{CFPpre} and $I_{CFPpost}$ are the background-corrected CFP fluorescence intensities before and after photobleaching. YFP Scale bar represents 10 m. Data shown are mean ± SEM (n = 20). (*$P < 0.01$). Measurements of the FRET efficiency were carried out in the laboratories of Dr. Zheng Liu and Dr. Terence Wagenknecht.

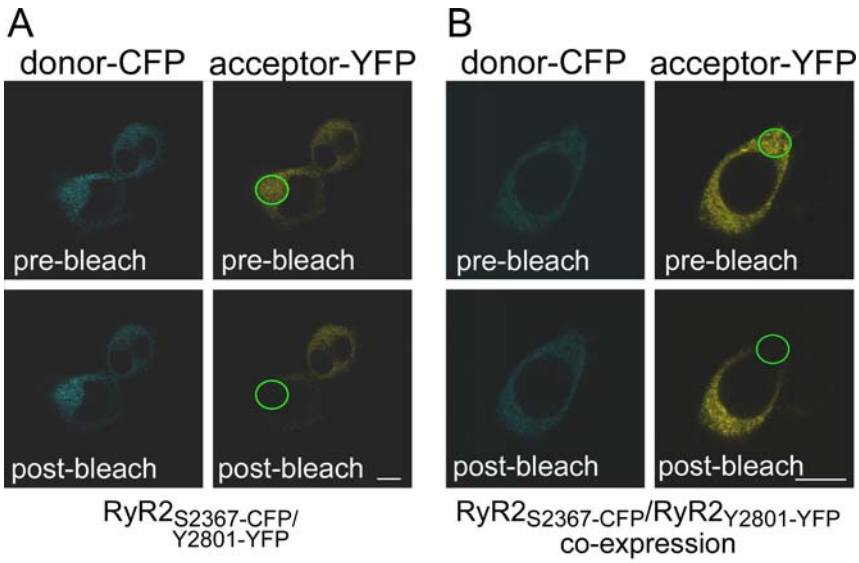

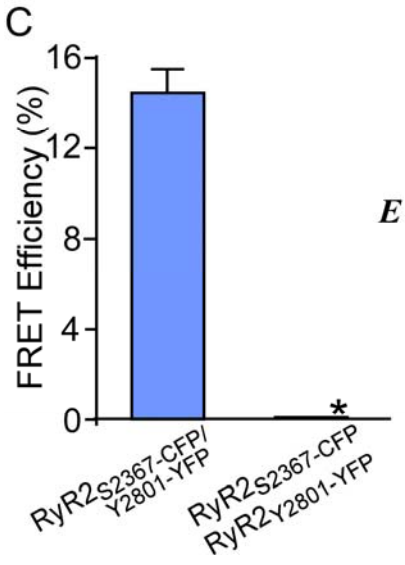

$$E = \left(\frac{I_{CFPpost} - I_{CFPpre}}{I_{CFPpost}} \right) \times 100\%$$

5.2.2 S2367-CFP/Y2801-YFP FRET probe is a dynamic, functional conformation sensor

We next determined whether this intra-subunit FRET probe (S2367-CFP/Y2801-YFP) is capable of sensing conformational changes in RyR2. We activated $RyR2_{S2367\text{-}CFP/Y2801\text{-}YFP}$ with various concentrations of caffeine to alter the conformational and functional state of the channel, and continuously monitored the FRET signal by determining the fluorescence ratio of YFP and CFP upon CFP excitation. We reasoned that if caffeine activation of RyR2 leads to conformational changes in the clamp region, it would alter the relative positions of S2367-CFP and Y2801-YFP and thus their FRET signals. Indeed, as shown in Fig. 25A, caffeine reduced the FRET signal in HEK293 cells expressing $RyR2_{S2367\text{-}CFP/Y2801\text{-}YFP}$ in a concentration dependent manner. The effect of caffeine on FRET is reversible. Upon caffeine wash off, the FRET signal recovered to a level similar to that before caffeine treatment.

To assess whether caffeine-induced FRET changes are associated with functional changes, we monitored caffeine-induced Ca^{2+} release in HEK293 cells by determining the ER luminal Ca^{2+} level using a FRET-based ER luminal Ca^{2+} sensor, D1ER. We have previously shown that caffeine reduces the ER luminal Ca^{2+} level at which spontaneous Ca^{2+} release occurs (i.e. the threshold for spontaneous store-overload induced Ca^{2+} release, SOICR) [151,165,251,343]. The threshold for SOICR reflects the propensity (or functional state) of the RyR2 channel for spontaneous Ca^{2+} release [151,251]. As shown in Fig. 25, we found that caffeine concentration-dependently and reversibly reduced the SOICR threshold in HEK293 cells expressing $RyR2_{S2367\text{-}CFP/Y2801\text{-}YFP}$ (Fig. 25B) and RyR2(wt) (Fig. 25C) to a similar extent (Fig. 25D). Note that the CFP or YFP

fluorescence intensity in HEK293 cells expressing $RyR2_{S2367\text{-}CFP/Y2801\text{-}YFP}$ alone is only ~10% of that in cells expressing both D1ER and $RyR2_{S2367\text{-}CFP/Y2801\text{-}YFP}$ (Fig.26). Thus, the FRET signal detected in cells expressing both D1ER and $RyR2_{S2367\text{-}CFP/Y2801\text{-}YFP}$ largely reflects that of the D1ER luminal Ca^{2+} sensor. Taken together, these data indicate that the concentration-dependence of caffeine-induced FRET changes is similar to that of caffeine-induced changes in the SOICR threshold (Fig. 25D). Hence, caffeine-induced FRET changes closely correlate with the functional states of the channel.

To ascertain whether the large N-terminal cytosolic domain of RyR2 itself is sufficient to confer FRET between S2367-CFP and Y2801-YFP and its response to caffeine, we determined the FRET efficiency of a C-terminally truncated RyR2 containing the same S2367-CFP/Y2801-YFP FRET pair, $RyR2(1\text{-}4770)_{S2367\text{-}CFP/Y2801\text{-}YFP}$ (a channel lacking the small pore-forming domain) [221]. We found that $RyR2(1\text{-}4770)_{S2367\text{-}CFP/Y2801\text{-}YFP}$ still exhibited significant FRET (Fig. 27). However, caffeine did not change the FRET efficiency of $RyR2(1\text{-}4770)_{S2367\text{-}CFP/Y2801\text{-}YFP}$, while caffeine reduced the FRET efficiency of $RyR2_{S2367\text{-}CFP/Y2801\text{-}YFP}$ in a concentration dependent manner (Fig. 27). Thus, the large N-terminal domain of RyR2 itself is not sufficient for caffeine-induced conformational changes in the clamp region. It should be noted that caffeine did not affect the CFP or YFP fluorescence intensity of HEK293 cells co-transfected with $RyR2_{S2367\text{-}CFP}$ and $RyR2_{Y2801\text{-}YFP}$ where FRET was not detected. (Fig. 28). The results of these control experiments indicate that caffeine-induced FRET changes in HEK293 cells expressing $RyR2_{S2367\text{-}CFP/Y2801\text{-}YFP}$ did not result from a direct effect of caffeine on the fluorescence of CFP or YFP. Taken together, these data indicate that the S2367-

Fig. 25 Caffeine induces correlated structural and functional changes in RyR2

(A) Stable, inducible HEK293 cells expressing $RyR2_{S2367\text{-}CFP/Y2801\text{-}YFP}$ were perfused with KRH buffer containing increasing levels of caffeine (0-10 mM) to induce conformational changes in RyR2. A representative recording of the S2367-CFP/Y2801-YFP FRET signal from a single HEK293 cell is shown. Changes in the S2367-CFP/Y2801-YFP FRET signal reflect structural changes in the clamp region of RyR2. Dashed lines indicate steady-state FRET levels at different concentrations of caffeine. (B) Stable, inducible HEK293 cells expressing $RyR2_{S2367\text{-}CFP/Y2801\text{-}YFP}$ were transfected with the FRET-based ER luminal Ca^{2+} sensing protein, D1ER. The transfected cells were perfused with KRH buffer containing increasing levels of caffeine (0-10 mM). The trace shows a representative FRET recording from a single HEK293 cell expressing both D1ER and $RyR2_{S2367\text{-}CFP/Y2801\text{-}YFP}$. Since the CFP or YFP fluorescence intensity in HEK293 cells expressing $RyR2_{S2367\text{-}CFP/Y2801\text{-}YFP}$ alone is only ~10% of that in cells expressing both the D1ER luminal Ca^{2+} sensor and $RyR2_{S2367\text{-}CFP/Y2801\text{-}YFP}$, the FRET signals detected largely came from those of D1ER. These D1ER FRET signals reflect the ER luminal Ca^{2+} levels. Dashed lines indicate the ER luminal Ca^{2+} levels at which store overload induced Ca^{2+} release (SOICR) occurs (i.e. the SOICR threshold), which reflects the functional state of RyR2. (C) Single cell D1ER FRET imaging of stable, inducible, RyR2(wt)-expressing HEK293 cells transfected with D1ER at increasing levels of caffeine. Dashed lines indicate SOICR thresholds. (D) Comparison of caffeine-induced, concentration-dependent changes in the S2367-CFP/Y2801-YFP FRET signal (structural changes) with those in the SOICR threshold (functional changes). The extents of changes in FRET and SOICR at each caffeine concentration were normalized to those at 10 mM caffeine

(100%). Data shown are mean ± SEM (n = 4-11). There are no significant differences between reductions in FRET and SOICR threshold under each condition.

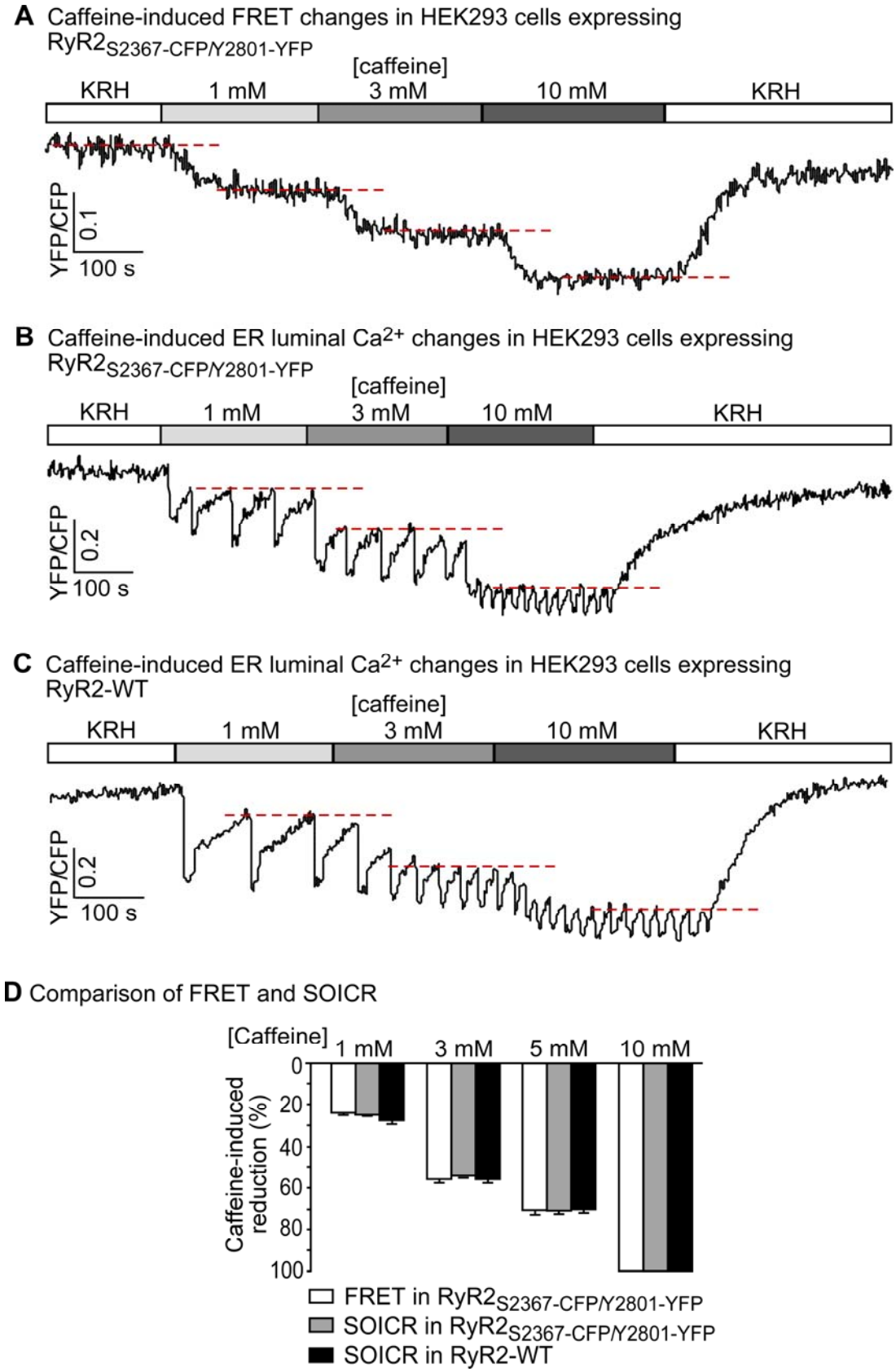
A Caffeine-induced FRET changes in HEK293 cells expressing RyR2S2367-CFP/Y2801-YFP
[caffeine]
KRH
1 mM
3 mM
10 mM
KRH
YFP/CFP
0.1
100 s
B Caffeine-induced ER luminal Ca2+ changes in HEK293 cells expressing RyR2S2367-CFP/Y2801-YFP
[caffeine]
KRH
1 mM
3 mM
10 mM
KRH
YFP/CFP
0.2
100 s
C Caffeine-induced ER luminal Ca2+ changes in HEK293 cells expressing RyR2-WT
[caffeine]
KRH
1 mM
3 mM
10 mM
KRH
YFP/CFP
0.2
100 s
D Comparison of FRET and SOICR
[Caffeine]
1 mM
3 mM
5 mM
10 mM
Caffeine-induced reduction (%)
0
20
40
60
80
100
FRET in RyR2S2367-CFP/Y2801-YFP
SOICR in RyR2S2367-CFP/Y2801-YFP
SOICR in RyR2-WT

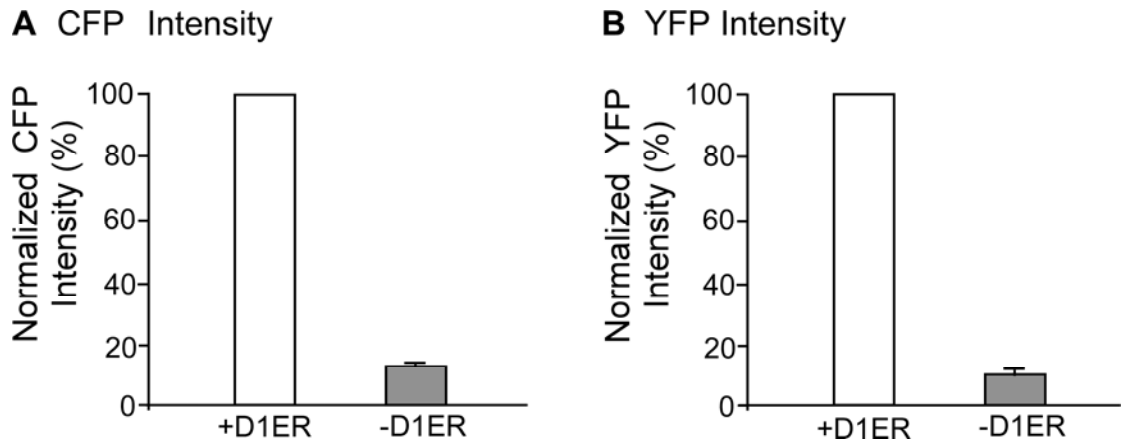

Fig. 26 Fluorescence intensity of CFP or YFP in HEK293 cells expressing $RyR2_{S2367\text{-}CFP/Y2801\text{-}YFP}$ with or without D1ER

HEK293 cells expressing $RyR2_{S2367\text{-}CFP/Y2801\text{-}YFP}$ were transfected with or without D1ER 48 h before imaging and induced for expression of the RyR2 double insertion 24 h before imaging. The CFP (A) and YFP (B) fluorescence intensity in D1ER transfected or non-transfected cells were recorded and compared. The level of CFP or YFP fluorescence intensity in cells without D1ER transfection were normalized to those in D1ER transfected cells (100%). Data shown are mean ± SEM (n = 3).

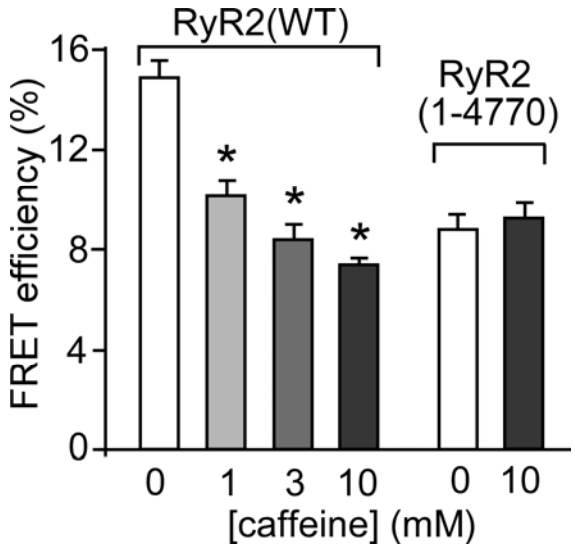

Fig. 27 Effect of caffeine on the FRET efficiency in HEK293 cells expressing $RyR2_{S2367\text{-}CFP/Y2801\text{-}YFP}$ or $RyR2(1\text{-}4770)_{S2367\text{-}CFP/Y2801\text{-}YFP}$

The FRET efficiencies in HEK293 cells expressing $RyR2_{S2367\text{-}CFP/Y2801\text{-}YFP}$ or a truncated RyR2, $RyR2(1\text{-}4770)_{S2367\text{-}CFP/Y2801\text{-}YFP}$, at various caffeine concentrations (0-10 mM) were determined using the photobleaching method as introduced in Fig. 24. Data shown are mean ± SEM (n = 30) (* $P < 0.05$; vs 0 mM caffeine). Measurements of the FRET efficiency were carried out in the laboratories of Dr. Zheng Liu and Dr. Terence Wagenknecht.

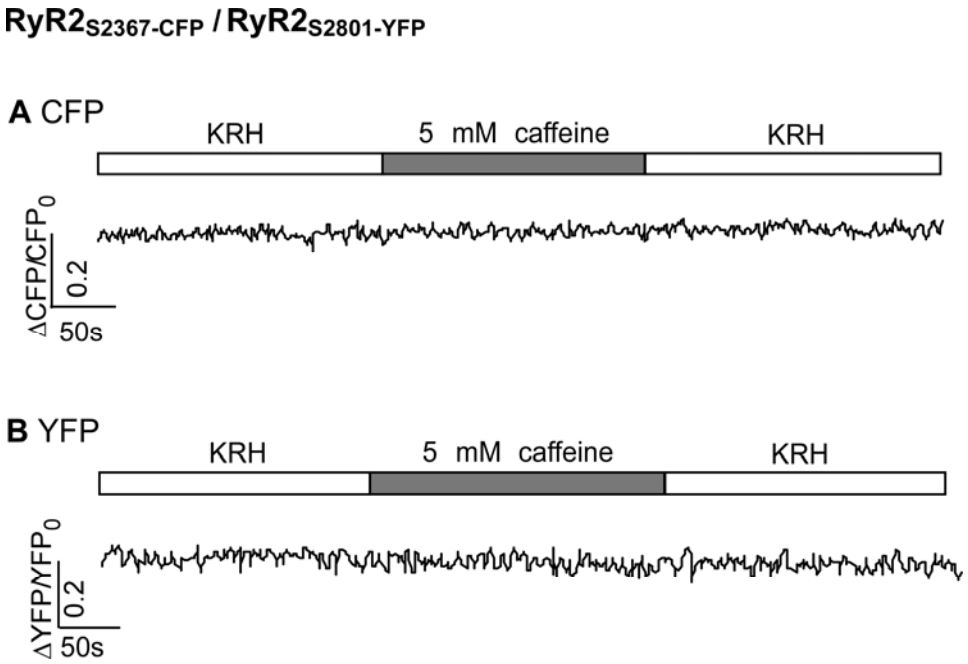

Fig. 28 Caffeine has no effect on fluorescence intensity of HEK293 cells co-transfected with $RyR2_{S2367\text{-}CFP}$ and $RyR2_{Y2801\text{-}YFP}$

HEK293 cells were co-transfected with $RyR2_{S2367\text{-}CFP}$ and $RyR2_{Y2801\text{-}YFP}$. The CFP signal and YFP signal in these cells were recorded during 5mM caffeine treatment and wash-off. Representative traces of the CFP (A) or YFP (B) signal are shown.

CFP/Y2801-YFP FRET probe is capable of sensing functionally correlated conformational changes in the clamp region of RyR2.

5.2.3 Ligand-dependent conformational changes in the clamp region of RyR2

A number of pharmacological and physiological ligands can activate RyR2, leading to Ca^{2+} release, but the molecular mechanisms of their activation are largely unknown. In the next series of experiments, we took advantage of our newly constructed conformation sensor to study the conformational changes in the clamp region of RyR2 activated by various ligands.

5.2.3.1 Pharmalogical compound aminophylline, theophylline and 4-CmC affect the channel conformation differently

In addition to caffeine, other pharmacological ligands, such as aminophylline, theophylline, and 4-CmC have been shown to activate RyR2 and induce SR Ca^{2+} release [165,253,263]. To determine whether different pharmacological ligands may have different effects on RyR2 conformation, we assessed the impact of aminophylline, theophylline and 4-CmC on FRET and the ER luminal Ca^{2+} level in HEK293 cells expressing $RyR2_{S2367\text{-}CFP/Y2801\text{-}YFP}$. Fig. 29 shows that like caffeine, aminophylline and theophylline reduced both the FRET level and the SOICR threshold, indicating that these two RyR2 agonists induce Ca^{2+} release and conformational changes in the clamp region. Interestingly, we found that 4-CmC did not cause any significant changes in the FRET signal, but it induced Ca^{2+} release (Fig. 30).

5.2.3.2 Distinct effects of cytosolic ATP and Ca^{2+} on the conformational dynamics of RyR2

Fig. 29 Effect of aminophylline and theophylline on the structure and function of RyR2

(A) HEK293 cells expressing $RyR2_{S2367\text{-}CFP/Y2801\text{-}YFP}$ were perfused with KRH buffer without or with caffeine (10 mM), aminophylline (10 mM), or theophylline (10 mM). A representative single cell recording of the S2367-CFP/Y2801-YFP FRET signal is shown. Dashed lines indicate steady-state FRET levels. (B) A representative single cell luminal Ca^{2+} recording of D1ER-transfected HEK293 cells expressing $RyR2_{S2367\text{-}CFP/Y2801\text{-}YFP}$ in the KRH buffer without or with caffeine, aminophylline, or theophylline. Dashed lines indicate the SOICR threshold. (C) Comparison of changes in the S2367-CFP/Y2801-YFP FRET signal (structural changes) with those in the SOICR threshold (functional changes) induced by caffeine, aminophylline, theophylline. The extents of changes in FRET and SOICR were normalized to those at 10 mM caffeine (100%). Data shown are mean ± SEM (n = 5-9).

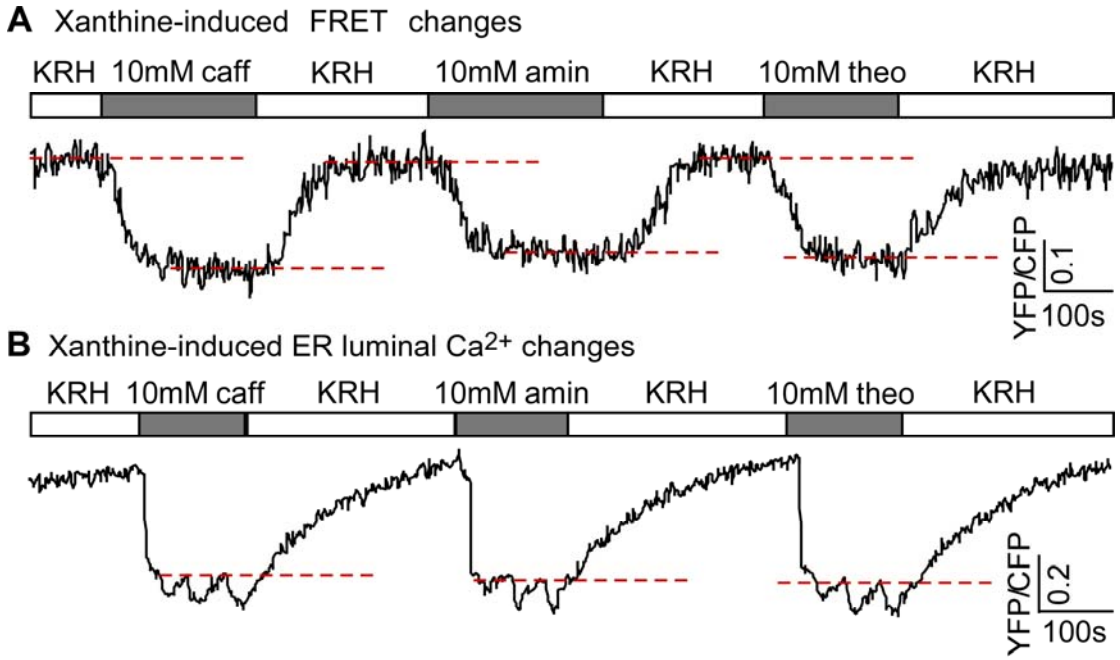
A Xanthine-induced FRET changes
KRH
10mM caff
KRH
10mM amin
KRH
10mM theo
KRH
YFP/CFP
0.1
100s
B Xanthine-induced ER luminal Ca2+ changes
KRH
10mM caff
KRH
10mM amin
KRH
10mM theo
KRH
YFP/CFP
0.2
100s

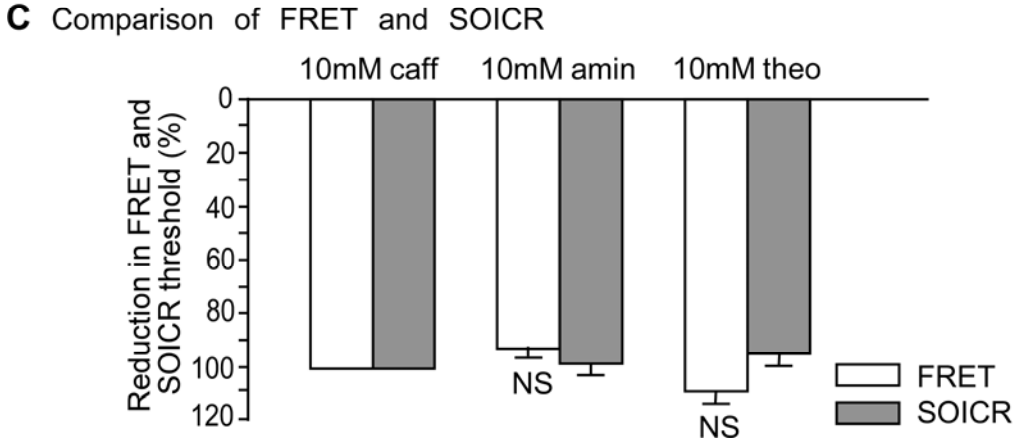
C Comparison of FRET and SOICR
10mM caff
10mM amin
10mM theo
Reduction in FRET and SOICR threshold (%)
0
20
40
60
80
100
120
NS
NS
FRET
SOICR

Fig. 30 Effect of 4-CmC on the structure and function of RyR2

(A) HEK293 cells expressing $RyR2_{S2367\text{-}CFP/Y2801\text{-}YFP}$ were permeabilized and perfused with the ICM buffer without or with caffeine (10 mM) or 4-CmC (1 mM). A representative single cell recording of the S2367-CFP/Y2801-YFP FRET signal is shown. (B) A representative single cell luminal Ca^{2+} recording of D1ER-transfected, permeabilized HEK293 cells expressing $RyR2_{S2367\text{-}CFP/Y2801\text{-}YFP}$ in ICM without or with caffeine or 4-CmC. Dashed lines indicate the SOICR threshold. (C) Comparison of changes in the S2367-CFP/Y2801-YFP FRET signal (structural changes) with those in the SOICR threshold (functional changes) induced by caffeine or 4-CmC. The extents of changes in FRET and SOICR were normalized to those at 10 mM caffeine (100%). Data shown are mean ± SEM (n = 7-11) (* $P < 0.01$; FRET vs. SOICR).

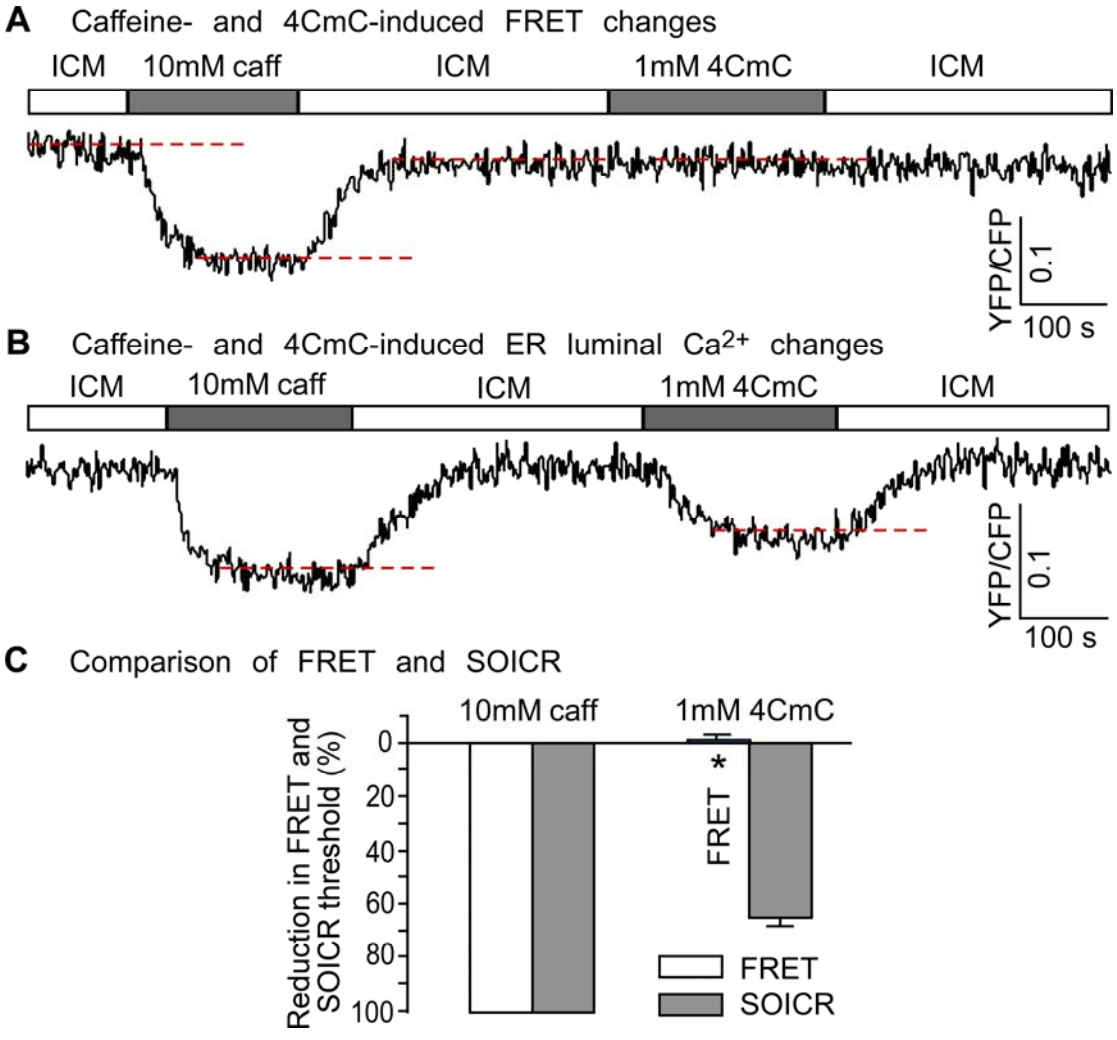
A Caffeine- and 4CmC-induced FRET changes
ICM
10mM caff
ICM
1mM 4CmC
ICM
YFP/CFP
0.1
100 s
B Caffeine- and 4CmC-induced ER luminal Ca2+ changes
ICM
10mM caff
ICM
1mM 4CmC
ICM
YFP/CFP
0.1
100 s
C Comparison of FRET and SOICR
10mM caff
1mM 4CmC
Reduction in FRET and SOICR threshold (%)
0
20
40
60
80
100
FRET *
FRET
SOICR

ATP and Ca^{2+} are two physiological agonists of RyR2 [324]. To assess the effect of cytosolic ATP and Ca^{2+} on the conformation and function of RyR2, we perfused permeabilized HEK293 cells expressing $RyR2_{S2367\text{-}CFP/Y2801\text{-}YFP}$ with an intracellular-like medium (ICM) or with ICM plus 5 mM ATP or 1 M Ca^{2+}. As shown in Fig. 31, ATP reversibly reduced both the FRET signal and the SOICR threshold, indicating that, like caffeine, ATP is able to induce conformational changes in the clamp region and concomitant intracellular Ca^{2+} release. Surprisingly, elevating cytosolic Ca^{2+} to 1 M induced little or no FRET changes in the $RyR2_{S2367\text{-}CFP/Y2801\text{-}YFP}$ expressing cells, but it did reduce the SOICR threshold (Fig. 32). Thus, unlike caffeine and ATP, cytosolic Ca^{2+} activates the RyR2 channel without inducing major conformational changes in the clamp region. Further, we determined the impact of ATP, Ca^{2+} and 4-CmC on the FRET efficiency in HEK293 cells expressing $RyR2_{S2367\text{-}CFP/Y2801\text{-}YFP}$. Similarly, we found that ATP reduced the FRET efficiency, whereas Ca^{2+} and 4-CmC had no effect on the FRET efficiency (Fig. 33). Taken together, these observations indicate that the activation of RyR2 by caffeine, aminophylline, theophylline, and ATP is associated with substantial conformational changes in the clamp region of RyR2, whereas the activation of RyR2 by cytosolic Ca^{2+} and 4-CmC is not. Thus, different ligands activate RyR2 and induce Ca^{2+} release by different mechanisms associated with distinct conformational changes.

5.2.3.3 Ryanodine keeps the channel open, but dose not lock RyR in a fixed conformation

It is well known that ryanodine binds to the open state of RyR and keeps the channel in an open, subconductance state [230,335,336,344]. It is unclear, however, whether ryanodine locks RyR in a fixed conformation. To address this question, we determined whether

Fig. 31 Effect of cytosolic ATP on the structure and function of RyR2

(A) HEK293 cells expressing $RyR2_{S2367\text{-}CFP/Y2801\text{-}YFP}$ were permeabilized and perfused with ICM without or with caffeine (10 mM) or ATP (5 mM). A representative single cell recording of the S2367-CFP/Y2801-YFP FRET signal is shown. (B) A representative single cell luminal Ca^{2+} recording of D1ER-transfected, permeabilized HEK293 cells expressing $RyR2_{S2367\text{-}CFP/Y2801\text{-}YFP}$ in the ICM buffer with or without caffeine or ATP. The SOICR threshold is indicated by a dashed line. (C) Comparison of changes in the S2367-CFP/Y2801-YFP FRET signal (structural changes) with those in the SOICR threshold (functional changes) induced by caffeine or ATP. The extents of changes in FRET and SOICR were normalized to those at 10 mM caffeine (100%). Data shown are mean ± SEM (n = 8-14).

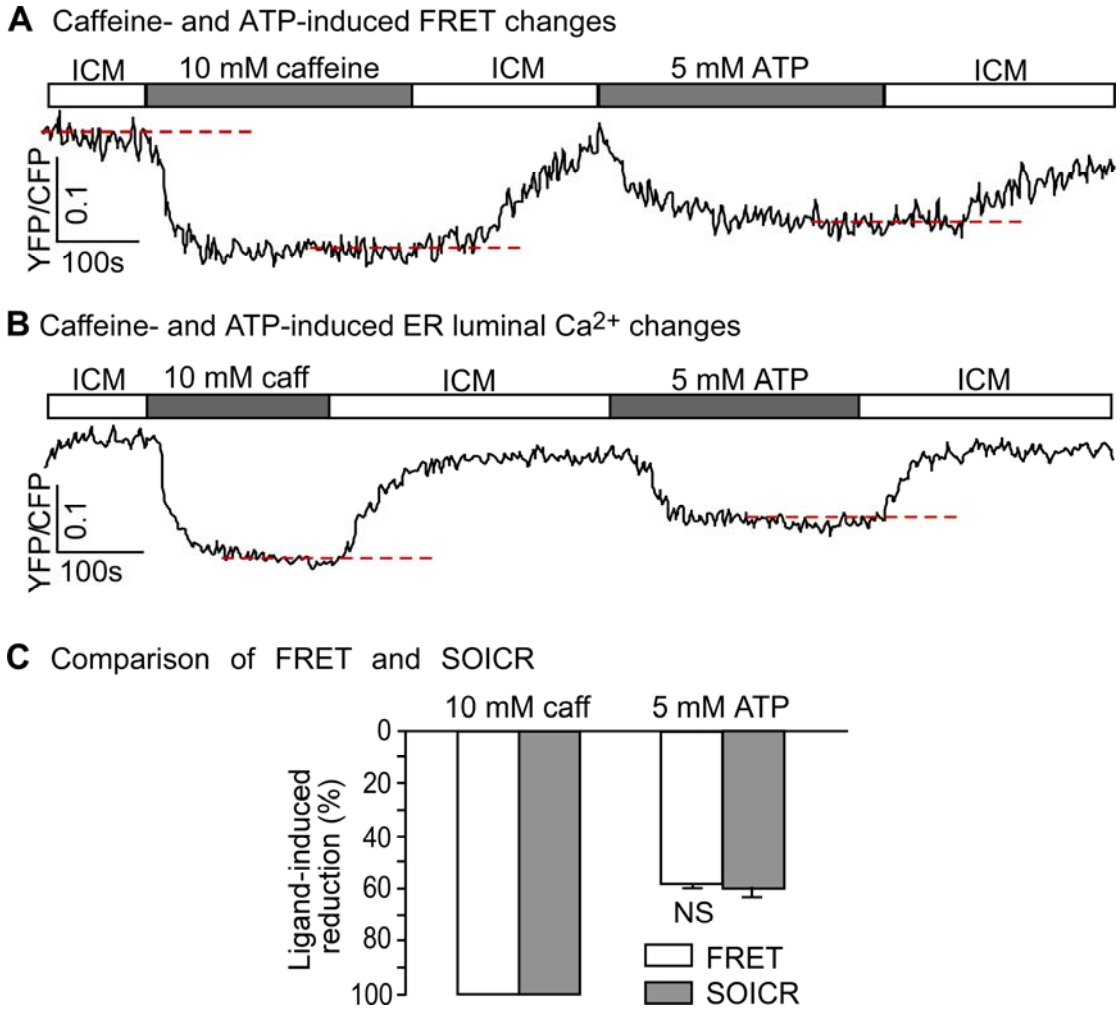
A Caffeine- and ATP-induced FRET changes
ICM
10 mM caffeine
ICM
5 mM ATP
ICM
YFP/CFP
0.1
100s
B Caffeine- and ATP-induced ER luminal Ca2+ changes
ICM
10 mM caff
ICM
5 mM ATP
ICM
YFP/CFP
0.1
100s
C Comparison of FRET and SOICR
10 mM caff
5 mM ATP
Ligand-induced reduction (%)
0
20
40
60
80
100
NS
FRET
SOICR

Fig. 32 Effects of cytosolic Ca^{2+} on the structure and function of RyR2

(A) HEK293 cells expressing $RyR2_{S2367\text{-}CFP/Y2801\text{-}YFP}$ were permeabilized and perfused with ICM without or with caffeine (10 mM) or Ca^{2+} (1 μM). A representative single cell recording of the S2367-CFP/Y2801-YFP FRET signal is shown. Note that unlike ATP, Ca^{2+} induced no changes in FRET. (B) A representative single cell luminal Ca^{2+} recording of D1ER-transfected, permeabilized HEK293 cells expressing $RyR2_{S2367\text{-}CFP/Y2801\text{-}YFP}$ in the ICM buffer without or with caffeine or Ca^{2+}. The dashed line indicates the SOICR threshold. (C) Comparison of changes in the S2367-CFP/Y2801-YFP FRET signal (structural changes) with those in the SOICR threshold (functional changes) induced by caffeine or Ca^{2+}. The extents of changes in FRET and SOICR were normalized to those at 10 mM caffeine (100%). Data shown are mean ± SEM (n = 7-8) (*$P < 0.01$; FRET vs. SOICR).

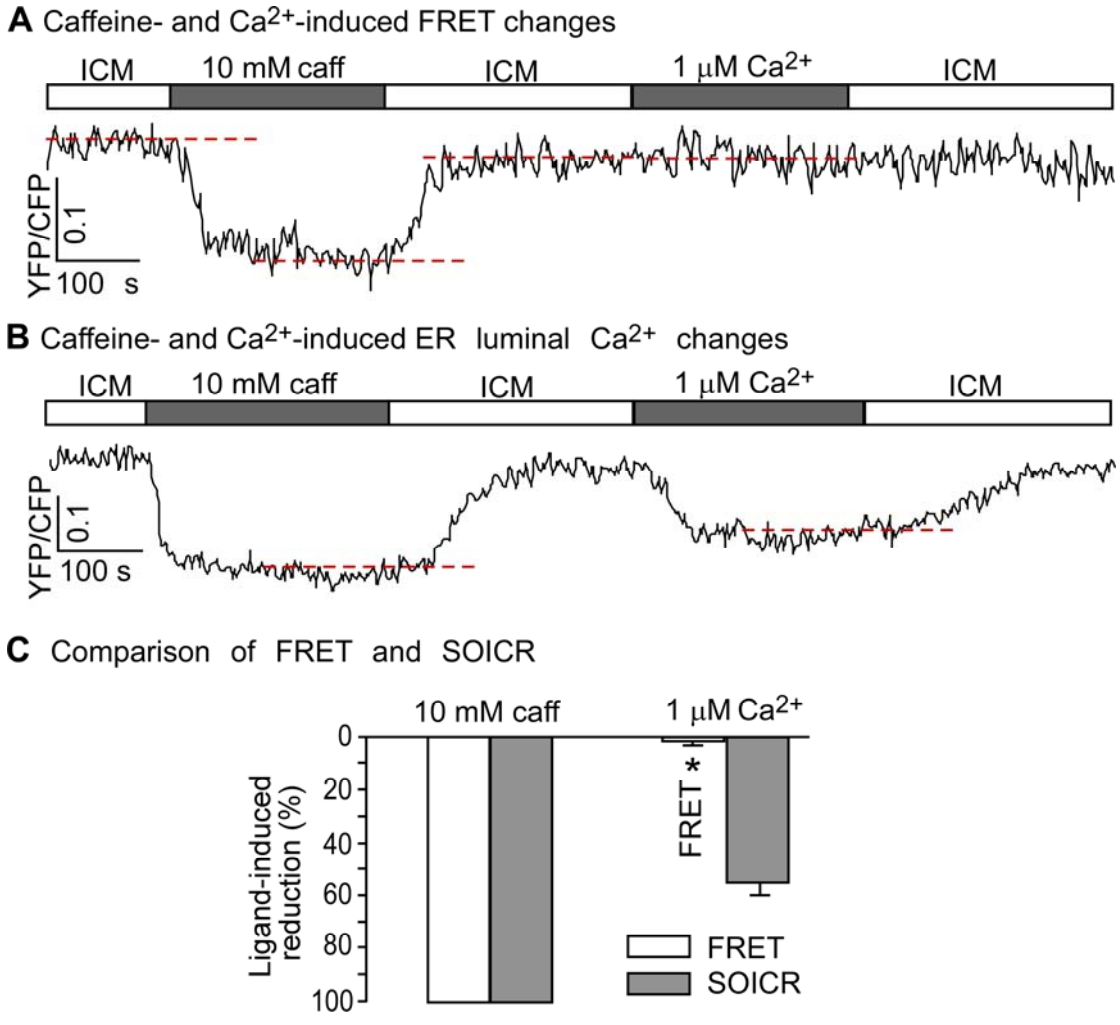
A Caffeine- and Ca2+-induced FRET changes
ICM
10 mM caff
ICM
1 μM Ca2+
ICM
YFP/CFP
0.1
100 s
B Caffeine- and Ca2+-induced ER luminal Ca2+ changes
ICM
10 mM caff
ICM
1 μM Ca2+
ICM
YFP/CFP
0.1
100 s
C Comparison of FRET and SOICR
10 mM caff
1 μM Ca2+
Ligand-induced reduction (%)
0
20
40
60
80
100
FRET *
FRET
SOICR

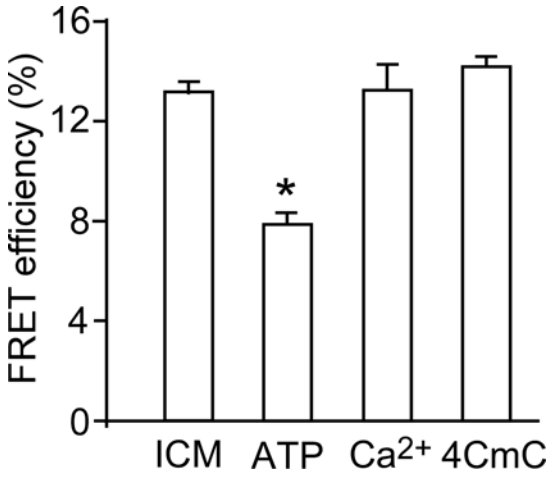

Fig. 33 Effect of ATP, Ca^{2+} or 4-CmC on the FRET efficiency in permeabilized HEK293 cells expressing $RyR2_{S2367\text{-}CFP/Y2801\text{-}YFP}$

HEK293 cells expressing $RyR2_{S2367\text{-}CFP/Y2801\text{-}YFP}$ were permeabilized with saponin and treated without or with ATP, Ca^{2+} or 4-CmC. The FRET efficiencies at each condition were determined using the photobleaching method as indicated in Fig. 24. Data shown are mean ± SEM (n = 20-30). (* $P < 0.01$; vs. ICM). Measurements of the FRET efficiency were carried out in the laboratories of Dr. Zheng Liu and Dr. Terence Wagenknecht.

caffeine could still induce conformational changes in a ryanodine-bound channel. To this end, we first perfused the permeabilized HEK293 cells expressing $RyR2_{S2367\text{-}CFP/Y2801\text{-}YFP}$ with caffeine (10 mM) to open the channel, and then with caffeine (10 mM) plus ryanodine (100 μM) to allow ryanodine binding to the caffeine-opened channels. These caffeine and ryanodine-treated cells were then perfused with the ICM buffer to remove caffeine and unbound ryanodine in order to reveal the effect of bound ryanodine, which is known to remain bound to RyR2. As shown in Fig. 34A, caffeine reduced the FRET signal. Caffeine plus ryanodine caused a small further reduction in FRET. After removing caffeine and unbound ryanodine, the FRET signal recovered partially to a level that is significantly lower than the FRET level before caffeine treatment (Fig. 34C).

To confirm that ryanodine remained bound to RyR2 after wash-off with the ICM buffer, we performed [^{3}H]ryanodine binding (see Methods). We found that the amount of [^{3}H]ryanodine binding to cells pre-treated with 100 μM non-labeled ryanodine plus 10 mM caffeine is only ~1% of that to control cells without ryanodine pre-treatment (Fig. 35). Thus, most of the RyR2 channels were bound with ryanodine after pre-treatment with 100 μM ryanodine plus 10 mM caffeine and remained bound with it after wash-off with the ICM buffer. Therefore, the FRET signal detected after wash-off with ICM (Fig. 34C) likely reflects the ryanodine-induced conformational changes in the ryanodine-bound channels.

We also determined the FRET efficiencies in permeabilized $RyR2_{S2367\text{-}CFP/Y2801\text{-}YFP}$ expressing cells in the absence or presence of caffeine or ryanodine or after wash-off (Fig. 34D). Similarly, we found that caffeine or caffeine plus ryanodine reduced the FRET efficiency to a similar extent, and that the FRET efficiency after removing caffeine and

Fig. 34. Impact of ryanodine on the structure and function of RyR2

(A) HEK293 cells transfected with $RyR2_{S2367\text{-}CFP/Y2801\text{-}YFP}$ were permeabilized and perfused with ICM, caffeine (10 mM), and caffeine (10 mM) plus ryanodine (100 μM), followed by wash-off with ICM. The cells were then perfused with caffeine (10 mM) again followed by wash-off with ICM. The illumination was turned off during part of the long incubation with caffeine plus ryanodine to minimize photobleaching. A representative single cell recording of the S2367-CFP/Y2801-YFP FRET signal is shown. (B) A representative single cell luminal Ca^{2+} recording of D1ER-transfected, permeabilized HEK293 cells expressing $RyR2_{S2367\text{-}CFP/Y2801\text{-}YFP}$. The cells were perfused in the same way as that described in panel A. Note that the ER Ca^{2+} store remained depleted after the addition of ryanodine. (C) Comparison of the changes in the S2367-CFP/Y2801-YFP FRET signal and those in the SOICR threshold under various conditions: (a) caffeine (10 mM) (control), (b) caffeine (10 mM) plus ryanodine (100 M), (c) after wash-off, and (d) re-application of caffeine (10 mM). The extents of changes in FRET and SOICR threshold were normalized to those in the control (100%). Data shown are mean ± SEM (n = 4-8). (* $P < 0.01$; FRET vs. SOICR; $^{\#}$ $P < 0.01$; vs. before or after caffeine treatment). (D) HEK293 cells expressing $RyR2_{S2367\text{-}CFP/Y2801\text{-}YFP}$ were permeabilized and perfused with ICM (a), caffeine (10 mM) (b), caffeine (10mM) plus ryanodine (100 M) (c), followed by wash-off (d). The FRET efficiency under each of these conditions was determined by the photobleaching method. Data shown are mean ± SEM (n = 30). (* $P < 0.01$; vs. ICM).

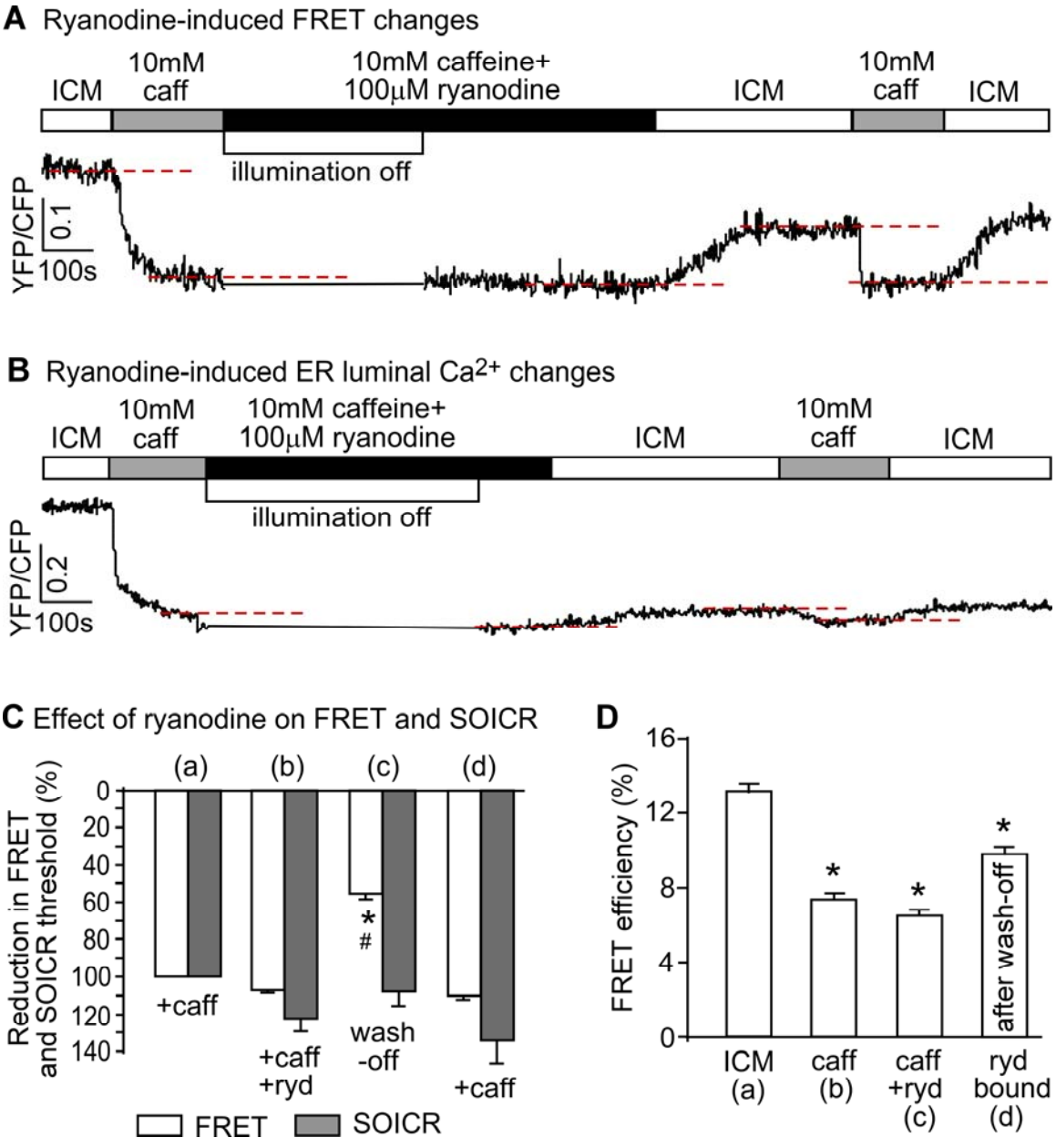
A Ryanodine-induced FRET changes
ICM
10mM caff
10mM caffeine+ 100μM ryanodine
ICM
10mM caff
ICM
illumination off
YFP/CFP
0.1
100s
B Ryanodine-induced ER luminal Ca2+ changes
ICM
10mM caff
10mM caffeine+ 100μM ryanodine
ICM
10mM caff
ICM
illumination off
YFP/CFP
0.2
100s
C Effect of ryanodine on FRET and SOICR
Reduction in FRET and SOICR threshold (%)
(a)
(b)
(c)
(d)
0
20
40
60
80
100
120
140
+caff
+caff +ryd
wash -off
+caff
*
#
FRET
SOICR
D
FRET efficiency (%)
16
12
8
4
0
*
*
*
after wash-off
ICM (a)
caff (b)
caff +ryd (c)
ryd bound (d)

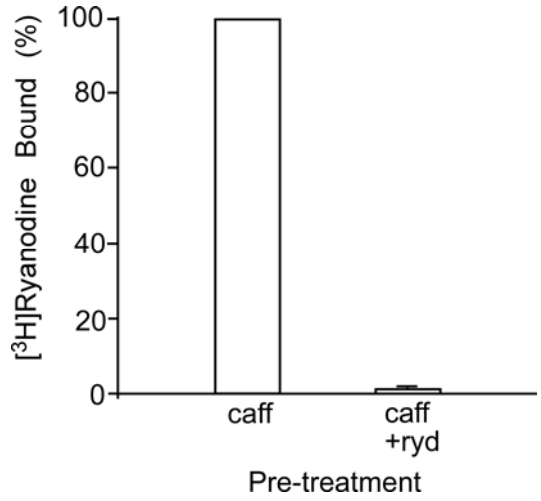

Fig. 35 [^{3}H]ryanodine binding to RyR2$_{S2367\text{-}CFP/Y2801\text{-}YFP}$

HEK293 cells expressing RyR2$_{S2367\text{-}CFP/Y2801\text{-}YFP}$ were permeabilized with saponin. The permeabilized cells were washed and incubated with or without 100 μM ryanodine plus 10 mM caffeine for 10 min to allow ryanodine to bind to RyR2. The ryanodine-treated or non-treated control cells were washed with the ICM buffer to remove caffeine and free ryanodine. The washed cells were solubilized with detergent to prepare cell lysates, which were then used for [^{3}H]ryanodine binding. The amounts of the [^{3}H]ryanodine binding in ryanodine pre-treated samples were normalized to that in ryanodine non-treated cells. Data shown are mean ± SEM (n = 3).

unbound ryanodine is lower than that before caffeine treatment (Fig. 34D). These data indicate that the bound ryanodine reduced the FRET signal or caused conformational changes in the clamp region, but to a lesser extent than caffeine (10 mM). Importantly, a subsequent addition of caffeine to the ryanodine-treated cells could still reduce the FRET signal (Fig. 34A,C). Thus, caffeine is still able to induce conformational changes in the ryanodine-bound RyR2 channel.

The impact of caffeine and ryanodine on RyR2 function is shown in Fig. 34B. Consistent with their known actions, caffeine caused store Ca^{2+} depletion. The addition of ryanodine in the presence of caffeine caused a small further reduction in store Ca^{2+} (Fig. 34B). The store Ca^{2+} level remained depleted after removing caffeine and unbound ryanodine (Fig. 34B,C). These observations are in agreement with the view that ryanodine interacts with the caffeine-opened RyR2 and keeps the channel in the open state, leading to store Ca^{2+} depletion. Taken together, these results indicate that ryanodine induces conformational changes in the clamp region of RyR2, and that the ryanodine-induced conformation can still be altered by caffeine.

5.3 Summary

Global conformational changes in the 3D structure of the Ca^{2+} release channel, RyR, occur upon ligand activation. A number of ligands are able to activate the RyR channel, but whether these structurally diverse ligands induce the same or different conformational changes in the channel is largely unknown. Here a FRET-based probe was constructed by inserting a CFP after residue Ser-2367 and a YFP after residue Tyr-2801 in RyR2 to yield a CFP- and YFP-dual labeled RyR2 ($RyR2_{S2367\text{-}CFP/Y2801\text{-}YFP}$). Both of these insertion sites

have previously been mapped to the "clamp" region in the four corners of the square-shaped cytoplasmic assembly of the 3D structure of RyR2.

Using this novel FRET probe, we monitored the extent of conformational changes in the clamp region of $RyR2_{S2367\text{-}CFP/Y2801\text{-}YFP}$ induced by various ligands. Meanwhile, the extent of Ca^{2+} release induced by the same ligands was also recorded in HEK293 cells expressing $RyR2_{S2367\text{-}CFP/Y2801\text{-}YFP}$. Conformational changes were detected in the clamp region upon triggering by ligands caffeine, aminophylline, theophylline, ATP, and ryanodine, but not Ca^{2+} or 4-CmC, although they all induced Ca^{2+} release. Interestingly, caffeine is able to induce further conformational changes in the clamp region of the ryanodine-modified channel, suggesting that ryanodine does not lock RyR in a fixed conformation.

Our data demonstrate that conformational changes in the clamp region of RyR are ligand dependent, and suggest the existence of multiple ligand dependent RyR activation mechanisms associated with distinct conformational changes. Limited by the resolution of cryo-EM, previous studies failed to observe detailed conformational changes in the clamp region of RyR2 induced by various ligands. Using a novel FRET probe, we were able to investigate the conformation changes in the clamp region induced by various ligands. We also correlated these conformational changes to channel function, which is not possible to perform using conventional methods of structural studies.

CHAPTER VI: MOLECULAR BASIS OF CARDIOMYOPATHY-ASSOCIATED RYR2 MUTATIONS

6.1 Introduction

Not only can impaired regulation by modulators lead to defective function of RyR2, but also inherited RyR2 mutations. RyR2 mutation-induced abnormal SR Ca^{2+} release is a well-known cause of ventricular tachyarrhythmias and sudden death [345,346]. To date, more than 150 disease-associated RyR2 mutations have been identified[274,347]. Most of these RyR2 mutations are associated with stress-induced ventricular tachyarrhythmias and sudden death in structurally normal hearts. Interestingly, some of the RyR2 mutations are associated with cardiomyopathies as well as cardiac arrhythmias[274,347]. For example, an in-frame deletion of 35 amino acid residues (Asn57-Gly91) in the N-terminal region, corresponding to exon-3 of the RYR2 gene, was identified in several unrelated families. This deletion was found to be associated with an expanding spectrum of phenotypes, including sinoatrial nodal dysfunction, atrial fibrillation, AV block, depressed left ventricular function, increased trabeculation, and DCM, in addition to CPVT[269,270,347]. Furthermore, a number of RyR2 N-terminal point mutations, including A77V, R176Q/T2504M, R420W, and L433P, have been associated with ARVD2 [274,279-283,347]. RyR2 mutations may also be associated with HCM [272]. Although a definitive link between RyR2 mutations and a specific type of cardiomyopathy has not been firmly established due to the small number of RyR2-mutation carriers and their variable clinical phenotypes, an increasing body of evidence does suggest that defective RyR2 is associated not only with cardiac arrhythmias but also with cardiomyopathies.

An important unresolved question is how mutations in RyR2 can lead to these different phenotypes. Since RyR2 mediates SR Ca^{2+} release, different RyR2 mutations may alter different aspects of SR Ca^{2+} release. One important aspect is the

initiation/activation of SR Ca^{2+} release. Mutations in RyR2 can cause cardiac arrhythmias by altering the activation of SR Ca^{2+} release. Our laboratory has recently demonstrated that a number of RyR2 mutations associated with CPVT reduce the threshold for spontaneous Ca^{2+} waves, also termed SOICR [151,251]. A reduced SOICR threshold will increase the propensity for DADs and thus triggered arrhythmias. Therefore, abnormal activation of Ca^{2+} release due to inappropriate opening of RyR2 represents a common mechanism for RyR2-associated CPVT[274].

The mechanism for RyR2-associated cardiomyopathies remains unknown. In addition to activation, the termination of SR Ca^{2+} release is also thought to be critical in maintaining stable EC coupling and in controlling the cytosolic Ca^{2+} transients[20,162,323,348]. Interestingly, impaired cytosolic Ca^{2+} transients have been proposed to trigger cardiac remodeling [306,307], leading to cardiomyopathies [65,67,83]. Thus, abnormal activation and termination of SR Ca^{2+} release could lead to impaired cytosolic Ca^{2+} transients and subsequently cardiomyopathies. It is, therefore, possible that RyR2 mutations associated with cardiomyopathies may alter the termination of Ca^{2+} release in addition to the change of activation threshold. To test this possibility, in the present study, we assessed the impact on Ca^{2+} release of a number of N-terminal RyR2 mutations mentioned above that are associated with cardiomyopathies. The DCM and ARVD2 linked mutations were found to slightly decrease the activation threshold but markedly reduce the termination threshold, and thus increase the fractional Ca^{2+} release. By contrast, the HCM associated mutation A1107M increased the termination threshold and reduced the fractional Ca^{2+} release. Our data demonstrate, for the first time, that the N-terminal region of RyR2 is an

important determinant of both activation and termination and that altered Ca^{2+} release termination is a common defect of RyR2 mutations associated with cardiomyopathies.

6.2 Results

6.2.1 The N-terminal region of RyR2 is an important determinant of Ca^{2+} release termination

The N-terminal region of RyR2 contains more than 20 disease-causing mutations, some of which are associated with cardiomyopathies [274,347], but the functional attributes of this region are unclear. To gain insight into the role of the N-terminal region in Ca^{2+} release, we used a deletion approach in which we removed the first 305 N-terminal residues of RyR2 (Del-305) (Fig. 36A). Ca^{2+} release assays and immunoblotting analysis revealed that the Del-305 mutant was expressed in HEK293 cells and remained functional (Figs. 36B and C). Note that in Ca^{2+} release assays, the addition of ryanodine (100 μM) following the addition of caffeine (0.25 mM) caused a slow release of Ca^{2+}. This is likely to be due to the binding of ryanodine to a small population of RyR2 channels that have been activated by the low concentration of caffeine (0.25 mM) and consequently an increase in Po of these channels. The subsequent addition of 2.5 mM caffeine activated the remaining ryanodine-unmodified RyR2 channels and caused a large Ca^{2+} release. In the continuous presence of ryanodine, the caffeine-activated channels would be modified by ryanodine into a fully activated state, leading to a depletion of intracellular Ca^{2+} store. The released Ca^{2+} would be extruded from the cytosol into the extracellular space, resulting in a transient Ca^{2+} release. Subsequent additions of caffeine yielded little or no Ca^{2+} release. This is because the ryanodine-modified channels are

already in the fully activated state with little or no intracellular Ca^{2+} store. The sharp decreases in fluorescence intensity immediately after the addition of caffeine were due to fluorescence quenching by caffeine. Importantly, the pattern of caffeine- and ryanodine-response of the Del-305 mutant is indistinguishable from that of the RyR2 WT (Fig. 36B). Thus, the deletion of the first 305 N-terminal residues of RyR2 does not abolish the expression or function of the channel.

To determine whether the N-terminal deletion alters SOICR, HEK293 cell expressing WT and Del-305 were transfected with D1ER for detecting luminal Ca^{2+} dynamics. SOICR was observed in HEK293 cells expressing the RyR2 Del-305 mutant upon elevation of extracellular Ca^{2+} as in cells expressing the RyR2 WT (Fig. 37A,B). Importantly, the Del-305 mutant cells exhibited a marked reduction in the termination threshold (35% vs 57% in WT, $P < 0.01$) and a slightly lowered activation threshold (90% vs 94% in WT, $P < 0.01$) (Figs.37C and D). Thus, the N-terminal deletion exerted a greater impact on the termination than on the activation of Ca^{2+} release. As a result, the fractional Ca^{2+} release during SOICR (activation threshold – termination threshold) is significantly greater in the Del-305 cells (55%) than in the WT cells (36%) ($P < 0.01$) (Fig.37E). On the other hand, there were no significant differences in the store capacity between the WT and Del-305 mutant cells (Figs. 37F). Thus, these results suggest that the N-terminal region of RyR2 plays an important role in the termination of Ca^{2+} release.

6.2.2 Deletion of Exon-3 in RyR2 reduces the threshold for Ca^{2+} release termination

Give the important role of the N-terminal region of RyR2 in the termination of Ca^{2+} release, we assessed whether the deletion of exon-3 (Del-Exon-3) within the N-terminal region (Fig. 38A) that is associated not only with CPVT but also with conduction

Fig. 36 Construction and functional expression of an N-terminally truncated RyR2 in HEK293 cells

(A) Schematic liner structure of the N-terminal region of RyR2, depicting the three structural domains (A, B, and C) [129]. The first 305 N-terminal residues covering the entire domain A and part of the domain B were removed to form the RyR2-Del-305 mutant. (B) HEK293 cells were transfected with RyR2 WT or the RyR2 deletion mutant, Del-305. Fluorescence intensity of the Fluo-3-loaded transfected cells was monitored continuously before and after the additions of caffeine or ryanodine. Traces shown are from representative experiments. Similar results were obtained from 3-4 separate experiments. (C) Immunoblotting of RyR2-WT and the Del-305 mutant from the same amount of cell lysates with the anti-RyR antibody (34c) (n=3).

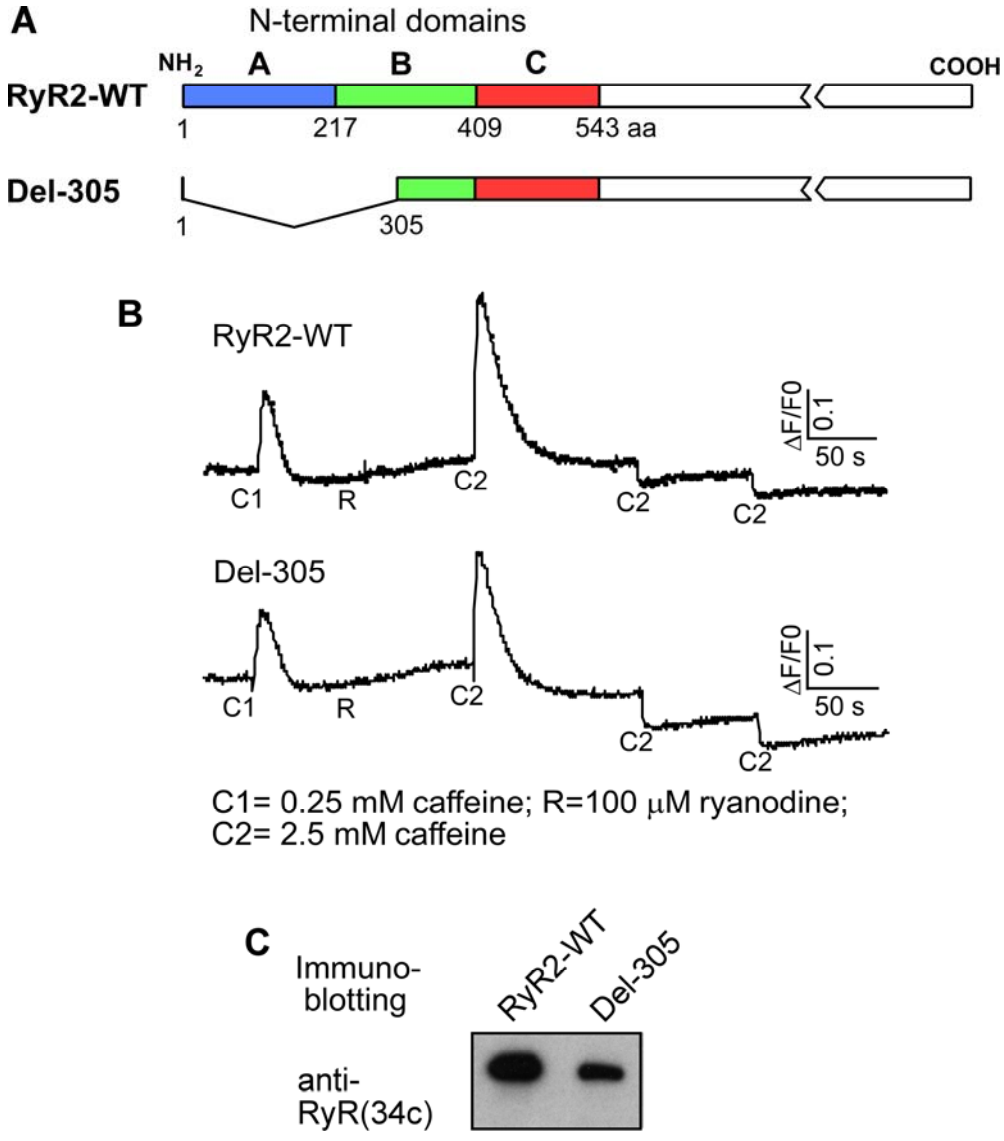
A
N-terminal domains
NH2
A
B
C
COOH
RyR2-WT
1
217
409
543 aa
Del-305
1
305
B
RyR2-WT
ΔF/F0
0.1
50 s
C1
R
C2
C2
C2
Del-305
ΔF/F0
0.1
50 s
C1
R
C2
C2
C2
C1= 0.25 mM caffeine; R=100 μM ryanodine;
C2= 2.5 mM caffeine
C
Immuno-
blotting
anti-
RyR(34c)
RyR2-WT
Del-305

Fig. 37 Effect of deleting the first 305 N-terminal residues of RyR2 on Ca^{2+} release activation and termination

Stable, inducible HEK293 cell lines expressing RyR2 WT or RyR2-Del-305 were transfected with the FRET-based ER luminal Ca^{2+} sensing protein D1ER 48 h before single cell FRET imaging. The expression of RyR2 WT and Del-305 was induced 24 h before imaging. The cells were perfused with KRH buffer containing increasing levels of extracellular Ca^{2+} (0-2 mM) to induce SOICR, followed by the addition of 1.0 mM tetracaine to inhibit SOICR, and then 20 mM caffeine to deplete the ER Ca^{2+} stores. FRET recordings from representative RyR2 WT (A) and Del-305 (B) cells (113-139) are shown. The activation threshold (C), termination threshold (D), fractional Ca^{2+} release (E), store capacity (F) were determined as described in the legend to Fig. 6. Data shown are mean ± SEM (n = 7-9) (* $P < 0.01$; vs WT).

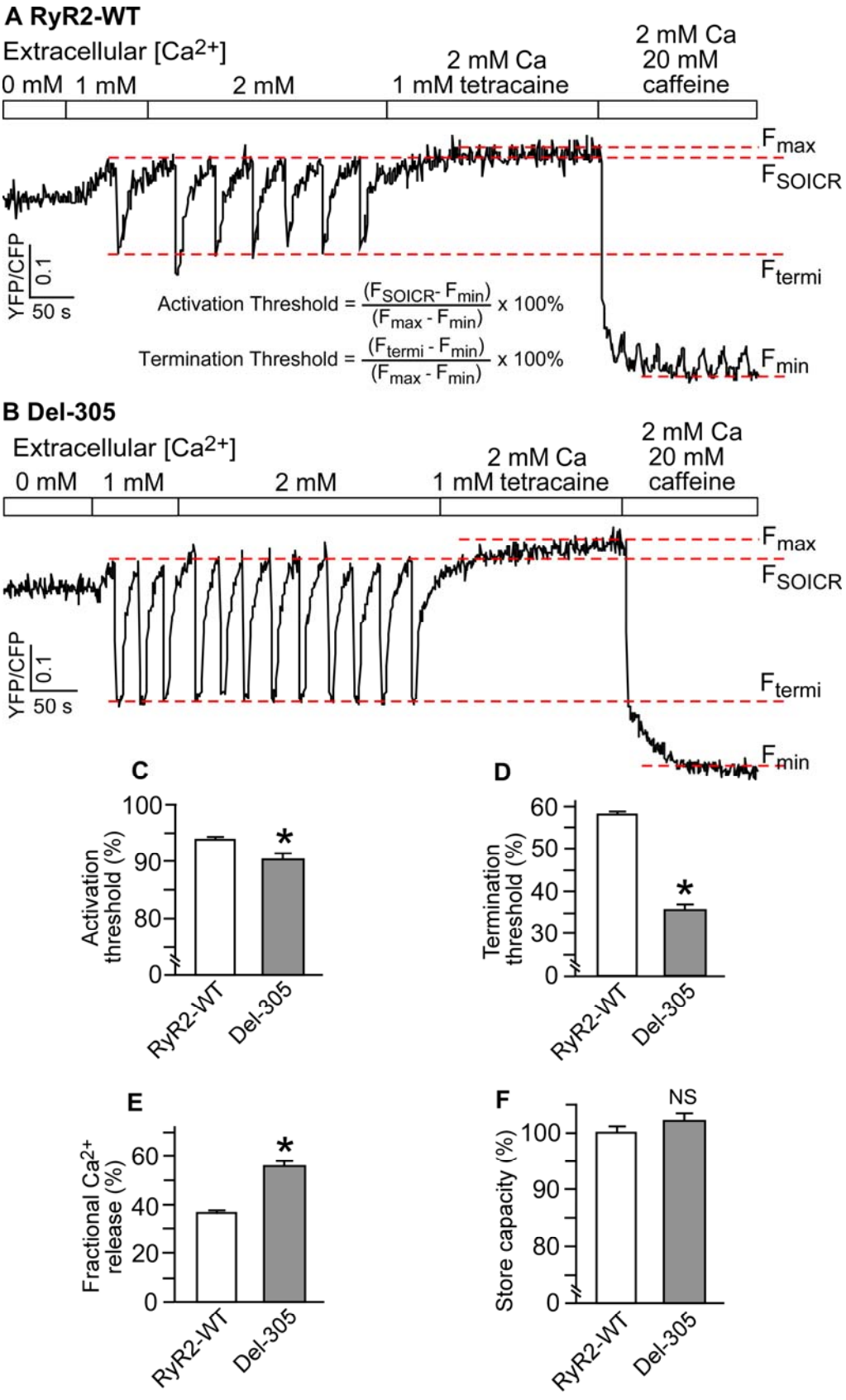
A RyR2-WT
Extracellular [Ca2+]
0 mM
1 mM
2 mM
2 mM Ca
1 mM tetracaine
2 mM Ca
20 mM
caffeine
Fmax
FSOICR
Ftermi
Fmin
YFP/CFP
0.1
50 s
Activation Threshold = (FSOICR- Fmin) / (Fmax - Fmin) x 100%
Termination Threshold = (Ftermi - Fmin) / (Fmax - Fmin) x 100%
B Del-305
Extracellular [Ca2+]
0 mM
1 mM
2 mM
2 mM Ca
1 mM tetracaine
2 mM Ca
20 mM
caffeine
Fmax
FSOICR
Ftermi
Fmin
YFP/CFP
0.1
50 s
C
Activation threshold (%)
100
90
80
0
*
RyR2-WT
Del-305
D
Termination threshold (%)
60
50
40
30
0
*
RyR2-WT
Del-305
E
Fractional Ca2+ release (%)
60
40
20
0
*
RyR2-WT
Del-305
F
Store capacity (%)
NS
100
90
80
0
RyR2-WT
Del-305

abnormalities and DCM [269,270,347] alters SOICR properties. Fig. 38 showed that the Del-Exon-3 mutant formed a functional Ca^{2+} release channel in HEK293 cells (Fig. 38B) and was expressed at a level similar to that of WT (Fig. 38C). Note that the pattern of caffeine- and ryanodine-response of the Del-Exon-3 mutant is indistinguishable from that of the RyR2 WT (Figs. 36B and38B). The ER luminal Ca^{2+} dynamics in these Del-Exon-3 mutant cells was then assessed. As seen in Fig. 39, the Del-Exon-3 mutant cells displayed a slightly lowered SOICR activation threshold (88% vs 94% in WT, $P < 0.01$) and a markedly reduced termination threshold (39% vs 57% in WT, $P < 0.01$) (Figs. 39A-D). The fractional Ca^{2+} release in the Del-Exon-3 cells (49%) is significantly greater than that in the WT cells (36%) ($P < 0.01$) (Fig.39E). There were no significant differences in store capacity between WT and Del-Exon-3 cells (Figs. 39F). These results demonstrate that the DCM-associated exon-3 deletion in RyR2 reduces the threshold for Ca^{2+} release termination and increases the fractional Ca^{2+} release.

6.2.3 Exon-3 deletion enhances the propensity for SOICR and the magnitude of Ca^{2+} transients

A reduced threshold for Ca^{2+} release termination is expected to increase the magnitude of Ca^{2+} release into the cytosol. To directly test this, we monitored the cytosolic Ca^{2+} transients in HEK293 cells expressing RyR2 WT and the Del-Exon-3 mutant using the cytosolic Ca^{2+} dye, Fura-2 AM. Fig. 40 shows that elevating extracellular Ca^{2+} induced SOICR in the form of cytosolic Ca^{2+} oscillations in both the WT (Fig. 40A) and Del-Exon-3 (Fig. 40B) cells. Importantly, the Del-Exon-3 mutant cells exhibited an enhanced propensity for SOICR (Fig. 40C). Furthermore, the Del-Exon-3 cells displayed increased amplitude (127 ± 1.3% of WT, $P < 0.05$) (Fig. 40D) and

Fig. 38 Construction and functional expression of the RyR2 Exon-3 deletion mutant

(A) Schematic linear structure of the N-terminal region of RyR2 WT and the RyR2 exon-3 deletion mutant (Del-Exon-3). The amino acid sequence of exon-3 and its secondary structures are also shown. (B) HEK293 cells were transfected with Del-Exon-3. Fluorescence intensity of the Fluo-3-loaded transfected cells was monitored continuously before and after the additions of caffeine or ryanodine. The trace shown is from a representative experiment. Similar results were obtained from 3 separate experiments. (C) Immunoblotting of RyR2-WT and the Del-Exon-3 mutant from the same amount of cell lysates with the anti-RyR antibody (34c) (n=3).

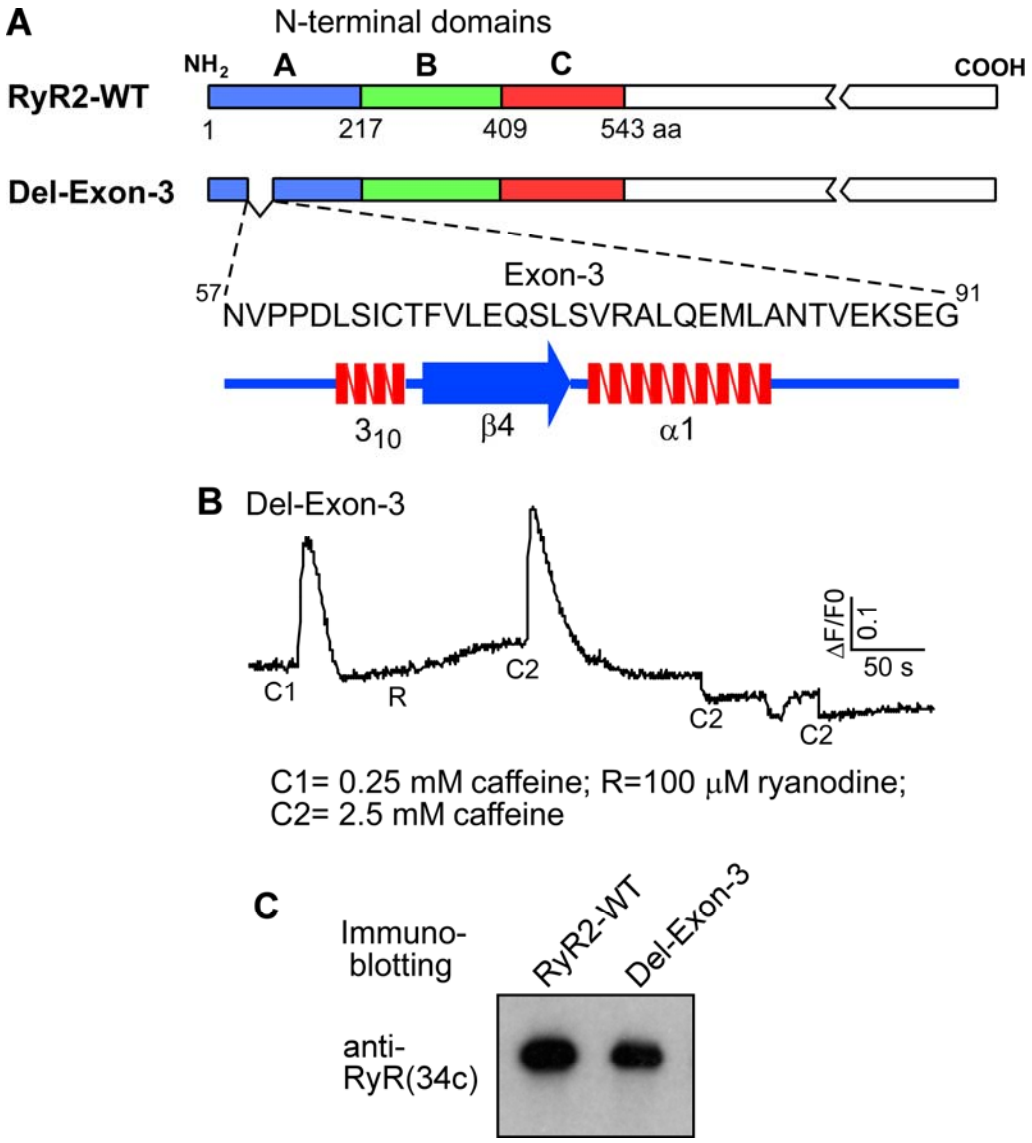
A
N-terminal domains
NH2
A
B
C
COOH
RyR2-WT
1
217
409
543 aa
Del-Exon-3
Exon-3
57
91
NVPPDLSICTFVLEQSLSVRALQEMLANTVEKSEG
310
β4
α1
B
Del-Exon-3
C1
R
C2
C2
C2
ΔF/F0
0.1
50 s
C1= 0.25 mM caffeine; R=100 μM ryanodine;
C2= 2.5 mM caffeine
C
Immuno-
blotting
anti-
RyR(34c)
RyR2-WT
Del-Exon-3

Fig. 39 Disease-causing RyR2 mutation, Exon-3 deletion, reduces the threshold for Ca^{2+} release termination

D1ER FRET signals were recorded in HEK293 cells expressing RyR2 WT (A) or the RyR2 exon-3 deletion mutant (Del-Exon-3) (B) using single cell FRET imaging. The activation threshold (C), termination threshold (D), fractional Ca^{2+} release (E), F_{max} (F), F_{min} (G), and store capacity (H) in RyR2 WT (139) and Del-Exon-3 (111) cells were determined as described in the legend to Fig. 6. Data shown are mean ± SEM (n = 6-9) (* $P < 0.01$; vs WT).

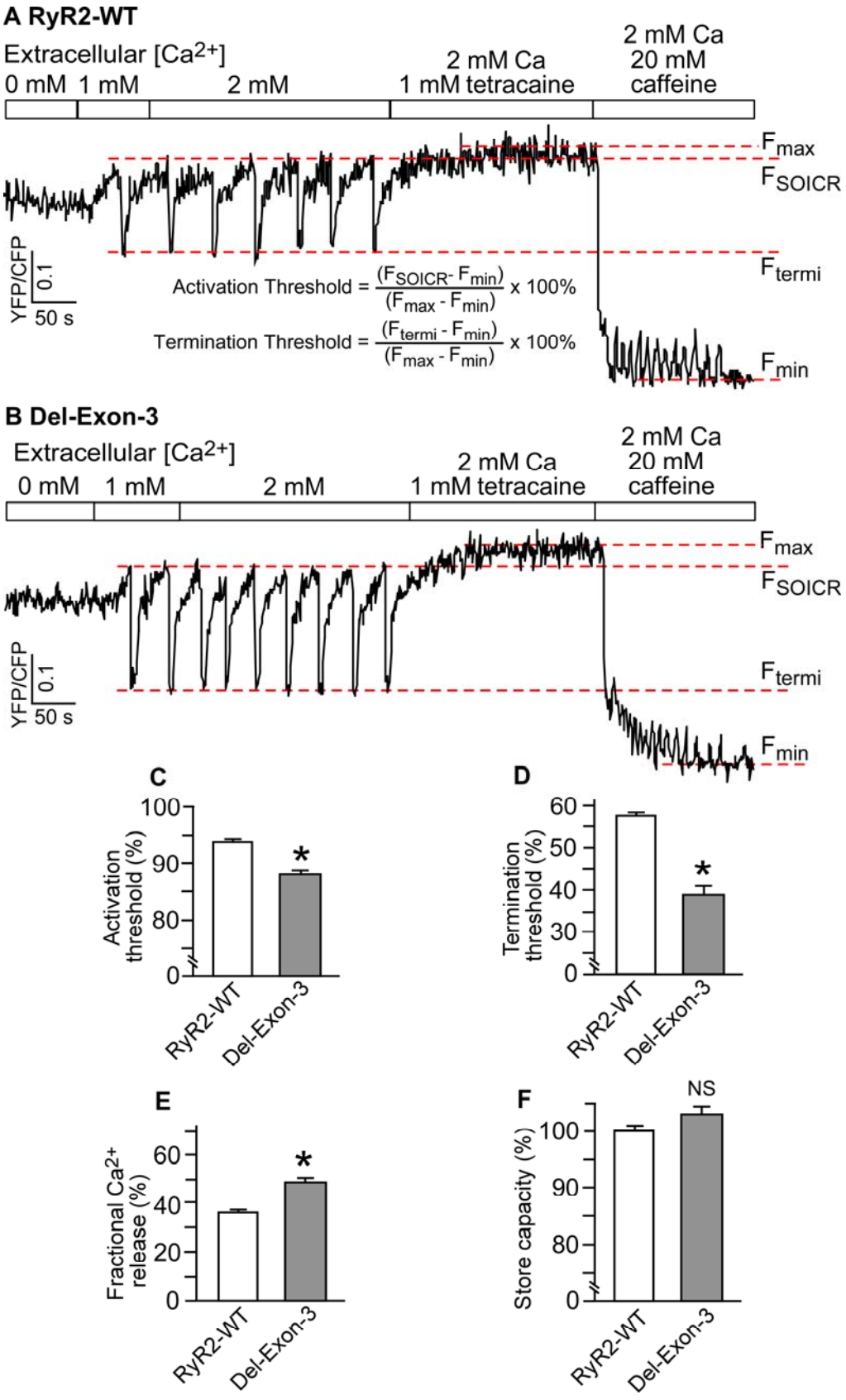
A RyR2-WT
Extracellular [Ca2+]
0 mM
1 mM
2 mM
2 mM Ca
1 mM tetracaine
2 mM Ca
20 mM
caffeine
Fmax
FSOICR
Ftermi
Fmin
YFP/CFP
0.1
50 s
Activation Threshold = (FSOICR - Fmin) / (Fmax - Fmin) x 100%
Termination Threshold = (Ftermi - Fmin) / (Fmax - Fmin) x 100%
B Del-Exon-3
C
Activation threshold (%)
D
Termination threshold (%)
E
Fractional Ca2+ release (%)
F
Store capacity (%)
NS
RyR2-WT
Del-Exon-3

Fig. 40 Exon-3 deletion enhances the occurrence, amplitude and frequency of SOICR in HEK293 cells

Stable, inducible HEK293 cells expressing RyR2 WT and the RyR2 exon-3 deletion mutant (Del-Exon-3) were loaded with 5 μM Fura-2 AM in KRH buffer. The cells were then perfused continuously with KRH buffer containing increasing levels of extracellular Ca^{2+} (0 - 2 mM) to induce SOICR. Fura-2 ratios of representative RyR2 WT (A) and Del-Exon-3 (B) cells were recorded using single cell Ca^{2+} imaging. (C) The percentages of RyR2 WT (337) and Del-Exon-3 (443) cells that display Ca^{2+} oscillations at various extracellular Ca^{2+} concentrations. (D, E) The amplitude (D) and frequency (E) of SOICR in RyR2 WT and Del-Exon-3 cells was determined by measuring the averaged peak and frequency of Ca^{2+} oscillations at 2 mM extracellular Ca^{2+}, and was normalized to that in the RyR2 WT cells (100%). Data shown are mean ± SEM (n = 8-9) ($^{\#}P < 0.05$; $^{*}P < 0.01$; vs WT).

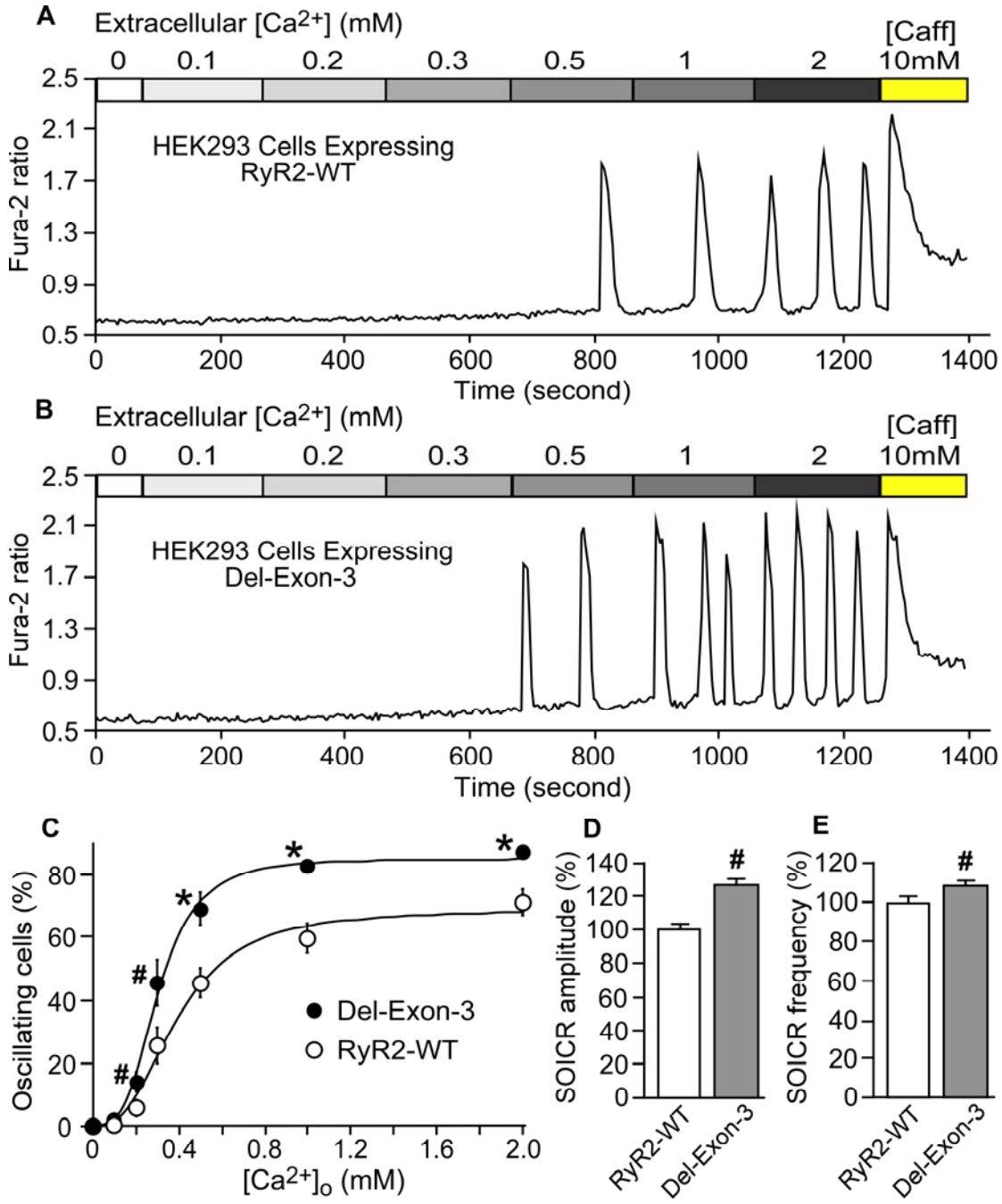
A
Extracellular [Ca2+] (mM)
0 0.1 0.2 0.3 0.5 1 2
[Caff]
10mM
HEK293 Cells Expressing
RyR2-WT
Fura-2 ratio
Time (second)
B
Extracellular [Ca2+] (mM)
0 0.1 0.2 0.3 0.5 1 2
[Caff]
10mM
HEK293 Cells Expressing
Del-Exon-3
Fura-2 ratio
Time (second)
C
Oscillating cells (%)
Del-Exon-3
RyR2-WT
[Ca2+]o (mM)
D
SOICR amplitude (%)
RyR2-WT
Del-Exon-3
E
SOICR frequency (%)
RyR2-WT
Del-Exon-3

Fig. 41 Deletion of the first 305 N-terminal residues of RyR2 enhances the propensity for SOICR and the amplitude of Ca^{2+} release

Stable, inducible HEK293 cells expressing RyR2 WT and the N-terminal deletion mutant (Del-305) were loaded with 5 μM Fura-2 AM in KRH buffer. The cells were then perfused continuously with KRH buffer containing increasing levels of extracellular Ca^{2+} (0 - 2 mM) to induce SOICR. Fura-2 ratios of representative RyR2-WT (A) and Del-305 (B) cells were recorded using single cell Ca^{2+} imaging. (C) The percentages of RyR2 WT (318) and Del-305 (410) cells that display Ca^{2+} oscillations at various extracellular Ca^{2+} concentrations. (D, E) The amplitude (D) and frequency (E) of SOICR in RyR2 WT and Del-305 expressing HEK293 cells were determined by measuring the averaged peak amplitude and frequency of Ca^{2+} oscillations at 2 mM extracellular Ca^{2+}, and normalized to that in the RyR2 WT cells (100%). Data shown are mean ± SEM (n = 7) (#$P < 0.05$; *$P < 0.01$ vs WT).

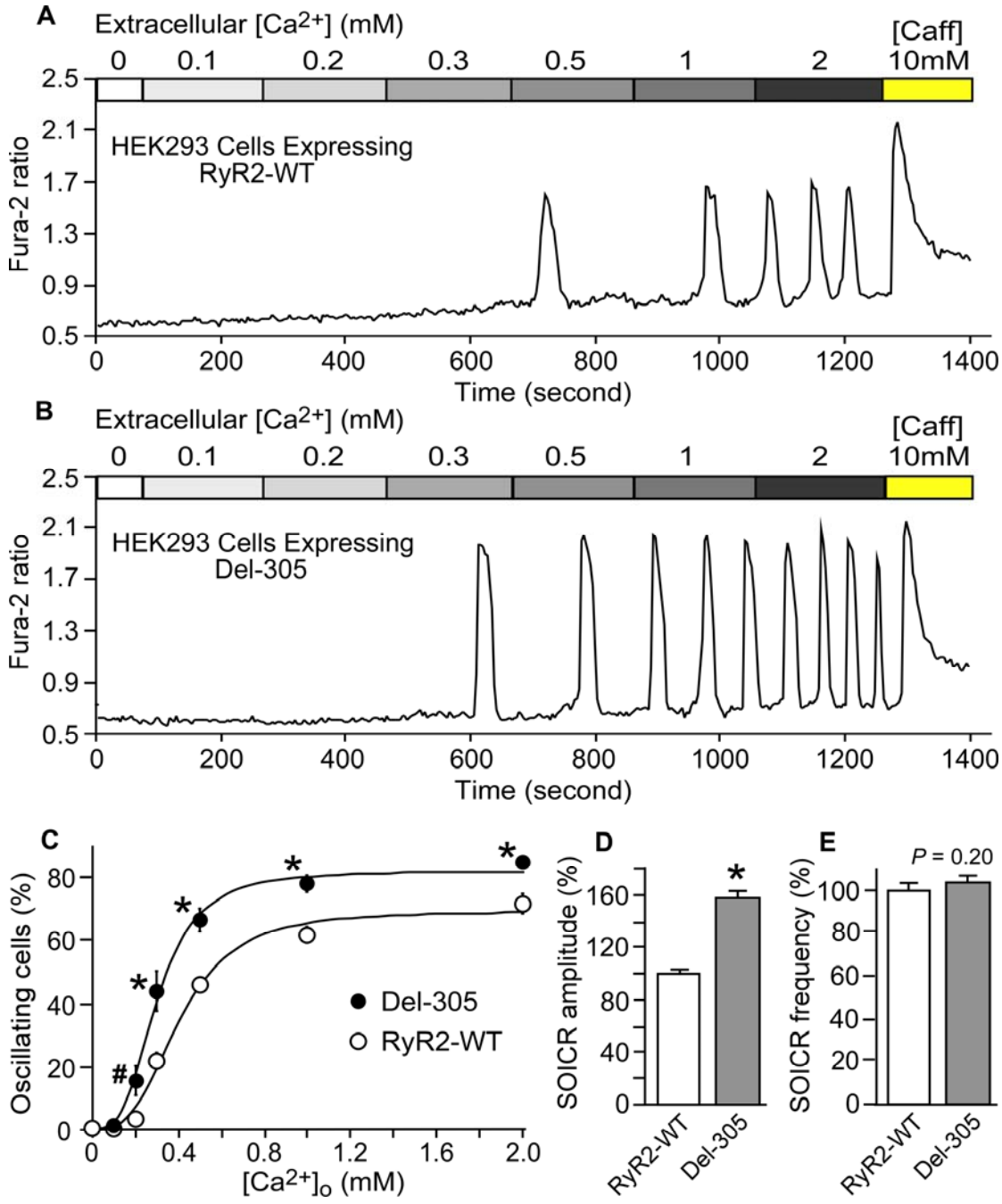
A
Extracellular [Ca2+] (mM)
0 0.1 0.2 0.3 0.5 1 2
[Caff]
10mM
HEK293 Cells Expressing
RyR2-WT
Fura-2 ratio
Time (second)
B
Extracellular [Ca2+] (mM)
HEK293 Cells Expressing
Del-305
Fura-2 ratio
Time (second)
C
Oscillating cells (%)
Del-305
RyR2-WT
[Ca2+]o (mM)
D
SOICR amplitude (%)
RyR2-WT
Del-305
E
P = 0.20
SOICR frequency (%)
RyR2-WT
Del-305

frequency (108 ± 2.2% of WT, $P < 0.05$) (Fig. 40E) of SOICR. Similarly, we found that the deletion of the first 305 N-terminal residues encompassing exon-3 also enhanced the occurrence and amplitude (164 ± 14% of WT, $P < 0.01$) of SOICR (Fig. 41). It should be noted that the store Ca^{2+} contents in RyR2 WT (100%), Del-Exon-3 (98 ± 1.0% of WT), and Del-305 (104 ± 3.9% of WT) cells are not significantly different.

To investigate whether the Del-Exon-3 deletion exerts its effect on SOICR in the context of cardiac cells, we transfected the HL-1 cardiac cells, a mouse atrial cell line, with GFP-tagged RyR2 WT or GFP-tagged Del-Exon-3 mutant and monitored the cytosolic Ca^{2+} transients during SOICR (Figs. 42A,B). Similar to those observed in HEK293 cells, we found that the exon-3 deletion increased the occurrence (Fig. 42C), amplitude (193 ± 1.0% of WT, $P < 0.01$) (Fig. 42D), and frequency (133 ± 13% of WT, $P = 0.06$) (Fig. 42E) of SOICR. There was no significant difference in the store Ca^{2+} contents between the WT (100%) and Del-Exon-3 (104 ± 1.0% of WT) transfected HL-1 cardiac cells. Taken together, these results demonstrate that the disease-causing exon-3 deletion enhances the occurrence of SOICR by reducing the activation threshold, and increases the amplitude of Ca^{2+} transients by reducing the termination threshold.

6.2.4 RyR2 N-terminal mutations associated with ARVD2 reduce the threshold for Ca^{2+} release termination

A number of point mutations in the N-terminal region of RyR2 have been associated with ARVD2 cardiomyopathy[274,279-283,347]. To determine whether these N-terminal ARVD2-associated RyR2 mutations also affect Ca^{2+} release termination, we generated HEK293 cell lines that express the RyR2 mutations, A77V, R176Q/T2504M, R420W, and L433P, and determined their SOICR properties. As shown in Fig. 43, each of these

Fig. 42 Effect of RyR2 Exon-3 deletion on SOICR in mouse HL-1 cardiac cells

Mouse HL-1 cardiac cells were transfected with a GFP-tagged RyR2 WT or a GFP-tagged Del-Exon-3 mutant using the Nucleofection method (Amaxa). Transfected cells were loaded with 5 μM Fura-2 AM and were then perfused continuously with KRH buffer containing increasing levels of extracellular Ca^{2+} (0.3-5 mM). Fura-2 ratios of representative HL-1 cardiac cells expressing the GFP-tagged RyR2 WT (A) and the GFP-tagged Del-Exon-3 mutant (B), identified based on their GFP fluorescence, were recorded using single cell Ca^{2+} imaging. (C) The percentages of GFP-tagged RyR2 WT (142) and GFP-tagged Del-Exon-3 (153) cells that display Ca^{2+} oscillations at various extracellular Ca^{2+} concentrations. (D, E) SOICR amplitude (D) and frequency (E) in RyR2 WT and Del-Exon-3 cells, normalized to that in the GFP-tagged RyR2 WT cells (100%). Data shown are mean ± SEM (n = 6-8) ($^{\#}P < 0.05$; $^{*}P < 0.01$; vs WT).

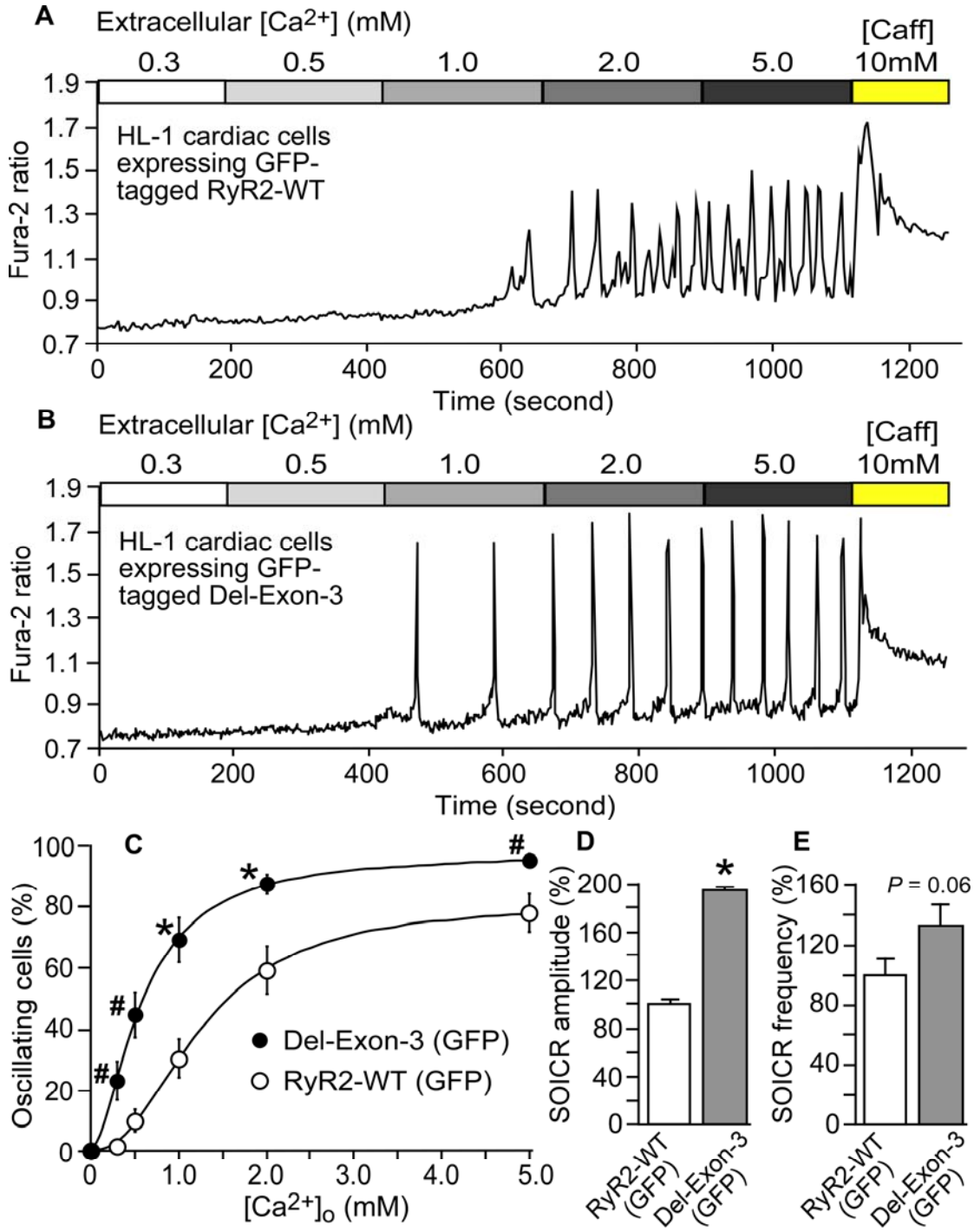
A
Extracellular [Ca2+] (mM)
0.3
0.5
1.0
2.0
5.0
[Caff]
10mM
HL-1 cardiac cells expressing GFP-tagged RyR2-WT
Fura-2 ratio
Time (second)
B
Extracellular [Ca2+] (mM)
HL-1 cardiac cells expressing GFP-tagged Del-Exon-3
Fura-2 ratio
Time (second)
C
Oscillating cells (%)
Del-Exon-3 (GFP)
RyR2-WT (GFP)
[Ca2+]o (mM)
D
SOICR amplitude (%)
RyR2-WT (GFP)
Del-Exon-3 (GFP)
E
SOICR frequency (%)
P = 0.06
RyR2-WT (GFP)
Del-Exon-3 (GFP)

RyR2 mutations reduced both the activation (Fig. 43A) and termination (Fig. 43B) thresholds for Ca^{2+} release. Each of these mutations also increased the fractional Ca^{2+} release due to a greater reduction in the termination threshold than in the activation threshold (Fig. 43C). Interestingly, CPVT mutations E189D and R4496C that are not associated with cardiomyopathy [250,349] reduced the activation and termination thresholds to a similar extent (Figs. 43A,B). As a result, the E189D mutation did not significantly alter the fractional Ca^{2+} release (Fig. 43C). There were no significant differences in store capacity between WT and mutant cells (Fig. 43D). Furthermore, these RyR2 N-terminal mutants were expressed in HEK293 cells at a level comparable to that of WT (Fig. 43E). Together, these observations show that increased fractional Ca^{2+} release due to reduced Ca^{2+} release termination is a common defect of ARVD2-associated RyR2 mutations.

6.2.5 HCM-linked RyR2 mutation A1107M increases the threshold for Ca^{2+} release termination

The human RyR2 mutation, T1107M, has been shown to be associated with HCM [272]. It is of interest to determine whether this mutation alters SOICR in a manner similar to those associated with DCM or ARVD2. To this end, we generated stable, inducible HEK293 cell line expressing the mouse RyR2 mutation A1107M, corresponding to the human HCM-associated RyR2 mutation, T1107M. Interestingly, the A1107M mutation significantly increased the termination threshold (61% vs 57% in WT, $P < 0.05$), but it did not significantly affect the activation threshold (Figs. 44A-C). This increase in the termination threshold but not in the activation threshold resulted in a significant reduction in the fractional Ca^{2+} release (32% vs 36% in WT, $P < 0.01$) (Fig.44D). There were no

Fig. 43 ARVD2-associted RyR2 N-terminal mutations decrease the termination threshold and increase the fractional Ca^{2+} release

D1ER FRET imaging was performed in single HEK293 cells expressing the RyR2 WT, ARVD2-associated RyR2 mutations (A77V, R176Q/T2504M, R420W, and L433P), and the E189D and R4496C RyR2 mutation associated with CPVT-only. The activation threshold (A), termination threshold (B), fractional Ca^{2+} release (C) and the store capacity (D) in RyR2 WT (250) and mutant (87-110) cells were determined as described in the legend to Fig. 6. Data shown are mean ± SEM (n = 5-13) (*P < 0.01; vs WT). (E) Immunoblotting of RyR2 WT and RyR2 mutants from the same amount of cell lysate using the anti-RyR antibody (34c) (n = 3).

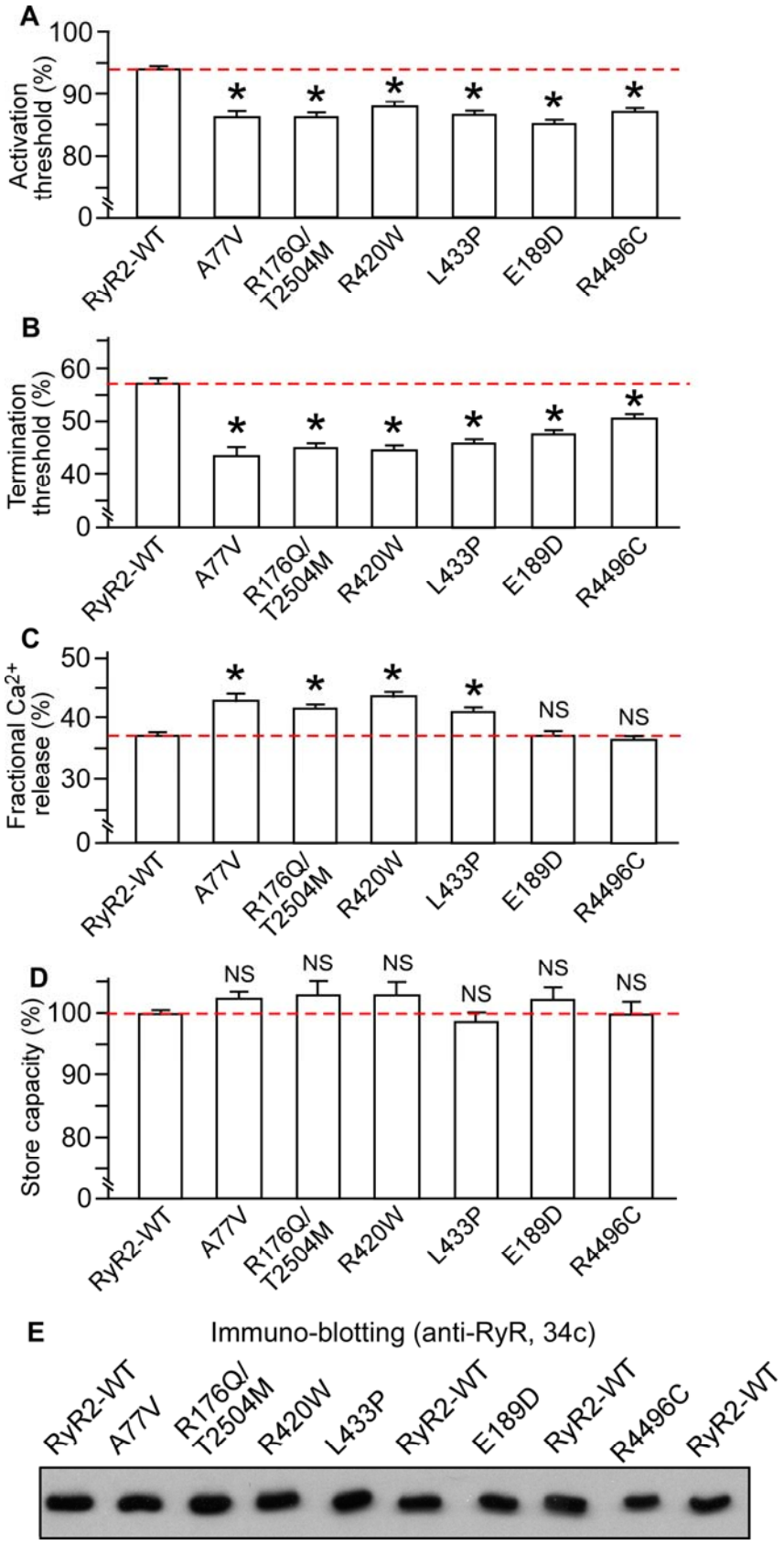
A
Activation threshold (%)
100
90
80
0
B
Termination threshold (%)
60
50
40
0
C
Fractional Ca2+ release (%)
50
40
30
0
NS
D
Store capacity (%)
100
90
80
0
NS
E
Immuno-blotting (anti-RyR, 34c)
RyR2-WT
A77V
R176Q/ T2504M
R420W
L433P
E189D
R4496C

Fig. 44 HCM-associated RyR2 mutation A1107M increases the termination threshold and decreases the fractional Ca^{2+} release

D1ER FRET signals were recorded in HEK293 cells expressing the RyR2 mutation A1107M (A) using single cell FRET imaging. The activation threshold (B), termination threshold (C), fractional Ca^{2+} release (D) and store capacity (E) in RyR2 WT (250) and the A1107M mutant (111) cells were determined as described in the legend to Fig. 6. Data shown are mean ± SEM (n = 7-13) ($^{\#}P < 0.05$; $*P < 0.01$; vs WT). (F) Immunoblotting of RyR2 WT and the A1107M mutant from the same amount of cell lysate using the anti-RyR antibody (34c) (n = 3).

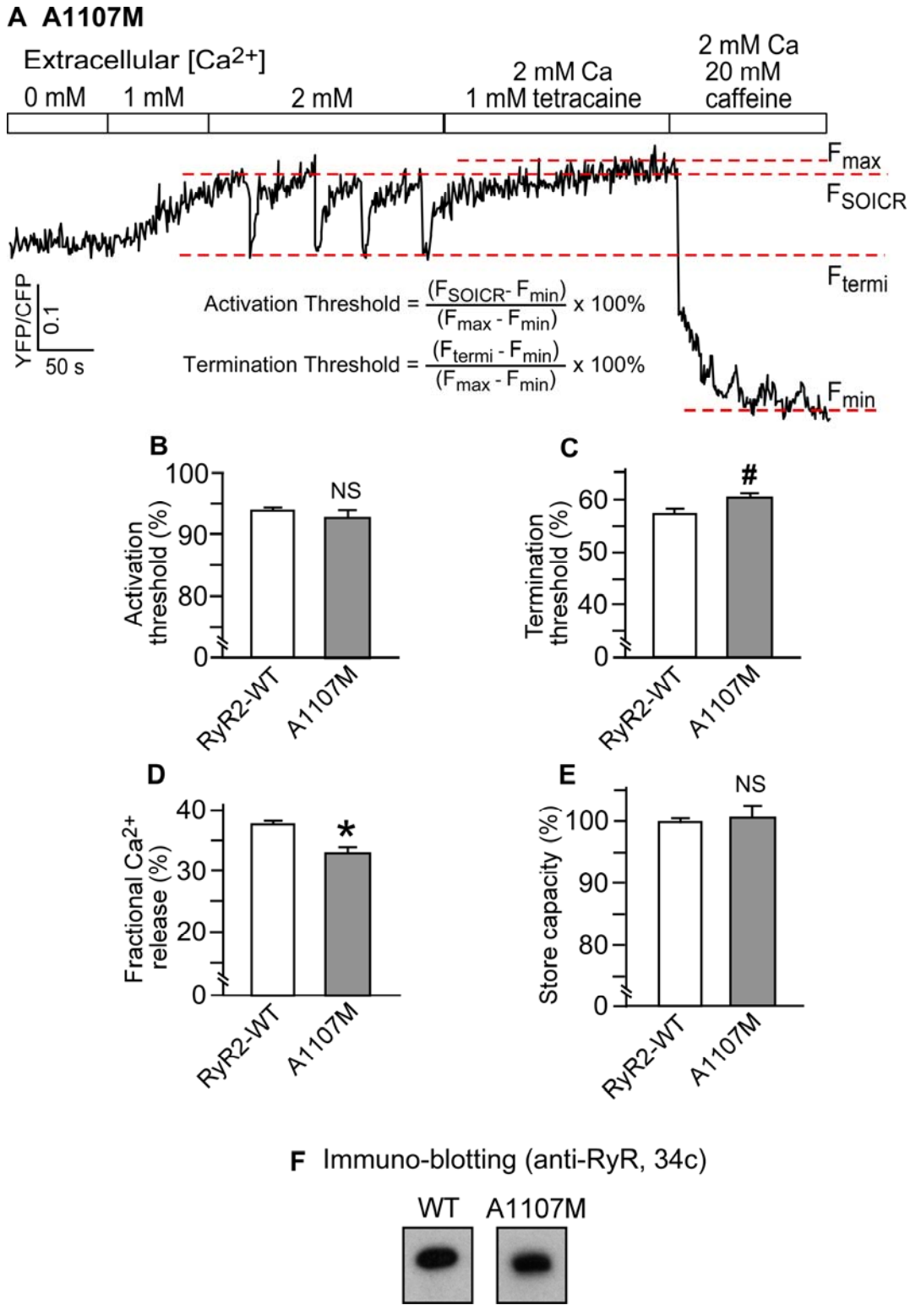
A A1107M
Extracellular [Ca2+]
0 mM
1 mM
2 mM
2 mM Ca
1 mM tetracaine
2 mM Ca
20 mM
caffeine
Fmax
FSOICR
Ftermi
Fmin
YFP/CFP
0.1
50 s
Activation Threshold = (FSOICR- Fmin) / (Fmax - Fmin) x 100%
Termination Threshold = (Ftermi - Fmin) / (Fmax - Fmin) x 100%
B
Activation threshold (%)
NS
C
Termination threshold (%)
#
D
Fractional Ca2+ release (%)
*
E
Store capacity (%)
NS
RyR2-WT
A1107M
F Immuno-blotting (anti-RyR, 34c)
WT
A1107M

significant differences in store capacity between the WT and A1107M mutant cells (Fig. 44E). The expression level of the RyR2 WT and A1107M mutant was also similar (Fig.44F). Therefore, in contrast to the effect of RyR2 mutations associated with DCM and ARVD2, the A1107M mutation associated with HCM increases the threshold for Ca^{2+} release termination and decreases the fractional Ca^{2+} release.

6.3 Summary

Naturally occurring mutations in RyR2 have been associated with both cardiac arrhythmias and cardiomyopathies. While it has become clear that DAD resulting from abnormal activation of SR Ca^{2+} release is the primary cause of RyR2-associated cardiac arrhythmias, the mechanism underlying RyR2-associated cardiomyopathies is completely unknown. We aimed to investigate the role of the N-terminal region of RyR2 in and the impact of a number of cardiomyopathy-associated RyR2 mutations on the activation and termination of Ca^{2+} release.

Single cell luminal Ca^{2+} imaging analysis revealed that the deletion of the first 305 N-terminal resides encompassing exon-3 or the deletion of exon-3 in RyR2, which is associated with DCM, markedly reduced the luminal Ca^{2+} threshold at which Ca^{2+} release terminates and increased the fractional Ca^{2+} release. Single cell cytosolic Ca^{2+} imaging also showed that both RyR2 deletions enhanced the amplitude of store overload induced Ca^{2+} transients in HEK293 cells and HL-1 cardiac cells. Furthermore, the RyR2 N-terminal mutations, A77V, R176Q/T2504M, R420W, and L433P, that are associated with ARVD2, also reduced the luminal Ca^{2+} threshold for Ca^{2+} release termination and increased the fractional Ca^{2+} release. Interestingly and in contrast, the RyR2 mutation

A1107M associated with HCM increased the luminal Ca^{2+} threshold for Ca^{2+} release termination and reduced the fractional Ca^{2+} release. In summary, cardiomyopathy-linked mutations in the N-terminal region of RyR2 all show altered termination threshold and fractional Ca^{2+} release. These results provide the first evidence that the N-terminal region of RyR2 is an important determinant of Ca^{2+} release termination, and that abnormal fractional Ca^{2+} release due to impaired Ca^{2+} release termination is a common defect for RyR2-associated cardiomyopathies.

CHAPTER VII: DISCUSSION AND FUTURE STUDIES

7.1 Molecular determinants of Ca^{2+} release activation and termination in RyR2

EC coupling is one of the most fascinating cellular processes in muscle physiology, whereby external electrical signals (excitation) are transmitted to chemical signals (Ca^{2+}) and ultimately lead to muscle contraction [2,3,350].

Investigations over the past half century have greatly advanced our understanding of the signal transduction pathway involved in EC coupling. The most important step in EC coupling is CICR via the RyR2 channel, which acts to amplify the Ca^{2+} signal. The 'local control' theory has been proposed to account for the initiation and gradation of CICR. In response to Ca^{2+} influx through L-type Ca^{2+} channel, graded CICR can be achieved by recruiting various numbers of Ca^{2+} release units (Ca^{2+} sparks) [28,31,33,34]. For each release unit, one would expect that all of the stored Ca^{2+} would be released upon stimulation due to the regenerative nature of CICR. However, the SR Ca^{2+} store is only partially depleted during Ca^{2+} sparks or global Ca^{2+} transients. [39-42]. Robust mechanisms that turn off the SR Ca^{2+} release are essential for stable EC coupling and muscle relaxation [20].

7.1.1 Ca^{2+} release terminates at a fixed threshold of ER luminal Ca^{2+} in HEK293 cells

Despite its pivotal role in muscle function, the molecular basis of Ca^{2+} release termination is largely unknown. Since growing evidence suggests that Ca^{2+} release termination is controlled by luminal Ca^{2+} dependent inactivation of RyR2 [40-42,54-56], direct monitoring of luminal Ca^{2+} should provide us with useful information to help understand the mechanism of Ca^{2+} release termination. However, the luminal Ca^{2+} probes currently used, such as Fluo-5N, are ineffective for monitoring SR Ca^{2+} dynamics in mouse cardiac cells for some unknown reasons, although they can be used for studies in rat, rabbit and canine cardiac cells [42,53,322,323]. In addition, difficulties in the introduction of the large

RyR2 cDNA (~15kb) to isolated cardiomyocytes have hampered the luminal Ca^{2+} studies. Here we established a system using D1ER, a FRET-based ER luminal Ca^{2+} sensing protein, to monitor the luminal Ca^{2+} dynamics in HEK293 cells. By directly monitoring the SR luminal Ca^{2+} level in rabbit cardiomyocytes, Zima et al. showed that spontaneous SR Ca^{2+} release terminates when the SR luminal Ca^{2+} level declines to a critical threshold (~60% of the SR Ca^{2+} content) [42]. Interestingly, we found that spontaneous Ca^{2+} release due to Ca^{2+} overload (or SOICR) in HEK293 cells expressing RyR2 WT also terminates when the ER luminal Ca^{2+} level declines to ~57% of the ER store capacity (Fig. 6). These observations indicate that termination of Ca^{2+} release is not unique to cardiomyocytes, rather it reflects the intrinsic properties of RyR2. Thus, our HEK293 cell system is an effective and easy-to-use method to assess the molecular mechanism of Ca^{2+} release termination. Using this system, we have identified several molecular determinants of Ca^{2+} release activation and termination.

7.1.2 Pore-forming region

7.1.2.1 Luminal Ca^{2+} sensing residue E4872 is important for Ca^{2+} release termination

Our laboratory has previously found that the helix bundle crossing of RyR2, which constitutes the ion gate of the channel, plays a primary role for luminal Ca^{2+} activation. Some negatively charged amino acids located at this helix bundle crossing were found to be involved in the formation of a luminal Ca^{2+} sensor. Among these residues, E4872 was proposed to be the major luminal Ca^{2+} sensing residue. A single mutation to alanine at E4872 abolished the luminal Ca^{2+} activation but not cytosolic Ca^{2+} activation. We also found that introducing metal-binding histidines at E4872 and its adjacent site converted RyR2 into a Ni^{2+}-gated channel, indicating the pivotal role of the E4872 residue in

luminal Ca^{2+} sensing (unpublished data). Consistent with these observations, the present study shows that the E4872A mutation increases both the activation and termination thresholds for Ca^{2+} release (Fig.9). In other words, higher luminal Ca^{2+} concentrations are required to activate the E4872A mutant channel as compared to the WT channel. On the other hand, less luminal Ca^{2+} depletion is needed to inactivate the mutant channel and to terminate Ca^{2+} release. These new data suggest that the E4872A mutation reduces the binding affinity for luminal Ca^{2+}, thus weakening the luminal Ca^{2+}-dependent activation of Ca^{2+} release. It is possible that this reduced affinity for luminal Ca^{2+} binding may increase the rate of dissociation of luminal Ca^{2+} from the sensor during Ca^{2+} depletion, thus promoting luminal Ca^{2+}-dependent inactivation of the channel and the termination of Ca^{2+} release.

Previous studies also showed that introducing a negative charge next to residue E4872 (G4871E) was capable of restoring the missing luminal Ca^{2+} activation of the E4872A mutant channel. Consistent with this observation, this double mutation, G4871E/E4872A, not only rescued luminal Ca^{2+} activation, but also re-established the termination of Ca^{2+} release (Fig.10). Taken together, these results indicate that the E4872 residue as a luminal Ca^{2+} binding site plays a crucial role in both luminal Ca^{2+} activation and termination.

7.1.2.2 Mechanism of luminal Ca^{2+} dependent activation and termination of Ca^{2+} release

A number of other mutations in the helix bundle crossing and TM10 have also been studied. Diverse patterns of changes in Ca^{2+} release induced by these mutations were observed. Some of these mutations including A4869G, Q4876A, F4870A, V4880A and K4881A lowered both the activation and termination thresholds for Ca^{2+} release (Fig. 11).

Other mutations including I4862A, G4864A, G4871R, E4882A and D4896A only affected the activation or the termination of Ca^{2+} release (Figs. 12&13). Interestingly, mutation of the negatively charged amino acid D4868 showed an increased threshold for Ca^{2+} release activation, but a decreased threshold for Ca^{2+} release termination (Fig. 14). These observations suggest that residues in the pore-forming region of RyR2 contribute diversely to Ca^{2+} release activation and termination. Residues E4872, D4868, A4869, Q4876, F4870, V4880 and K4881 control both the activation and termination of Ca^{2+} release. Residues I4862, G4864, G4871, E4882 and D4896 seem to be mainly involved in the regulation of one of these release phases. These studies provide novel information on critical residues in the pore-forming region that are critical for Ca^{2+} release activation and termination.

Based on these observations, it could be proposed that the pathways for Ca^{2+} release termination and activation are distinct but overlap. In other words, the activation and termination of Ca^{2+} release take place in two different states of the channel: activation of Ca^{2+} release (channel opening) may result from the binding of Ca^{2+} to the luminal Ca^{2+} sensor in the closed state, whereas termination of Ca^{2+} release (channel closing) occurs when the bound Ca^{2+} dissociates from the luminal Ca^{2+} sensor in the open state. The luminal Ca^{2+} level required for the activation of Ca^{2+} release (Ca^{2+} binding to the closed state) is always higher than that required for the termination of Ca^{2+} release (Ca^{2+} unbinding from the open state), suggesting that the affinity of Ca^{2+} binding to the luminal Ca^{2+} sensor in the closed state is lower than that in the open state.

A number of mutations in the pore-forming region affect either Ca^{2+} release activation or Ca^{2+} release termination or both. This indicates that residues in the pore

forming region involved in luminal Ca^{2+} activation and those involved in Ca^{2+} release termination are different. However, the exact mechanism by which they differentially contribute to the activation or termination of Ca^{2+} release is unknown. 3D structural modeling has revealed a close proximity of residues D4868, E4872 and R4874 in the channel pore. Furthermore, previous studies suggest that these residues are involved in the formation of salt bridges and play a role in stabilizing the closed state of the channel. Thus, one could imagine that mutations of residues D4868 and E4872 could affect the threshold for Ca^{2+} release activation. This is indeed the case. However, it is unclear why these salt-bridge forming residues, D4868 and E4872, contribute oppositely to the termination of Ca^{2+} release. Solving the crystal structures of the RyR2 pore in both the open and closed states would allow us to define the roles of each residue in the pore region in channel gating.

7.1.3 Other regions in RyR2 critical for Ca^{2+} release activation and termination

The activation and termination of Ca^{2+} release reflect the gating properties of the RyR2 channel. Specifically, the activation of Ca^{2+} release (channel opening) depends on the gating properties of the channel in the closed state, whereas the termination of Ca^{2+} release (channel closing) results from deactivation of the channel from the open state. Therefore, regions in RyR2 that could affect the channel gating properties are potentially involved in determining Ca^{2+} release activation and termination. It is clear that the pore-forming region interacts with luminal Ca^{2+} to initiate the activation or termination of Ca^{2+} release. We also found that several other regions that undergo conformational changes during gating are crucial for Ca^{2+} release activation and termination.

7.1.3.1 N-terminal region of RyR2

The 3D structure of the N-terminal region of RyR has recently been solved [128-130,352]. This 3D structure reveals that the N-terminal region of RyR contains 3 domains that interact with each other to form the cytoplasmic vestibule at the center of the channel. Interestingly, most of the disease-causing RyR mutations are located in interfaces between the 3 N-terminal domains or between the N-terminal domains and other parts of the channel [129]. Importantly, the cytoplasmic vestibule corresponding to the N-terminal region has been shown to undergo conformational changes during channel gating [136]. Based on these observations, it has been proposed that the N-terminal region of RyR is allosterically coupled to the transmembrane pore region [352]. Thus, mutations in the N-terminal region may affect the gating of the channel and the properties of Ca^{2+} release by disrupting the allosteric coupling between the N-terminal domains and the channel pore region. Consistent with this prediction, we found that the N-terminal Del-305 deletion interrupted both the Ca^{2+} release activation and termination (Fig 37). Other disease-linked N-terminal mutations also affected the Ca^{2+} release properties to various levels (Fig. 39, 43 and 44).

7.1.3.2 CaMBD of RyR2

Cross-linking studies revealed that disulfide bonds could be formed between subunits by treating RyR1 with oxidizing agents, and that the formation of these disulfide bonds was prevented by Ca^{2+}-CaM or apoCaM [353,354], indicating that CaM may bind to a site of inter-subunit contact. 3D structural studies have shown that the CaMBD (amino acids 3614-3643 in RyR1; amino acids 3583-3603 in RyR2) is located midway between the clamp region and the transmembrane region[107,207-209], suggesting its potential role in

cross-talk between the cytoplasmic domain and the channel gate. Therefore, CaMBD may also be involved in determining the channel gating properties. Consistently, we found that deletion or triple/single mutations in the CaMBD all reduced Ca^{2+} release termination, while one of these mutations also interrupted Ca^{2+} release activation (Fig 17, 18 and19).

In summary, the pore-forming region of RyR2, the primary region involved in luminal Ca^{2+}-dependent activation and channel gating, also determines Ca^{2+} release termination. In addition, the N-terminal region and CaMBD are also important determinants of Ca^{2+} release activation and termination.

7.2 RyR2 modulators in Ca^{2+} release activation and termination

RyR2 has been found to interact with a number of modulators, such as CaM, FKBP12.6, and Ca^{2+}. Impaired interactions of RyR2 with these modulators have been shown to cause or affect the development of cardiac disease as a result of altered SR Ca^{2+} release. However, it is unclear whether these RyR2-interacting proteins affect Ca^{2+} release primarily by modulating the activation or the termination aspect of Ca^{2+} release.

7.2.1 CaM and CaMBD

7.2.1.1 Ca^{2+}-CaM facilitates Ca^{2+} release termination

CaM has been found to reduce the P_o of RyR2 activated either by cytosolic Ca^{2+} or luminal Ca^{2+}. When the cytosolic Ca^{2+} decreased to less than 10 μM, more potent inhibition by CaM was observed at the single channel level. Based on these observations, it has been suggested that CaM may play a role in the termination of SR Ca^{2+} release by reducing the probability of channel reopening when the local cytosolic Ca^{2+} decreases to

less than 10 μM [49].

The role of CaM in the termination of Ca^{2+} release has not been well established at the cellular level. To directly address this issue, the effect of CaM on luminal Ca^{2+} dynamics in HEK293 cells was characterized. Consistent with the proposed role of CaM in Ca^{2+} release termination, overexpression of CaM was found to enhance Ca^{2+} release termination (Fig. 16). It was also found that the inhibitory effect of CaM depends largely on its Ca^{2+} binding capability since the Ca^{2+}-binding deficient mutant of CaM, CaM (1-4), was ineffective in hastening the termination of Ca^{2+} release (Fig. 16). This is consistent with the previous finding from other groups that RyR2 was unaffected by apoCaM [49,199,200] but different from the observation from one group that apoCaM was also capable of inhibiting RyR2 [201]. On the other hand, substitution of the endogenous CaM with CaM (1-4) delayed Ca^{2+} release termination, indicating the role of endogenous Ca^{2+}-CaM as an inhibitor of Ca^{2+} release. In future studies, it will be of interest to dissect which lobes (N- or C-lobes) of CaM are responsible for the CaM effect on Ca^{2+} release termination using CaM (1,2), in which the two Ca^{2+} binding sites in the N-lobe are mutated, and CaM (3,4), in which the two Ca^{2+} binding sites in the C-lobe of CaM are mutated.

As CaM is known to be involved in a wide range of cellular processes [193], it is necessary to confirm that the effect of CaM on the termination of Ca^{2+} release is mediated by RyR2, but not by other processes triggered by overexpression of CaM or CaM (1-4). A CaMBD of RyR2 has been located at residues 3583-3603. Deletion of this CaMBD resulted in background [^{35}S] CaM binding and impaired CaM inhibition of RyR2 in single channel measurements [200]. Similarly, we found that CaM and CaM (1-4) failed to change the threshold for Ca^{2+} release termination in cells expressing the Del-

3583-3603 mutant, which is incapable of binding CaM (Fig. 17). This result indicates that the inhibition of Ca^{2+} release by CaM is mediated by RyR2 but not by other secondary effects. Meanwhile, we found that Del-3583-3603 delayed the termination of Ca^{2+} release and generated a large fractional Ca^{2+} release as seen in RyR2 WT cells co-expressed with CaM (1-4), indicating that defective CaM binding leads to impaired Ca^{2+} release. These results consistently support the view that Ca^{2+}-CaM is able to inhibit the activity of RyR2 and thus strengthen Ca^{2+} release termination.

It is also interesting to note that, in Meissner's model of CaM-dependent inhibition of RyR2, substantial inhibition of RyR2 by CaM only occurs at low cytosolic Ca^{2+} concentrations. During diastole, CaM binds to RyR2 and stabilizes the channel in a closed state at 100nM cytosolic Ca^{2+}. During the initial phase of Ca^{2+} release, RyR2 is not significantly affected by CaM in the presence of a high local cytosolic Ca^{2+} concentration. This is because that CaM can only take effect when the local cytosolic Ca^{2+} concentration has been reduced to a low level in the later phase of Ca^{2+} release. Accordingly, CaM mainly contributes to the termination of Ca^{2+} release as a late-stage inhibitor [49]. By simultaneous recording of luminal Ca^{2+} and cytosolic Ca^{2+} during spontaneous Ca^{2+} release, Maxwell et al. show that the cytosolic Ca^{2+} is approaching its highest level when luminal Ca^{2+} reaches its minimal level [355]. If Meissner's theory were true, the termination threshold would not have been altered by CaM, because CaM would not inhibit the channel when the cytosolic Ca^{2+} is high. However, this is not the case. Our data clearly show that CaM affects the termination threshold. Overexpression of CaM WT was found to increase the termination threshold. Impaired CaM binding due to a CaM mutation or a RyR2 deletion resulted in markedly lowered termination threshold.

Thus, our data indicate that Ca^{2+}-CaM facilitates Ca^{2+} release termination at an early stage of Ca^{2+} release when cytosolic Ca^{2+} concentrations are high.

7.2.1.2 The CaMBD of RyR2 is important for channel function

Homozygous knock-in mice harboring three key RyR2 mutations (W3587A/L3591D/F3603A) in the CaMBD showed hypertrophy and died at 9-16 days of age [50]. Yamaguchi et al. attributed this severe phenotype solely to the impaired CaM inhibition of RyR2. However, the role of CaMBD itself in channel function has been overlooked.

Previous studies of RyR1 have provided some clues that CaMBD itself may be important for channel function. A fragment of RyR1 (amino acids 4064-4210), the so called calmodulin-like domain (CaMLD) has been reported to interact with and activate the CaMBD [205,206,356]. CaM binding to the CaMBD was suggested to interfere with the interaction between CaMBD and CaMLD, promoting channel closure. Moreover, the inter-domain contact between these two domains has been shown to be a ubiquitous regulatory target in RyR1, since multiple ligands such as 4-CmC, Ca^{2+} and Mg^{2+} were able to manipulate the interaction independent of CaM [206]. These findings indicate that the interaction between CaMBD and CaMLD serves as a mechanism of ligand-dependent activation of the RyR1 channel.

On the other hand, increased interaction between CaMBD and some other domains may stabilize the channel in the closed state and prevent hyperactivity of the channel. Ikemoto et al. have suggested that removal of the inter-domain interaction between N-terminal and the central domain destabilizes the channel, thereby resulting in hyper-sensitization of the channel [357,358]. Similarly, if the interaction between the CaMBD and

some other domain is disrupted, the channel may increase its propensity to open. Indeed, addition of synthetic exogenous peptides corresponding to the CaMBD (3614-3643) increased the occurrence of spontaneous Ca^{2+} sparks in skeletal muscle. This could be due to interfered inter-subunit interactions or impaired CaM binding. However, a single mutation (L3624D) within this CaMBD peptide allowed CaM binding but did not increase the Ca^{2+} spark frequency. Apparently, the increased Ca^{2+} spark frequency is not due to the lack of endogenous CaM binding, because the L3624D peptide is still capable of binding CaM. Therefore, it is proposed that the CaMBD of RyR1 is a site of inter-subunit contact within RyR1 that stabilizes the closed state of the channel [326].

Similar to the interactions suggested for RyR1, we found that the CaMBD of RyR2 may also be critical for channel function itself rather than only responsible for CaM binding. In HEK293 cells co-expressing RyR2-WT and CaM (1-4) and those co-expressing RyR2-Del-3583-3603 and CaM (1-4), one would expect that the overexpression of CaM(1-4) mutant in these cells would suppress the effect of endogeneous CaM on RyR2-WT and RyR2-Del-3583-3603, and thus the termination of Ca^{2+} release to a similar extent, if the RyR2 mutation Del-3583-3603 only affects CaM binding. However, we found that cells co-expressing RyR2-Del-3583-3603 and CaM (1-4) mutant displayed a much lower termination threshold (33%) than cells co-expressing RyR2-WT and CaM (1-4) (49%), suggesting that this region plays an additional role in accelerating Ca^{2+} release termination (Figs. 16,17). Furthermore, Del-3583-3603 completely eliminated [^{35}S]CaM binding and abolished CaM inhibition of RyR2 in single channel studies, whereas the single mutation W3587A only partially removed CaM binding and inhibition of RyR2. At higher Ca^{2+} concentrations, W3587A even bound

CaM in a mode equivalent to WT [200]. Surprisingly, W3587A was as effective as Del-3583-3603 in weakening Ca^{2+} release termination (Figs. 17&18). This discrepancy could be explained by the direct allosteric impact of W3587A on the channel rather than on CaM binding. These observations strongly indicate that the CaMBD itself is key to the termination process. Finally, a single mutation F3603A in CaMBD was found to increase the activation threshold and reduce the termination threshold for Ca^{2+} release (Figs. 19). The increased activation threshold was not observed in Del-3583-3603 or other two single mutants. Besides, F3603 is not required for CaM binding and CaM inhibition of the RyR2 [200]. Therefore the altered Ca^{2+} release in this F3603A mutant is unlikely caused by defective binding of CaM. Instead, the mutation F3603A in the CaMBD may generate some unique structural changes that affect channel activation, indicating that the CaMBD is also crucial for Ca^{2+} release activation. Taken together, the CaMBD of RyR2 plays an important role in both Ca^{2+} release activation and termination.

The exact mechanism by which the RyR2 channel is regulated by the CaMBD is unknown. Similar to those observed in RyR1, it is possible that the CaMBD of RyR2 and its adjacent domains form a complex that regulates the channel function. Mutations in the CaMBD may alter the interaction between the CaMBD and its binding partners, causing distinct functional consequences. Future studies are required to identify the binding partners of CaMBD in RyR2 that cooperatively modulate the function of the channel. Since the CaMLD of RyR1 has been identified as the interacting-domain of the CaMBD, the corresponding region (amino acids 4020–4166) of RyR2 may be a potential candidate for interacting with CaMBD of RyR2.

7.2.2 FKBP12.6 accelerates Ca^{2+} release termination

FKBP12.6 is tightly associated with the RyR2 channel and considered to be a major regulator of RyR2, but the precise role of FKBP12.6 in modulating RyR2 function is complex and controversial. On one hand, Andrew Marks's group has shown that dissociation of FKBP12.6 from RyR2 increases the sensitivity of the channel to cytosolic Ca^{2+} activation and induces subconductance states, and that FKBP12.6 knock-out mice display enhanced propensity for stress-induced ventricular arrhythmias [174,359,360]. On the other hand, others, including us, have shown that the removal of FKBP12.6 does not alter the conductance and activation of the RyR2 channel or the susceptibility to stress-induced ventricular arrhythmias [176-178,217,218]. Nevertheless, considering that FKBP12.6 is a physiological protein tightly bound to RyR2, it is reasonable to propose that FKBP12.6 would play some important role in the channel function.

In order to study the role of FKBP12.6 in Ca^{2+} release, HEK293 cells were transfected with or without FKBP12.6 and luminal Ca^{2+} dynamics were compared in these cells. Consistent with our previous finding that FKBP12.6 did not alter the propensity for spontaneous Ca^{2+} release (or SOICR), FKBP12.6 did not modify the SOICR activation threshold (Fig. 20). On the other hand, it inhibited the channel by increasing the termination threshold and therefore shortened the fractional Ca^{2+} release (Fig. 20). This finding explains why no excise induced arrhythmia was detected in FKBP12.6 null mice, because FKBP12.6 does not target the activation threshold for SOICR, decrease of which will lead to the symptom of CPVT. Meanwhile, it also predicts that mice lacking of FKBP12.6 will display impaired Ca^{2+} release because of altered Ca^{2+} release termination. Indeed, impaired Ca^{2+} release has been observed in

FKBP12.6 null mice [329,361]. Considering the controversy surrounding the functional role of FKBP12.6, our findings are novel and exciting, as they point out, for the first time, that FKBP12.6 regulates RyR2 activity and Ca^{2+} release by modulating the termination of Ca^{2+} release, rather than the cytosolic Ca^{2+} activation or conduction of the RyR2 channel as previously believed.

While the CaM binding site has been located to residues K3583-F3603 in RyR2, the binding sites for FKBP12.6 are still controversial [123,174,221-223]. Multiple regions in the primary sequence of RyR2 have been suggested to contribute to the binding of FKBP12.6. Current conformational studies also suggest an adjacent binding location between CaM and FKBP12.6 [207,209,224,225]. CaM and FKBP12.6 appear to come in direct contact with domain 3 (handle domain) of RyR2 [209,226]. In line with these structural studies, both CaM and FKBP12.6 were found to increase the termination threshold without affecting the activation threshold (Fig.16,20), suggesting that the region of RyR2 that interacts with CaM and FKBP12.6 is important for Ca^{2+} release termination.

7.2.3 Cytosolic Ca^{2+} sensitizes Ca^{2+} release activation and delays Ca^{2+} release termination

Cytosolic Ca^{2+} is known to be the primary activator of CICR. Ca^{2+} influx through the L-type Ca^{2+} channels is capable of activating the RyR2 channels to generate a large Ca^{2+} release from the SR. While low levels of cytosolic Ca^{2+} (100 nM-10 μM) sensitize the channel, high concentrations (>1 mM) of cytosolic Ca^{2+} inhibit the channel. Based on this inhibitory effect of cytosolic Ca^{2+}, an early study has suggested that it is the highly elevated cytosolic Ca^{2+} during systole that inactivates the RyR2 channel and thus terminates SR Ca^{2+} release [48]. To date, no direct experimental evidence has been

provided to support this hypothesis, and whether cytosolic Ca^{2+} can reach such high concentrations (>1 mM) to block the channel under physiological condition is unclear. On the other hand, low concentrations of Ca^{2+} are known to activate the RyR2 channel, but, its effect on Ca^{2+} release termination has not been investigated.

To address these issues, HEK293 cells were permeabilized and spontaneous Ca^{2+} release upon elevated cytosolic Ca^{2+} (50 to 200 nM) was monitored. In these permeabilized cells, the released Ca^{2+} was rapidly removed by perfusion and buffered by EGTA. Thus, the cytosolic Ca^{2+} should remain relatively constant (50 or 200 nM). If high concentrations of cytosolic Ca^{2+} play a primary role in Ca^{2+} release termination, RyR2 channels would lose the ability to terminate and the Ca^{2+} stores would be depleted under the current conditions. However, at a given cytosolic Ca^{2+} concentration, Ca^{2+} release still terminated at a fixed luminal Ca^{2+} level similar to that observed in intact HEK293 cells, indicating that termination of Ca^{2+} release is unlikely due to elevated cytosolic Ca^{2+}. On the other hand, physiological levels of cytosolic Ca^{2+} were found to activate the channel, as expected, and, more interestingly, weaken the termination of Ca^{2+} release (Fig 20). These data suggest that cytosolic Ca^{2+} itself inhibits rather than accelerates Ca^{2+} release termination.

7.2.4 CaMKII lowers the SOICR activation threshold

CaMKII is a central signaling molecule responsible for the pathogenesis of various heart diseases [362]. The expression and activities of CaMKII are increased in both failing human heart [363,364] and animal models of hypertrophy and heart failure [186,365,366]. Down regulation of CaMKII improves cardiac function and protects the heart from hypertrophy or heart failure [330-333]. CaMKIIδ_c is the major cytosolic isoform that phosphorylates

multiple ion channels including RyR2 in cardiomyocytes[308]. Despite years of studies, the functional consequences of RyR2 phosphorylation by CaMKII remain controversial. Single channel, [^{3}H]ryanodine binding and cellular studies suggest that CaMKII phosphorylation either increases [173,186-188] or decreases [189,190] the sensitivity of the RyR2 channel to Ca^{2+} activation.

To clarify the apparent discrepancy, we investigated the effect of CaMKII on Ca^{2+} release activation and termination. It was found that HEK293 cells transfected with CaMKII displayed a dramatically enhanced SOICR propensity by reducing the Ca^{2+} release activation threshold. Meanwhile, the termination threshold was unaltered in these cells (Fig 21). However, the reduced SOICR threshold may not be entirely due to enhanced RyR2 phosphorylation by CaMKII. Hyperphosphorylation by CaMKII could activate multiple pathways and induce transcriptions of various genes [367]. These changes in cells may lead to secondary effects such as oxidative stress that modify RyR2 and alter spontaneous Ca^{2+} release. Interestingly, regardless of what directly modified the RyR2 channel, changes induced by CaMKII did not alter the termination of Ca^{2+} release.

Further studies are required to identify the direct role of CaMKII phosphorylation in regulating RyR2. S2815 in human RyR2 (corresponding to S2814 in mouse RyR2) has been suggested as the CaMKII phosphorylation site [187]. It will be of interest to study the luminal Ca^{2+} dynamics in HEK293 cells expressing S2814D which mimics CaMKII phosphorylation, or S2814A which abolishes CaMKII phosphorylation of RyR2. If CaMKII indeed activates the channel and does not influence the termination of Ca^{2+} release, one would expect to observe a decreased SOICR activation threshold in HEK293

cells expressing S2814D and an increased SOICR threshold in cells expressing S2814A. Termination thresholds in both cell lines would not be affected.

7.3 Ligand dependent conformational changes in the clamp region of RyR2

RyR2 is a gigantic ion channel functionally regulated by a number of ligands. It has long been appreciated that global conformational changes observed in the clamp region (close to the CaMBD), N-terminal region and the transmembrane domain are involved in the gating and regulation of the RyR channel [131-136]. Abnormal conformational changes in RyR are also believed to underlie a common cause of RyR-associated diseases [125,129,135,368]. However, the molecular basis of conformational changes in RyR remains incompletely understood.

In the present study, we built a FRET-based probe to assess the conformational changes in the corner region of the large square-shaped cytoplasmic assembly (clamp region) of the 3D architecture of RyR2. Using this novel conformation sensor, we demonstrate, for the first time, that ligand-induced Ca^{2+} release via activation of RyR2 is not always correlated with conformational changes in the clamp region, suggesting the existence of multiple mechanisms of RyR2 activation associated with unique conformational changes.

7.3.1 Multiple ligand-dependent RyR2 open states

Substantial structural rearrangements in the clamp region of the 3D architecture of RyR occur upon channel activation by an ATP analogue, AMP-PCP, or ryanodine in the presence of high concentrations of Ca^{2+} (100 μM) [133,134,341]. Interestingly, Ca^{2+} alone did not appear to cause significant conformational changes in the clamp region [134]. Consistent

with these cryo-EM findings, we also detected conformational changes in the clamp region induced by ATP and ryanodine but not by Ca^{2+} alone using our novel FRET-based conformation probe, confirming the utility and sensitivity of our FRET approach. However, the reason for the different effect of Ca^{2+} is unclear. It was suggested that the 3D reconstruction of RyR in the presence of Ca^{2+} alone represents the average of a channel population with both the open and closed states as Ca^{2+} alone only transiently activates the channel. On the other hand, the reconstruction of RyR in the presence of AMP-PCP/Ca^{2+} or ryanodine/Ca^{2+} represents mainly the open state as these ligands fully activated the channel. Although Ca^{2+} alone produced little conformational change in the clamp region, it induced structural rearrangements in the transmembrane domain of RyR to an extent similar to that observed with AMP-PCP/Ca^{2+} [134]. Thus, these observations raise the possibility that conformational changes in the clamp region may be ligand dependent.

Recently, a higher resolution (~10 Å) 3D reconstruction of RyR has been obtained in the presence of a potent RyR agonist, PCB 95 together with Ca^{2+} (50 μM) and FKBP12.6 [136]. Substantial differences in the clamp and central regions in the cytoplasmic assembly and in the transmembrane domain of RyR were noticed when comparing the 3D reconstruction in the presence of PCB 95/Ca^{2+} with intermediate resolution (~30 Å) 3D reconstruction in the presence of AMP-PCP/Ca^{2+} or ryanodine/Ca^{2+} [133,134]. These differences were thought to be due to the low resolution of the early 3D reconstructions. Alternatively, it is possible that PCB 95/Ca^{2+}/FKBP12.6 may induce different conformational changes in RyR compared to AMP-PCP/Ca^{2+} or ryanodine/Ca^{2+}.

To further assess the ligand dependence of conformational changes in the clamp region, we used our FRET probe to monitor the conformational changes in the clamp region of RyR upon binding to various ligands. These ligand-induced conformational changes were then correlated with the functional state of the channel in the presence of the same ligand. We found that caffeine, aminophylline, theophylline, ATP, and ryanodine induced conformational changes in the clamp region and concomitant Ca^{2+} release, whereas Ca^{2+} and 4-CmC induced Ca^{2+} release in a manner compatible to that induced by caffeine and ATP, but caused no detectable conformational changes in the clamp region (Fig 29-34). Thus, in a manner different from caffeine, ATP, and ryanodine, Ca^{2+} and 4-CmC activate RyR and Ca^{2+} release without inducing significant conformational changes in the clamp region.

Using a different FRET probe designed to monitor the conformational changes between the N-terminal domain and the central disease mutation hotspot of RyR2, we have previously shown that caffeine increased the FRET signal, while ATP and 4-CmC reduced it [342]. On the other hand, in the present study, we found that both caffeine and ATP decreased the FRET signal of the clamp FRET probe, while 4-CmC showed no effect. These studies using two different FRET probes indicate that the conformational changes induced by caffeine, ATP or 4-CmC are different. Taken together, our current FRET analysis and previous cryo-EM reconstructions demonstrate that conformational changes in RyR are ligand-dependent, and suggest that different ligands may activate the RyR channel via different mechanisms with distinct conformational changes.

7.3.2 Functional and structural impact of ryanodine on RyR

It is widely believed that ryanodine locks the RyR channel into an open, subconductance state, and that the ryanodine-modified channel is insensitive to further modulation by other channel ligands [230,335,336,344]. In contrast, it has been shown that ryanodine increases the sensitivity of single RyR2 channels to cytosolic Ca^{2+} activation by ~1,000-fold, and that single ryanodine-modified RyR2 channels remain sensitive to modulation by channel modulators such as Mg^{2+} and caffeine [369,370]. Thus, functionally, ryanodine does not lock the RyR channel into an open state. Instead, ryanodine dramatically sensitizes the channel to cytosolic Ca^{2+} activation. However, it is unclear whether, structurally, ryanodine locks the channel in a fixed conformational state. To address this question, we monitored the impact of caffeine on conformational changes in the clamp region of RyR2 before and after ryanodine modification. We found that ryanodine, upon binding, kept the channel open and induced conformational changes in the clamp region, which is consistent with the structural rearrangements in the 3D architecture of ryanodine-modified RyR observed by cryo-EM [133]. Importantly, we found that caffeine still induced further conformational changes in the clamp region of ryanodine-modified RyR2 channels. These data indicate that although ryanodine may keep the channel fully open by markedly sensitizing it to Ca^{2+} activation, it does not lock the receptor's conformation into a fixed state.

7.4 Impaired Ca^{2+} release in the genesis of cardiomyopathies

Mutations in RyR2 have been associated with stress-induced ventricular tachycardias and cardiomyopathies. Extensive investigations over the past decade have

demonstrated that spontaneous Ca^{2+} wave (or SOICR)-evoked DADs are the major cause of RyR2-associated CPVT [265,274,371]. We and others have shown that CPVT RyR2 mutations reduce the activation threshold for SOICR [151,250,251,275-278]. This reduced SOICR activation threshold will increase the likelihood of diastolic activation of SR Ca^{2+} release under conditions of SR Ca^{2+} overload, and thus the propensity for SOICR-evoked DADs and triggered arrhythmias [346,372-377]. However, how RyR2 mutations lead to cardiomyopathies in addition to CPVT remains unclear.

7.4.1 Sarcomeric proteins and cardiomyopathies

Cardiomyopathies are generally associated with mutations in sarcomeric proteins. Most disease-associated sarcomeric mutations have been shown to alter the sensitivity of myofilaments to Ca^{2+} [65,67,68,378]. Since myofilaments represent a major pool of Ca^{2+} binding sites, changes in the Ca^{2+} sensitivity of myofilaments will alter their responses to Ca^{2+} release, which will, in turn, change the systolic Ca^{2+} transients. Sarcomeric mutations associated with HCM tend to increase the myofilament Ca^{2+} sensitivity and reduce systolic Ca^{2+} transients, whereas those associated with DCM tend to decrease the myofilament Ca^{2+} sensitivity and increase systolic Ca^{2+} transients [65-69]. Impaired systolic Ca^{2+} transients as a result of altered myofilament Ca^{2+} sensitivity has been proposed to trigger cardiac remodeling via Ca^{2+}/CaM dependent signaling pathways, such as the calcineurin/NFAT pathway [306,307] or to stimulate apoptotic signaling [309], leading to HCM or DCM [306-309].

7.4.2 RyR2 and cardiomyopathies

Zima et al. have shown that both spontaneous (diastolic) and stimulated (systolic) SR Ca^{2+} release in cardiomyocytes terminate at the same SR Ca^{2+} threshold [42], suggesting

that the same mechanism governs the termination of systolic and diastolic Ca^{2+} release. In the present study, we have shown that cardiomyopathy-associated RyR2 mutations alter the termination of SOICR or diastolic Ca^{2+} release. Based on the findings of Zima et al., it is likely that these RyR2 mutations will also alter the termination of systolic Ca^{2+} release. Altering the termination threshold for Ca^{2+} release will affect the fractional Ca^{2+} release and thus the cytosolic Ca^{2+} transients. For example, a reduced termination threshold would delay the termination of Ca^{2+} release and increase the cytosolic Ca^{2+} transients, whereas an increased termination threshold would cause premature termination of Ca^{2+} release and decrease the cytosolic Ca^{2+} transients. In line with this view, we found that a DCM-associated RyR2 mutation exon-3 deletion reduces the termination threshold and increase the fractional Ca^{2+} release (Fig. 39, 40 and 42). On the other hand, an HCM-associated RyR2 mutation A1107M increases the termination threshold and decreases the fractional Ca^{2+} release (Fig. 44). These changes in fractional Ca^{2+} release would lead to altered cytosolic Ca^{2+} transients, an effect similar to that of the DCM- or HCM-associated sarcomeric mutations.

It is important to note that the fractional Ca^{2+} release (activation threshold-termination threshold) depends not only on the termination threshold but also on the activation threshold for Ca^{2+} release. Unlike the cardiomyopathy-associated RyR2 mutations, CPVT-only RyR2 mutations, E189D and R4496C, reduce the activation and termination thresholds to a similar extent, resulting in no significant changes in the fractional Ca^{2+} release (Fig. 43). Therefore, our data suggest that abnormal fractional Ca^{2+} release as a result of impaired Ca^{2+} release termination may underlie RyR2-associated cardiomyopathies.

Interestingly, a number of identified cardiomyopathy-associated RyR2 mutations are clustered in the N-terminal region of RyR2. The pore forming region, N-terminal region and the CaMBD of RyR2 are all recognized as the major determinants of Ca^{2+} release activation and termination in the present study. It is likely that additional cardiomyopathy-linked mutations will be identified in the other two key regions of RyR2 in the near future.

7.4.3 Mechanisms underlying cardiomyopathies

Apparently, cardiomyopathies induced by both sarcomere mutations and RyR mutations are all associated with changes in Ca^{2+} homeostasis. Increased myofilament Ca^{2+} sensitivity slows the decay of Ca^{2+} transients, whereas decreased myofilament Ca^{2+} sensitivity hastens the decay of Ca^{2+} transients [65-69]. Similarly, some RyR2 mutations are able to delay Ca^{2+} release termination and prolong the decay of Ca^{2+} transients, whereas some other mutations result in premature termination and enhanced decay of Ca^{2+} transients.

Other factors that impair cytosolic Ca^{2+} homeostasis are also involved in the genesis of cardiomyopathies. In the present study, we found that impaired regulation of RyR2 by FKBP12.6 and CaM altered Ca^{2+} release termination and thus the fractional Ca^{2+} release. Consistently, both FKBP12.6 null mice and CaM binding deficient mice with prolonged SR Ca^{2+} release displayed moderate to severe cardiomyopathies [50,329]. On the other hand, enhanced SERCA inhibition caused by a PLB mutation has been shown to delay the SR Ca^{2+} uptake and thus slow the decay of Ca^{2+} transients. Transgenic mice carrying this PLB mutation showed DCM [304].

Taken together, cardiomyopathies induced by various factors may share a similar

underlying mechanism. That is, these factors all generate abnormal Ca^{2+} homeostasis, which can lead to cardiomyopathy-linked gene reprogramming, causing changes in cell size, sarcomeric reorganization and gene expression [379].

7.4.4 Impaired Ca^{2+} release termination is a common target of cardiac disease

Impaired Ca^{2+} release activation has been recognized as the cause of cardiac arrhythmias, such as CPVT. Similarly, Ca^{2+} release termination may also play an equally important role in the genesis of disease. Here we found that the DCM-associated RyR2 exon-3 deletion and the ARVD2-associated RyR2 N-terminal mutations, A77V, R176Q/T2504M, R420W, and L433P, reduce the threshold for Ca^{2+} release termination, whereas an HCM-associated RyR2 mutation, A1107M, increases the termination threshold (Fig. 39, 43 and 44). These data demonstrate, for the first time, that RyR2 mutations associated with cardiomyopathies impair the termination of Ca^{2+} release.

The importance of Ca^{2+} release termination in cardiac physiology and pathophysiology has increasingly been recognized [20,162,348]. Reduced threshold for Ca^{2+} release termination has been shown in heart failure [323,380]. Moreover, aberrant Ca^{2+} release termination also contributes to CPVT. It is well known that both the magnitude and the rate of spontaneous Ca^{2+} release events are important for triggering arrhythmogenic DADs [381]. It has been estimated that a total release of 50-70% SR Ca^{2+} content is required to produce DADs with amplitudes that are sufficient to induce triggered activities. A reduction in the termination threshold for SOICR would lead to an increase in the fractional Ca^{2+} release and thus the amplitude of Ca^{2+} waves during SR Ca^{2+} overload. The increased amplitude of Ca^{2+} waves would, in turn, produce more robust DADs, and enhance the propensity for triggered activities. Thus, the reduced

termination threshold for SOICR of the DCM- and ARVD2-associated RyR2 mutations combined with their lowered activation threshold may explain their enhanced susceptibility to CPVT.

In summary, these observations suggest that impaired Ca^{2+} release termination may be a common defect associated with cardiomyopathies and other cardiac abnormalities.

7.5 Perspectives and future studies

7.5.1 Investigating the role of other RyR2 modulators in Ca^{2+} release activation and termination

In the present study, we defined three novel determinants of Ca^{2+} release activation and termination in RyR2 and investigated the role of FKBP12.6, CaM, CaMKII and cytosolic Ca^{2+} in Ca^{2+} release activation and termination. As an important Ca^{2+} release governor, RyR2 interacts with a large array of other channel modulators. These physiological modulators, such as triadin, junction, PKA, ATP and Mg^{2+} are also critically involved in RyR2 channel regulation [137,138]. Dysregulation by these modulators can lead to various cardiac diseases [181,382-384]. It will be interesting to know how these modulators alter Ca^{2+} release activation and termination as well as fractional Ca^{2+} release.

7.5.2 Generation of domain-specific FRET probes for studying conformational changes in RyR

Cryo-EM and 3D reconstructions have provided important information on the structural domains or regions that undergo conformational changes in RyR upon ligand binding. However, due to the relatively low resolutions of current 3D reconstructions, the amino acid sequences that are involved in ligand-induced conformational changes in RyR

have yet to be determined. Furthermore, little is known about the dynamics, ligand dependence, or functional correlations of these conformational changes. An alternative approach to studying conformational changes is the use of domain specific FRET-based probes. Using GFP as a structural marker, we have previously mapped a number of specific sites or sequences onto the 3D structure of RyR [123,124,126,182,315,316]. The docking of crystal structures of RyR fragments into the cryo-EM density map of RyR has also led to the sequence assignment of some specific domains [125,128,129,158,368]. These sequence-structure correlations allow us to design and build FRET-based probes in specific domains or regions of the RyR structure. Using this approach, we have previously constructed a FRET probe for monitoring the conformational dynamics involving the N-terminal and central regions of RyR2 [342]. In the present study, we built a FRET probe for studying the ligand dependence and functional correlation of the conformational dynamics in the clamp region. Hence, domain specific FRET probes are an effective approach to monitoring conformational changes in RyR. The generation of a network of domain-specific FRET probes should allow us to systematically and comprehensively study the conformational dynamics and ligand gating mechanisms of RyR.

7.5.3 Generation of knock-in mouse models for cardiomyopathies and development of a novel luminal Ca^{2+} sensing probe targeting mouse SR

The results of our studies in HEK293 cells demonstrate that cardiomyopathy-associated RyR2 mutations alter the activation and termination of Ca^{2+} release. Since HEK293 cells lack many cardiac-specific proteins, whether the impact on Ca^{2+} release of cardiomyopathy-associated RyR2 mutations observed in HEK293 cells will manifest in cardiac cells has yet to be confirmed. Knock-in mice harboring the cardiomyopathy-

associated RyR2 mutations are good models for studying the impact of mutations on Ca^{2+} release termination in native cardiomyocytes. RyR2 mutations have been associated with three distinct types of cardiomyopathies: DCM, HCM, and ARVD2. We have shown that DCM and ARVD2-associated RyR2 mutations delay Ca^{2+} release termination and increase the fractional Ca^{2+} release, whereas an HCM-associated mutation enhances the termination of Ca^{2+} release and decrease the fractional Ca^{2+} release. To further understand the molecular and cellular basis of each of these three types of RyR2-associated cardiomyopathies, it will be useful to have three different knock-in mouse models harboring the A1107M, the Exon-3 deletion or the R420W mutation, associated with HCM, DCM or ARVD2, respectively.

To directly assess the luminal Ca^{2+} thresholds at which Ca^{2+} release occurs and at which Ca^{2+} release terminates, it is important and necessary to monitor the SR luminal Ca^{2+} level in cardiomyocytes of these knock-in mice. However, there are currently no reliable luminal Ca^{2+} sensing probes that can be loaded into mouse cardiomyocytes. We have successfully used the luminal Ca^{2+} sensing protein D1ER to monitor the luminal Ca^{2+} dynamics in HEK293 cells. A novel probe targeting the SR could be generated by replacing the calreticulin signal peptide sequence and the KDEL ER retention signal sequence in the original D1ER construct with the SR-targeted CASQ2 sequence. Then the SR-targeted luminal Ca^{2+} sensing protein (D1SR) could be expressed in mouse cardiomyocytes via adenovirus-mediated in vivo gene delivery technique and used for monitoring luminal Ca^{2+} dynamics. Studying the luminal Ca^{2+} dynamics in these mouse models will likely provide novel insights into the mechanism of Ca^{2+} release termination and its role in the pathogenesis of cardiomyopathies.

7.5.4 Ca^{2+} release termination as a therapeutic drug target

Given the crucial role of Ca^{2+} release termination in the pathogenesis of cardiac diseases and its modulation by a number of factors and mutations, the termination of Ca^{2+} release represents a novel and promising therapeutic target for the treatment of cardiomyopathies and other diseases. For patients with increased termination threshold and reduced fractional SR Ca^{2+} release, drugs that lower the termination threshold and promote Ca^{2+} release would be beneficial. For patients with decreased termination threshold and increased fractional SR Ca^{2+} release, drugs that increase the termination threshold and suppress Ca^{2+} release would be effective. Our HEK293 cells provide a simple and effective system for testing the effect of potential therapeutic compounds on Ca^{2+} release termination.

On the other hand, under- or over-correction of Ca^{2+} release termination could be problematic. A number of anti-arrhythmic drugs have been shown to suppress the activation of Ca^{2+} release and thus lower the chance for abnormal spontaneous Ca^{2+} release and DADs. These drugs would benefit patients with reduced activation threshold [385]. However, the effect of these compounds on Ca^{2+} release termination has yet to be studied. These compounds may also alter Ca^{2+} release termination and the fractional Ca^{2+} release. Long-term changes in fractional Ca^{2+} release may alter cytosolic Ca^{2+} homoeostasis, which may, in turn, cause cardiomyopathies. Thus, the effect of anti-arrhythmic drugs on Ca^{2+} release termination and fractional Ca^{2+} release, in addition to Ca^{2+} release activation, should be carefully studied to ensure their proper use.

7.6 Summary

In conclusion, we demonstrate for the first time that termination of Ca^{2+} release is controlled by RyR2 itself and regulated by RyR2 modulators, and that altered Ca^{2+} release termination is associated with cardiomyopathies.

We have identified three novel molecular determinants of Ca^{2+} release activation and termination in RyR2, including the pore-forming region, the N-terminal region and the CaMBD. RyR2 mutations in these key regions and some modulators were found to modify the activation threshold or the termination threshold or both, indicating that Ca^{2+} release termination, in addition to activation, is an important regulatory target. We also demonstrate that multiple conformational changes in the clamp region of RyR2 occur upon activation by different ligands. Therefore, multiple open states of the channel may exist and provide the structural basis for multiple activation and termination pathways.

Enhanced Ca^{2+} release activation has been recognized as a common defect of RyR2 mutations associated with CPVT, but why patients harboring some of these CPVT mutations also display cardiomyopathies is unknown. Here we found that these mutations altered fractional Ca^{2+} release as a result of reduced or enhanced Ca^{2+} release termination, whereas CPVT-only mutations rarely changed the fractional Ca^{2+} release, indicating that abnormal fractional Ca^{2+} release due to impaired Ca^{2+} release termination is a common defect for RyR2-associated cardiomyopathies.

Since Ca^{2+} release termination is regulated by various RyR2 modulators and affected by RyR2 mutations, its role in cardiac disease should not be overlooked. Normalizing the threshold for Ca^{2+} release termination by controlling the activity of

RyR2 offers a promising and novel therapeutic strategy for the treatment of cardiomyopathies and other cardiac abnormalities.

BIBLIOGRAPHY

1. Kranias EG, Bers DM. Calcium and cardiomyopathies. *Subcell Biochem*. 2007;45:523-537.
2. Bers DM. Excitation-contraction coupling and cardiac contractile force, second edition. *Kluwer Academic Publishers, Dordrecht, The Netherlands*. 2001.
3. Bers DM. Cardiac excitation-contraction coupling. *Nature*. 2002;415(6868):198-205.
4. Dibb KM, Graham HK, Venetucci LA, Eisner DA, Trafford AW. Analysis of cellular calcium fluxes in cardiac muscle to understand calcium homeostasis in the heart. *Cell Calcium*. 2007.
5. Ono K, Iijima T. Cardiac T-type Ca^{2+} channels in the heart. *J Mol Cell Cardiol*. 2010;48(1):65-70.
6. Bodi I, Mikala G, Koch SE, Akhter SA, Schwartz A. The L-type calcium channel in the heart: The beat goes on. *J Clin Invest*. 2005;115(12):3306-3317.
7. Fearnley CJ, Roderick HL, Bootman MD. Calcium signaling in cardiac myocytes. *Cold Spring Harb Perspect Biol*. 2011;3(11):a004242.
8. Wang SQ, Song LS, Lakatta EG, Cheng H. Ca^{2+} signalling between single L-type Ca^{2+} channels and ryanodine receptors in heart cells. *Nature*. 2001;410(6828):592-596.
9. Pate P, Mochca-Morales J, Wu Y, et al. Determinants for calmodulin binding on voltage-dependent Ca^{2+} channels. *J Biol Chem*. 2000;275(50):39786-39792.
10. Erickson MG, Alseikhan BA, Peterson BZ, Yue DT. Preassociation of calmodulin with voltage-gated Ca^{2+} channels revealed by FRET in single living cells. *Neuron*. 2001;31(6):973-985.
11. Pitt GS, Zuhlke RD, Hudmon A, Schulman H, Reuter H, Tsien RW. Molecular basis of calmodulin tethering and Ca^{2+}-dependent inactivation of L-type Ca^{2+} channels. *J Biol Chem*. 2001;276(33):30794-30802.
12. Stathopulos PB, Seo MD, Enomoto M, Amador FJ, Ishiyama N, Ikura M. Themes and variations in ER/SR calcium release channels: Structure and function. *Physiology (Bethesda)*. 2012;27(6):331-342.
13. Bunney TD, Katan M. PLC regulation: Emerging pictures for molecular mechanisms. *Trends Biochem Sci*. 2011;36(2):88-96.
14. Parys JB, De Smedt H. Inositol 1,4,5-trisphosphate and its receptors. *Adv Exp Med Biol*. 2012;740:255-79. doi:255-279.
15. Lencesova L, Krizanova O. IP(3) receptors, stress and apoptosis. *Gen Physiol Biophys*. 2012;31(2):119-130.
16. Verkhratsky A. The endoplasmic reticulum and neuronal calcium signalling. *Cell Calcium*. 2002;32(5-6):393-404.
17. Narayanan D, Adebiyi A, Jaggar JH. Inositol trisphosphate receptors in smooth muscle cells. *Am J Physiol Heart Circ Physiol*. 2012;302(11):H2190-210.
18. Lamb GD. Excitation-contraction coupling in skeletal muscle: Comparisons with cardiac muscle. *Clin Exp Pharmacol Physiol*. 2000;27(3):216-224.
19. Fabiato A. Calcium-induced release of calcium from the cardiac sarcoplasmic reticulum. *Am J Physiol*. 1983;245(1):C1-14.

20. Stern MD, Cheng H. Putting out the fire: What terminates calcium-induced calcium release in cardiac muscle? *Cell Calcium*. 2004;35(6):591-601.
21. Stern MD, Lakatta EG. Excitation-contraction coupling in the heart: The state of the question. *FASEB J*. 1992;6(12):3092-3100.
22. Stern MD. Theory of excitation-contraction coupling in cardiac muscle. *Biophys J*. 1992;63(2):497-517.
23. Lopez-Lopez JR, Shacklock PS, Balke CW, Wier WG. Local, stochastic release of Ca^{2+} in voltage-clamped rat heart cells: Visualization with confocal microscopy. *J Physiol*. 1994;480 (Pt 1):21-29.
24. Wier WG, Egan TM, Lopez-Lopez JR, Balke CW. Local control of excitation-contraction coupling in rat heart cells. *J Physiol*. 1994;474(3):463-471.
25. Lopez-Lopez JR, Shacklock PS, Balke CW, Wier WG. Local calcium transients triggered by single L-type calcium channel currents in cardiac cells. *Science*. 1995;268(521395273973):1042-105.
26. Stern MD, Pizarro G, Rios E. Local control model of excitation-contraction coupling in skeletal muscle. *J Gen Physiol*. 1997;110(4):415-440.
27. Cheng H, Lederer MR, Lederer WJ, Cannell MB. Calcium sparks and $[Ca^{2+}]i$ waves in cardiac myocytes. *Am J Physiol*. 1996;270(1 Pt 1):C148-59.
28. Cheng H, Lederer MR, Xiao RP, et al. Excitation-contraction coupling in heart: New insights from Ca^{2+} sparks. *Cell Calcium*. 1996;20(2):129-40.
29. Cheng H, Lederer WJ, Cannell MB. Calcium sparks: Elementary events underlying excitation-contraction coupling in heart muscle. *Science*. 1993;262(5134):740-744.
30. Franzini-Armstrong C, Protasi F, Ramesh V. Shape, size, and distribution of Ca^{2+} release units and couplons in skeletal and cardiac muscles. *Biophys J*. 1999;77(3):1528-1539.
31. Cheng H, Lederer WJ. Calcium sparks. *Physiol Rev*. 2008;88(4):1491-1545.
32. Bers DM. Calcium cycling and signaling in cardiac myocytes. *Annu Rev Physiol*. 2008;70:23-49.
33. Cannell MB, Cheng H, Lederer WJ. The control of calcium release in heart muscle. *Science*. 1995;268(5213):1045-1049.
34. Smith GD, Keizer JE, Stern MD, Lederer WJ, Cheng H. A simple numerical model of calcium spark formation and detection in cardiac myocytes. *Biophys J*. 1998;75(1):15-32.
35. Gonzalez A, Kirsch WG, Shirokova N, et al. Involvement of multiple intracellular release channels in calcium sparks of skeletal muscle. *Proc Natl Acad Sci U S A*. 2000;97(8):4380-4385.
36. Schneider MF. Ca^{2+} sparks in frog skeletal muscle: Generation by one, some, or many SR Ca^{2+} release channels? *J Gen Physiol*. 1999;113(3):365-372.
37. Bers DM, Fill M. Coordinated feet and the dance of ryanodine receptors [comment]. *Science*. 1998;281(5378):790-791.
38. Sobie EA, Dilly KW, dos Santos Cruz J, Lederer WJ, Jafri MS. Termination of cardiac Ca^{2+} sparks: An investigative mathematical model of calcium-induced calcium release. *Biophys J*. 2002;83(1):59-78.
39. DelPrincipe F, Egger M, Niggli E. Calcium signalling in cardiac muscle: Refractoriness revealed by coherent activation. *Nat Cell Biol*. 1999;1(6):323-329.

40. Terentyev D, Viatchenko-Karpinski S, Valdivia HH, Escobar AL, Gyorke S. Luminal Ca^{2+} controls termination and refractory behavior of Ca^{2+}-induced Ca^{2+} release in cardiac myocytes. *Circ Res*. 2002;91(5):414-420.
41. Shannon TR, Guo T, Bers DM. Ca^{2+} scraps: Local depletions of free [Ca^{2+}] in cardiac sarcoplasmic reticulum during contractions leave substantial Ca^{2+} reserve. *Circ Res*. 2003;93(1):40-45.
42. Zima AV, Picht E, Bers DM, Blatter LA. Termination of cardiac Ca^{2+} sparks: Role of intra-SR [Ca^{2+}], release flux, and intra-SR Ca^{2+} diffusion. *Circ Res*. 2008;103(8):e105-15.
43. Marx SO, Ondrias K, Marks AR. Coupled gating between individual skeletal muscle Ca^{2+} release channels (ryanodine receptors). *Science*. 1998;281(5378):818-821.
44. Marx SO, Gaburjakova J, Gaburjakova M, Henrikson C, Ondrias K, Marks AR. Coupled gating between cardiac calcium release channels (ryanodine receptors). *Circ Res*. 2001;88(11):1151-1158.
45. Gyorke S. Ca^{2+} spark termination: Inactivation and adaptation may be manifestations of the same mechanism. *J Gen Physiol*. 1999;114(1):163-166.
46. Zahradnikova A, Dura M, Gyorke S. Modal gating transitions in cardiac ryanodine receptors during increases of Ca^{2+} concentration produced by photolysis of caged Ca^{2+}. *Pflugers Arch*. 1999;438(3):283-288.
47. Gyorke S, Fill M. Ryanodine receptor adaptation: Control mechanism of Ca^{2+}-induced Ca^{2+} release in heart. *Science*. 1993;260(5109):807-809.
48. Fabiato A. Time and calcium dependence of activation and inactivation of calcium-induced release of calcium from the sarcoplasmic reticulum of a skinned canine cardiac purkinje cell. *J Gen Physiol*. 1985;85(2):247-289.
49. Xu L, Meissner G. Mechanism of calmodulin inhibition of cardiac sarcoplasmic reticulum Ca^{2+} release channel (ryanodine receptor). *Biophys J*. 2004;86(2):797-804.
50. Yamaguchi N, Takahashi N, Xu L, Smithies O, Meissner G. Early cardiac hypertrophy in mice with impaired calmodulin regulation of cardiac muscle ca release channel. *J Clin Invest*. 2007;117(5):1344-1353.
51. Lokuta AJ, Meyers MB, Sander PR, Fishman GI, Valdivia HH. Modulation of cardiac ryanodine receptors by sorcin. *J Biol Chem*. 1997;272(40):25333-25338.
52. Farrell EF, Antaramian A, Benkusky N, et al. Regulation of cardiac excitation-contraction coupling by sorcin, a novel modulator of ryanodine receptors. *Biol Res*. 2004;37(4):609-612.
53. Brochet DX, Yang D, Di Maio A, Lederer WJ, Franzini-Armstrong C, Cheng H. Ca^{2+} blinks: Rapid nanoscopic store calcium signaling. *Proc Natl Acad Sci U S A*. 2005;102(8):3099-3104.
54. Lukyanenko V, Viatchenko-Karpinski S, Smirnov A, Wiesner TF, Gyorke S. Dynamic regulation of sarcoplasmic reticulum Ca^{2+} content and release by luminal Ca^{2+}-sensitive leak in rat ventricular myocytes. *Biophys J*. 2001;81(2):785-98.
55. Gyorke S, Gyorke I, Lukyanenko V, Terentyev D, Viatchenko-Karpinski S, Wiesner TF. Regulation of sarcoplasmic reticulum calcium release by luminal calcium in cardiac muscle. *Front Biosci*. 2002;7:d1454-63.

56. Stevens SC, Terentyev D, Kalyanasundaram A, Periasamy M, Gyorke S. Intra-sarcoplasmic reticulum ca oscillations are driven by dynamic regulation of ryanodine receptor function by luminal ca in cardiomyocytes. *J Physiol*. 2009.
57. Parmacek MS, Solaro RJ. Biology of the troponin complex in cardiac myocytes. *Prog Cardiovasc Dis*. 2004;47(3):159-176.
58. Gomes AV, Potter JD. Molecular and cellular aspects of troponin cardiomyopathies. *Ann N Y Acad Sci*. 2004;1015:214-224.
59. Hibberd MG, Jewell BR. Calcium- and length-dependent force production in rat ventricular muscle. *J Physiol*. 1982;329:527-540.
60. Kentish JC, ter Keurs HE, Ricciardi L, Bucx JJ, Noble MI. Comparison between the sarcomere length-force relations of intact and skinned trabeculae from rat right ventricle. influence of calcium concentrations on these relations. *Circ Res*. 1986;58(6):755-768.
61. Li L, Desantiago J, Chu G, Kranias EG, Bers DM. Phosphorylation of phospholamban and troponin I in beta-adrenergic-induced acceleration of cardiac relaxation. *Am J Physiol Heart Circ Physiol*. 2000;278(3):H769-79.
62. Kentish JC, McCloskey DT, Layland J, et al. Phosphorylation of troponin I by protein kinase A accelerates relaxation and crossbridge cycle kinetics in mouse ventricular muscle. *Circ Res*. 2001;88(10):1059-1065.
63. Pi Y, Kemnitz KR, Zhang D, Kranias EG, Walker JW. Phosphorylation of troponin I controls cardiac twitch dynamics: Evidence from phosphorylation site mutants expressed on a troponin I-null background in mice. *Circ Res*. 2002;90(6):649-656.
64. Pena JR, Wolska BM. Troponin I phosphorylation plays an important role in the relaxant effect of beta-adrenergic stimulation in mouse hearts. *Cardiovasc Res*. 2004;61(4):756-763.
65. Fatkin D, McConnell BK, Mudd JO, et al. An abnormal Ca^{2+} response in mutant sarcomere protein-mediated familial hypertrophic cardiomyopathy. *J Clin Invest*. 2000;106(11):1351-1359.
66. Knollmann BC, Kirchhof P, Sirenko SG, et al. Familial hypertrophic cardiomyopathy-linked mutant troponin T causes stress-induced ventricular tachycardia and Ca^{2+}-dependent action potential remodeling. *Circ Res*. 2003;92(4):428-436.
67. Robinson P, Griffiths PJ, Watkins H, Redwood CS. Dilated and hypertrophic cardiomyopathy mutations in troponin and alpha-tropomyosin have opposing effects on the calcium affinity of cardiac thin filaments. *Circ Res*. 2007;101(12):1266-1273.
68. Huke S, Knollmann BC. Increased myofilament Ca^{2+}-sensitivity and arrhythmia susceptibility. *J Mol Cell Cardiol*. 2010;48(5):824-833.
69. Schober T, Huke S, Venkataraman R, et al. Myofilament ca sensitization increases cytosolic ca binding affinity, alters intracellular ca homeostasis, and causes pause-dependent ca-triggered arrhythmia. *Circ Res*. 2012;111(2):170-179.
70. Bers DM, Despa S, Bossuyt J. Regulation of Ca^{2+} and na+ in normal and failing cardiac myocytes. *Ann N Y Acad Sci*. 2006;1080:165-177.
71. Shigekawa M, Iwamoto T. Cardiac Na+-Ca^{2+} exchange: Molecular and pharmacological aspects. *Circ Res*. 2001;88(9):864-876.

72. Litwin SE, Li J, Bridge JH. Na-ca exchange and the trigger for sarcoplasmic reticulum ca release: Studies in adult rabbit ventricular myocytes. *Biophys J*. 1998;75(1):359-371.
73. Weber CR, Piacentino V,3rd, Ginsburg KS, Houser SR, Bers DM. Na+-Ca^{2+} exchange current and submembrane [Ca^{2+}] during the cardiac action potential. *Circ Res*. 2002;90(2):182-189.
74. Weisser-Thomas J, Piacentino V,3rd, Gaughan JP, Margulies K, Houser SR. Calcium entry via Na/Ca exchange during the action potential directly contributes to contraction of failing human ventricular myocytes. *Cardiovasc Res*. 2003;57(4):974-985.
75. Pott C, Philipson KD, Goldhaber JI. Excitation-contraction coupling in na+-Ca^{2+} exchanger knockout mice: Reduced transsarcolemmal Ca^{2+} flux. *Circ Res*. 2005;97(12):1288-1295.
76. Bers DM. Altered cardiac myocyte ca regulation in heart failure. *Physiology (Bethesda)*. 2006;21:380-387.
77. Martonosi AN, Pikula S. The structure of the Ca^{2+}-ATPase of sarcoplasmic reticulum. *Acta Biochim Pol*. 2003;50(2):337-365.
78. Brini M, Carafoli E. Calcium pumps in health and disease. *Physiol Rev*. 2009;89(4):1341-1378.
79. Periasamy M, Kalyanasundaram A. SERCA pump isoforms: Their role in calcium transport and disease. *Muscle Nerve*. 2007;35(4):430-442.
80. Sakata S, Lebeche D, Sakata N, et al. Targeted gene transfer increases contractility and decreases oxygen cost of contractility in normal rat hearts. *Am J Physiol Heart Circ Physiol*. 2007;292(5):H2356-63.
81. Bhupathy P, Babu GJ, Periasamy M. Sarcolipin and phospholamban as regulators of cardiac sarcoplasmic reticulum Ca^{2+} ATPase. *J Mol Cell Cardiol*. 2007;42(5):903-911.
82. MacDougall LK, Jones LR, Cohen P. Identification of the major protein phosphatases in mammalian cardiac muscle which dephosphorylate phospholamban. *Eur J Biochem*. 1991;196(3):725-734.
83. Haghighi K, Gregory KN, Kranias EG. Sarcoplasmic reticulum ca-ATPase-phospholamban interactions and dilated cardiomyopathy. *Biochem Biophys Res Commun*. 2004;322(4):1214-1222.
84. Erkasap N. SERCA in genesis of arrhythmias: What we already know and what is new? *Anadolu Kardiyol Derg*. 2007;7 Suppl 1:43-46.
85. Jenden DJ, Fairhurst AS. The pharmacology of ryanodine. *Pharmacol Rev*. 1969;21(1):1-25.
86. Procita L. The action of ryanodine on mammalian skeletal muscle in situ. *J Pharmacol Exp Ther*. 1956;117(4):363-373.
87. Hajdu S, Leonard E. Action of ryanodine on mammalian cardiac muscle: Effects on contractility, and reversal of digitalis-induced ventricular arrhythmias. *Circ Res*. 1961;9:1291-1298.
88. Fabiato A. Effects of ryanodine in skinned cardiac cells. *Fed Proc*. 1985;44(15):2970-2976.

89. Cannell MB, Vaughan-Jones RD, Lederer WJ. Ryanodine block of calcium oscillations in heart muscle and the sodium-tension relationship. *Fed Proc*. 1985;44(15):2964-2969.
90. Bonilla E. Staining of transverse tubular system of skeletal muscle by tannic acid-glutaraldehyde fixation. *J Ultrastruct Res*. 1977;(2):162-165.
91. Somlyo AV. Bridging structures spanning the junctioning gap at the triad of skeletal muscle. *J Cell Biol*. 1979;80(3):743-750.
92. Campbell KP, Franzini-Armstrong C, Shamoo AE. Further characterization of light and heavy sarcoplasmic reticulum vesicles. identification of the 'sarcoplasmic reticulum feet' associated with heavy sarcoplasmic reticulum vesicles. *Biochim Biophys Acta*. 1980;602(1):97-116.
93. Campbell KP, Knudson CM, Imagawa T, et al. Identification and characterization of the high affinity [3H]ryanodine receptor of the junctional sarcoplasmic reticulum Ca^{2+} release channel. *J Biol Chem*. 1987;262(14):6460-6463.
94. Inui M, Saito A, Fleischer S. Purification of the ryanodine receptor and identity with feet structures of junctional terminal cisternae of sarcoplasmic reticulum from fast skeletal muscle. *J Biol Chem*. 1987;262(4):1740-1747.
95. Hakamata Y, Nakai J, Takeshima H, Imoto K. Primary structure and distribution of a novel ryanodine receptor/calcium release channel from rabbit brain. *FEBS Lett*. 1992;312(2-3):229-235.
96. Furuichi T, Furutama D, Hakamata Y, Nakai J, Takeshima H, Mikoshiba K. Multiple types of ryanodine receptor/Ca^{2+} release channels are differentially expressed in rabbit brain. *J Neurosci*. 1994;14(8):4794-4805.
97. Neylon CB, Richards SM, Larsen MA, Agrotis A, Bobik A. Multiple types of ryanodine receptor/Ca^{2+} release channels are expressed in vascular smooth muscle. *Biochem Biophys Res Commun*. 1995;215(3):814-821.
98. Murayama T, Ogawa Y. Properties of Ryr3 ryanodine receptor isoform in mammalian brain. *J Biol Chem*. 1996;271(9):5079-5084.
99. Hosoi E, Nishizaki C, Gallagher KL, Wyre HW, Matsuo Y, Sei Y. Expression of the ryanodine receptor isoforms in immune cells. *J Immunol*. 2001;167(9):4887-494.
100. Futatsugi A, Kuwajima G, Mikoshiba K. Tissue-specific and developmentally regulated alternative splicing in mouse skeletal muscle ryanodine receptor mRNA. *Biochem J*. 1995;305(Pt 2):373-378.
101. Miyatake R, Furukawa A, Matsushita M, et al. Tissue-specific alternative splicing of mouse brain type ryanodine receptor/calcium release channel mRNA. *FEBS Lett*. 1996;395(2-3):123-126.
102. Marziali G, Rossi D, Giannini G, Charlesworth A, Sorrentino V. cDNA cloning reveals a tissue specific expression of alternatively spliced transcripts of the ryanodine receptor type 3 (RyR3) calcium release channel. *FEBS Lett*. 1996;394(1):76-82.
103. Dulhunty AF, Pouliquin P. What we don't know about the structure of ryanodine receptor calcium release channels. *Clin Exp Pharmacol Physiol*. 2003;30(10):713-723.

104. Takeshima H, Nishimura S, Matsumoto T, et al. Primary structure and expression from complementary DNA of skeletal muscle ryanodine receptor. *Nature*. 1989;339(6224):439-445.
105. Zorzato F, Fujii J, Otsu K, et al. Molecular cloning of cDNA encoding human and rabbit forms of the Ca^{2+} release channel (ryanodine receptor) of skeletal muscle sarcoplasmic reticulum. *J Biol Chem*. 1990;265(4):2244-2256.
106. Du GG, Sandhu B, Khanna VK, Guo XH, MacLennan DH. Topology of the Ca^{2+} release channel of skeletal muscle sarcoplasmic reticulum (RyR1). *PNAS*. 2002;99(26):16725-16730.
107. Samso M, Wagenknecht T, Allen PD. Internal structure and visualization of transmembrane domains of the RyR1 calcium release channel by cryo-EM. *Nat Struct Mol Biol*. 2005;12(6):539-544.
108. Ludtke SJ, Serysheva II, Hamilton SL, Chiu W. The pore structure of the closed RyR1 channel. *Structure*. 2005;13(8):1203-1211.
109. Serysheva II, Ludtke SJ, Baker ML, et al. Subnanometer-resolution electron cryomicroscopy-based domain models for the cytoplasmic region of skeletal muscle RyR channel. *Proc Natl Acad Sci U S A*. 2008;105(28):9610-9615.
110. Zhao M, Li P, Li X, Zhang L, Winkfein RJ, Chen SR. Molecular identification of the ryanodine receptor pore-forming segment. *J Biol Chem*. 1999;274(37):25971-25974.
111. Du GG, Guo X, Khanna VK, MacLennan DH. Functional characterization of mutants in the predicted pore region of the rabbit cardiac muscle Ca^{2+} release channel (ryanodine receptor isoform 2). *J Biol Chem*. 2001;276(34):31760-31771.
112. Balshaw D, Gao L, Meissner G. Luminal loop of the ryanodine receptor: A pore-forming segment? *Proc Natl Acad Sci U S A*. 1999;96(7):3345-3347.
113. Gao L, Balshaw D, Xu L, Tripathy A, Xin C, Meissner G. Evidence for a role of the lumenal M3-M4 loop in skeletal muscle Ca^{2+} release channel (ryanodine receptor) activity and conductance. *Biophys J*. 2000;79(2):828-840.
114. Welch W, Rheault S, West DJ, Williams AJ. A model of the putative pore region of the cardiac ryanodine receptor channel. *Biophys J*. 2004;87(4):2335-2351.
115. Franzini-Armstrong C. STUDIES OF THE TRIAD : I. structure of the junction in frog twitch fibers. *J Cell Biol*. 1970;47(2):488-499.
116. Radermacher M, Wagenknecht T, Grassucci R, et al. Cryo-EM of the native structure of the calcium release channel/ryanodine receptor from sarcoplasmic reticulum. *Biophys J*. 1992;61(4):936-940.
117. Radermacher M, Rao V, Grassucci R, et al. Cryo-electron microscopy and three-dimensional reconstruction of the calcium release channel/ryanodine receptor from skeletal muscle. *J Cell Biol*. 1994;127(2):411-423.
118. Serysheva II, Orlova EV, Chiu W, Sherman MB, Hamilton SL, van Heel M. Electron cryomicroscopy and angular reconstitution used to visualize the skeletal muscle calcium release channel. *Nat Struct Biol*. 1995;2(1):18-24.
119. Serysheva II, Ludtke SJ, Baker MR, Chiu W, Hamilton SL. Structure of the voltage-gated L-type Ca^{2+} channel by electron cryomicroscopy. *Proc Natl Acad Sci U S A*. 2002;99(16):10370-10375.

120. Paolini C, Fessenden JD, Pessah IN, Franzini-Armstrong C. Evidence for conformational coupling between two calcium channels. *Proc Natl Acad Sci U S A*. 2004;101(34):12748-12752.
121. Paolini C, Protasi F, Franzini-Armstrong C. The relative position of RyR feet and DHPR tetrads in skeletal muscle. *J Mol Biol*. 2004;342(1):145-153.
122. Liu Z, Zhang J, Wang R, Wayne Chen SR, Wagenknecht T. Location of divergent region 2 on the three-dimensional structure of cardiac muscle ryanodine receptor/calcium release channel. *J Mol Biol*. 2004;338(3):533-545.
123. Zhang J, Liu Z, Masumiya H, et al. Three-dimensional localization of divergent region 3 of the ryanodine receptor to the clamp-shaped structures adjacent to the FKBP binding sites. *J Biol Chem*. 2003;278(16):14211-14218.
124. Liu Z, Wang R, Zhang J, Chen SR, Wagenknecht T. Localization of a disease-associated mutation site in the three-dimensional structure of the cardiac muscle ryanodine receptor. *J Biol Chem*. 2005;280(45):37941-37947.
125. Yuchi Z, Lau K, Van Petegem F. Disease mutations in the ryanodine receptor central region: Crystal structures of a phosphorylation hot spot domain. *Structure*. 2012;20(7):1201-1211.
126. Meng X, Xiao B, Cai S, et al. Three-dimensional localization of serine 2808, a phosphorylation site in cardiac ryanodine receptor. *J Biol Chem*. 2007;282(35):25929-25939.
127. Zhou Q, Wang QL, Meng X, et al. Structural and functional characterization of ryanodine receptor-natrin toxin interaction. *Biophys J*. 2008;95(9):4289-4299.
128. Amador FJ, Liu S, Ishiyama N, et al. Crystal structure of type I ryanodine receptor amino-terminal beta-trefoil domain reveals a disease-associated mutation "hot spot" loop. *Proc Natl Acad Sci U S A*. 2009;106(27):11040-11044.
129. Tung CC, Lobo PA, Kimlicka L, Van Petegem F. The amino-terminal disease hotspot of ryanodine receptors forms a cytoplasmic vestibule. *Nature*. 2010;468(7323):585-588.
130. Lobo PA, Van Petegem F. Crystal structures of the N-terminal domains of cardiac and skeletal muscle ryanodine receptors: Insights into disease mutations. *Structure*. 2009;17(11):1505-1514.
131. Ohkusa T, Kang JJ, Morii M, Ikemoto N. Conformational change of the foot protein of sarcoplasmic reticulum as an initial event of calcium release. *J Biochem*. 1991;109(4):609-615.
132. el-Hayek R, Yano M, Ikemoto N. A conformational change in the junctional foot protein is involved in the regulation of Ca^{2+} release from sarcoplasmic reticulum. studies on polylysine-induced Ca^{2+} release. *J Biol Chem*. 1995;270(26):15634-15638.
133. Orlova EV, Serysheva II, van Heel M, Hamilton SL, Chiu W. Two structural configurations of the skeletal muscle calcium release channel. *Nat Struct Biol*. 1996;3(6):547-552.
134. Serysheva I, Schatz M, van Heel M, Chiu W, Hamilton SL. Structure of the skeletal muscle calcium release channel activated with Ca^{2+} and AMP-PCP. *Biophys J*. 1999;77(4):1936-1944.

135. Ikemoto N, Yamamoto T. Regulation of calcium release by interdomain interaction within ryanodine receptors. *Front Biosci*. 2002;7:d671-83.
136. Samso M, Feng W, Pessah IN, Allen PD. Coordinated movement of cytoplasmic and transmembrane domains of RyR1 upon gating. *PLoS Biol*. 2009;7(4):e85.
137. Bers DM. Macromolecular complexes regulating cardiac ryanodine receptor function. *J Mol Cell Cardiol*. 2004;37(2):417-429.
138. Song DW, Lee JG, Youn HS, Eom SH, Kim do H. Ryanodine receptor assembly: A novel systems biology approach to 3D mapping. *Prog Biophys Mol Biol*. 2011;105(3):145-161.
139. Meissner G, Darling E, Eveleth J. Kinetics of rapid Ca^{2+} release by sarcoplasmic reticulum. effects of Ca^{2+}, Mg^{2+}, and adenine nucleotides. *Biochemistry*. 1986;25(1):236-244.
140. Laver DR, Owen VJ, Junankar PR, Taske NL, Dulhunty AF, Lamb GD. Reduced inhibitory effect of Mg^{2+} on ryanodine receptor-Ca^{2+} release channels in malignant hyperthermia. *Biophys J*. 1997;73(4):1913-1924.
141. Chen SR, Ebisawa K, Li X, Zhang L. Molecular identification of the ryanodine receptor Ca^{2+} sensor. *J Biol Chem*. 1998;273(24):14675-14678.
142. Du GG, MacLennan DH. Functional consequences of mutations of conserved, polar amino acids in transmembrane sequences of the Ca^{2+} release channel (ryanodine receptor) of rabbit skeletal muscle sarcoplasmic reticulum. *J Biol Chem*. 1998;273(48):31867-31872.
143. Li P, Chen SR. Molecular basis of Ca^{2+} activation of the mouse cardiac Ca^{2+} release channel (ryanodine receptor). *J Gen Physiol*. 2001;118(121322505):33-44.
144. Du GG, MacLennan DH. Ca^{2+} inactivation sites are located in the COOH-terminal quarter of recombinant rabbit skeletal muscle Ca^{2+} release channels (ryanodine receptors). *J Biol Chem*. 1999;274(37):26120-26126.
145. Gao L, Tripathy A, Lu X, Meissner G. Evidence for a role of C-terminal amino acid residues in skeletal muscle Ca^{2+} release channel (ryanodine receptor) function. *FEBS Lett*. 1997;412(1):223-226.
146. Du GG, Khanna VK, MacLennan DH. Mutation of divergent region 1 alters caffeine and Ca^{2+} sensitivity of the skeletal muscle Ca^{2+} release channel (ryanodine receptor). *J Biol Chem*. 2000;275(16):11778-11783.
147. Lukyanenko V, Gyorke I, Gyorke S. Regulation of calcium release by calcium inside the sarcoplasmic reticulum in ventricular myocytes. *Pflugers Arch*. 1996;432(6):1047-1054.
148. Gyorke I, Gyorke S. Regulation of the cardiac ryanodine receptor channel by luminal Ca^{2+} involves luminal Ca^{2+} sensing sites. *Biophys J*. 1998;75(6):2801-2810.
149. Ching LL, Williams AJ, Sitsapesan R. Evidence for Ca^{2+} activation and inactivation sites on the luminal side of the cardiac ryanodine receptor complex. *Circ Res*. 2000;87(3):201-206.
150. Fabiato A, Fabiato F. Excitation-contraction coupling of isolated cardiac fibers with disrupted or closed sarcolemmas. calcium-dependent cyclic and tonic contractions. *Circ Res*. 1972;31(3):293-307.
151. Jiang D, Wang R, Xiao B, et al. Enhanced store overload-induced Ca^{2+} release and channel sensitivity to luminal Ca^{2+} activation are common defects of RyR2

mutations linked to ventricular tachycardia and sudden death. *Circ Res*. 2005;97(11):1173-1181.
152. Jiang D, Chen W, Wang R, Zhang L, Chen SRW. Loss of luminal Ca^{2+} activation in the cardiac ryanodine receptor is associated with ventricular fibrillation and sudden death. *Proc Natl Acad Sci U S A*. 2007;104(46):18309-18314.
153. Tripathy A, Meissner G. Sarcoplasmic reticulum lumenal Ca^{2+} has access to cytosolic activation and inactivation sites of skeletal muscle Ca^{2+} release channel. *Biophys J*. 1996;70(6):2600-2615.
154. Xu L, Meissner G. Regulation of cardiac muscle Ca^{2+} release channel by sarcoplasmic reticulum lumenal Ca^{2+}. *Biophys J*. 1998;75(5):2302-2312.
155. Sitsapesan R, Williams A. Regulation of the gating of the sheep cardiac sarcoplasmic reticulum Ca^{2+}-release channel by luminal Ca^{2+}. *J Membr Biol*. 1994;137(3):215-226.
156. Sitsapesan R, Williams A. The gating of the sheep skeletal sarcoplasmic reticulum Ca^{2+}-release channel is regulated by luminal Ca^{2+}. *J Membr Biol*. 1995;146(2):133-144.
157. Seo MD, Velamakanni S, Ishiyama N, et al. Structural and functional conservation of key domains in InsP3 and ryanodine receptors. *Nature*. 2012;483(7387):108-112.
158. Sharma P, Ishiyama N, Nair U, et al. Structural determination of the phosphorylation domain of the ryanodine receptor. *FEBS J*. 2012;279(20):3952-3964.
159. Truong K, Sawano A, Miyawaki A, Ikura M. Calcium indicators based on calmodulin-fluorescent protein fusions. *Methods Mol Biol*. 2007;352:71-82.
160. Truong K, Sawano A, Mizuno H, et al. FRET-based in vivo Ca^{2+} imaging by a new calmodulin-GFP fusion molecule. *Nat Struct Biol*. 2001;8(12):1069-1073.
161. Gyorke I, Hester N, Jones LR, Gyorke S. The role of calsequestrin, triadin, and junctin in conferring cardiac ryanodine receptor responsiveness to luminal calcium. *Biophys J*. 2004;86(4):2121-2128.
162. Gyorke S, Terentyev D. Modulation of ryanodine receptor by luminal calcium and accessory proteins in health and cardiac disease. *Cardiovasc Res*. 2008;77(2):245-255.
163. Knollmann BC, Chopra N, Hlaing T, et al. Casq2 deletion causes sarcoplasmic reticulum volume increase, premature Ca^{2+} release, and catecholaminergic polymorphic ventricular tachycardia. *J Clin Invest*. 2006;116(9):2510-2520.
164. Sitsapesan R, Williams AJ. Regulation of current flow through ryanodine receptors by luminal Ca^{2+}. *J Membr Biol*. 1997;159(3):179-185.
165. Kong H, Jones PP, Koop A, Zhang L, Duff HJ, Chen SR. Caffeine induces Ca^{2+} release by reducing the threshold for luminal Ca^{2+} activation of the ryanodine receptor. *Biochem J*. 2008;414(3):441-452.
166. Kermode H, Williams AJ, Sitsapesan R. The interactions of ATP, ADP, and inorganic phosphate with the sheep cardiac ryanodine receptor. *Biophys J*. 1998;74(3):1296-1304.
167. Laver DR, Lenz GK, Lamb GD. Regulation of the calcium release channel from rabbit skeletal muscle by the nucleotides ATP, AMP, IMP and adenosine. *J Physiol*. 2001;537(Pt 3):763-778.

168. Meissner G. Adenine nucleotide stimulation of Ca^{2+}-induced Ca^{2+} release in sarcoplasmic reticulum. *J Biol Chem*. 1984;259(4):2365-2374.
169. Meissner G, Henderson JS. Rapid calcium release from cardiac sarcoplasmic reticulum vesicles is dependent on Ca^{2+} and is modulated by Mg^{2+}, adenine nucleotide, and calmodulin. *J Biol Chem*. 1987;262(7):3065-3073.
170. Tencerova B, Zahradnikova A, Gaburjakova J, Gaburjakova M. Luminal Ca^{2+} controls activation of the cardiac ryanodine receptor by ATP. *J Gen Physiol*. 2012;140(2):93-108.
171. Takasago T, Imagawa T, Furukawa K, Ogurusu T, Shigekawa M. Regulation of the cardiac ryanodine receptor by protein kinase- dependent phosphorylation. *J Biochem*. 1991;109(1):163-170.
172. Yoshida A, Takahashi M, Imagawa T, Shigekawa M, Takisawa H, Nakamura T. Phosphorylation of ryanodine receptors in rat myocytes during beta- adrenergic stimulation. *J Biochem*. 1992;111(2):186-190.
173. Witcher DR, Kovacs RJ, Schulman H, Cefali DC, Jones LR. Unique phosphorylation site on the cardiac ryanodine receptor regulates calcium channel activity. *J Biol Chem*. 1991;266(17):11144-11152.
174. Marx SO, Reiken S, Hisamatsu Y, et al. PKA phosphorylation dissociates FKBP12.6 from the calcium release channel (ryanodine receptor): Defective regulation in failing hearts. *Cell*. 2000;101(4):365-376.
175. Timerman AP, Onoue H, Xin HB, et al. Selective binding of FKBP12.6 by the cardiac ryanodine receptor. *J Biol Chem*. 1996;271(34):20385-20391.
176. Jiang MT, Lokuta AJ, Farrell EF, Wolff MR, Haworth RA, Valdivia HH. Abnormal Ca^{2+} release, but normal ryanodine receptors, in canine and human heart failure. *Circ Res*. 2002;91(11):1015-1022.
177. Stange M, Xu L, Balshaw D, Yamaguchi N, Meissner G. Characterization of recombinant skeletal muscle (ser-2843) and cardiac muscle (ser-2809) ryanodine receptor phosphorylation mutants. *J Biol Chem*. 2003;278(51):51693-51702.
178. Xiao B, Sutherland C, Walsh MP, Chen SRW. Protein kinase A phosphorylation at serine-2808 of the cardiac Ca^{2+}-release channel (ryanodine receptor) does not dissociate 12.6-kDa FK506-binding protein (FKBP12.6). *Circ Res*. 2004;94(4):487-495.
179. Guo T, Cornea RL, Huke S, et al. Kinetics of FKBP12.6 binding to ryanodine receptors in permeabilized cardiac myocytes and effects on ca sparks. *Circ Res*. 2010;106(11):1743-1752.
180. Xiao B, Jiang MT, Zhao M, et al. Characterization of a novel PKA phosphorylation site, serine-2030, reveals no PKA hyperphosphorylation of the cardiac ryanodine receptor in canine heart failure. *Circ Res*. 2005;96(8):847-855.
181. Xiao B, Tian X, Xie W, et al. Functional consequence of protein kinase A-dependent phosphorylation of the cardiac ryanodine receptor: Sensitization of store overload-induced Ca^{2+} release. *J Biol Chem*. 2007;282(41):30256-30264.
182. Jones PP, Meng X, Xiao B, et al. Localization of PKA phosphorylation site, ser(2030), in the three-dimensional structure of cardiac ryanodine receptor. *Biochem J*. 2008;410(2):261-270.

183. Wagner S, Dybkova N, Rasenack EC, et al. Ca^{2+}/calmodulin-dependent protein kinase II regulates cardiac na+ channels. *J Clin Invest*. 2006;116(12):3127-3138.
184. Tessier S, Karczewski P, Krause EG, et al. Regulation of the transient outward K(+) current by Ca^{2+}/calmodulin-dependent protein kinases II in human atrial myocytes. *Circ Res*. 1999;85(9):810-819.
185. Maier LS, Bers DM. Role of Ca^{2+}/calmodulin-dependent protein kinase (CaMK) in excitation-contraction coupling in the heart. *Cardiovasc Res*. 2007;73(4):631-640. doi: 10.1016/j.cardiores.2006.11.005.
186. Maier LS, Zhang T, Chen L, DeSantiago J, Brown JH, Bers DM. Transgenic CaMKII{delta}C overexpression uniquely alters cardiac myocyte Ca^{2+} handling: Reduced SR Ca^{2+} load and activated SR Ca^{2+} release. *Circ Res*. 2003;92(8):904-911.
187. Wehrens XH, Lehnart SE, Reiken SR, Marks AR. Ca^{2+}/Calmodulin-dependent protein kinase II phosphorylation regulates the cardiac ryanodine receptor. *Circ Res*. 2004;94(6):e61-70.
188. Currie S, Loughrey C, Craig M, Smith G. Calcium/calmodulin-dependent protein kinase IIdelta associates with the ryanodine receptor complex and regulates channel function in rabbit heart. *Biochem J*. 2004;377(Pt 2):357-366.
189. Lokuta AJ, Rogers TB, Lederer WJ, Valdivia HH. Modulation of cardiac ryanodine receptors of swine and rabbit by a phosphorylation-dephosphorylation mechanism. *J Physiol (Lond)*. 1995;487(Pt 3):609-622.
190. Yang D, Zhu WZ, Xiao B, et al. Ca^{2+}/calmodulin kinase II-dependent phosphorylation of ryanodine receptors suppresses Ca^{2+} sparks and Ca^{2+} waves in cardiac myocytes. *Circ Res*. 2007;100(3):399-407. doi: 10.1161/01.RES.0000258022.13090.55.
191. Witcher DR, Strifler BA, Jones LR. Cardiac-specific phosphorylation site for multifunctional Ca^{2+}/calmodulin-dependent protein kinase is conserved in the brain ryanodine receptor. *J Biol Chem*. 1992;267(7):4963-4967.
192. Rodriguez P, Bhogal MS, Colyer J. Stoichiometric phosphorylation of cardiac ryanodine receptor on serine-2809 by calmodulin-dependent kinase II and protein kinase A. *J Biol Chem*. 2003;278:38593-38600.
193. Saucerman JJ, Bers DM. Calmodulin binding proteins provide domains of local Ca^{2+} signaling in cardiac myocytes. *J Mol Cell Cardiol*. 2012;52(2):312-316.
194. Demaurex N, Frieden M. Measurements of the free luminal ER Ca^{2+} concentration with targeted "cameleon" fluorescent proteins. *Cell Calcium*. 2003;34(2):109-119.
195. Miyawaki A, Llopis J, Heim R, et al. Fluorescent indicators for Ca^{2+} based on green fluorescent proteins and calmodulin. *Nature*. 1997;388(6645):882-887.
196. Ikeda M, Sugiyama T, Wallace CS, et al. Circadian dynamics of cytosolic and nuclear Ca^{2+} in single suprachiasmatic nucleus neurons. *Neuron*. 2003;38(2):253-263.
197. Palmer AE, Jin C, Reed JC, Tsien RY. Bcl-2-mediated alterations in endoplasmic reticulum Ca^{2+} analyzed with an improved genetically encoded fluorescent sensor. *Proc Natl Acad Sci U S A*. 2004;101(50):17404-17409.
198. Balshaw DM, Yamaguchi N, Meissner G. Modulation of intracellular calcium-release channels by calmodulin. *J Membr Biol*. 2002;185(1):1-8.

199. Fruen BR, Black DJ, Bloomquist RA, et al. Regulation of the RYR1 and RYR2 Ca^{2+} release channel isoforms by Ca^{2+}-insensitive mutants of calmodulin. *Biochemistry*. 2003;42(9):2740-2747.
200. Yamaguchi N, Xu L, Pasek DA, Evans KE, Meissner G. Molecular basis of calmodulin binding to cardiac muscle Ca^{2+} release channel (ryanodine receptor). *J Biol Chem*. 2003;278(26):23480-23486.
201. Balshaw DM, Xu L, Yamaguchi N, Pasek DA, Meissner G. Calmodulin binding and inhibition of cardiac muscle calcium release channel (ryanodine receptor). *J Biol Chem*. 2001;276(23):20144-20153.
202. Rodney GG, Schneider MF. Calmodulin modulates initiation but not termination of spontaneous Ca^{2+} sparks in frog skeletal muscle. *Biophys J*. 2003;85(2):921-932.
203. Moore CP, Rodney G, Zhang JZ, Santacruz-Toloza L, Strasburg G, Hamilton SL. Apocalmodulin and Ca^{2+} calmodulin bind to the same region on the skeletal muscle Ca^{2+} release channel. *Biochemistry (N Y)*. 1999;38(26):8532-8537.
204. Yamaguchi N, Xin C, Meissner G. Identification of apocalmodulin and Ca^{2+}-calmodulin regulatory domain in skeletal muscle Ca^{2+} release channel, ryanodine receptor. *J Biol Chem*. 2001;276(25):22579-22585.
205. Xiong L, Zhang JZ, He R, Hamilton SL. A Ca^{2+}-binding domain in RyR1 that interacts with the calmodulin binding site and modulates channel activity. *Biophys J*. 2006;90(1):173-182.
206. Gangopadhyay JP, Ikemoto N. Interaction of the lys(3614)-asn(3643) calmodulin-binding domain with the cys(4114)-asn(4142) region of the type 1 ryanodine receptor is involved in the mechanism of Ca^{2+}/agonist-induced channel activation. *Biochem J*. 2008;411(2):415-423.
207. Wagenknecht T, Radermacher M, Grassucci R, Berkowitz J, Xin HB, Fleischer S. Locations of calmodulin and FK506-binding protein on the three- dimensional architecture of the skeletal muscle ryanodine receptor. *J Biol Chem*. 1997;272(51):32463-32471.
208. Samso M, Wagenknecht T. Apocalmodulin and Ca^{2+}-calmodulin bind to neighboring locations on the ryanodine receptor. *J Biol Chem*. 2002;277(2):1349-1353.
209. Huang X, Fruen B, Farrington DT, Wagenknecht T, Liu Z. Calmodulin-binding locations on the skeletal and cardiac ryanodine receptors. *J Biol Chem*. 2012;287(36):30328-30335.
210. Cornea RL, Nitu F, Gruber S, et al. FRET-based mapping of calmodulin bound to the RyR1 Ca^{2+} release channel. *Proc Natl Acad Sci U S A*. 2009;106(15):6128-6133.
211. Chelu MG, Danila CI, Gilman CP, Hamilton SL. Regulation of ryanodine receptors by FK506 binding proteins. *Trends Cardiovasc Med*. 2004;14(6):227-234.
212. Kaftan E, Marks AR, Ehrlich BE. Effects of rapamycin on ryanodine receptor/Ca^{2+}-release channels from cardiac muscle. *Circ Res*. 1996;78(6):990-997.
213. McCall E, Li L, Satoh H, Shannon TR, Blatter LA, Bers DM. Effects of FK-506 on contraction and Ca^{2+} transients in rat cardiac myocytes. *Circ Res*. 1996;79(6):1110-1121.

214. Xiao RP, Valdivia HH, Bogdanov K, Valdivia C, Lakatta EG, Cheng H. The immunophilin FK506-binding protein modulates Ca^{2+} release channel closure in rat heart. *J Physiol (Lond)*. 1997;500(Pt 2):343-354.
215. Su Z, Sugishita K, Li F, Ritter M, Barry WH. Effects of FK506 on $[Ca^{2+}]i$ differ in mouse and rabbit ventricular myocytes. *J Pharmacol Exp Ther*. 2003;304(1):334-341.
216. Barg S, Copello JA, Fleischer S. Different interactions of cardiac and skeletal muscle ryanodine receptors with FK-506 binding protein isoforms. *Am J Physiol*. 1997;272(5 Pt 1):C1726-33.
217. Xiao J, Tian X, Jones PP, et al. Removal of FKBP12.6 does not alter the conductance and activation of the cardiac ryanodine receptor or the susceptibility to stress-induced ventricular arrhythmias. *J Biol Chem*. 2007;282(48):34828-34838.
218. Hunt DJ, Jones PP, Wang R, et al. K201 (JTV519) suppresses spontaneous Ca^{2+} release and [3H]ryanodine binding to RyR2 irrespective of FKBP12.6 association. *Biochem J*. 2007;404(3):431-438.
219. Gaburjakova M, Gaburjakova J, Reiken S, et al. FKBP12 binding modulates ryanodine receptor channel gating. *J Biol Chem*. 2001;276(20):16931-1695.
220. Bultynck G, Rossi D, Callewaert G, et al. The conserved sites for the FK506-binding proteins in ryanodine receptors and inositol 1,4,5-trisphosphate receptors are structurally and functionally different. *J Biol Chem*. 2001;276(50):47715-4724.
221. Masumiya H, Wang R, Zhang J, Xiao B, Chen SRW. Localization of the 12.6-kDa FK506-binding protein (FKBP12.6) binding site to the NH2-terminal domain of the cardiac Ca^{2+} release channel (ryanodine receptor). *J Biol Chem*. 2003;278(6):3786-3792.
222. Zissimopoulos S, Lai FA. Evidence for a FKBP12.6 binding site at the C-terminus of the cardiac ryanodine receptor. *Biophys J*. 2002;82:59a.
223. Zissimopoulos S, Lai FA. Interaction of FKBP12.6 with the cardiac ryanodine receptor C-terminal domain. *J Biol Chem*. 2005;280(7):5475-5485.
224. Wagenknecht T, Grassucci R, Berkowitz J, Wiederrecht GJ, Xin HB, Fleischer S. Cryoelectron microscopy resolves FK506-binding protein sites on the skeletal muscle ryanodine receptor. *Biophys J*. 1996;70(4):1709-1715.
225. Samso M, Shen X, Allen PD. Structural characterization of the RyR1-FKBP12 interaction. *J Mol Biol*. 2006;356(4):917-927.
226. Sharma MR, Jeyakumar LH, Fleischer S, Wagenknecht T. Three-dimensional visualization of FKBP12.6 binding to an open conformation of cardiac ryanodine receptor. *Biophys J*. 2006;90(1):164-172.
227. Cornea RL, Nitu FR, Samso M, Thomas DD, Fruen BR. Mapping the ryanodine receptor FK506-binding protein subunit using fluorescence resonance energy transfer. *J Biol Chem*. 2010;285(25):19219-19226.
228. Lai FA, Misra M, Xu L, Smith HA, Meissner G. The ryanodine receptor-Ca^{2+} release channel complex of skeletal muscle sarcoplasmic reticulum. evidence for a cooperatively coupled, negatively charged homotetramer. *J Biol Chem*. 1989;264(28):16776-16785.
229. Pessah IN, Zimanyi I. Characterization of multiple [3H]ryanodine binding sites on the Ca^{2+} release channel of sarcoplasmic reticulum from skeletal and cardiac

muscle: Evidence for a sequential mechanism in ryanodine action. *Mol Pharmacol*. 1991;39(5):679-689.
230. Meissner G. Ryanodine activation and inhibition of the Ca^{2+} release channel of sarcoplasmic reticulum. *J Biol Chem*. 1986;261(14):6300-6306.
231. McGrew SG, Wolleben C, Siegl P, Inui M, Fleischer S. Positive cooperativity of ryanodine binding to the calcium release channel of sarcoplasmic reticulum from heart and skeletal muscle. *Biochemistry (N Y)*. 1989;28(4):1686-1691.
232. Coronado R, Morrissette J, Sukhareva M, Vaughan DM. Structure and function of ryanodine receptors. *Am J Physiol*. 1994;266(6 Pt 1):C1485-504.
233. Witcher DR, McPherson PS, Kahl SD, et al. Photoaffinity labeling of the ryanodine receptor/Ca^{2+} release channel with an azido derivative of ryanodine. *J Biol Chem*. 1994;269(18):13076-13079.
234. Callaway C, Seryshev A, Wang JP, et al. Localization of the high and low affinity [3H]ryanodine binding sites on the skeletal muscle Ca^{2+} release channel. *J Biol Chem*. 1994;269(22):15876-15884.
235. Chen SR, Li P, Zhao M, Li X, Zhang L. Role of the proposed pore-forming segment of the Ca^{2+} release channel (ryanodine receptor) in ryanodine interaction. *Biophys J*. 2002;82(5):2436-247.
236. Wang R, Zhang L, Bolstad J, et al. Residue Gln4863 within a predicted trans-membrane sequence of the Ca^{2+}-release channel (ryanodine receptor) is critical for ryanodine interaction. *J Biol Chem*. 2003;278(51):51557-51565.
237. Loke J, MacLennan DH. Malignant hyperthermia and central core disease: Disorders of Ca^{2+} release channels. *Am J Med*. 1998;104(5):470-486.
238. Joseph X, Whitehurst V, Bloom S, Balazs T. Enhancement of cardiotoxic effects of beta-adrenergic bronchodilators by aminophylline in experimental animals. *Fundam Appl Toxicol*. 1981;1(6):443-447.
239. Varriale P, Ramaprasad S. Aminophylline induced atrial fibrillation. *Pacing Clin Electrophysiol*. 1993;16(10):1953-1955.
240. Whitehurst VE, Joseph X, Vick JA, Alleva FR, Zhang J, Balazs T. Reversal of acute theophylline toxicity by calcium channel blockers in dogs and rats. *Toxicology*. 1996;110(1-3):113-121.
241. Rousseau E, Ladine J, Liu QY, Meissner G. Activation of the Ca^{2+} release channel of skeletal muscle sarcoplasmic reticulum by caffeine and related compounds. *Arch Biochem Biophys*. 1988;267(1):75-86.
242. Rousseau E, Meissner G. Single cardiac sarcoplasmic reticulum Ca^{2+}-release channel: Activation by caffeine. *Am J Physiol*. 1989;256(2 Pt 2):H328-33.
243. Sitsapesan R, Williams AJ. Mechanisms of caffeine activation of single calcium-release channels of sheep cardiac sarcoplasmic reticulum. *J Physiol*. 1990;423:425-439.
244. Cheek TR, Moreton RB, Berridge MJ, Stauderman KA, Murawsky MM, Bootman MD. Quantal Ca^{2+} release from caffeine-sensitive stores in adrenal chromaffin cells. *J Biol Chem*. 1993;268(36):27076-27083.
245. Dettbarn C, Gyorke S, Palade P. Many agonists induce "quantal" Ca^{2+} release or adaptive behavior in muscle ryanodine receptors. *Mol Pharmacol*. 1994;46(3):502-507.

246. Gaburjakova J, Gaburjakova M. Comparison of the effects exerted by luminal Ca^{2+} on the sensitivity of the cardiac ryanodine receptor to caffeine and cytosolic Ca^{2+}. *J Membr Biol*. 2006;212(1):17-28.
247. Porta M, Zima AV, Nani A, et al. Single ryanodine receptor channel basis of caffeine's action on Ca^{2+} sparks. *Biophys J*. 2011;100(4):931-938.
248. Tong J, Oyamada H, Demaurex N, Grinstein S, McCarthy TV, MacLennan DH. Caffeine and halothane sensitivity of intracellular Ca^{2+} release is altered by 15 calcium release channel (ryanodine receptor) mutations associated with malignant hyperthermia and/or central core disease. *J Biol Chem*. 1997;272(42):26332-26339.
249. Tong J, McCarthy TV, MacLennan DH. Measurement of resting cytosolic Ca^{2+} concentrations and Ca^{2+} store size in HEK-293 cells transfected with malignant hyperthermia or central core disease mutant Ca^{2+} release channels. *J Biol Chem*. 1999;274(2):693-702.
250. Jiang D, Jones PP, Davis DR, et al. Characterization of a novel mutation in the cardiac ryanodine receptor that results in catecholaminergic polymorphic ventricular tachycardia. *Channels (Austin)*. 2010;4(4):302-310.
251. Jiang D, Xiao B, Yang D, et al. RyR2 mutations linked to ventricular tachycardia and sudden death reduce the threshold for store-overload-induced Ca^{2+} release (SOICR). *Proc.Natl.Acad.Sci.U.S.A.* 2004;101(35):13062-13067.
252. Jiang D, Xiao B, Zhang L, Chen SR. Enhanced basal activity of a cardiac Ca^{2+} release channel (ryanodine receptor) mutant associated with ventricular tachycardia and sudden death. *Circ Res*. 2002;91(3):218-25.
253. Zorzato F, Scutari E, Tegazzin V, Clementi E, Treves S. Chlorocresol: An activator of ryanodine receptor-mediated Ca^{2+} release. *Mol Pharmacol*. 1993;44(6):1192-1201.
254. Choisy S, Huchet-Cadiou C, Leoty C. Sarcoplasmic reticulum Ca^{2+} release by 4-chloro-m-cresol (4-CmC) in intact and chemically skinned ferret cardiac ventricular fibers. *J Pharmacol Exp Ther*. 1999;290(2):578-586.
255. Fessenden JD, Wang Y, Moore RA, Chen SR, Allen PD, Pessah IN. Divergent functional properties of ryanodine receptor types 1 and 3 expressed in a myogenic cell line. *Biophys J*. 2000;79(5):2509-2525.
256. Herrmann-Frank A, Richter M, Sarkozi S, Mohr U, Lehmann-Horn F. 4-chloro-m-cresol, a potent and specific activator of the skeletal muscle ryanodine receptor. *Biochim Biophys Acta*. 1996;1289(1):31-40.
257. Herrmann-Frank A, Richter M, Lehmann-Horn F. 4-chloro-m-cresol: A specific tool to distinguish between malignant hyperthermia-susceptible and normal muscle. *Biochem Pharmacol*. 1996;52(1):149-155.
258. Ording H, Glahn K, Gardi T, Fagerlund T, Bendixen D. 4-chloro-m-cresol test--a possible supplementary test for diagnosis of malignant hyperthermia susceptibility. *Acta Anaesthesiol Scand*. 1997;41(8):967-972.
259. Gilly H, Musat I, Fricker R, Bittner RE, Steinbereithner K, Kress HG. Classification of malignant hyperthermia-equivocal patients by 4-chloro-M-cresol. *Anesth Analg*. 1997;85(1):149-154.

260. Baur CP, Bellon L, Felleiter P, et al. A multicenter study of 4-chloro-m-cresol for diagnosing malignant hyperthermia susceptibility. *Anesth Analg*. 2000;90(1):200-205.
261. Choisy S, Huchet-Cadiou C, Leoty C. Differential effects of 4-chloro-m-cresol and caffeine on skinned fibers from rat fast and slow skeletal muscles. *J Pharmacol Exp Ther*. 2000;294(3):884-893.
262. Choisy S, Divet A, Huchet-Cadiou C, Leoty C. Sarcoplasmic reticulum Ca^{2+} content affects 4-CmC and caffeine contractures of rat skinned skeletal muscle fibers. *Jpn J Physiol*. 2001;51(6):661-669.
263. Fessenden JD, Perez CF, Goth S, Pessah IN, Allen PD. Identification of a key determinant of ryanodine receptor type 1 required for activation by 4-chloro-m-cresol. *J Biol Chem*. 2003;278(31):28727-28735.
264. Fessenden JD, Feng W, Pessah IN, Allen PD. Amino acid residues Gln4020 and Lys4021 of the ryanodine receptor type 1 are required for activation by 4-chloro-m-cresol. *J Biol Chem*. 2006;281(30):21022-21031.
265. George CH, Jundi H, Thomas NL, Fry DL, Lai FA. Ryanodine receptors and ventricular arrhythmias: Emerging trends in mutations, mechanisms and therapies. *J Mol Cell Cardiol*. 2007;42(1):34-50.
266. Liu N, Ruan Y, Priori SG. Catecholaminergic polymorphic ventricular tachycardia. *Prog Cardiovasc Dis*. 2008;51(1):23-30.
267. Liu N, Priori SG. Disruption of calcium homeostasis and arrhythmogenesis induced by mutations in the cardiac ryanodine receptor and calsequestrin. *Cardiovasc Res*. 2008;77(2):293-301.
268. Blayney LM, Lai FA. Ryanodine receptor-mediated arrhythmias and sudden cardiac death. *Pharmacol Ther*. 2009;123(2):151-177.
269. Bhuiyan ZA, van den Berg MP, van Tintelen JP, et al. Expanding spectrum of human RYR2-related disease: New electrocardiographic, structural, and genetic features. *Circulation*. 2007;116(14):1569-1576.
270. Marjamaa A, Laitinen-Forsblom P, Lahtinen AM, et al. Search for cardiac calcium cycling gene mutations in familial ventricular arrhythmias resembling catecholaminergic polymorphic ventricular tachycardia. *BMC Med Genet*. 2009;10:12.
271. Marjamaa A, Laitinen-Forsblom P, Wronska A, Toivonen L, Kontula K, Swan H. Ryanodine receptor (RyR2) mutations in sudden cardiac death: Studies in extended pedigrees and phenotypic characterization in vitro. *Int J Cardiol*. 2011;147(2):246-252.
272. Noboru Fujino, Hidekazu Ino, Kenshi Hayashi, et al. A novel missense mutation in cardiac ryanodine receptor gene as a possible cause of hypertrophic cardiomyopathy: Evidence from familial analysis. *Circulation*. 2006;114(II):165.
273. MacLennan DH, Chen SR. Store overload-induced Ca^{2+} release as a triggering mechanism for CPVT and MH episodes caused by mutations in RYR and CASQ genes. *J Physiol*. 2009;587(Pt 13):3113-3115.
274. Priori SG, Chen SR. Inherited dysfunction of sarcoplasmic reticulum Ca^{2+} handling and arrhythmogenesis. *Circ Res*. 2011;108(7):871-883.

275. Kannankeril PJ, Mitchell BM, Goonasekera SA, et al. Mice with the R176Q cardiac ryanodine receptor mutation exhibit catecholamine-induced ventricular tachycardia and cardiomyopathy. *Proc Natl Acad Sci U S A*. 2006;103(32):12179-12184.
276. Fernandez-Velasco M, Rueda A, Rizzi N, et al. Increased Ca^{2+} sensitivity of the ryanodine receptor mutant RyR2R4496C underlies catecholaminergic polymorphic ventricular tachycardia. *Circ Res*. 2009;104(2):201-9, 12p following 209.
277. Sedej S, Heinzel FR, Walther S, et al. Na+-dependent SR Ca^{2+} overload induces arrhythmogenic events in mouse cardiomyocytes with a human CPVT mutation. *Cardiovasc Res*. 2010.
278. Uchinoumi H, Yano M, Suetomi T, et al. Catecholaminergic polymorphic ventricular tachycardia is caused by mutation-linked defective conformational regulation of the ryanodine receptor. *Circ Res*. 2010.
279. d'Amati G, Bagattin A, Bauce B, et al. Juvenile sudden death in a family with polymorphic ventricular arrhythmias caused by a novel RyR2 gene mutation: Evidence of specific morphological substrates. *Hum Pathol*. 2005;36(7):761-767.
280. Tiso N, Stephan DA, Nava A, et al. Identification of mutations in the cardiac ryanodine receptor gene in families affected with arrhythmogenic right ventricular cardiomyopathy type 2 (ARVD2). *Hum Mol Genet*. 2001;10(321096894):189-94.
281. Tester DJ, Spoon DB, Valdivia HH, Makielski JC, Ackerman MJ. Targeted mutational analysis of the RyR2-encoded cardiac ryanodine receptor in sudden unexplained death: A molecular autopsy of 49 medical examiner/coroner's cases. *Mayo Clin Proc*. 2004;79(11):1380-1384.
282. Bauce B, Rampazzo A, Basso C, et al. Screening for ryanodine receptor type 2 mutations in families with effort-induced polymorphic ventricular arrhythmias and sudden death: Early diagnosis of asymptomatic carriers. *J Am Coll Cardiol*. 2002;40(2):341-349.
283. Nishio H, Iwata M, Suzuki K. Postmortem molecular screening for cardiac ryanodine receptor type 2 mutations in sudden unexplained death: R420W mutated case with characteristics of status thymico-lymphatics. *Circ J*. 2006;70(11):1402-1406.
284. Milting H, Lukas N, Klauke B, et al. Composite polymorphisms in the ryanodine receptor 2 gene associated with arrhythmogenic right ventricular cardiomyopathy. *Cardiovasc Res*. 2006;71(3):496-505.
285. Ahmad F, Seidman JG, Seidman CE. The genetic basis for cardiac remodeling. *Annu Rev Genomics Hum Genet*. 2005;6:185-216.
286. McCartan C, Mason R, Jayasinghe SR, Griffiths LR. Cardiomyopathy classification: Ongoing debate in the genomics era. *Biochem Res Int*. 2012:796926.
287. Maron BJ. Hypertrophic cardiomyopathy: A systematic review. *JAMA*. 2002;287(10):1308-1320.
288. Karkkainen S, Peuhkurinen K. Genetics of dilated cardiomyopathy. *Ann Med*. 2007;39(2):91-107.
289. Corrado D, Basso C, Thiene G. Arrhythmogenic right ventricular cardiomyopathy: Diagnosis, prognosis, and treatment. *Heart*. 2000;83(5):588-595.

290. Keren A, Syrris P, McKenna WJ. Hypertrophic cardiomyopathy: The genetic determinants of clinical disease expression. *Nat Clin Pract Cardiovasc Med*. 2008;5(3):158-168.
291. Geisterfer-Lowrance AA, Kass S, Tanigawa G, et al. A molecular basis for familial hypertrophic cardiomyopathy: A beta cardiac myosin heavy chain gene missense mutation. *Cell*. 1990;62(5):999-1006.
292. Mirza M, Marston S, Willott R, et al. Dilated cardiomyopathy mutations in three thin filament regulatory proteins result in a common functional phenotype. *J Biol Chem*. 2005;280(31):28498-28506.
293. Du CK, Morimoto S, Nishii K, et al. Knock-in mouse model of dilated cardiomyopathy caused by troponin mutation. *Circ Res*. 2007;101(2):185-194.
294. Chang AN, Parvatiyar MS, Potter JD. Troponin and cardiomyopathy. *Biochem Biophys Res Commun*. 2008;369(1):74-81.
295. Knollmann BC, Blatt SA, Horton K, et al. Inotropic stimulation induces cardiac dysfunction in transgenic mice expressing a troponin T (I79N) mutation linked to familial hypertrophic cardiomyopathy. *J Biol Chem*. 2001;276(13):10039-10048.
296. Sirenko SG, Potter JD, Knollmann BC. Differential effect of troponin T mutations on the inotropic responsiveness of mouse hearts--role of myofilament Ca^{2+} sensitivity increase. *J Physiol*. 2006;575(Pt 1):201-213.
297. Lutucuta S, Tsybouleva N, Ishiyama M, et al. Induction and reversal of cardiac phenotype of human hypertrophic cardiomyopathy mutation cardiac troponin T-Q92 in switch on-switch off bigenic mice. *J Am Coll Cardiol*. 2004;44(11):2221-2230.
298. Hernandez OM, Szczesna-Cordary D, Knollmann BC, et al. F110I and R278C troponin T mutations that cause familial hypertrophic cardiomyopathy affect muscle contraction in transgenic mice and reconstituted human cardiac fibers. *J Biol Chem*. 2005;280(44):37183-37194.
299. James J, Zhang Y, Osinska H, et al. Transgenic modeling of a cardiac troponin I mutation linked to familial hypertrophic cardiomyopathy. *Circ Res*. 2000;87(9):805-811.
300. Wen Y, Pinto JR, Gomes AV, et al. Functional consequences of the human cardiac troponin I hypertrophic cardiomyopathy mutation R145G in transgenic mice. *J Biol Chem*. 2008;283(29):20484-20494.
301. Juan F, Wei D, Xiongzhi Q, et al. The changes of the cardiac structure and function in cTnTR141W transgenic mice. *Int J Cardiol*. 2008;128(1):83-90.
302. Semsarian C, Ahmad I, Giewat M, et al. The L-type calcium channel inhibitor diltiazem prevents cardiomyopathy in a mouse model. *J Clin Invest*. 2002;109(8):1013-1020.
303. Zheng M, Dilly K, Dos Santos Cruz J, et al. Sarcoplasmic reticulum calcium defect in ras-induced hypertrophic cardiomyopathy heart. *Am J Physiol Heart Circ Physiol*. 2004;286(1):H424-33.
304. Schmitt JP, Kamisago M, Asahi M, et al. Dilated cardiomyopathy and heart failure caused by a mutation in phospholamban. *Science*. 2003;299(5611):1410-1413.

305. Minamisawa S, Hoshijima M, Chu G, et al. Chronic phospholamban-sarcoplasmic reticulum calcium ATPase interaction is the critical calcium cycling defect in dilated cardiomyopathy. *Cell*. 1999;99(3):313-322.
306. Wilkins BJ, Molkentin JD. Calcineurin and cardiac hypertrophy: Where have we been? where are we going? *J Physiol*. 2002;541(Pt 1):1-8.
307. Houser SR, Molkentin JD. Does contractile Ca^{2+} control calcineurin-NFAT signaling and pathological hypertrophy in cardiac myocytes? *Sci Signal*. 2008;1(25):pe31.
308. Zhang T, Brown J. Role of Ca^{2+}/calmodulin-dependent protein kinase II in cardiac hypertrophy and heart failure. *Cardiovasc Res*. 2004;63(3):476-486.
309. Toko H, Takahashi H, Kayama Y, et al. Ca^{2+}/calmodulin-dependent kinase IIdelta causes heart failure by accumulation of p53 in dilated cardiomyopathy. *Circulation*. 2010;122(9):891-899.
310. Frey N, McKinsey TA, Olson EN. Decoding calcium signals involved in cardiac growth and function. *Nat Med*. 2000;6(11):1221-1227.
311. Kolodziejczyk SM, Wang L, Balazsi K, DeRepentigny Y, Kothary R, Megeney LA. MEF2 is upregulated during cardiac hypertrophy and is required for normal post-natal growth of the myocardium. *Curr Biol*. 1999;9(20):1203-1206.
312. Lu J, McKinsey TA, Nicol RL, Olson EN. Signal-dependent activation of the MEF2 transcription factor by dissociation from histone deacetylases. *Proc Natl Acad Sci U S A*. 2000;97(8):4070-4075.
313. Passier R, Zeng H, Frey N, et al. CaM kinase signaling induces cardiac hypertrophy and activates the MEF2 transcription factor in vivo. *J Clin Invest*. 2000;105(10):1395-1406.
314. Ho SN, Hunt HD, Horton RM, Pullen JK, Pease LR. Site-directed mutagenesis by overlap extension using the polymerase chain reaction. *Gene*. 1989;77(1):51-59.
315. Wang R, Chen W, Cai S, et al. Localization of an NH(2)-terminal disease-causing mutation hot spot to the "clamp" region in the three-dimensional structure of the cardiac ryanodine receptor. *J Biol Chem*. 2007;282(24):17785-17793.
316. Liu Z, Zhang J, Li P, Chen SR, Wagenknecht T. Three-dimensional reconstruction of the recombinant type 2 ryanodine receptor and localization of its divergent region 1. *J Biol Chem*. 2002;277(48):46712-46719.
317. Yang D, Song LS, Zhu WZ, et al. Calmodulin regulation of excitation-contraction coupling in cardiac myocytes. *Circ Res*. 2003;92(6):659-667.
318. Baus E, Urbain J, Leo O, Andris F. Flow cytometric measurement of calcium influx in murine T cell hybrids using fluo-3 and an organic-anion transport inhibitor. *J Immunol Methods*. 1994;173(1):41-47.
319. Papadopoulos S, Leuranguer V, Bannister RA, Beam KG. Mapping sites of potential proximity between the dihydropyridine receptor and RyR1 in muscle using a cyan fluorescent protein-yellow fluorescent protein tandem as a fluorescence resonance energy transfer probe. *J Biol Chem*. 2004;279(42):44046-44056.
320. Ide T, Tsutsui H, Kinugawa S, et al. Mitochondrial electron transport complex I is a potential source of oxygen free radicals in the failing myocardium. *Circ Res*. 1999;85(4):357-363.

321. Wang R, Bolstad J, Brown C, Zhang L, Chen SR. Role of the TM10 transmembrane helix in cardiac ryanodine receptor function. *Biophys J*. 2003;84:427a.
322. Kubalova Z, Gyorke I, Terentyeva R, et al. Modulation of cytosolic and intra-sarcoplasmic reticulum calcium waves by calsequestrin in rat cardiac myocytes. *J Physiol (Lond)*. 2004;561(2):515-524.
323. Domeier TL, Blatter LA, Zima AV. Alteration of sarcoplasmic reticulum Ca^{2+} release termination by ryanodine receptor sensitization and in heart failure. *J Physiol*. 2009;587(Pt 21):5197-5209.
324. Fill M, Copello JA. Ryanodine receptor calcium release channels. *Physiol Rev*. 2002;82(4):893-922.
325. Meissner G. Molecular regulation of cardiac ryanodine receptor ion channel. *Cell Calcium*. 2004;35(6):621-628.
326. Rodney GG, Wilson GM, Schneider MF. A calmodulin binding domain of RyR increases activation of spontaneous Ca^{2+} sparks in frog skeletal muscle. *J Biol Chem*. 2005;280(12):11713-11722.
327. Lam E, Martin MM, Timerman AP, et al. A novel FK506 binding protein can mediate the immunosuppressive effects of FK506 and is associated with the cardiac ryanodine receptor. *J Biol Chem*. 1995;270(44):26511-26522.
328. Jeyakumar L, Ballester L, Cheng D, et al. FKBP binding characteristics of cardiac microsomes from diverse vertebrates. *Biochem Biophys Res Commun*. 2001;281(4):979-986.
329. Xin HB, Senbonmatsu T, Cheng DS, et al. Oestrogen protects FKBP12.6 null mice from cardiac hypertrophy. *Nature*. 2002;416(687821904899):334-38.
330. Zhang R, Khoo MS, Wu Y, et al. Calmodulin kinase II inhibition protects against structural heart disease. *Nat Med*. 2005;11(4):409-417.
331. Backs J, Backs T, Neef S, et al. The delta isoform of CaM kinase II is required for pathological cardiac hypertrophy and remodeling after pressure overload. *Proc Natl Acad Sci U S A*. 2009;106(7):2342-2347.
332. Ling H, Zhang T, Pereira L, et al. Requirement for Ca^{2+}/calmodulin-dependent kinase II in the transition from pressure overload-induced cardiac hypertrophy to heart failure in mice. *J Clin Invest*. 2009;119(5):1230-1240.
333. Sossalla S, Fluschnik N, Schotola H, et al. Inhibition of elevated Ca^{2+}/calmodulin-dependent protein kinase II improves contractility in human failing myocardium. *Circ Res*. 2010;107(9):1150-1161.
334. Anderson ME. CaMKII and a failing strategy for growth in heart. *J Clin Invest*. 2009;119(5):1082-1085.
335. Zucchi R, Ronca-Testoni S. The sarcoplasmic reticulum Ca^{2+} channel/ryanodine receptor: Modulation by endogenous effectors, drugs and disease states. *Pharmacol Rev*. 1997;49(1):1-51.
336. Xu L, Tripathy A, Pasek DA, Meissner G. Potential for pharmacology of ryanodine receptor/calcium release channels. *Ann N Y Acad Sci*. 1998;853:130-148.
337. Eisner DA, Diaz ME, O'Neill SC, Trafford AW. Physiological and pathological modulation of ryanodine receptor function in cardiac muscle. *Cell Calcium*. 2004;35(6):583-589.

338. Eisner DA, Kashimura T, Venetucci LA, Trafford AW. From the ryanodine receptor to cardiac arrhythmias. *Circ J*. 2009;73(9):1561-1567.
339. Capes EM, Loaiza R, Valdivia HH. Ryanodine receptors. *Skelet Muscle*. 2011;1(1):18.
340. Maclennan DH, Zvaritch E. Mechanistic models for muscle diseases and disorders originating in the sarcoplasmic reticulum. *Biochim Biophys Acta*. 2011;1813(5):948-964.
341. Sharma MR, Jeyakumar LH, Fleischer S, Wagenknecht T. Three-dimensional structure of ryanodine receptor isoform three in two conformational states as visualized by cryo-electron microscopy. *J Biol Chem*. 2000;275(13):9485-9491.
342. Liu Z, Wang R, Tian X, et al. Dynamic, inter-subunit interactions between the N-terminal and central mutation regions of cardiac ryanodine receptor. *J Cell Sci*. 2010;123(Pt 10):1775-1784.
343. Jones PP, Jiang D, Bolstad J, et al. Endoplasmic reticulum Ca^{2+} measurements reveal that the cardiac ryanodine receptor mutations linked to cardiac arrhythmia and sudden death alter the threshold for store-overload-induced Ca^{2+} release. *Biochem J*. 2008;412(1):171-178.
344. Rousseau E, Smith JS, Meissner G. Ryanodine modifies conductance and gating behavior of single Ca^{2+} release channel. *Am J Physiol*. 1987;253(3 Pt 1):C364-8.
345. Pogwizd SM, Bers DM. Cellular basis of triggered arrhythmias in heart failure. *Trends Cardiovasc Med*. 2004;14(2):61-66.
346. Venetucci LA, Trafford AW, O'Neill SC, Eisner DA. The sarcoplasmic reticulum and arrhythmogenic calcium release. *Cardiovasc Res*. 2008;77(2):285-292.
347. Medeiros-Domingo A, Bhuiyan ZA, Tester DJ, et al. The RYR2-encoded ryanodine receptor/calcium release channel in patients diagnosed previously with either catecholaminergic polymorphic ventricular tachycardia or genotype negative, exercise-induced long QT syndrome: A comprehensive open reading frame mutational analysis. *J Am Coll Cardiol*. 2009;54(22):2065-2074.
348. Sobie EA, Lederer WJ. Dynamic local changes in sarcoplasmic reticulum calcium: Physiological and pathophysiological roles. *J Mol Cell Cardiol*. 2011.
349. Priori SG, Napolitano C, Tiso N, et al. Mutations in the cardiac ryanodine receptor gene (hRyR2) underlie catecholaminergic polymorphic ventricular tachycardia. *Circulation*. 2001;103(2):196-200.
350. Fozzard HA. Heart: Excitation-contraction coupling. *Annu Rev Physiol*. 1977;39:201-220.
351. Meng X, Wang G, Viero C, et al. CLIC2-RyR1 interaction and structural characterization by cryo-electron microscopy. *J Mol Biol*. 2009;387(2):320-334.
352. Lobo PA, Kimlicka L, Tung CC, Van Petegem F. The deletion of exon 3 in the cardiac ryanodine receptor is rescued by beta strand switching. *Structure*. 2011;19(6):790-798.
353. Aghdasi B, Zhang JZ, Wu Y, Reid MB, Hamilton SL. Multiple classes of sulfhydryls modulate the skeletal muscle Ca^{2+} release channel. *J Biol Chem*. 1997;272(6):3739-3748.
354. Zhang JZ, Wu Y, Williams BY, et al. Oxidation of the skeletal muscle Ca^{2+} release channel alters calmodulin binding. *Am J Physiol*. 1999;276(1 Pt 1):C46-53.

355. Maxwell JT, Blatter LA. Facilitation of cytosolic calcium wave propagation by local calcium uptake into the sarcoplasmic reticulum in cardiac myocytes. *J Physiol*. 2012;590(Pt 23):6037-6045.
356. Gangopadhyay JP, Ikemoto N. Role of the Met3534-Ala4271 region of the ryanodine receptor in the regulation of Ca^{2+} release induced by calmodulin binding domain peptide. *Biophys J*. 2006;90(6):2015-2026.
357. Yamamoto T, El-Hayek R, Ikemoto N. Postulated role of interdomain interaction within the ryanodine receptor in Ca^{2+} channel regulation. *J Biol Chem*. 2000;275(16):11618-11625.
358. Kobayashi S, Yano M, Suetomi T, et al. Dantrolene, a therapeutic agent for malignant hyperthermia, markedly improves the function of failing cardiomyocytes by stabilizing interdomain interactions within the ryanodine receptor. *J Am Coll Cardiol*. 2009;53(21):1993-2005.
359. Wehrens XH, Lehnart S, Huang F, et al. FKBP12.6 deficiency and defective calcium release channel (ryanodine receptor) function linked to exercise-induced sudden cardiac death. *Cell*. 2003;113(7):829-840.
360. Marks AR. Ryanodine receptors, FKBP12, and heart failure. *Front Biosci*. 2002;7:d970-7.
361. Liu Y, Chen H, Ji G, et al. Transgenic analysis of the role of FKBP12.6 in cardiac function and intracellular calcium release. *Assay Drug Dev Technol*. 2011;9(6):620-627.
362. Couchonnal LF, Anderson ME. The role of calmodulin kinase II in myocardial physiology and disease. *Physiology (Bethesda)*. 2008;23:151-9. doi:151-159.
363. Kirchhefer U, Schmitz W, Scholz H, Neumann J. Activity of cAMP-dependent protein kinase and Ca^{2+}/calmodulin-dependent protein kinase in failing and nonfailing human hearts. *Cardiovasc Res*. 1999;42(1):254-261.
364. Hoch B, Meyer R, Hetzer R, Krause EG, Karczewski P. Identification and expression of delta-isoforms of the multifunctional Ca^{2+}/calmodulin-dependent protein kinase in failing and nonfailing human myocardium. *Circ Res*. 1999;84(6):713-721.
365. Zhang T, Maier LS, Dalton ND, et al. The {delta}C isoform of CaMKII is activated in cardiac hypertrophy and induces dilated cardiomyopathy and heart failure. *Circ Res*. 2003;92(8):912-919.
366. Ai X, Curran JW, Shannon TR, Bers DM, Pogwizd SM. Ca^{2+}/Calmodulin-dependent protein kinase modulates cardiac ryanodine receptor phosphorylation and sarcoplasmic reticulum Ca^{2+} leak in heart failure. *Circ Res*. 2005;97(12):1314-1322.
367. Anderson ME, Brown JH, Bers DM. CaMKII in myocardial hypertrophy and heart failure. *J Mol Cell Cardiol*. 2011;51(4):468-473.
368. Van Petegem F. Ryanodine receptors: Structure and function. *J Biol Chem*. 2012;287(38):31624-31632.
369. Du GG, Guo X, Khanna VK, MacLennan DH. Ryanodine sensitizes the cardiac Ca^{2+} release channel (ryanodine receptor isoform 2) to Ca^{2+} activation and dissociates as the channel is closed by Ca^{2+} depletion. *Proc Natl Acad Sci U S A*. 2001;98(24):13625-13630.

370. Masumiya H, Li P, Zhang L, Chen SR. Ryanodine sensitizes the Ca^{2+} release channel (ryanodine receptor) to Ca^{2+} activation. *J Biol Chem*. 2001;276(43):39727-3935.
371. Mohamed U, Napolitano C, Priori SG. Molecular and electrophysiological bases of catecholaminergic polymorphic ventricular tachycardia. *J Cardiovasc Electrophysiol*. 2007;18(7):791-797.
372. Kass RS, Tsien RW. Fluctuations in membrane current driven by intracellular calcium in cardiac purkinje fibers. *Biophys J*. 1982;38(3):259-69.
373. Stern M, Kort A, Bhatnagar G, Lakatta E. Scattered-light intensity fluctuations in diastolic rat cardiac muscle caused by spontaneous Ca^{2+}-dependent cellular mechanical oscillations. *J Gen Physiol*. 1983;82(1):119-153.
374. Orchard C, Eisner D, Allen D. Oscillations of intracellular Ca^{2+} in mammalian cardiac muscle. *Nature*. 1983;304(5928):735-738.
375. Marban E, Robinson SW, Wier WG. Mechanisms of arrhythmogenic delayed and early afterdepolarizations in ferret ventricular muscle. *J Clin Invest*. 1986;78(5):1185-192.
376. Lakatta EG. Functional implications of spontaneous sarcoplasmic reticulum Ca^{2+} release in the heart. *Cardiovasc Res*. 1992;26(3):193-214.
377. Diaz ME, Trafford AW, O'Neill SC, Eisner DA. Measurement of sarcoplasmic reticulum Ca^{2+} content and sarcolemmal Ca^{2+} fluxes in isolated rat ventricular myocytes during spontaneous Ca^{2+} release. *J Physiol*. 1997;501 (Pt 1):3-16.
378. Baudenbacher F, Schober T, Pinto JR, et al. Myofilament Ca^{2+} sensitization causes susceptibility to cardiac arrhythmia in mice. *J Clin Invest*. 2008;118(12):3893-3903.
379. Bers DM, Guo T. Calcium signaling in cardiac ventricular myocytes. *Ann N Y Acad Sci*. 2005;1047:86-98.
380. Kubalova Z, Terentyev D, Viatchenko-Karpinski S, et al. Abnormal intrastore calcium signaling in chronic heart failure. *Proc Natl Acad Sci U S A*. 2005;102(39):14104-14109.
381. Schlotthauer K, Bers DM. Sarcoplasmic reticulum Ca^{2+} release causes myocyte depolarization. underlying mechanism and threshold for triggered action potentials. *Circ Res*. 2000;87(9):774-80.
382. Wehrens XH, Lehnart SE, Reiken S, Vest JA, Wronska A, Marks AR. Ryanodine receptor/calcium release channel PKA phosphorylation: A critical mediator of heart failure progression. *Proc Natl Acad Sci U S A*. 2006;103(3):511-518.
383. Roux-Buisson N, Cacheux M, Fourest-Lieuvin A, et al. Absence of triadin, a protein of the calcium release complex, is responsible for cardiac arrhythmia with sudden death in human. *Hum Mol Genet*. 2012;21(12):2759-2767.
384. Cai WF, Pritchard T, Florea S, et al. Ablation of junctin or triadin is associated with increased cardiac injury following ischaemia/reperfusion. *Cardiovasc Res*. 2012;94(2):333-341.
385. Zhou Q, Xiao J, Jiang D, et al. Carvedilol and its new analogs suppress arrhythmogenic store overload-induced Ca^{2+} release. *Nat Med*. 2011;17(8):1003-1009.